WATER EXCHANGE AND CIRCULATION IN SELECTED KENYAN
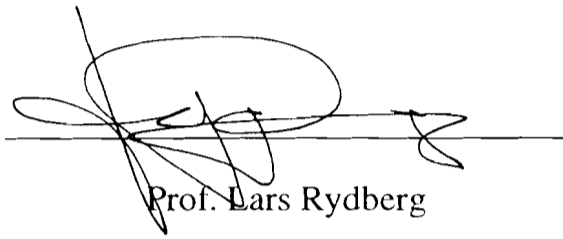
CREEKS

By

Michael Mutua Nguli

A Thesis Submitted in fulfillment of the requirement for the Degree of Doctor of

Philosophy (Physical Oceanography) of the University of Dar es Salaam
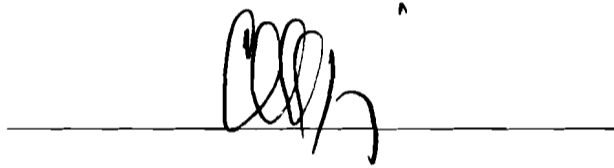
University of Dar es Salaam

(July 2002)

CERTIFICATION

The undersigned certify that they have read and hereby recommend for acceptance by the University of Dar es Salaam a thesis entitled: **Water exchange and circulation in selected Kenyan creeks**, in fulfillment of the requirement for the Degree of Doctor of Philosophy (Physical Oceanography).

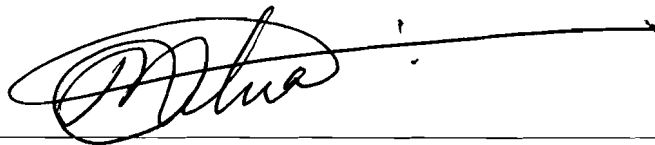Prof. Lars Rydberg

(FIST SUPERVISOR)

Prof. E. C. Njau

(SECOND SUPERVISOR)

Date 04 November 2002

DECLARATION

AND

COPYRIGHT

I, **MICHAEL MUTUA NGULI**, declare that this is my own original work and that it has not been presented and will not be presented to any other university for a similar or any other degree award.

Signature _____

ACKNOWLEDGEMENT

Prof. V. Masanja of the Department of Mathematics UDSM provided unfailing encouragement and generated enthusiasm during the course and to her also I am thankful. I thank also Prof. Y. Mgaya (UDSM) who on numerous occasions has inspired and envisioned a new strategy in developing oceanography (as a core unit in aquatic sciences) in Eastern Africa Region to which this thesis and similar ones in the future would hopefully constitute an important effort in the foundation of aquatic knowledge in the region.

DEDICATION

Dedicated to

Rydberg, Mueni, Mark, Mathew and Moses

ABSTRACT

Water exchange and circulation dynamics in shallow water ecosystems characterized by three selected creeks in the Kenyan coastal zone are analyzed and discussed. Two of the creeks (Kilifi and Tudor Creeks) have each narrow and relatively deep single channel that connects an inner relatively wide and shallow mangrove fringed inner basins to the ocean. The third is characterized by a relatively broad opening to the ocean giving it the characteristics of a small mangrove fringed bay (Gazi Bay). Several river streams drain in each of the creeks; hence they are essentially estuarine creek systems. Morphological configuration, dimensions, sizes, depth and orientations of each system are some of the factors influencing water exchange and circulation dynamics. The driving forces come from sea surface buoyancy fluxes influenced by climatic factors, rainfall, freshwater, evaporation and heat flux which cause changes in salinity temperature, and density structure. Tide or sea level fluctuations are everywhere of importance both as a driving force generating barotropic flow and mixing. The wind also affects the sea level and hence is sometimes the primary mixing source and occasionally drives circulation and water exchange.

Measurements of hydrographic parameters (temperature and salinity), sea levels and velocities are used to study water exchange and heat flux in three selected sites within the context of four monsoon climatic conditions: The inter-monsoon long-rain IMLR season (May), occasionally overlapping April, the southeast monsoon (SEM) season (June-September), (the inter-monsoon-short rain (IMSR) season (October-November) and the northeast monsoon (NEM) season (December-March). Each of the study sites is basically divided into three almost distinct ecological regimes-the inner shallow estuarine proper basins close to the river mouths, the inlet channel, the entrance and the immediate shelf slope environment. During IMLR and the IMSR-seasons as well as during SEM season, longitudinally averaged salinity revealed that salinity is lower inside the creeks but higher in the ocean water. This longitudinal salinity gradient is the result of interaction between fresh water discharge, sea water brought by the tide, gravitation circulation and tidal dispersion.

Thus the IMLR and IMSR seasons suggest near classical estuarine condition and stratification particularly in May, and net-out flow-exchange consistent with density induced gravitation (baroclinic) circulation. The relatively higher salinity in the inner parts of the creek than in the ambient water during NEM season suggest negative estuarine condition driven by excess evaporation over precipitation and imply net-inflow-exchange of water or trapping tendency. Salinity and temperature vary form maximum (35.5, 30°C) in NEM particularly in February-early March to minimum values (28, 25°C) in IMLR and SEM (particularly August) respectively.

Following the rain and diminished freshwater input, both the basin and the channel water display partial stratification characterized by the decrease in salinity gradient as SEM and NEM seasons progress. The channels deep water retains more stratification than the basin water, which becomes almost homogeneous due to intense mixing. The results indicate that, in addition to local rainfall influences, the shifting of the offshore major currents bring water of low salinity in the SEM season and temperatures and vice versa in NEM season.

On shorter (daily and fortnightly time scales) salinity increases within the creeks and reach highest fluctuations during flood and spring tides, whereas during neap tide the conditions are reversed. The creeks reveal low salinity during ebb and neap tides. Stratification is found to be maximum near low water spring (LWS) and minimum around high water spring (HWS). Temperature show variation with solar radiation, maximum daily temperatures occur at 15 hours and minimum temperature at around 5 a.m. Temperature is low the creeks during spring tide, but high during the neap tides. The variation of salinity and temperature during flood and spring tides is attributed to large tidal prism during flood and spring tides that result in cooling of the creeks by ocean water, whereas during ebb and neap tides variations in salinity and temperature is caused by smaller tidal prism with low salinity water from upper reaches in the creeks and solar heating.

Tidal characteristics, harmonics, range, asymmetries and phase lags are also determined. At the entrance to each study site a tidal asymmetry with a combination of long ebb periods and high flood velocities is observed. The water and heat exchange is calculated

from simultaneous sea level and temperature data. The seas level results show that tide in the creeks is predominantly semi-diurnal M_2 tide, with a form number less than 0.21 for the three creeks. The M_2 tide and other two main tidal constituents (S_2, and N_2) account for more than 90% of the variation in tidal amplitude in Tudor Creek, whereas in Kilifi Creek they contribute 64%. Shallow water tides are also obtained for the three creeks; however, their amplitudes contribute 25% of M_2. M_4 is suggested as the cause of distortion observed in the tidal curves in Gazi Bay and Tudor Creek. Tidal ranges are found to show very slight variation form one study area to the other. The spring tidal ranges from the entrance areas were 4m, 3m, 3.2m mean tidal range 3m, 2.3m, 2.3m and neap range of 1.4m, 1.0m, and 1.2m for Gazi Bay, Tudor and Kilifi Creeks respectively, and are of the same order of magnitude within the creeks. In Tudor M_2 and S_2 do not show any reduction in amplitude; however N_2 decreases in amplitude by 16%, while K_2 increases by 50% of M_2 amplitude. It is found that the average temperature within the creeks is higher than the oceanic temperature; despite this, however, there is an apparent import of the heat from the ocean falling within 40-60Wm^{-2}. Thus the sum of the long wave back radiation, evaporation and sensible heat flux exceeds the net incoming solar radiation. A set of figures featuring, variation in the temperature, salinity, and sea level as a function of time are used to support the results.

Seasonal changes hydrographic parameters in each of the four seasons are presented as longitudinal sections that allow along-the-creek and vertical variation of water structure to be observed. Taking Tudor Creek as a typically representation of the three creeks, the results distinctly show how salinity and temperature vary within the creek in the three ecological regimes and also with the seasons. The channel, the entrance and the immediate slope area are together considered as frontal zone. The zone constitutes the most critical are of the creeks that govern the physical processes, the net spring-neap exchange dynamics as well as the long-term ventilation processes. Its position is a result of a shear-production as the tidal current responds to rapid change in depth at the entrance and in the creek channel, as well as in the morphology of each channel. During the flooding phase water of oceanic origin is pumped into the shallow basins. Part of the increasing tidal current energy is expended in mixing the water in the basin area, first due to stratification from the freshwater input during the IMLR and IMSR seasons period and latter due to added buoyancy resulting from heat input in the NEM input. During

the ebbing phase (and even long-term low tidal level in SEM season). the tidal mixing (seasonal changes) occurs in the channel as the part of the potential energy as the well-mixed water in the basin mixes with the deep stratified water in the channel.

Thus the mechanism of mixing is viewed as controlled by the dynamics in the zone which change with the local and non-local (monsoonal) influences. Almost throughout the year the front acts as a physical boundary in trapping water in the shallow inner basins and the net exchange between the basins and the ocean is small. However, in peak IMLR season the dynamics are changed as the gravitation circulation enhances the exchange. the position of the front moves into and is aligned with the channel resulting increased water exchange.

Similarly as the evaporation exceeds precipitation particularly during NEM, the creeks basins tend to develop reverse estuarine circulation, whereas in the oceanic side, due to prevailing wind and meeting of the Somali Current and EACC enhanced offshore Eckman circulation occurs. It is suggested that the gravitation circulation arising from the hypersaline conditions induce shoreward and creek-ward movements of material from the ocean. The differences in exchange dynamics imply ecological differences in terms of biological productivity and suitability of the three creeks as nursery grounds for fish. The seasonal change in the water structure is supported by vertical profiles of the offshore water featuring temperature, salinity, density, oxygen and nutrients profiles, time depended progression of oceanographic parameters and fish-landing plot, as well as schematics depicting various processes. The thermocline fluctuates and shoals during NEM season but deepens in SEM season. leading to the speculation whether the mechanisms that affect water structure and the thermocline position may relate to enhanced biological productivity and changes in fish-landing. Although the findings do not allow firm conclusion on 'fish-thermocline' relation, the seasonality in the oceanographic and meteorological parameters suggest that opposed gravitation circulation patterns in the creeks and in the offshore, may be crucial to biological enrichment and improved artisanal fishery.

Hence it is hypothesized that during NEM season the sea level rises as the Somali Current (SC) water 'backs-up' the East African Coastal Current (EACC), and the near

hypersaline conditions within the creeks induce internal anti-clockwise circulation with a vertical sense similar to an offshore 'upwelling-favorable-conditions' circulation generated by non-local forcing (Kelvin wave) mechanism which is probably linked to Findlater Jet. Conversely, during SEM season the sea level is low probably due to the relaxation of the 'back-up' as water is swiftly removed from the East African Bight by enhanced northerly transport in the EACC, mixing is intensified by relatively strong winds, the water in the creeks is less saline with a positive salinity gradient, hence an internal clock-wise circulation is postulated with downward sense of flow as that of the offshore 'down-welling favorable conditions'. Net outward water exchange (creek-ventilation) begins in the IMLR season when high salinity water at the end of NEM is replaced by fresh water which causes salinity to plummet from high values just before the onset of the NEM season to the low salinity in May. The swift coastal current rapidly removes from the entrance any out-welled plume from the creeks and replaces it with different water masses. The implication of the internal circulation is that upwelling frontal features are set up inside the creek during SEM season, but near the entrance and shelf edge during the NEM season. However, the apparent trapping mechanism due to net creek-ward gravitation flow during NEM season make it more favorable as nursery and recruiting period for fish and crustaceans, whereas the circulation during the SEM season may suggest outward migration or loss of material from the creeks.

TABLE OF CONTENTS

CHAPTER ONE

GENERAL INTRODUCTION, RESESEARCH QUESTIONS, OBJECTIVES AND SIGNIFICANCE OF THE STUDY

LIST OF FIGURES

xxiv

xxv

xxx

.

xxxviii

LIST OF TABLES

LIST OF ABREVIATIONS

EAB	East Africa Bight
EACC	East African Coastal Current
ECC	Equatorial Counter Current
COMEC model	Creek-Ocean Monsoon Eco-process model
GLOSS	Global Sea level Observing System
IMLR	Inter-monsoon Long Rain Season
IMSR	Inter-monsoon short Rain Season
ITCZ	Inter-tropical Convergence Zone
KMFRI	Kenya Marine and Fisheries Research Institute
KMC	Kenya Meat Commission
KMD	Kenya Meteorological Department
MIAMS	Moi Inter-national Airport Meteorological Station
NEM	Northeast Monsoon
NEC	North Equatorial Current
RCM	Rotor Current Meter
SC	Somali Current
SEC	South Equatorial Current
SEM	Southeast Monsoon
PCM	Pendulum Current Meter
UDSM	University of Dar es Salaam
UG	University of Gothenburg
NARA	National Research and Administration of Sri Lanka

CHAPTER ONE

GENERAL INTRODUCTION, RESEARCH QUESTIONS, OBJECTIVES AND SIGNIFICANCE OF STUDY

1.1 GENERAL INTRODUCTION

While most coastal areas of the World Ocean feature more or less wide shelf areas, the Kenyan shelf is virtually non-existent. It means from oceanographic point of view, that the stronger currents flowing along the coast will have a strong impact on the coastal water exchange including that of the tidal creeks of Kenya, which is the main subject of this study. The exchange will also, probably, be affected by the changing monsoon climate also a main factor influencing the hydrography of East Africa: at least it is a hypothesis of this thesis.

Kenyan tidal creeks are inlets usually formed at present (or former) river mouths that start inland, usually with mangrove swamps and mudflats, drained by smaller tidal creeks to shallow wide basins, which in turn are connected by one or several channels to the ocean. If receiving freshwater the creeks may be classified as estuaries.

They were formed as a result of rivers cutting through the reefs during periods of lower eustatic sea level. About 18000 yrs ago the mean sea level was at 120m below the present level (see e.g. Kjerve, 1991), which coincided with the period of maximum ice cover. The sea level reached its present elevation about 5000 years ago, but has undergone fluctuations of a few meters since then (Fairbridge, 1980) as a result of coastal processes during the period of rise, but also thereafter barriers such as coral reefs, formed. Such barriers now constitute the margins of the creeks (Lankford, 1976). All creeks are also

1

currently on transition. They are being filled with both fluvial material and marine input reshaping their boundaries (Meade, 1969). At the same time tidal flow re-suspend settled material and tends to keep the creeks open.

Some particular features of today may be pointed out. The entrance is often relatively long and deep and cuts through old coral rocks. Inside the inlets the creeks widen and may have far reaching tidal channels, whereas others are relatively short and narrow. The areas inside the entrance are generally shallow. Our goal here is to study some of the Kenyan creeks from oceanographic point of view.

An important factor, particularly, from the point of view of biological processes and water quality is that of exchange of water with the ocean. The exchange of water is important not only to maintain water quality, but also for importing and exporting nutrients and plankton. Within the creeks, mangroves and sea grass have colonized the sediments. Nzioka (1985) pointed out that the Kenyan creeks act as nursery areas for commercially important fish species. Similar observations have been made elsewhere (Wolanski et al., 1980; Robertson et al., 1987; Ridd et al., 1988; Boto and Bunt, 1981). Hence the creeks are both ecologically and economically important environments.

The water exchange and thus the mass transport between the creeks and the inner continental shelf occur for example due to river discharge. This fresh water (mass flux or buoyancy input) tends to flow on top of the denser ocean water.

SINGLE CHANNEL

SHALLOW

BAY (CREEK)

OCEA:

P

E

R

(b)

V

A2

A1

BAY (CREEK)

G

OCEAl
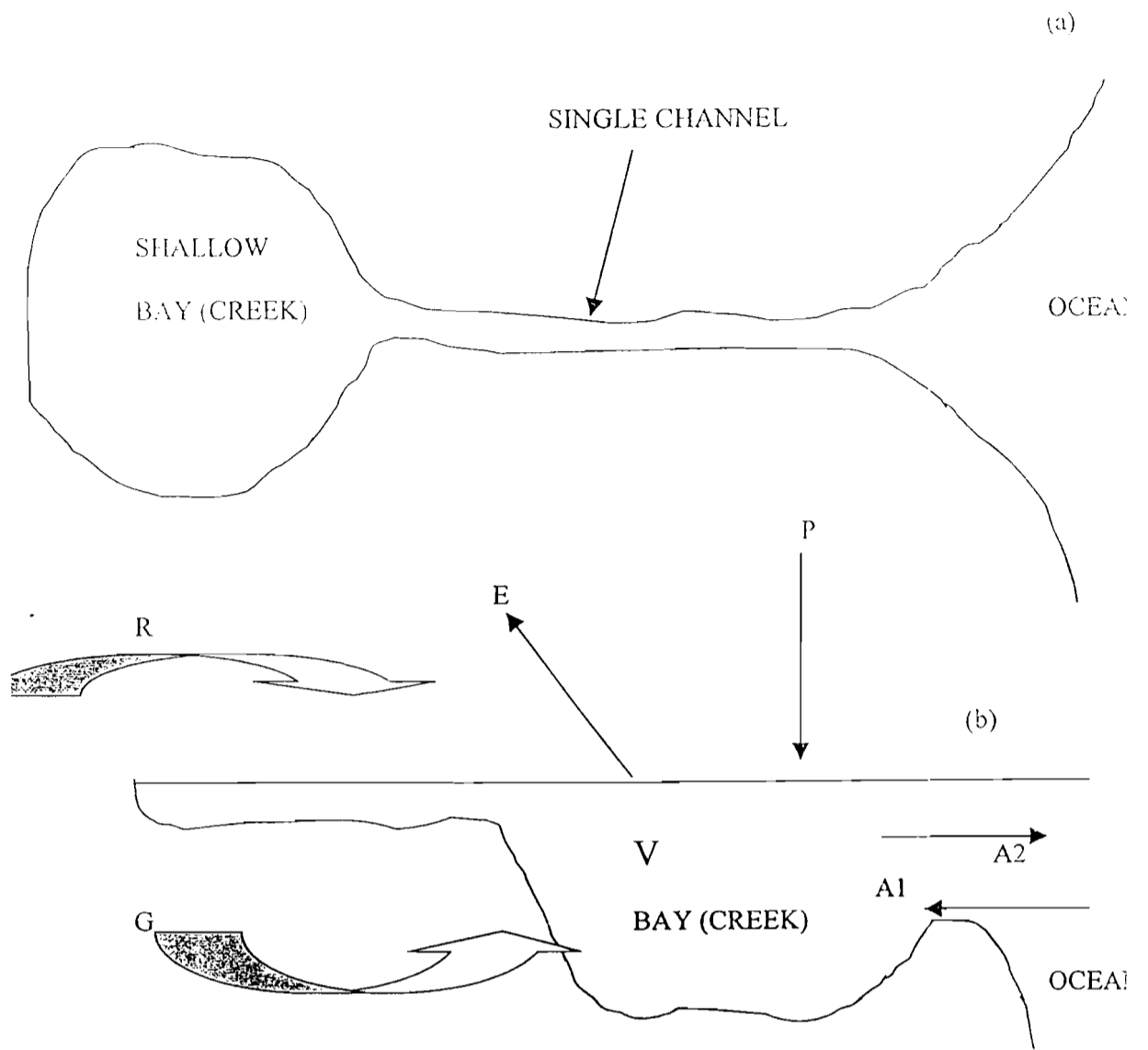
Figure 1.1a Schematic showing (a) features of a typical creek system such as considered in this study, (b) various forcing parameters: E-evaporation, P-precipitation, R-river input; G-ground water input, A1-incoming water A2-outgoing water, V -creek volume.
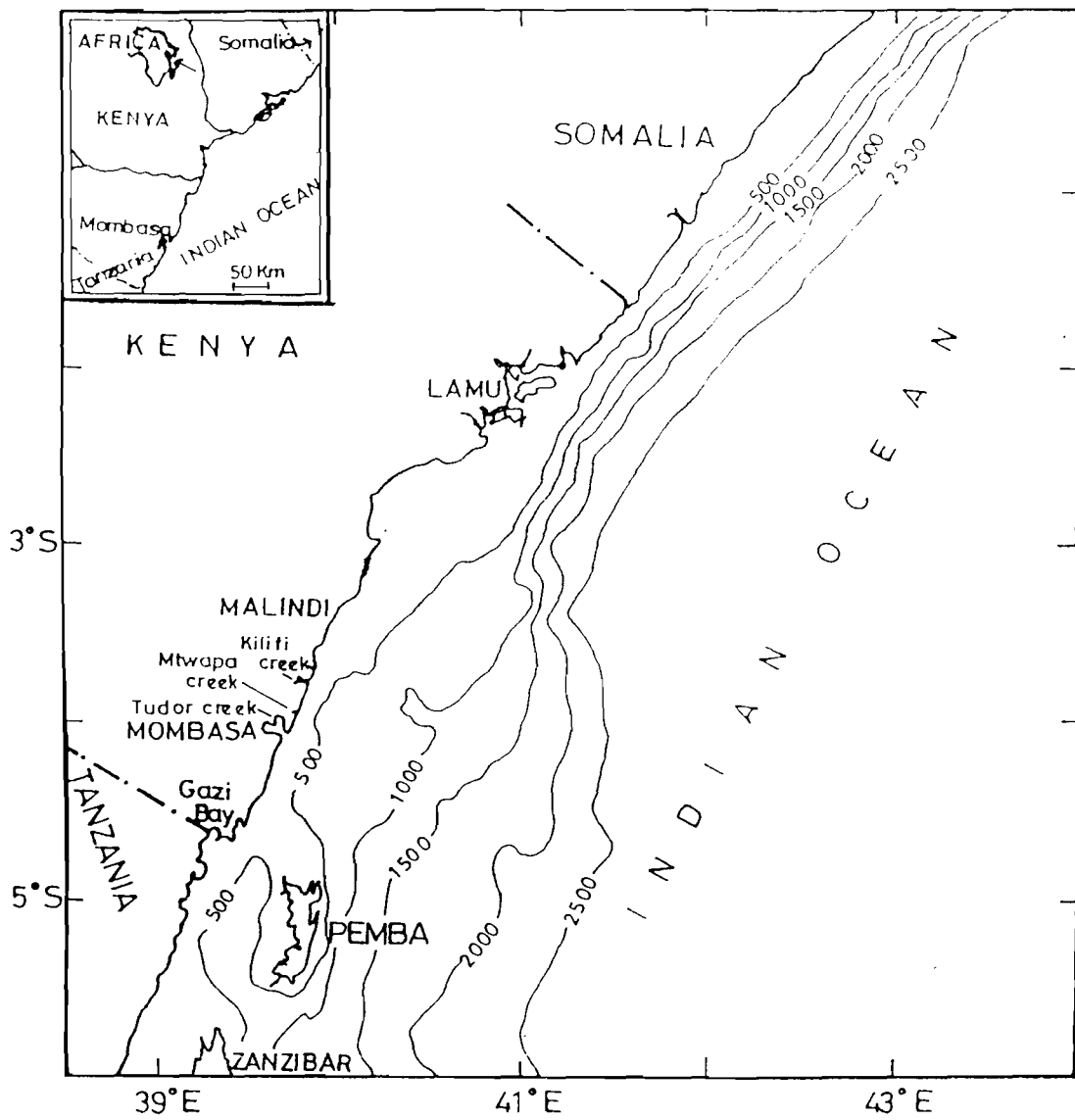
Figure1.1b Bathymetry of Kenya Coast. Note the closeness of 200 and 500 m contour near Gazi Bay, Tudor Creek and Kilifi Creek in the southern part the coast.

4

However, in most creek areas, the fresh water is rapidly mixed with the oceanic water due to high tides along the Kenyan coast of with spring tide rage is 3-4m (Pugh, 1979). Tides together with fresh water mutually force water exchange, however, there are other factors such as wind, oceanic variation of sea level and density and even heat flux that may influence the exchange between the creek systems and the ocean. The exchange is also affected by the variability in currents along and across the shelf, which transport the creek water away from the primary influenced area. Strong winds give rise to storm surge and cause wave set up along the coastline there by affecting the mixing and flushing of the coastal waters. Although the time scales associated with these processes may range from days to years and this relative importance varies with location, it is appropriate to relate the water exchange to the strong monsoon signal which in various ways influences the hydrography and climate of this area. At least both the related currents and hydrography play direct or indirect roles in changing the efficiency of the water exchange.

Both for management and secure future of the tidal creeks, it is necessary to quantify and describe the importance of the various physical processes driving creek-shelf exchange. An appropriate management requires understanding the individual processes including also the coastal currents, wind, precipitation, and radiation fluxes through sea surface. Most knowledge on the various physical processes occurring in inlets and river mouths is based on research in North America and Northern Europe where fjord-type estuaries similar to the Kenyan creeks exist. In the Scandinavia studies were carried out (see e.g. Stigebrandt, 1980, 1983, 1985, 1990; Andersson and Rydberg, 1993; Pejrup et al., 1993).

Tropical estuarine systems, on the other hand, are often shallow and therefore tidally dominated. Such systems have been studied e.g. by Kjerve and Magill (1989) and by Oliviera and Kjerve (1993), in Australia and Southeast Asia by Wolanski *et al.* (1980); Ridd *et al.* (1990); Wattayakorn et al. (1990) and by Wolanski (1986). From the coast of Kenya (and Tanzania), except for some tidal studies by Pugh (1979), Lwiza and Bigendako (1988), and also by Nguli (1994), Odido (1994) and Norconsult (1995) e.g. in Tudor Creek, there is very little done in terms of tides, currents and even hydrography. The investigations in Tudor Creek (north of Mombasa Island) included some currents and salinity observations, and some rudimentary model of creek exchange. However, these studies were insufficient for any detailed description of the processes occurring in the creeks.

The purpose of this work, therefore, is to investigate the physical processes, which influence circulation, mixing and waters exchange, from observations inside the creek as well as in the adjoining shelf water. The creeks systems under consideration are Gazi Bay, Tudor Creek and Kilifi Creek. A typical example of the creek is shown in Figure 1.1a. The three systems are shown in Figure 1.1b, which also shows the shelf topographic features of the Kenya continental shelf including the relatively wider part between Malindi and Lamu i.e. the vicinity of Ungwana Bay at the location the North Kenyan Banks. Each of the study areas is described separately later in the section. Supply of fresh water is normally small but input during the monsoon periods may be considerable and a strongly eroding landscape gives a large supply of suspended matter. The continental shelf off Kenya is otherwise very narrow and the main coastal current

comes close (Newell, 1959, Johnson et al., 1982) to each of the creek's entrance implying, presumably, seasonal variations in the creek circulation.

Oceanographic characteristics of the Kenyan outer-shelf waters were studied during the International Indian Ocean expeditions of 1965 and the Monsoon Experiment (MONEX) of late 1970'ies. In addition studies were carried out in between 1992 and 1993 during the Kenya-Dutch Tyro expedition.

1.1.2 Statement of the research problem

Despite several offshore cruises in the equatorial western Indian Ocean (see Ch.3.2.1) and the knowledge of the main coastal currents that occur offshore, there is practically no information on the effects in the shallow near shore waters. Not even up-welling and down-welling conditions associated with the main offshore coastal current have been studied. Such conditions variability would result in enhanced ventilation of the creeks (see e.g. Stigebrandt, 1990). Obviously the type of creeks with deep and long inlets (which are not restricted), an outside bar reef topography and extremely narrow shelf are uncommon, comparable sites are hardly found elsewhere in the world. Therefore a main objective of this thesis is to present, in some detail, the hydrography between the creeks and the open ocean. This also includes some deeper studies of various oceanographic processes that appear. For this we have carried out observations of tide levels, currents, salinity, and temperature and to a limited extent nutrient in the creeks and at the bordering ocean. We hope to throw some light on the physical mechanisms governing circulation patterns and their variations with the monsoon seasons. Particular attention is given to climatic characteristics, heat flux, hydrography, currents, tides, salt

and water balance, friction and to bottom layer profiles characteristics within the inlet channel of Tudor Creek. In order to have a holistic understanding of the oceanic influences, we also include analysis of unpublished oceanographic cruise data sets from selected stations in the ambient (adjacent coastal) waters. The data sets are from Kenya Marine and Fishery Institute (KMFRI) Data Center. The author of this thesis participated in almost all the of the cruises from which the data sets obtained.

1.1.3 Research questions

Strictly water exchange and circulation in Gazi Bay, Tudor and Kilifi Creeks are expected to be unique in each creek due to variability in the magnitudes of the forcing parameters. Such parameters are the meteorological factors e.g. solar radiation, cloud cover, wind direction and intensity, precipitation that may give rise to variable precipitation, and hydrographic factors such as variability in temperature, salinity and water density and tidal characteristics of each study site. These forcing parameters together with morphological features, considered at short time scales of daily and fortnightly fluctuations or seasonal and inter-seasonal monsoon time scales are important for circulation and water exchange between the creeks and the ocean. For these particular study sites, some key research question can be raised:

1. How do the meteorological parameters vary with time, for the years under investigation, what parameters can be use to define climatic seasons and distinguish one from the other? What are the merits of such divisions? Still further how do the local parameters variability compare to the general climatic characteristics of the coastal region?

2. Which are the various forcing factors that drive circulation and water exchange between the creeks and the ocean?

3. Is the monsoon climatic signal identifiable in the local meteorological parameters and how are the monsoon seasons related to hydrographic structure (temperature and salinity) and the water exchange?

4. The tide is commonly a dominating factor for water exchange, but to what extent are other driving forces such as freshwater, winds and shelf processes important in this case? Also how does the tidal amplitude and range vary and are the creeks floods or ebb dominant?

5. The flow of the East African Coastal Current (EACC) is northward but strongly variable. During the NE monsoon the Somali Current (SC) meets the EACC in the general vicinity of the study site and the strength of the EACC is reduced, but it is strengthened during SE monsoon, how do these variable flow conditions affect the inshore-offshore exchange?

6. The deep and narrow but rather long inlet channels that connect Tudor and Kilifi Creeks with the ocean are topographically different from most other coastal water bodies in the world. In a normal fjord like estuary, the inlet channel is narrow and the basin is deep. Here it is the other way round. Thus, to what extent is the mixing that takes place within the channel important in relation to mixing and circulation within the creek inside the channel?

7. Still further how do the hydrographic and nutrient structures look like in the ambient water, is the thermocline position and intensity influenced by monsoon seasons?

8. The creek water is part of the surface water of the East African Coastal Current. To what extent do the water masses brought by this current and its fluctuating speed affect the water exchange in the creeks?

9. More interestingly what, circulation patterns, water condition or mechanisms can be postulated to explain biological enhancement within the creeks as well as in the ambient shelf water?

1.1.4 Objectives of the study

The specific objectives are:

1. To quantify meteorological parameters and describe their variability in the context of regional climate.

2. To determine tidal characteristics of the creeks.

3. To estimate river discharge into the creeks, including evaporation and local precipitation cross-sections flows and mean velocities with a view to establishing seasonal water budget and flushing rates.

4. To determine radiation and heat budget from Weather Mast data and from also local meteorological stations.

5. To investigated nutrient concentrations in the creeks and the ocean.

6. Investigate and describe the oceanography of the offshore in the context of monsoon seasons, and identify water masses.

7. To describe the circulation mechanisms related sea level, vertical structure changes in the EACC, seas level and link this to biological enrichment in the creeks and coastal water.

1.1.5 Significance of the study

The creek waters of Kenya are likely to be an important ecological platform in providing a sheltered, nutrient rich and productive environment, conducive to spawning and breeding of fish as well as for other resources such as mangroves. Therefore it is important to understand the physics of the creek waters. Knowledge of the exchange and flushing rates are particularly important for pollution problems and thus for resource management of the creeks. Such knowledge is needed in handling of the wastewater from hotels and tourist industry in these already densely populated areas along the coastline.

The organization of this thesis is as follows: In the second chapter we look into the settings of the region and the study area giving meteorology and oceanographic background. In Chapter 3-literature review is considered, followed in Chapter 4 by material and methods, in which the various instruments used in the study, the stations, the measurements and treatment of raw data are presented. In addition, in Chapter 4 we have a section on theories and analysis where we have considered various useful theoretical techniques. Chapter 5 takes up results on meteorology; in each study site results are given for hydrography, currents, tide and water exchange and other calculations. In Chapter 6 some aspects of the oceanography of ambient (adjoining shelf) water are considered. Chapter 7 takes up discussion beginning with climate, hydrography, tides and mechanism that cause the thermocline to up-well and down-well, ocean sea level change and seasonal water exchange or ventilation. As the mechanisms are important for fisheries their biological implication is also discussed. Under Chapter 8, conclusions and recommendations are presented.

CHAPTER TWO

GENERAL BACKGROUND SETTING TO THE STUDY AREA

2.1 GEOMORPHOLOGY AND CONTINENTAL SHELF

2.1.1 The Kenya continental shelf

The Kenya continental shelf is part of the larger East Africa Bight (EAB), which is basically the Kenya-Tanzania shelf. EAB can be taken as the indented East African coastline, eastward of a straight line drawn northwards from Mafia Island to Kiunga off Tanzania and Kenya respectively. The continental shelf is characterised by a relatively narrow continental shelf (Figure 1.1b). This is particularly true of the Kenya continental shelf, which has a narrow width of only 4-15km only. The length of the Kenya coast is approximately 600-km stretching from 1°42'S to 4°40'S bordering Somali in the north and Tanzania in the south. Well-developed fringing reef systems are present all along the coastline except where the major rivers discharge into the ocean.

While old bathymetric charts are available existing scanty literature give only general description (e.g. Johnson *et al.*, 1982). The width of the Kenyan shelf varies considerably (Figure 1.1b). In the south coast it varies between 3 and 5km. In the coastal area from Kilifi Creek to Wasin Island, the bottom contours are roughly parallel to the coast and border a narrow shelf. This is shown particularly by the 200 and 500m depth contour range, which indicates that this area has width of 2 km only.

Off Malindi Bay the width is 10-15km attaining a maximum width of 60km in Ungwana Bay area before tapering to 5km off Lamu and Kiwayu. The location of the maximum width, just 2°S of the equator, is also where the two larger rivers. Tana and Sabaki, enter

12

the ocean and the submarine banks known as the North Kenya Banks form. The banks and their surrounding area constitute the Kenya's largest marine fishing ground.

The Ungwana Bay is an interesting region where the Somali Current during the Northeast Monsoon is said to meet with the East African Coastal Current, as discussed in Chapter 2.3. The shelf covers an estimated area of about 20,000 km^2 most within is in this region. The study areas, Gazi Bay, Tudor Creek and Kilifi Creek appear as relatively small embayments of estuarine type, at least in their upper reaches. They occur at equal distances of 50 km from each other in the coastal districts of Kilifi, Mombasa and Kwale (Figure 1.1b). Tudor Creek is a name given to the entire creek from Mombasa Old Port to Tudor Harbor including the Kombeni and Tsivu River mouths. Tudor Creek is the old harbor of Mombasa the site of Fort Jesus. Gazi Bay, located further south near the Pemba channel, is situated in a rural area of Kenya and has a small village located near it. Kilifi Creek is much like Tudor Creek but with no major harbor. Kilifi town, which has a large population, and the districts fish landing market is located near the creek. Both the entrance and the inner part of the creek are used as fishing grounds. The inner areas are important for shrimp fishery, which occurs between July and August (Fishery Dept. comm.).

2.1.2 Geomorphologic settings

According to Inman and Nordstrom (1971), the East African coast is an Afro-trailing edge type coast, which has experienced eustatic sea level oscillation and/or isostatic and differential tectonic movements. These have considerably influenced the coastal geomorphologic configuration. In the Kenya coast, the pertinent geological and

13

geomorphologic features are discussed by Caswell (1953), Thompson (1956), Ase (1978, 1981), Ojany (1984), Oosterom (1988), Abuodha (1989, 1992). Although the coast may look like uniform it is established that the Kenya coast shows great diversity in terms the shoreline configuration; sandy beaches, dunes, mangrove creek systems, muddy tidal flats and rocky shores bordered by cliffs. Thomson (1956) and Abuodha (1989) noted that the coastal plain rises from sea to 140 m and is 3-6km wide in the south but attains a width of more than 50km towards the Tana delta. In his earlier work Caswell (1953), had distinguished three zones in the coast. The Nyika lies at 600 m above sea level and represents the higher ground covered by the Duruma sand stone series and older rocks to the west. The Foot Plateau occurs between 140 and 600 m above sea level and coincides well with the relatively young Jurassic rocks. The geomorphology of the coastal plain is dominated by a series of raised old sea terraces. Most of the coastal environment and the recently formed shore configuration follow the 0-5 m and 5-15 m sea level terrace complexes.

Due to its evolutionary history, the principal rocks observed along the coastal margin are of sedimentary origins ranging from Triassic to recent. Raise-Assa (1988) has pointed out that the Duruma Sandstone series, the oldest formation, is represented by the Mariakani and Mazeras sand stone which were deposited during periods of sub-aqueous, deltaic, lacustrine or possibly neritic conditions that prevailed during the opening of the Indian Ocean. Marine limestone with occasional horizons of sandstone and earlier limestone represent the upper Mesozoic. Cainozoic to recent rocks comprise mostly of marls and limestone, and is represented by the sandstone, clays, conglomerates and gravel such as the Marafa beds. Quaternary representatives include windblown magarine

14

sands. limestone. cemented sands and coral sands. Recent unconsolidated windblown sands. beach sands and clay overlie the older units, in the north Kenyan Coast off Mambrui. In the coastal plains within Gazi Bay to the south and in Tudor and Kilifi Creeks the Cainozoic rock is generally low lying and characterised by extensive fossil reef. which lies a few meters above present sea level (e.g. see Abuodha. 1989).

The most westerly, the middle to upper Jurassic marine shale. sandstone and conglomerates of the Kambe Formation, are resistant to incision and forms a broad ridge northwest of the creek systems. Tudor and Kilifi Creek occur within the outcrop of Upper Jurassic marine shale, sandstone and limestone of the Mto Mkuu formation (Raise-Assa, 1988). Marine shale of this formation is extensively exposed around the edge of the peripheral lagoons in the backwaters. Gazi Bay occurs over wave-cut Pleistocene limestone reef and back-reef deposits (Caswell, 1953; 1956), which separate the backwater areas of the creek systems from the coast. The rocks also form the cliff-terrain along and on either side of the entrances to the two creeks. The Pleistocene forms the fringing barrier reef system that traverses Tudor and Kilifi Creeks protecting them from the pounding waves (Abuodha, 1989).

2.2 CLIMATIC SETTINGS

2.2.1   Air pressure variability and Inter-tropical Convergence Zone

The Kenya coast lies in the equatorial region. Its climate and weather that is dominated by the large-scale pressure systems of the western Indian Ocean that affects the ocean indirectly through the association with the monsoon wind systems. The key features that further affect the climate are the Inter-tropical Convergence Zone (ITCZ),

and the equatorial trough of low pressure and also the distribution of land and water that largely affect basic air pressure seasonal pattern. Low and high pressure alternates over the land and the ocean respectively. By July the pressure a low-pressure system of 1000 mb is well established over the northern Pakistan, as part of low-pressure trough along 20°N latitude. A corresponding high-pressure ridge occurs south of 20"S latitude. Wind blow clockwise around a high and give rise to the southeast winds. which blow form mid-March to August, characterizing the southeast monsoon (SEM). From December to March the low over the Pakistan is replaced by high pressure, which reaches a value of 1020 mb by January. The low pressure moves southward and by January the low-pressure trough occurs over Madagascar and the African mainland and over the western Indian Ocean. During this time the anti-clockwise wind system give rise to northeasterly winds, and thus characterize the northeast monsoon (NEM). The monsoons periods are illustrated in Figure 2.2.1, for January, which is representative for the Northeast monsoon (NEM) season dry period, and for July/August, which is a representative of the dry Southeast Monsoon (SEM) season. The seasons are described later in details.

The ITCZ is found where the northeast and southeast winds meet as they blow towards the low pressure in the trough. This zone basically follows the sun's movement with a lag of about one month. It is a region of confluence of air and is thus likely to give rise to rain. In Kenya, however the local variation, due the presence of highlands and lakes, introduce significant modifications such that the ITCZ pattern is not quite predictable.

16

January Circulation

July/August Circulation
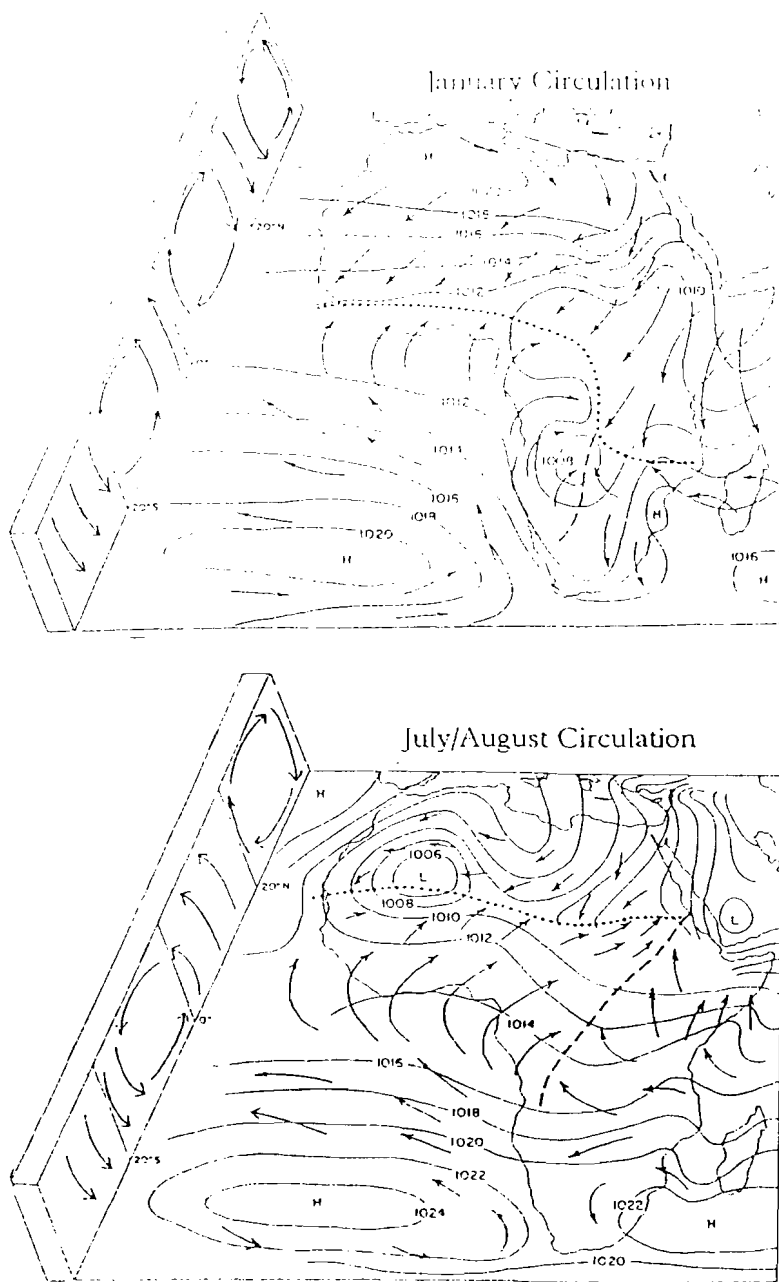
Figure 2.2.1 Atmospheric circulation showing winds, air pressure and vertical motion in the study area. Note the movement of the ITCZ - dotted line and dashed lines convergence as winds from southeast and Congo region basin respectively (Source, Wallace and Hobbs, 1997).

17

The ITCZ movement indirectly relates to the monsoon winds, which also drive the surface ocean currents in the western Indian Ocean. Broadly speaking, SEM and NEM are two distinct monsoon seasons that occur in the study area, although, later for the purpose of more detailed treatment in this document the four monsoon-seasons are introduced.

Hence, the movement of the ITCZ controls the rainfall in Kenya. There is a strong seasonal cycle in rainfall with pronounced dry seasons in between. The NEM rains appear in October-November, whereas the SEM rains peak from April to June (see further below). The changes from dry to wet seasons (inter-monsoons) occur as the dominant influence at the coast shifts from the subtropical high with descending air to ascending air connected to the low pressure system of the Westerlies (Figure 2.2.1).

2.2.2 Cloud cover and evaporation

Just before the onset of SEM and the long rains, in March, both the sea surface temperatures and humidity are high and there is an upward movement of the air dominated by an approaching low pressure. Thus the passage of the ITCZ, which occurs about this time, brings extensive cumulonimbus clouds along the coast. The cloud cover over the ocean is high, 55 % between 0-10 °S (Orville, 1996). The upward movement of the air is forced by the convergence of the trade winds of the Northern Hemisphere, which blow in the southwestern direction and those of the Southern Hemisphere, which blow towards Northwest as shown in Figure 2.2.1. The clouds appearing from April to August and have a high concentration of raindrops and ice crystals which grow to large sizes. Consequently, these clouds have high reflectivity, and since they reach high

altitudes. they also have strong effects on the amount of infrared radiation emitted to the space. An increase in cloud reduces the amount of sunlight during this period and cooling results. Evaporation occurs when relatively dry air comes into contact with relatively wet surface. particularly in relation to strong winds (see e.g. Gill, 1982). Figure 2.2.2.1 shows monthly (a) mean temperatures and (b) evaporation of the study area. The evaporation along the coast is between 2000 and 2100 mm (Michieka et al., 1978). Within about 25 km from the coast and even at the upper reaches of Tudor and Kilifi Creek the evaporation is somewhat higher, 2100-2200 mm. The monthly average evaporation varies between 140 mm in June/July to 200 mm in December/January. The term evapo-transpiration represents the aggregate of moisture transfer into the atmosphere by the process of evaporation and the transpiration by green plants.

2.2.2.2 The regimes of the monsoon and the winds

Since much of our results will be based on the context of seasonality, it is important to clearly identify the monsoon regimes. As already mentioned there are seasonal patterns whereas the year is divided into four seasons based on wind direction and rainfall. The inter-monsoon long-rain season (IMLR season) is from April to June. To the north of the Equator this is referred to as Southwest Monsoon, since the general wind system (Figure 2.3.1) tends eastward instead of north due to coriolis effect. Viewed from Kenya the winds come generally from the Southeast, hence the Southeast monsoon. The proper Southeast monsoon (SEM) is from July to September/October. This period is usually referred to as the summer although the area is south of the equator.

19
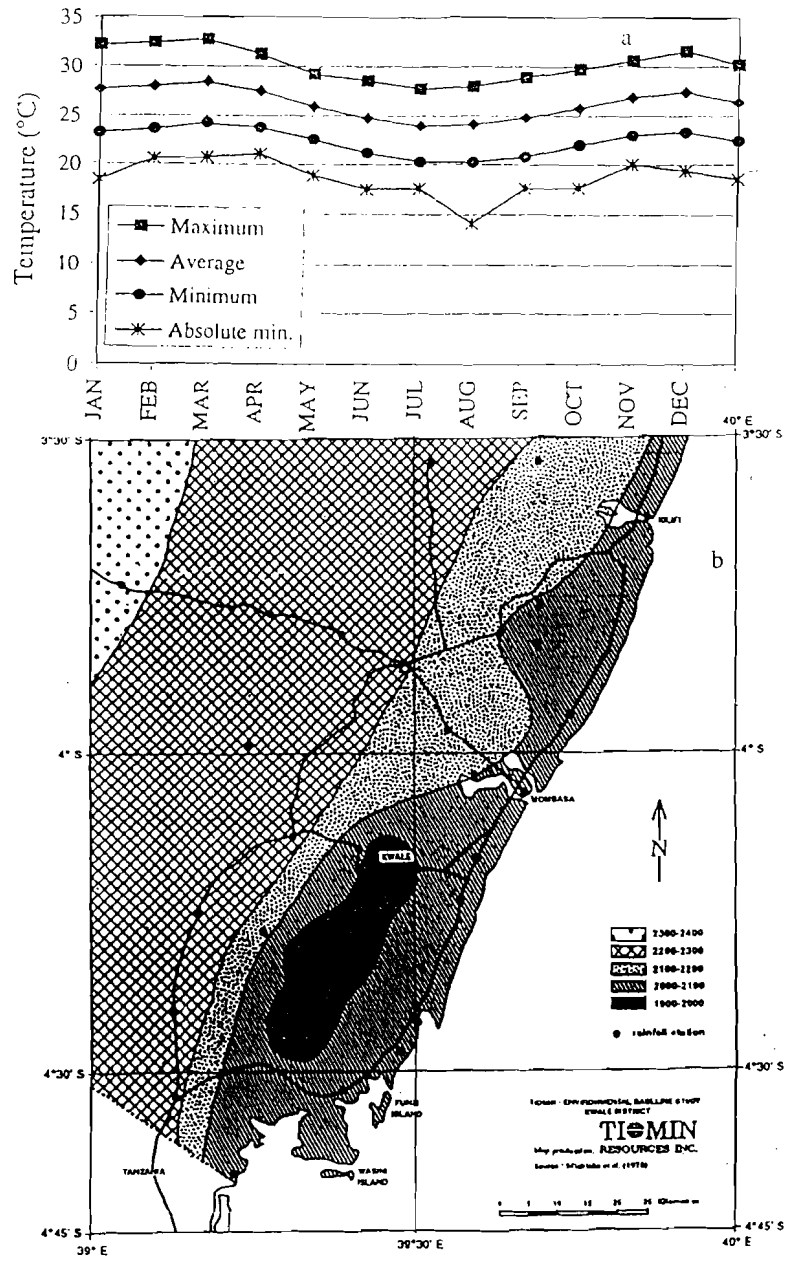
Figure 2.2.2.1a-b Typical (a) annual temperature and (b) evaporation changes for the study area (Source, Michieka et al., 1978).
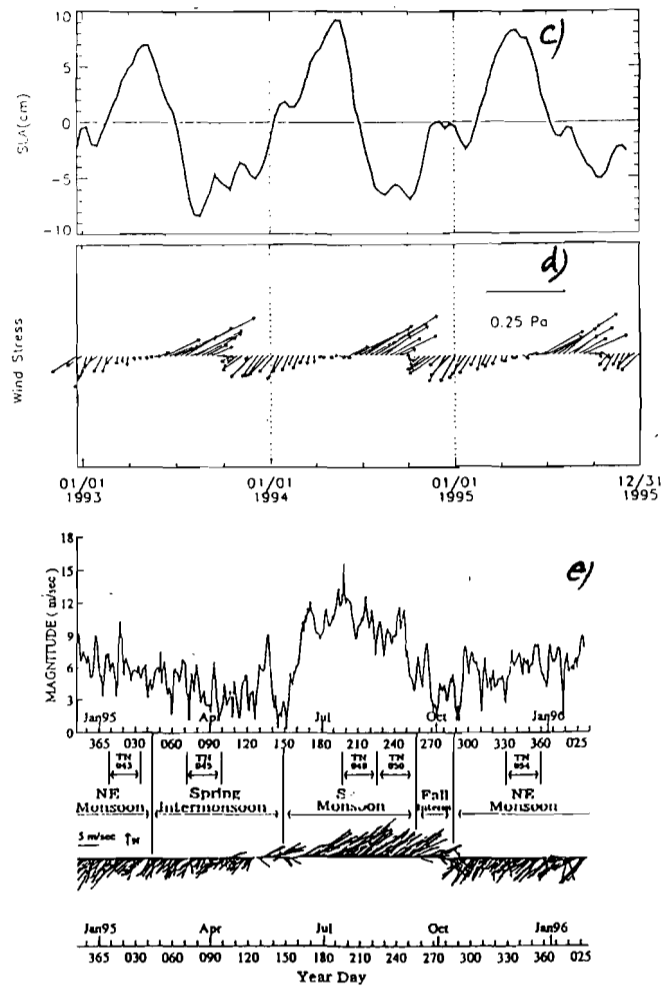
Figure 2.2.2.1c-e Example of (c) Sea level anomaly (SLA), (d) wind stress in stick diagram and (e) magnitude of wind stress in relation to the four monsoon seasons in the western Indian Ocean (Source, KMFRI Oceanography series Nguli. 1996).

21

The short-rain occurs during the next inter-monsoon from October to November coinciding with the fall season; it is referred to as the IMSR season. The Northeast Monsoon season (NEM) finally is from January to March and corresponds to the winter period. Figure 2.2.2.1c-e illustrates the concept of the four monsoon seasons. The figure also shows the magnitude and direction of wind to be found in the monsoon parts of the Indian Ocean. Additional wind speed and direction is shown for the equatorial Indian Ocean in Figures 2.2.2.1f-i from NCEP.

2.2.3 Rainfall and temperature

In general, maximum rainfall should occur around equinox in March and September, when the ITCZ traverses the equator, while the dry seasons occur after the solstices in December and June respectively. In the coastal region, where the rainfall is modified due to maritime effects, the long rains (IMLR) season peak from April to May. The short rain (IMSR) is from October to November (and sometimes in December), thus there is a delay of 1-2 months.

In Kwale district, and thus in Gazi Bay. Rainfall varies from 1500 mm along the coast and decreases gradually less than 500 mm in the hinterland (Jaetzold and Schmidt, 1983). The annual rainfall ranges from 1300-1400 mm in Kwale south, towards Kwale north 1100-1200 mm. The isolines run basically parallel to the coast. Higher rainfall in the southeastern part seems to be caused by the configuration of the coast and the presence of the Shimba Hills (Michieka et al., 1978).

22
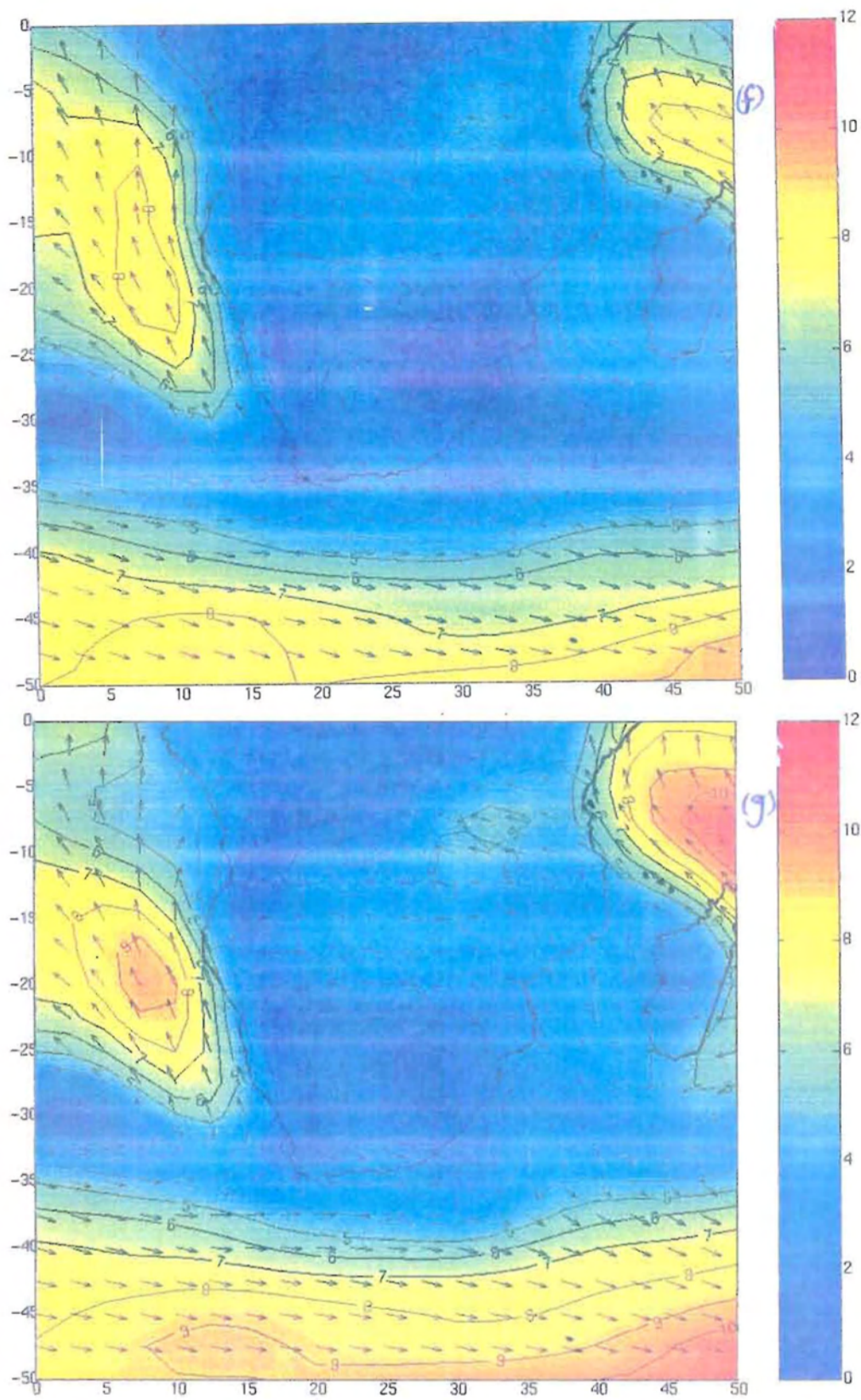
Figure 2.2.2.1f-g NCEP, mean wind speed and direction, panel (f) IMLR season
(May), panel (g) SEM season (August).
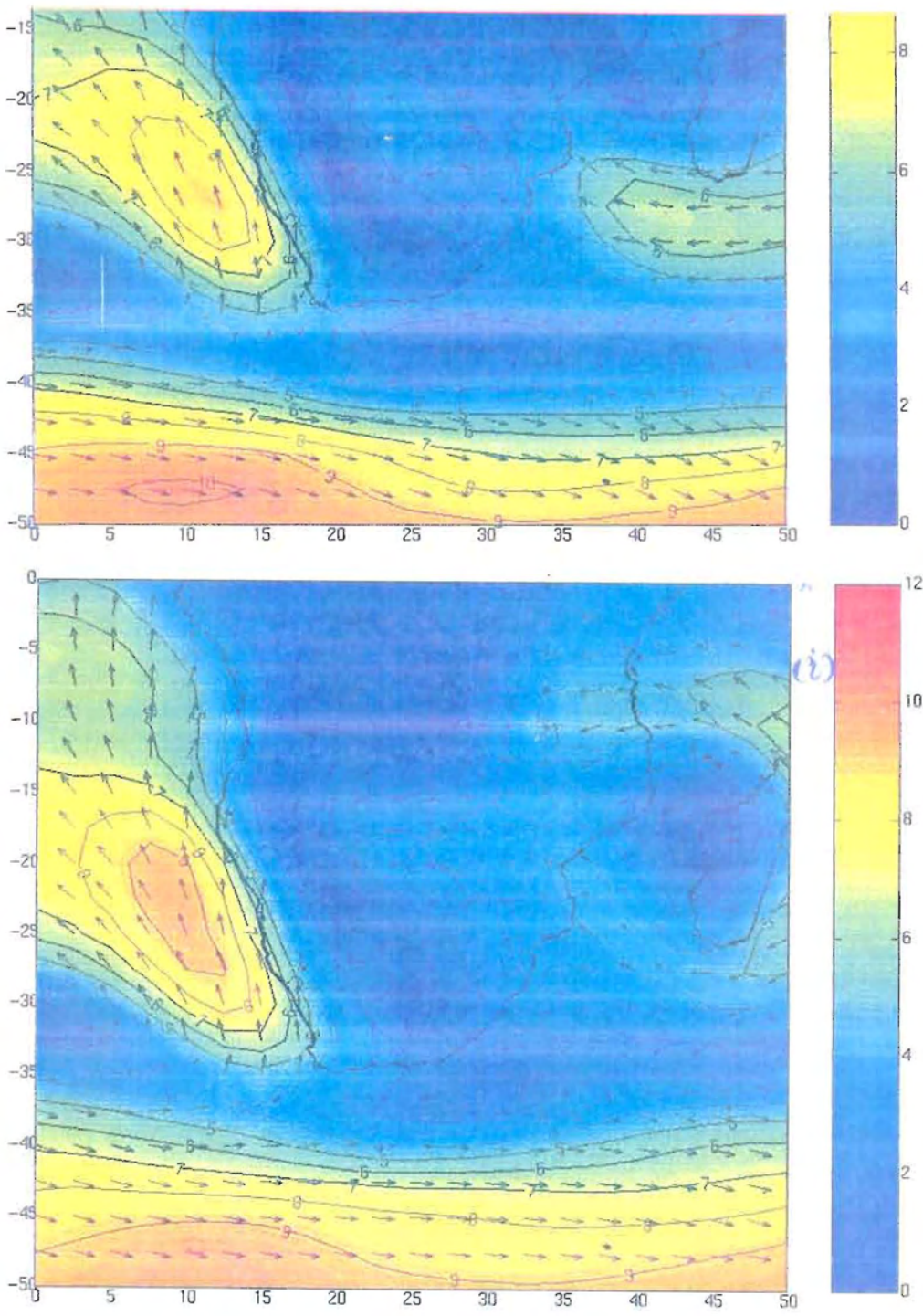
Figure 2.2.2.1h-i NCEP, mean wind speed and direction, panel (h) NEM season (February), panel (i) IMSR season (November).

The mean annual rainfall ranges from about 500 mm in the drier hinterland in the north to 1,150 mm in the more wet area south of Malindi. When the long-term meteorological data (1957-1987), from Kikoneni near Gazi is examined, the recorded maximum rainfall is 600 mm; the lowest is 50mm while the mean is about 300mm for the IMLR. During the IMSR the same station shows a maximum 200mm and there are some years when there was no rain. The mean precipitation is about 30mm. The rainfall varies considerably from one station to another, depending on their location, particularly in relation to the distance from the coast (Michieka et al., 1978).

The air temperatures are relatively constant through out the year, with a mean monthly maximum of about 30 °C and a monthly minimum of around 22 °C (Figure 2.2.2.1b). The warmest period is between November and April with daily mean temperatures of 26 °C to 28 °C. The rest of the year, from May to October, is cooler with temperatures between 24 and 26 °C. The coldest month is August, while the warmest is March. The "summer" corresponds to the high rain season while the "winter" matches the long dry season (Jaetzold and Schmidt, 1983). Average maximum temperature in Mombasa ranges from 28-32°C, highest from January to March and lowest in July and August. Average minimum temperatures in Mombasa range from 21 °C in July and August to 24 °C from February to April.

2.3 OCEANOGRAPHIC SETTINGS

2.3.1 Wind regime and their related oceanic currents

The wind direction over the ocean shows a pattern following the monsoon seasons. Northeast winds are predominant from December to March. In April, the wind gradually changes direction whereas southerly winds dominate, at the onset of the IMLR season and SEM inclusive. From September to December again the wind direction changes to northerly. The stick plots of Figure 2.2.2.1b and 2.2.2.c illustrate wind stress and wind direction illustrates the succession. Figure 2.3.1a-b and 2.3.1c-d also illustrate the character of the monsoon system but also the corresponding surface currents of the Indian Ocean for the months of May, August, October and February.

Four major oceanic currents show in Figure 2.3.1a-b and 2.3.1c-d. influence the Kenyan coastal waters. These are the South Equatorial Current (SEC), the East African Coastal Current (EACC) the Equatorial Counter Current (ECC) and the Somali Current (SC). The westward flowing SEC is divided into two currents north of Madagascar. One is the Mozambique Current, which flows southward into the Mozambique Channel and while the other is the EACC. The EACC flows northward from latitudes 11 °S and 3 °S, almost throughout the year with a surface speeds exceeding 1 ms^{-1} in Southeast Monsoon (Swallow et al., 1991). It continues north across the equator. where it changes name to Somali Current. During this period and with the strengthening of the SEM winds the SC continues northward (Figure 2.3.1c-d) right to the Horn of Africa. and also causes upwelling off the Somali coast in June. Under the influence of the NEM monsoon winds, the SC reverses direction to southwest and flows at a speed of about 1.5-2 ms^{-1} (Duing and Schott (1978). It meets the northward moving EACC, somewhere between

26

Malindi and Lamu on the Kenyan Coast to form the eastward moving ECC, which is non-existent during SEM season when the flow is continuous along the Eastern Africa coast. The convergence slows the speed of the EACC to about half its speed during the Southeast Monsoon (Figure 2.3.1a). There has been very few analysed oceanographic data in the region north of Zanzibar. The surface current patterns which represent the flow condition during NEM season and the IMLR season shown in Figure 2.3.1a and 2.3.1b respectively, while those of the SEM and the IMLR season are also shown in Figure 2.3.1c and 2.3.1d. Note that during the IMSR season there is a weak North Equatorial Current (NEC) flowing in an anti-clockwise direction, however. during the IMLR season the is a tendency for the water off Somali and Arabian sea to rotated in a clockwise sense.

27
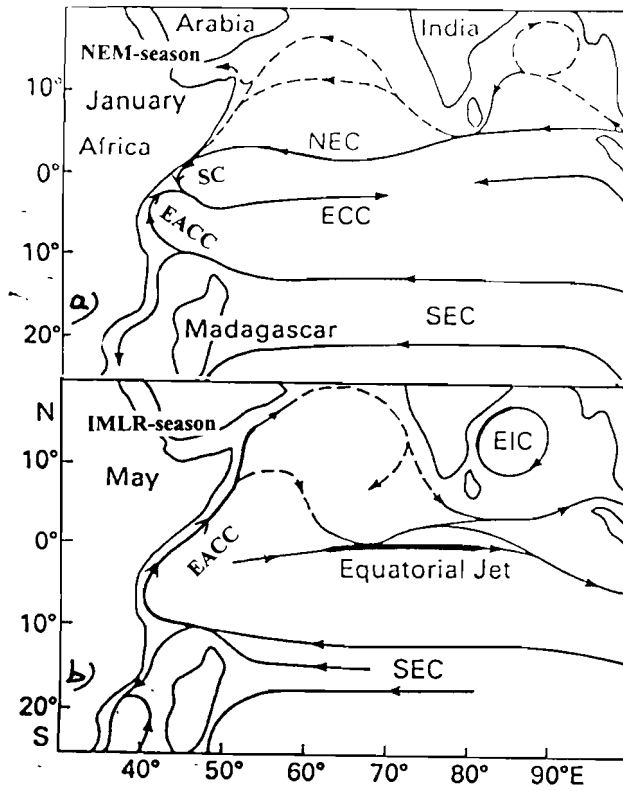
Figure 2.3.1a-b Surface currents in Eastern African region. Current (a) during NEM season are depicted for January. EACC and SC converge off Kenya Coast and move oceanward as the ECC. Circulation during (a) the IMLR season shows EACC along the entire EA coast and an Equatorial Jet (The Figure is redrawn from Tomczak and Godfrey, 1994).

28
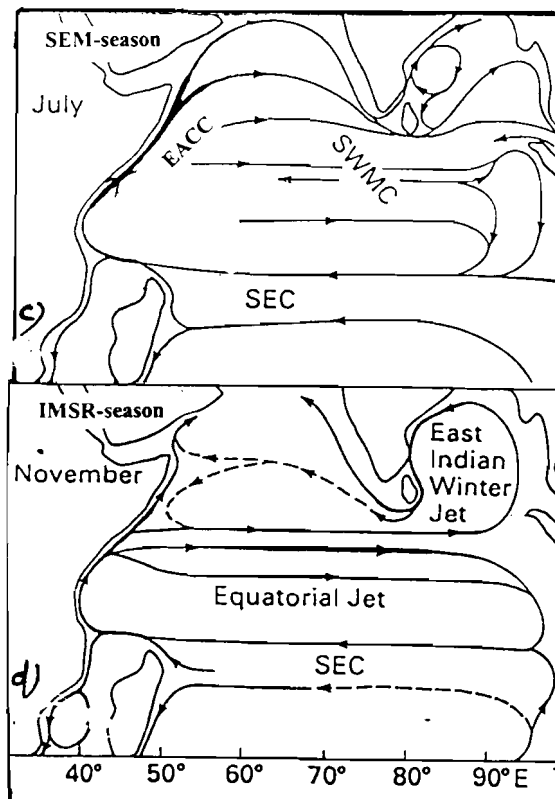
Figure 2.3.1c-d Surface currents in East Africa during (c) SEM-season depicted for July, Strong EACC flows along the coast to the Arabian Sea. Currents during (d) IMSR season are depicted for November Note, weakened EACC, the Southwest Monsoon Current (SWMC) and the Equatorial Jet (The Figure redrawn from Tomczak and Godfrey, 1994).

An eastward flowing jet first noted by Findlater (1971) characterises both inter-monsoon periods. Water masses, although were preliminarily discussed by Newell (1959), are those found generally in the Indian Ocean and have been discussed by Tomczak and Godfrey (1994). However, during the time of Newell (1959) very few temperature and salinity data existed and so the precise identity of water masses on the Kenyan shelf was not clearly defined. Understanding the seasonal characteristics of the water types formed in then inshore areas (see Chapter 5) and of the oceanic water masses and their distribution is important for understanding fishery resources and the dynamics of the surface layer of the ocean. In the next section we look briefly at the water characteristics in terms of the offshore water and the inshore (creeks and bays) in the region. We return to water masses later in the thesis.

2.3.2 Water characteristics

2.3.2.1 Offshore water

See surface temperature and to a lesser extent salinity are influenced by the monsoons and tides. During the SEM the shifting of the ocean currents brings water of lower salinity into the SEC, while during the NEM the SEC draws water of higher salinity. Rain and discharges of all major rivers during the heavy rains of April -May may further decrease the salinity on the coast. This is clearly seen from Levitus Atlas (Levitus, 1994) where also temperature is shown to vary in to high values in March and minimum in August and September. From the Levitus (1994), we find that the oceanic salinity increases towards the west from low salinity areas in the East.

Off the East Africa coast the salinity increases gradually in the surface region. Higher salinity occurs off the Red Sea and Arabian Sea.

The water masses of the ocean are important as they are usually formed in one part of the ocean and advected by the currents to different parts of the ocean. Obviously, the character may change considerably during the year along the East African Coast, but it is not clear what role they play in the structure of the creek and bay water. Salinity and temperature mainly determine the oceanic structure. Thus more interesting information can be obtained by analyzing past oceanographic data collected off Gazi Bay, Tudor Creek and Kilifi Creek (see Chapter 6), and attempt to describe the oceanographic variability that influence the water structure in the selected creeks.

2.3.2.2 Inshore waters of creeks and bays

Even less is known about the inshore waters. Tudor and Kilifi Creek and Gazi Bay have not been studied much from the oceanographic point of view. Some research work has been carried out in relation to biological work. Those studies are described in Section 3.2.3 of Chapter 3, on literature review and after each study sites is considered in more details (see, Chapter 4).

31

CHAPTER THREE

LITERATURE REVIEW

3.1 INTRODUCTION

The creeks considered in this study are essentially partially like fjords or tidal inlets but partially typical coastal plain tidal embayments. through which a moderate discharge finds its way to the ocean. Water circulation and water exchange between any such natural water body and the ocean is of complex nature affected by a variety of factors. In general the pertinent factors are inlet and estuarine geometry, net freshwater input (precipitation, evaporation, runoff), and current velocities, wave action, tides and bottom shear (on longer scales also sediment load and littoral drift). Inlet configuration and dimensions, bay and creek sizes, depth and orientation with respect to the prevailing winds are all hydrographic factors influencing water exchange in coastal water bodies. The driving forces comes from sea surface buoyancy fluxes influenced by rainfall, evaporation and plus heat flux. Tides are almost everywhere of importance both as driving force and for mixing. Winds are sometimes the primary mixing sources and occasionally drive water exchange. Our aim is to later estimate the magnitudes of forcing functions that drive water exchange between the creeks (bay) and the ocean in terms of volume flux (mass transport through transverse cross-section at the entrance of each study site), but also how water balance is affected by seasonal (monsoon) changes. Therefore, we begin this Section by reviewing these types of coastal water bodies or estuarine systems after which follows a general review of the various processes that might appear.

3.1.1 Background

3.1.1.1 Creeks and bays as an estuarine environment

The two creeks and a bay to be investigated in this study, and discussed in some detail in Section 4.1.1 to 4.1.3 have seasonal rivers draining into them in their upper secondary creek channels. They are areas of interaction between fresh and salt water, and for most of oceanographers, engineers and natural scientist they are estuaries. However. Perillo (1995) pointed out that there over 40 different definitions of estuaries, based on one's immediate view point and in most of the definitions some key influences are omitted. Cameron and Pritchard (1963) defined estuaries as semi-enclosed body of water, having a more or less free connection with the ocean and within which seawater is measurably diluted by fresh water and does not include tidal influence. Dione (1993) used tide in the definition. He stated that 'an estuary is an inlet of the sea, reaching into the river valley as far as the upper limit of the tidal rise. Usually it is divided into three sectors: a) a marine or lower estuary, in free connection with the open ocean: a middle estuary subject to strong salt and fresh water mixing; and c) an upper or fluvial estuary, characterised by fresh water but subject to daily tidal action'.

Most recent there has been attempt to include sediments and wave processes, and biological species in the definition. Dalrymple et al. (1992) have defined an estuary as: 'the seaward portion of a drowned valley system which receives sediment from both fluvial and marine resources and which contains facies influenced by tide, wave and fluvial processes. The estuary is considered to extend from the landward influence of marine facies at its head to the ocean-ward limit of coastal facies at its mouth'. Perillo (1995) definition is: 'An estuary is a semi-enclosed coastal body of water that extends to

33

the effective limit of tidal influence. Within this body, sea water entering from one or more free connections with the open sea, or any other saline coastal body of water, is significantly diluted with fresh water derived from land drainage, and can sustain euryhaline biological species for either part or the whole of their life cycle'.

Possibly a most satisfactory definition over all definition for creeks and bays considered in this study would be an adaptation of Dionne's definition. It allows for three sectors or regimes, a) a marine or lower estuary, referred to as 'the entrance' with free connection to the ocean. b) middle estuary; 'the inlet channel' with its immediate opening to the shallow mangrove –fringed-basin; and c) an upper or fluvial estuary in our case the secondary creek channel with their mangrove –fringed peripheral lagoons.

In addition to the definition of an estuary a classification is required within which to predict the characteristics of estuaries. Many classifications have been put forward. Some of the classifications are based on combinations of geomorphology and physical processes and topographic dimensions (Hansen and Rattray, 1966; Dyer, 1973 and Officer, 1976; and Kjerve and Magill, 1989). These workers have each used different classification schemes; however they found that topography, and river flow and tidal action are important factors that influence the rate of mixing of salt and fresh water. Locally, and depending on the season, wind and heat flux may also be important. The resultant mixing will be reflected in density structure (see water structure later) and the presence of stratification may cause modification in the circulation and water exchange. We consider a few of the classification schemes. Pritchard (1952a) classified estuaries as *positive* and *negative*. A *positive* estuary is one where the fresh water inflow derived from river discharge and precipitation exceeds the output from evaporation. Salinity is

consequently lower than within the estuary than in the sea. In the negative estuaries evaporation exceeds river flow and precipitation, and hypersaline conditions exist. Davis (1994) classification was as *Microtidal <2m range, Mesotidal <4m> 2m. Macrotidal <6m> 4m and Hypertidal> 6m.* Depending on the morphology and friction influence on a tidal wave propagating into an estuary Nichols and Biggs (1995) have introduced three terms. These terms are, *Hypersynchronous estuaries* for funnel shaped estuaries; *synchronous estuaries* where the rage is constant except in the riverine section; and *hypersynchronous estuaries* where friction exceeds the effect of convergence and the velocities are highest in the mouth.

There are also classification by topography, morphology or physiographic features and salinity structure. In the topographic classification the estuaries are divided into *coastal plain estuaries or drowned river valleys, fjords and bar-built estuaries* (Pritchard (1952b). In morphological classification, Fairbridge (1980) and Dalrymple et al. (1992) have provided comprehensive classification by coming up *wave-dominated estuaries and tide-dominated classifications.*

Pritchard (1955) proposed a division according to the circulation and stratification of the estuary, where thus density stratification largely due to salinity differences rather than temperature differences. This way he identified three types of estuaries: *highly stratified partially stratified* and *well-mixed estuaries.* Each type exhibits unique circulation characteristics.

Although. as mentioned above, most work on estuaries and lagoons stem from non-equatorial regions in the north, several studies from lagoons and tidal creek in tropical Asia, South America and Australia exist. Wolanski et al. (1980; 1990), Ridd et

35

al. (1990), Wattayakorn et al. (1990), Wolanski (1986), Oliviera and Kjerfve (1993) and Medeiros and Kjerfve (1993) discuss how the exchange processes are controlled by tides, currents and winds. Cheng et al. (1993), notes that most biochemical processes take place over time scales of several tidal periods and that even though tides are important for the mixing, water exchange has to be considered over longer periods as well. In some cases, the zone between the river mouths and the open water has been characterised in terms of salinity and temperature into three zones: turbid zone of the marsh systems which are predominantly inter-tidal marshes similar to the mangrove areas mentioned earlier in this document. The second turbid zone is the near-shore areas corresponding to the creek entrances where the hydraulics of the creek channel, wave climate and wind set up and long-shore currents are important. A third zone is the boundary zone that is the area between the near-shore and the relatively "clear" water above the inner continental shelf (see e.g. Oertel and Dunstan, 1980).

As already mentioned, water movement, mixing and material transport occur as a result of tides, winds and buoyancy forcing by freshwater discharge or even heat radiation. Sometimes forcing is driven from outside due to seas level or thermocline motion. It is seldom possible to analyse the, instantaneous velocity field in tidal estuaries. Rather, the circulation is investigated through temporally averaged spatial water flow. Some aspects of water movement regarded in estuarine systems are those of dispersion, entrainment and turbulent diffusion. The movement arises as a result of the competition between stratification and mixing and is governed by the *gradient Richardson number Ri*. *Ri* is a comparison between the stabilising forces of density stratification to the stabilising influence of the velocity shear, for $Ri>1$ the stratification is stable, $Ri=0$ it is neutral and

Ri<0 it is unstable. *Dispersion* is a gradient process and refers to the transport of waterborne characteristics by advection and eddy diffusion (spreading) processes over the same time scale for which the circulation is calculated, which are usually one or several complete tidal cycles. Turbulence or mixing is a form of water movement generated by shear at the seabed and by shear at the halocline or the interface and depending on timing during the tide as well as estuarine type.

Depending on the thickness of the velocity interface and density interface internal mixing can occur and lead to *entrainment* which occurs when Ri >1/4 as a one-way process where the less turbulent water mass becomes drawn into a more turbulent layer. *Turbulent diffusion* occurs Ri<1 and is a two way process in which equal volume of water are exchanged between the two layers, and though no net exchange of water, salt is transported upwards and the potential energy of the water column in enhanced (Dyer, 1997). Advective and diffusive processes are important in tidal estuarine systems. The ratio between advective and diffusive fluxes depends on the time scale over which averaging is made. A long time scale will always increase the diffusive flux. The same is true for horizontal averaging. The ratio differentiation applied to lagoon systems allow for classification such as *choked, restricted or leaky* (Kjerfve, 1989). *Choked lagoons* are characterised by long narrow entrance(s), longer residence times and. and dominant wind forcing. *Restricted* lagoons usually exhibit one or two or more channels or inlets, have a well-defined tidal circulation, are strongly influenced by wind and are usually vertically mixed. *Leaky lagoons* occupy the opposite end of the spectrum from *choked lagoons* which are characterised by wide tidal passes, unimpaired water exchange with the ocean strong tidal currents and existence of sharp salinity and turbidity fronts.

Tidal currents in estuarine systems. coupled to mixing of ocean and river waters affect the vertical as well as the horizontal density stratification. With intense mixing or weak fresh water supply the water column becomes homogeneous. More fresh water on the other hand is likely to induce a vertical stratification and a horizontal. gravitational circulation (see below).

3.1.1.2 Mixing and stratification

Stratification is an intrinsic aspect of stirring or mixing by tidally driven flows in estuarine systems. Bottom stress produces turbulence in the flow and this turbulent kinetic energy mix the water column. Horizontal gradients on the other hand are set up e.g. by a combination of fresh water supply and consecutive mixing which causes high saline dense water to flow inwards underneath low saline, less dense surface water. The horizontal density gradient is associated with the variation of salinity along the estuarine system. So-called baroclinic currents or buoyancy forced currents in estuarine systems are a result of non-parallel isopycnal and isobaric surfaces. The baroclinic current tend to redistribute the density fields to equilibrium

Fischer et al. (1979) investigated effect in estuaries of vertical and lateral shear influenced by tidal oscillations and how it affected the circulation. Most comprehensive studies on exchange mechanisms from estuaries and fjords were done (e.g. Stigebrandt, 1983; Rattray and Hansen, 1966; Robinson, 1983; Prandle, 1985; Bjork et al., 2000, Stigebrandt, 1980; Brown and Trask, 1980; Hill, 1994; Rydberg and Wickbom, 1996). The exchange appears over a broad range of time and length scales (Smith. 1979 and Sitgebrandt, 1980).

38

In many estuaries the tidal circulation is the most obvious means by which flushing occurs. However, significant exchange may occur over much longer time scales where also, buoyancy forcing, atmospheric forcing and far field effects such as shelf waves (Kjerve et al., 1978) or even radiation balance may be important. Thus in tidally dominated estuaries, the exchange processes reduce to the problem of polarised transport that of flood and ebb where the net long-term movement is largely a function of the fluid velocity and discharge. In this case variables depend on the basin hypsometry. That is the distribution of the estuarine basin surface area with height (e.g. Boon and Byrne, 1981). Results from such studies show that the circulation in inlets is profoundly affected by the interaction between the water flows and inlet bathymetry, but also, that the topography is always of utmost importance. The hydrodynamic processes of tidal inlets have been investigated using various one-dimensional models from inside the lagoon out through the inlet (cf. Ye, 1987a; Robinson, 1983; Rydberg and Wickbom, 1996). Officer (1996) used the one-dimensional equations to study the estuaries with large tidal prism and low river runoff, which may fit with our setting.

3.1.1.3 Heat flow

The properties of ocean water in tidal creeks are modified not only by the fresh water, but also by heating or cooling. Heating is a result of solar radiation absorbed in the water column. The heat is retained by creek water through vertical mixing. Bulk equations for calculation of solar radiation, sensible heat and heat loss by long wave radiation and evaporation, have been developed in order to establish heat budget. For example, Varma and Kurup (1996) used the formulas in their study in the northern part of

the Somali Current, which is affected by the monsoon climate. Sultan and Ahmad (1993, 1994) carried out similar studies in the Arabian Sea, while Reed (1983) and De Lisle (1970) also carried out similar work in the eastern Pacific Ocean and in the Tasmania Sea respectively. Vugts and Zimmerman (1975) demonstrated effects of interaction between the daily heat and tidal cycles from measurement in the Dutch Wadden Sea but failed to include variable tidal volume in the heat transfer equations. Heath (1977) carried out similar studies in a New Zealand inlet. He found that fluctuations in temperature produced by the tidal exchange and by the solar cycle are both important.

In Chwaka Bay, Tanzania, a bay almost similar to Gazi Bay considered in this study, Mahongo (1998, 1997) investigated heat budget. He considered radiative fluxes and turbulent fluxes and applies several cloud correlation factors, such as used by Kimball (1928), Laevastu (1960), Budyko (1963), Tabata (1964) and Reed (1977) to arrive at reasonable fluctuations of the fluxes. He recommended the application of the factors given by Tabata (1964) and Reed (1977). Further Ulf Cerdelöf et al. (1995) carried out heat flux studies in the same bay.

3.1.1.4 Tides in ocean and coastal waters

One of our objectives is to determine tidal characteristics, and see how astronomical tide becomes distorted during its propagation from the ocean into the shallow inlets/creek systems such as selected in this study. The astronomical tide spectrum is composed of a large number of constituents whose mutual non-linear interactions represent a complex physical problem (Gallagher and Munk, 1971). Therefore, we will focus on the predominant species and our analysis will seek to extract

the amplitudes and the phase of the major tidal constituents from pressure gauge records. In this section we review briefly tide-producing forces.

According to Newton's law the gravitation force between the earth and the moon, is proportional to their masses, and inversely proportional to the square of the distance between them. Revolution of the earth/moon system introduces a centrifugal force. The horizontal component of the difference between the gravitational and centripetal force is what drives the tides. These horizontal tidal tractive forces are very small and are inversely proportional to the cube of the distance between earth and moon and because they are not balanced they cause the water movement. The patterns of these tide-producing forces produce bulges of water over the areas on the near and far side to the moon where the forces are directed outward from the earth's surface, but depressed between those areas where the forces are directed inwards. As the earth rotates about its polar axis, each point on the surface of the earth, pass through a whole pattern of forces in one day with two passes under the bulges and two under the depressions. This is the basis for the existence of semi-diurnal tides on a diurnally rotating earth. The earth/sun system sets up a similar pattern of forces to that for earth/moon pair but the forces involved are much smaller because of the much greater distance. The fact that the sun and the moon do not move in a synchronous fashion, their path are ellipses, the planes of rotational move north and south (with annual cycles of the sun, and the monthly circles of the moon) add complications to the pattern of tide producing forces. Despite this complications the motion of the sun and the moon are known very precisely and are responsible for the tidal motion observed by sea level records in coastal stations.

phases and amplitudes. Each constituent can be represented by a sine curve with its own period and phase, whose amplitude represents its contribution to the total tide. Harmonic analysis procedure extracts from the tide record the response to the specified gravitational force constituents.

Sea level changes occur due to different reasons. Wind waves; for example produce high frequencies, while air pressure, wind, and tidal fluctuations cause lower frequencies. Tidal frequencies can be determined with extremely high accuracy from classical celestial mechanics. The extraction of their amplitudes and phases from sea-level records is known as the harmonic analysis. A longer record implies a higher accuracy in determination of the tidal characteristics. At least a one-month sea-level record is needed to obtain a reasonable resolution of the major components. Harmonic analysis uses the "method of least squares" to extract the tidal constituent of given frequencies from a sea level record (Chapter 4).

Tidal constituents

The distribution of the tide producing potential over the surface of the earth can be expressed as a series expansion in spherical harmonics. Theses functions form a complete set for describing distributions on the surface of a sphere (Jeffreys and Jeffreys, 1956). The coefficient of which can be expanded as Fourier series with frequencies that are linear combination of the basic frequencies of the solar system.

A very detail classification of tidal constituents by Doodson involves 390 components, includes the three major periods, but also longer ones such as lunar perigee (8.85 years),

42

where the estuary tide is in phase with the outside tide. If the time taken to do this is equal to the tidal period, the reflected wave meet the next wave entering from the sea, thus a resonance appears. Long estuaries are also subject to friction and the tidal wave is completely dissipated before reaching the end of the estuary. The tidal wave is then solely progressive wave in nature. Elevation and currents are in phase. However, in most estuaries at least some of the tidal energy dissipates before and after reflection and the tidal response is a mixture of a standing wave with a progressive contribution of variable magnitude. Although there are some 160 known constituents, with about 60 recognized as significant, only 14 will be considered during the harmonic calculations using least square method (Chapter 4).

3.1.1.5 Basic concepts of near bottom flow

A most important issue in any study of the dynamics of flows in shelf seas is the bottom friction and the flow in the near bottom boundary layers. More over the profile near the bed is important not only for water mixing as much, but also for sediment transport and distribution. There is a considerable research on the form of the boundary flow, and the related distribution of shear stresses and turbulent eddy viscosity within the water column (e.g. Lesser, 1951; Weatherly, 1972; Dyer, 1970; Kundu. 1990). Many studies are based on the velocity profile where a logarithmic profile (assuming that $\frac{\partial u}{\partial t} \alpha \frac{u.}{z}$ (see later) is fitted to the near-bed velocity data to estimate various characteristics of the near bed flow. In recent times first response current meters have been in use (cf. Gordon and Dohne, 1973; Harvey and Vicent, 1977).

As the flows passes near the bed over bottom elements a velocity shear is produced by the friction drag. The flow is considerably slowed down near the bed than higher up, and elements produce turbulence which according to Offen and Kline (1975), and Robinson (1991), occurs as transverse vortices developed from streak of velocities near the bed. The vortices are ejected to the surface and then travel down stream in 'horseshoe shapes' before decaying. During high flow these vortices erupt at the surface as 'boils' (Jackson, 1976). The velocity profile across the bottom varies according to the conditions in the water column. For unstratified conditions they conform to *the von Karman-Prandtl equation*, which relates the friction velocity and the stream flow above the bottom to the roughness depth. The friction velocity u* is related to the bed shear

stress τ_0 as $u^{*} = \left(\frac{\tau_o}{\rho} \right)^{1/2}$. Anwar (1983) found that the equation is valid for

homogeneous (well-mixed) flow over flat bed and can be used for determining the bed shear stress from the velocity profiles. The equation does not hold for unsteady flow, in density stratification or uneven beds (Dyer, 1986). Thus, for stratified flows the profile modifies to the equation shown in Section 4.4.1. Alternatively experiments have shown to a good approximation that the bed shear stress is proportional to the squire of the velocity in the bottom boundary layer according *to the quadratic friction law:* $\tau_o = \rho C_d U^2$. The drag coefficient Cd can be related to the bed roughness and the value of the roughness depth (see Dyer, 1986).

There is need to establish the type of flow regime, estimate the drag coefficient and roughness length and the residual drift at different heights above the creek-bed.

The relation of the tidal regimes and the drag coefficient used in calculating the bottom stress, and hence variability in the roughness depth (see Appendix C).

3.2.2 Previous studies in the adjoining coastal water

3.2.2.1 Coastal currents

Adjoining coastal water, for the purpose of this document, means the coastal water immediately off the entrance to the creeks and bays. This is the water on the shelf, which is likely to be exchanged with that of the creek or bay. Newell (1957, 1959) pointed out that the shelf water in this region is that of the East African Coastal Current (EACC) and the Somali Current (SC), which reverses direction under the influence of the monsoon winds for along time (Huntingfold, 1980). Only in recent times efforts have been made to study the currents and largely focused where the Somali Current (SC) meets the EACC. Leetmaa (1972, 1973) did the first observations in March-April, near 2°S latitude off Kenya. He found that the SC current reversed direction, and starts as an intrusion from south triggered by 8-10ms^{-1} winds in the last week of March. He concluded that the onset of the SC occurred south of the equator one month before the onset of the SW monsoon over the interior of the northern Indian Ocean. He further concludes that the local winds and a switching action on the EACC cause the onset. This implies that in earlier April the current direction is very sensitive to the small variations in wind direction. There have been several studies related to the current behaviour in this region.

Duing and Schott (1977) moored several current meters between Mombasa and Kiwayu from mid-January to mid-July 1976 (see Figure 3.2.2.2). They come to the same

conclusion. Johnson et al. (1982) investigated the onset mechanism and arrived also at the same conclusion. They suggested that the switching of the Somali Current was due to topographic control at the location of the Northern Kenya Banks (see Figure 1.1b) and that the switch occurred in mid-March at the onset of SEM, just preceding the Inter-monsoon long rain (IMLR) season. The differences on the onset time seem to confirm 'multiple onsets' as suggested by Fieux and Stommel (1977). Other investigators arrived at the same conclusion regarding the onset (Duing and Szekielda, 1971; Cox. 1976). Also Anderson and Rowlands (1976) arrived at the same conclusion from theoretical studies which discriminated between local and remote forcing. Other contributing work are (e.g. Swallow and Bruce, 1966; Lutjeharms, 1972; Citeau et al., 1973; Magnier and Piton, 1973; 1974, and Swallow et al., 1991; Schott al et., 1990, and Quadfasel and Schott, 1982). Swallow et al. (1991) has defined the EACC, as the part of the boundary current that flow northward through out the years. This follows the nomenclature by Newell (1957). Thus a summary of the current flow can be made. It is similar to that given earlier in Figures 2.2.1a-b, and 2.2.1c-d, and by Wyrtki (1971).

Anonymous (1981) and R.V.Tyro (1992-93) made further current measurements along the coast. Both will be taken up in Chapter 6.

The EACC was recently defined by Swallow et al. (1991) as that part of the boundary current system off East Africa that flow northward through out the year, in the climatologically mean. They saw the current as linking the boundary current north of Madagascar and at the equator. The source of the EACC is thus the South Equatorial Current (SEC). The SEC flows westward along the latitude 10 -12°S. bringing low salinity water from the eastern Indian Ocean to the East Africa coast.

47

The SEC in the Indian Ocean split into the southward going Mozambique Current and the north-going EACC. During the SEM (northern summer) the EACC continues to transport water across the equator into Somali Coast. In NEM season (northern winter) the EACC meets the southward flowing SC at the latitude of 2-3°S and together they flow eastward as the ECC (Figure 2.3.1c). Duing and Schott (1972) studied the progression of wind in Lamu and currents at various depths and showed that considerable change occurred off Lamu i.e. after the Northern Kenya Banks (Figures 3.2.2.1a and Figure 3.2.2.1b).

Figure 3.2.2.2 (also see Swallow et al., 1992) shows the flow of the EACC from south of Malindi (3°S). The EACC monthly mean northward component of surface currents off Gazi Bay-Tudor Creek (4°-5°S) increased from the end of March up to the maximum speeds of slightly more than $1ms^{-1}$ by in April then decreased by 40% between May and July (Figure 3.2.2.2, panel a). The maximum is followed by slow decrease to a minimum of about $0.3ms^{-1}$ in NEM. At the latitude 3 ° -4 ° S which is off Kilifi Creek (i.e. Mombasa-Malindi shelf) the current has a broad maximum of $1.1ms^{-1}$(Figure 3.2.2.2,panel b). The current off Gazi Bay moves at greater speed than off Kilifi Creek during NEM (February). Swallow found that the current increases offshore reaching maximum speeds between 20 and 75km (Figure 3.2.2.2, panel c) agreeing with Bell (1972). He pointed out that the maximum speed occurs between 16 and 80m offshore and the width of the current to be more than 160km. The speed off Gazi Bay and Kilifi is almost double those at 8°-9 °S and 9°-10°S (Figure 3.2.2.2), which indicate that the EACC accelerates considerably off our study area. The transport structure is reviewed below.

The possible events causing variation between 3 and 5 °S are taken up in results and discussion Chapters.

3.2.1.2 Transport structure

The transport structure between 11°S and 3°S of the EACC was investigated by Swallow et al. (1991) who showed that a mean northward transport of 106 m³s⁻¹ off Gazi Bay and Tudor Creek (4°-5°S) in the upper 500m. Duing (1977) after reviewing work by Swallow and Bruce (1966), Leetmaa (1973) and Duing and Schott (1977), showed a transport of 14.4x 106 m^3s^{-1} at 2°S during IMLR season (May) in the upper 100m and a current width of 120km flowing at a mean velocity of 1.2 ms⁻¹. However, this transport increased to 17x106 m^3s^{-1} between 1°N and 2.8°N an increase of 42% per 100km. Swallow and Bruce (1966) report further north maximum transport of 71x106 m^3s^{-1} and 15x106 m^3s^{-1} in the upper 1000m. They also found a zone of extremely high velocities (>3 ms⁻¹) and vertical current shear in the upper 50m of the SC and revealed a strongly amplified baroclinic structure in the upper layer. Bruce and Volkmann (1969) indicated powerful subsurface anticyclonic gyres with transports of approximately 70x10 m^3s^{-1} during SEM and NEM respectively was located 150km offshore. The observations reveal that that local forcing must play a very important role along the Kenya-Somali coast from say 3°S to 9°N. The mechanism is complex and little understood it is taken up in the discussion (Chapter 7).

3.2.1.3 Salinity and temperature and the thermocline

The first work on salinity and temperature is that of Newell (1959), and is based on data from cruise No.67 carried out by M.V. *Tchita* in 1952-54 and previous data from *Valdivia*, *Dana* and *John Murray* expeditions of 1898-99, 1928-30 and 1933-4 respectively. In addition to the surface flow Newell (1959) documented temperature, salinity and water mass. He discussed four water masses: (a) the Tropical Surface Water with high temperature, high salinity, and oxygen saturated. (b) Arabian Sea Water with high salinity and high oxygen. (c) Antarctica Intermediate Water with low salinity and high oxygen and (d) the North Indian Deep Water with a Red Sea outflow of high salinity and low oxygen.

Magner and Pinto (1973, 1974) gave a similar account of the water masses of the region down to 600m, based on data from *R.V. Vauban*. Harvey (1977) carried out similar work off Tanzania coast and indicated characteristics similar to those observed by Newell (1959). Quadfasel and Schott (1982) and Duing and Schott (1978) have indicated that mass transport, position of the thermocline and the oceanographic characteristics of the coastal current change with the monsoon season. Repeated hydrographic measurement around 3°S (Leetmaa and Trusdale, 1972), reveal surface salinity of 35.5 in March and 35.0 in May. They attribute the former to Arabian Sea Water carried south during the NEM, and the latter as corresponding to the SEM and coastal runoff carried northward by the Somali Current. Unanalysed oceanographic data is available from more recent cruises off Kenya e.g. Dr. Fidjof Nansen (1982-83), R.V. Kusi (1979), and in R.V. Tyro expedition of 1992-93. The data is selectively considered for analysis in Chapter 6.

50
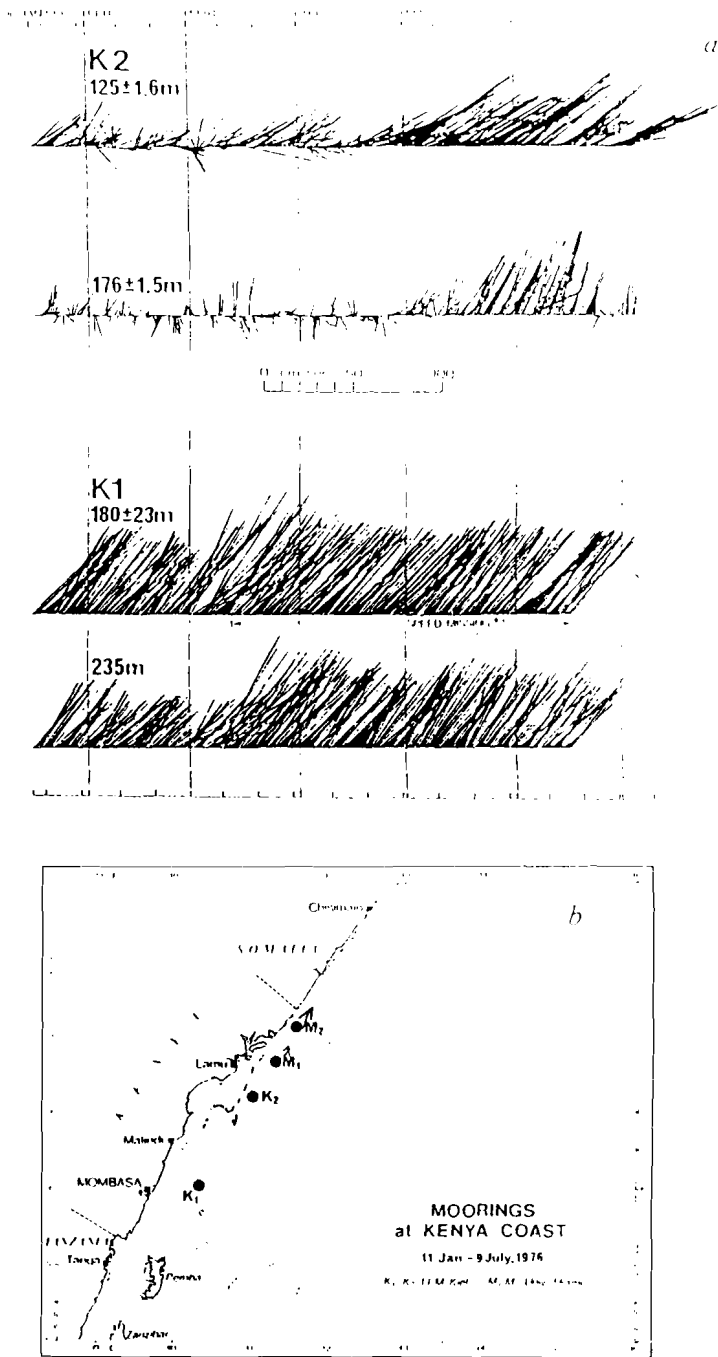
Figure 3.2.2.1a Panel (a) stick diagrams for current off Kilifi Creek at position

K1, K2 and panel (b) the mooring position for the current meters K1, K2, M1 and

M2 (Source, Swallow et al., 1992).
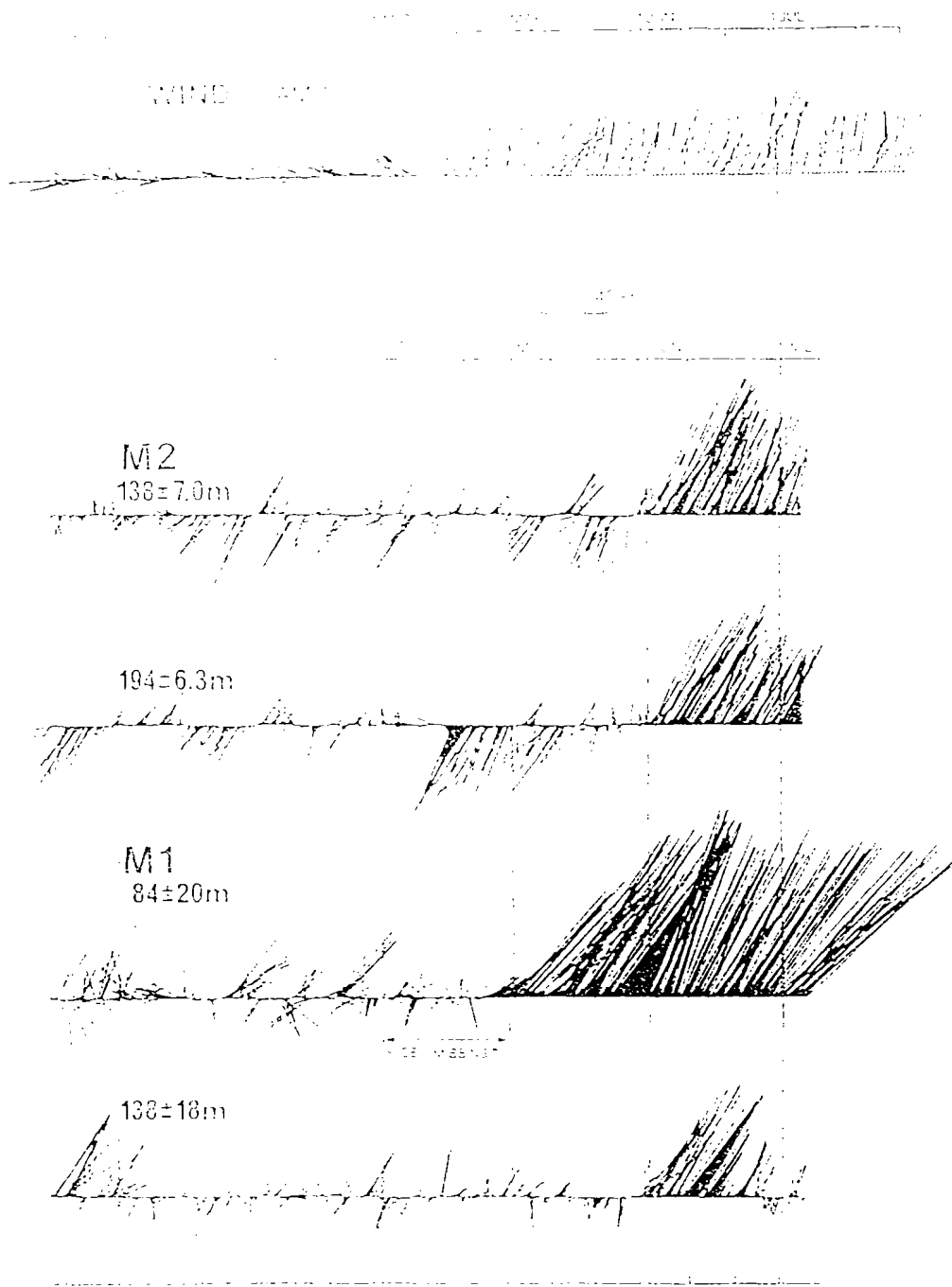
Figure 3.2.2.1b Stick diagram for wind and currents off Lamu (M1 and M2),

Note, the change of direction, compare to K1 and K2 in Figure 3.2.2.1a (Source,

Swallow et al., 1992).
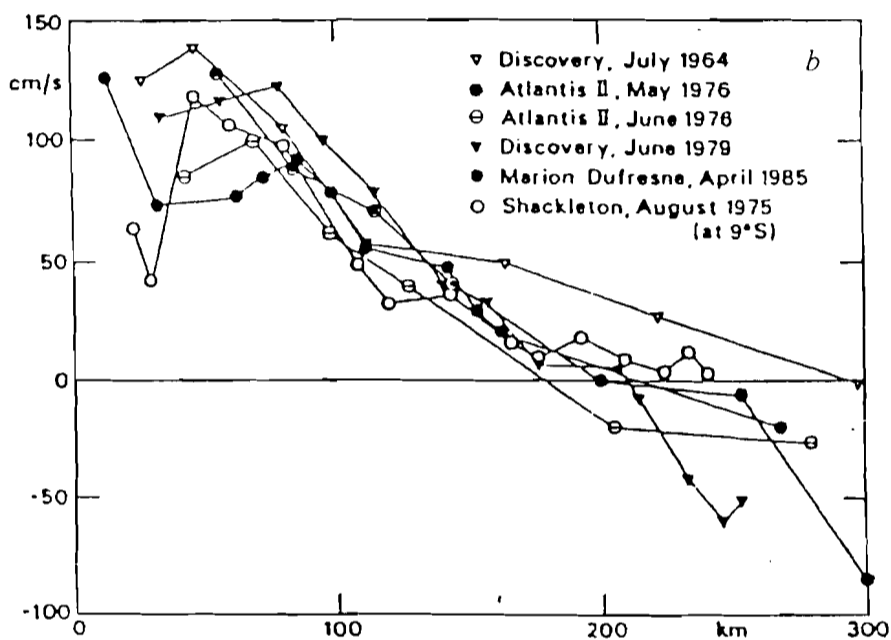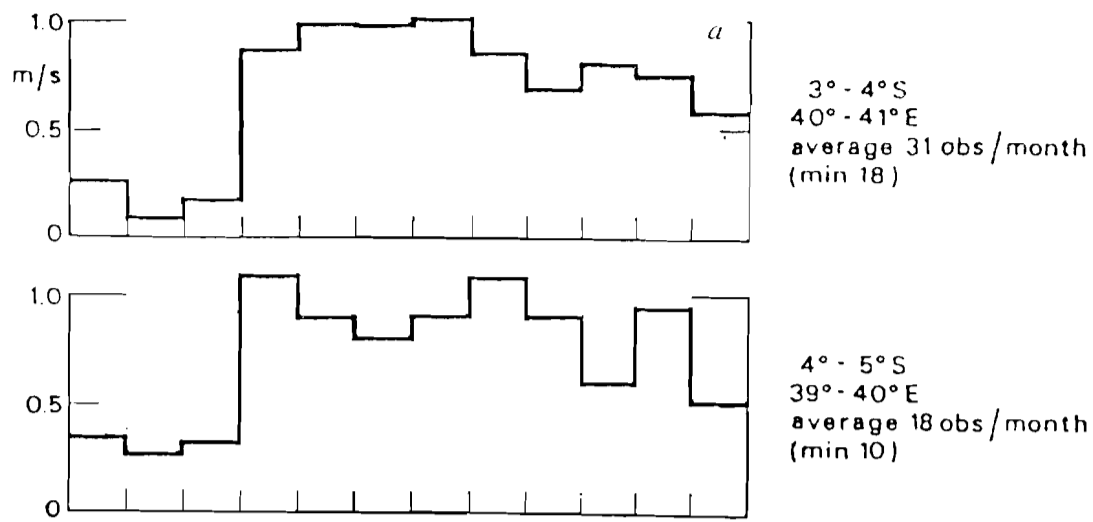
Figure 3.2.2.2 Seasonal cycle of monthly mean component of historical ship

drift currents at selected latitudes in the EACC, Panel (a) Off Kilifi Tudor Creek

area, Panel (b) off Tudor creek-Gazi Bay area, panel (c) current perpendicular to

the Kilifi-Gazi Bay shelf area (Source, Swallow et al., 1992).

3.2.3 Scientific work in the proposed study sites.

Several studies, although not uniquely dealing with physical oceanography, have been carried out in Gazi Bay and Tudor Creek, which are the two of three selected study sites proposed for investigation (see Chapter 4). The third one is Kilifi Creek. The Morphological aspects of the study site are taken up in Chapter 4. However, the past work or literature on these study sites is taken up in this Section. Work concerned hydrography where preliminary salinity and temperature were carried out. Some tide measurements were also done including currents and nutrients (silicate, phosphate, nitrates, nitrites and amonia). Kilifi Creek, which is morphologically similar to Tudor Creek (see Chapter 4), has received not much attention and there is apparently no literature available.

3.2.3.1 Previous studies on salinity and temperature in Gazi Bay and Tudor Creek

In Gazi Bay Ohowa et al. (1997) used a vane for current and a refractometer for salinity during measurements and reported variable distribution of currents during high and low river discharge. They found that salinity in the bay ranged from 24 to 35 during the wet period but remained at 35 in the whole of the bay during the dry period. The discharge from river Mkurumuji caused the salinity to drop from values 10-25 near its mouth and to 0 in the Kindogweni river mouth. They indicated that the circulation in the bay during flood in the wet period (Figure 3.2.3.1) was clockwise. Kitheka (1996) reported salinity and temperature range 28 - 35 and 25-31.5°C respectively. He showed

that salinity in the upper parts of the estuary dropped to near zero during the IMLR season, but only up to 15 during the dry season. He also observed the water in the bay was vertically well mixed (homogeneous), and attributed this to tidal mixing. He concluded that the variability of these parameters was seasonal. Thus in Gazi Bay there is a considerable effect of the rivers entering in north and west, respectively. However, it is not obvious whether fresh water input has an influence on the circulation.

Norconsult (1975) carried some hydrographic measurements on 20 stations both in Tudor Creek, Kilindini harbour and offshore (within 5km from Shore) from Tiwi to Mtwapa Creek, i.e. 20km north of Tudor Creek. He found that salinity in the offshore water shows small variations during the year, averaging about 35. He suggested that the salinity of the water in the harbour and creeks is determined by the salinity of the ocean water entering them by the tide, evaporation and the fresh water runoff from tributaries catchment areas. During the dry seasons of SEM and NEM the evaporation in shallow wide the estuarine basins exceeds the fresh water inflow, resulting in slightly higher salinity as compared to the offshore waters. During the IMSR and IMLR seasons the fresh water inflow exceeds the evaporation, causing a slightly lower salinity in the creeks. His results showed that throughout the year the salinity distribution was uniform with depth both in the offshore and inshore waters. The highest mean monthly temperature of the offshore water occurs in the month of March and April of NEM reaching 28-29°C. The lowest temperature of 24-25°C occurs during July and August of SEM. He pointed that the cause of the temperatures of up to 2°C higher in the creeks than in the offshore water observed through out the year is caused by sun radiation in the shallow estuarine basins. He concluded that the fresh-water runoff results in slightly lower density of the

creek waters. The density distribution was found close to uniform with depth both in the inshore and offshore water suggesting vertically homogeneous water.

Measurements on a series of stations similar to those of Norconsult (1975) in the lower part of Tudor Creek but with extended coverage to the Kombeni River mouth was done by Okemwa (1988, 1990), Kazungu (1989), Kimaro (1987) and Nguli (1994). During the IMLR season they reported longitudinal salinity gradient, with low salinity where the rivers debauched into the creeks but found salinity in the lower reaches of the creek were close to that reported by Norconsult. Nguli (1994) confirmed the salinity gradient and estimated flushing time of about 14 days of the water in the upper reaches of the creek. A number of other studies carried out in Tudor Creek that have focused on biological aspects of the creek (e.g. Okemwa and Revis, 1988 and Kimaro, 1987). They argued that the seasonal changes observed in zooplankton concentration are related to different water types. Kazungu (1989) worked on chemical aspects and his studies also included temperature and salinity. He showed salinity range of 34.8 - 35.5 with low values occurring during the wet period was reported. More over he found low saline water in the upper reaches of the creek and a salinity range of 2 - 36.2 from the shallow inner basin to near the entrance area of the creek. The gradient decreased considerably by June becoming more or less uniform through out the creek in July. Kazungu further pointed out that creek becomes an estuary during the rain season, and but after the rain the oceanic conditions are established. This had implied that Tudor Creek is likely to have a neutral and even an inverse circulation (see e.g. Dyer, 1979).
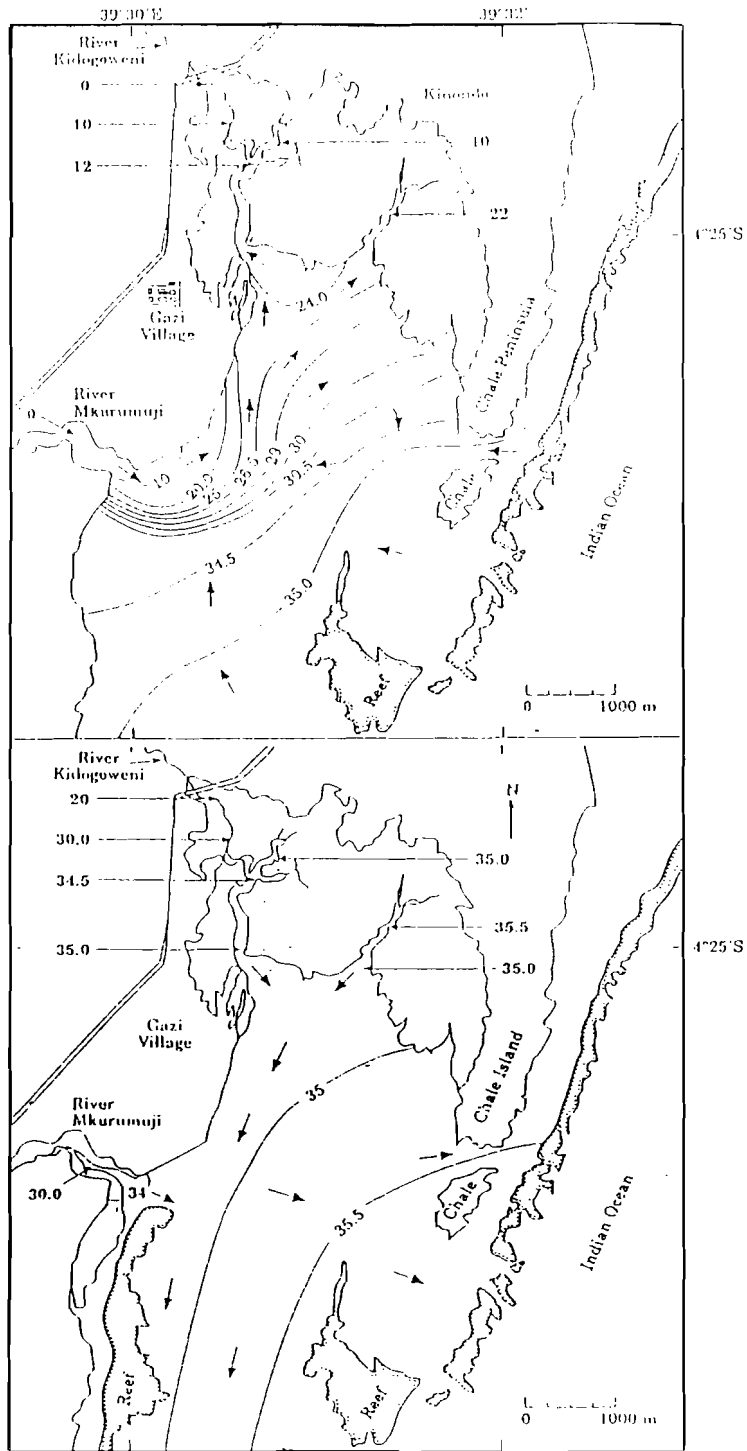
Figure 3.2.3.1 Spatial distribution of salinity in both wet (a) and dry (b) seasons for Gazi Bay (Source, Ohowa et al., 1997).

3.2.3.2 Previous studies on tide and currents in Gazi Bay and Tudor Creek

Pugh (1979), Nguli (1994), and Odido (1994) all studied tides of the region. Pugh carried out harmonic analysis using sea level data from the tide gauge in Mombasa and other stations of the western Indian Ocean. He found semi-diurnal (M_2) tide dominated with amplitude of 0.933m. For the S_2 constituents he found amplitudes of 0.460m. He estimated a tidal a spring tidal range ($2(M_2+S_2)$) of 2.8m. Nguli (1994), Odido (1994), and Magori (1997) carried similar analyses but based on short period (two weeks) sea level records. Elsewhere along the nearby part of the East African coast, Lwiza and Bigendako (1988) at Kunduchi, north of Dar es Salaam did tidal observations. Their results closely agreed with those of Pugh (1979), for more representative results longer sea level record (at least 29 days) is necessary.

Few current measurements have been carried in the inshore (40m) area along the Kenyan coast. Norconsult (1975) measured currents in Tudor Creek inlet channel using Pendulum Current Meters such as those used in this study and discussed by Cederlof. (1996). He showed that mean flood tide lasts for 6.5 hours and the mean ebb tide for 6.3 hours, with maximum currents in the range 0.4- 0.6 ms^{-1} (Figure 3.2.3.2). According to Norconsult (1975) slack water appears more or less exactly at high water, where as inflow starts some time 10-20minutes before low water. The small delay implies week constriction by of tidal flow by Tudor Creek. Kimaro (1987) during her plankton studies found a clockwise eddy near KMFRI, thus indicating transverse circulation may be important in lower part of the Tudor inlet channel.
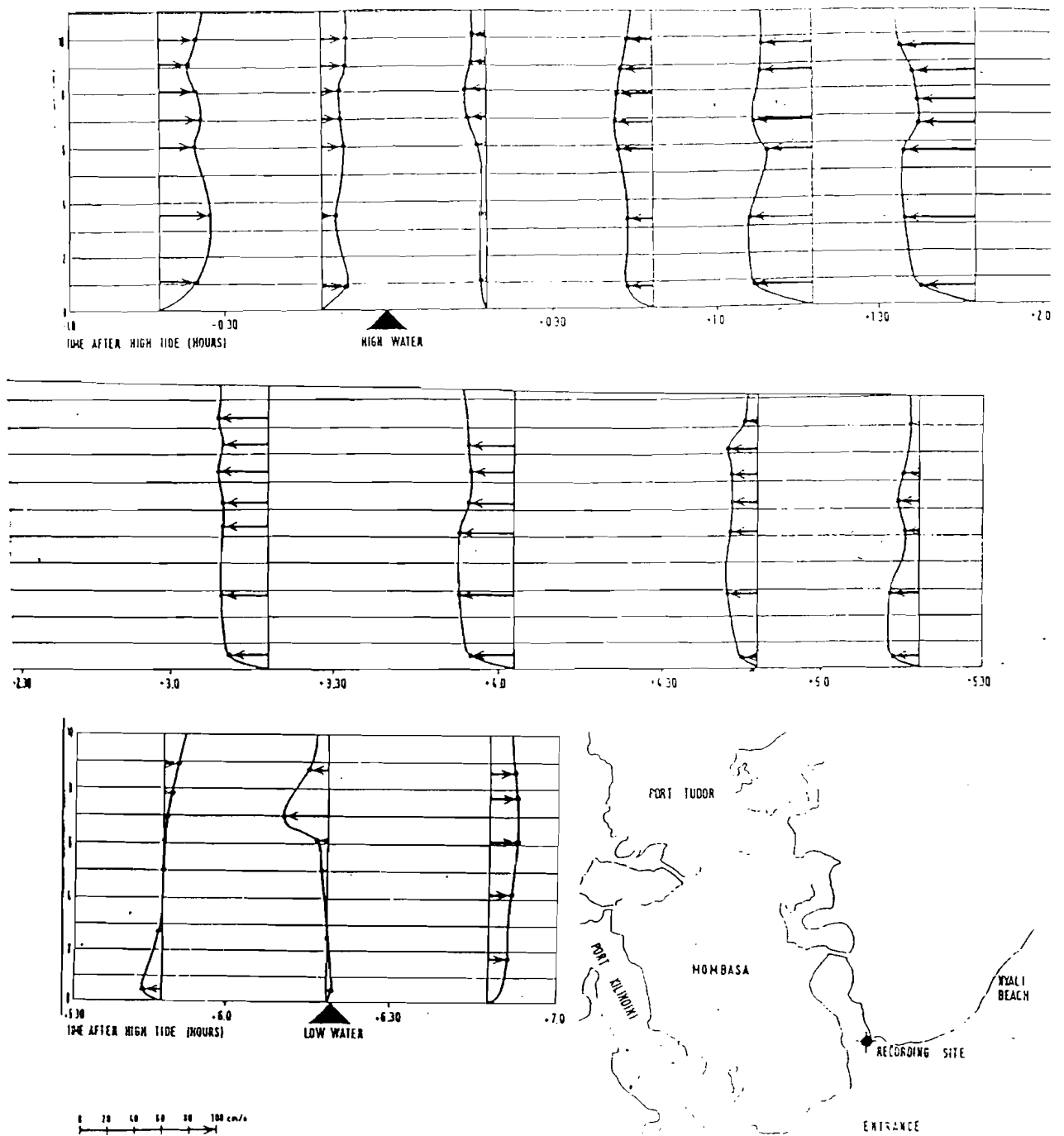
Figure 3.2.3.2 Vertical variation of current from high water to low water. Note the one-direction almost through out the flood and ebb period (Source. Norconsult, 1975).

3.2.3.3 Previous studies work on nutrients in Gazi Bay and Tudor creek

Phosphorus, nitrogen, and silicon are the most important nutrients for plant growth. They are taken from water by the organisms and replenished through resolution or decomposition. Since the water in an estuarine is influenced by runoff and is in exchange with the ocean nutrient cycles are interfered with by various conditions in the estuary.

In Tudor Creek and Gazi Bay, it was found that nutrient (nitrate) variations were depended on rain (Kazungu, 1986, 1989; Hemminga et al., 1994). In Tudor Creek Kazungu (1986) showed that in April the concentration was of the order 9.4 μg-at/l. A maximum (22.6 μg-at/l) occurred in May while after the rains (June and July) the concentrations were less than 1.0 μg-at/l. For the entire creek the nutrient range was below 10-40ug at/l, which led to the conclusion that Tudor Creek is 'low nutrient estuary'. To be a high nutrient range the range would be 100-350μg-at/l (Sharp, 1983; Bale and Howland, 1981). The values during the rain season were higher than those found in the open waters of the western Indian Ocean. According to Smith and Cordisporti (1980) rarely the values exceed 5μg-at/l. Kazungu pointed out that the nutrient range 13-20μg at /l found by Smith and Cordisporti (1980) for the Somali upwelling region compared well with those of Tudor Creek.

Much lower nutrient values were found in Gazi Bay during the rain season and very low values in dry season (Hemminga et al., 1994; Ohowa et al., 1998). A time series summarising typical variation of dissolve inorganic nitrogen (DIN) during the wet and dry seasons of 1992-4, form Ohowa et al. (1998) is shown in Figure 3.2.3.3

Elsewhere, it has also been shown in shallow estuarine systems nutrients are supplied into the shallow estuarine systems by various sources, mainly by river inputs and human influences (McCarthy et al., 1984; Nixon and Pilson, 1993). This is different from the open ocean, where primary production is controlled by regeneration process (Glibert, 1988), while in an upwelling region the vertical movement of water assist primary production by allochthonous input of nutrients into the euphotic zone from deep water. Of the various nutrients in the systems phosphorus is increasingly being accepted as the limiting factor in algal growth than phosphorus (Graneli et al., 1986, Rydberg, 1986). Although, there are no specific studies on nutrients as a limiting factor in the Kenyan creeks, there have been measurements on chemical aspects of the shelf water. As mentioned earlier and, on the preposition that the oceanic surface layer may enter the creeks, we have included results on nutrients in the ambient water in Chapter 6.
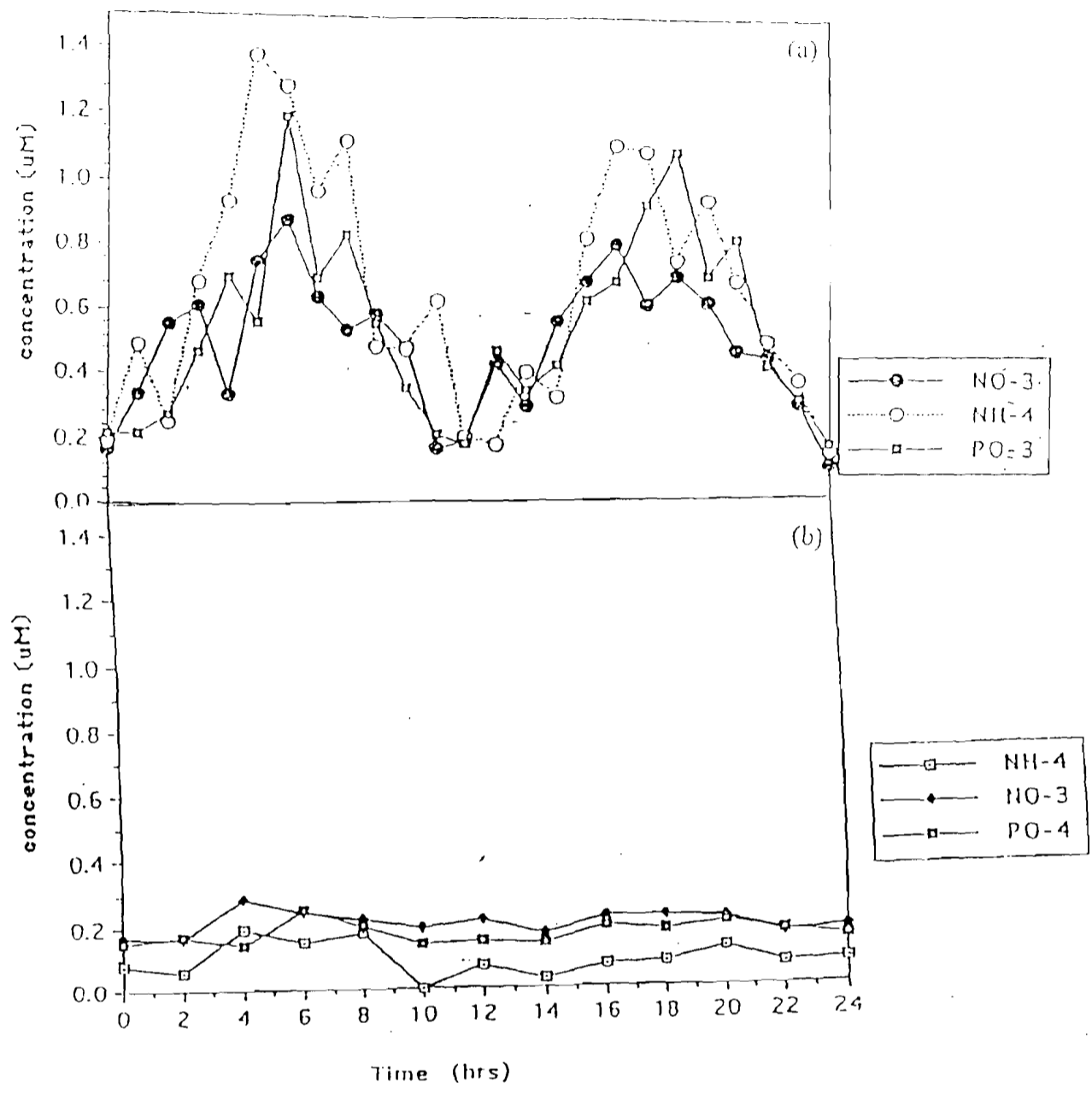
Figure 3.2.3.3 Summarising of 24-hour observation of dissolved inorganic nutrients during the rain (a) and dry (b) seasons of 1992-4, in Gazi Bay (Source, Kitheka et al. 1996, EEC report).

62

CHAPTER FOUR

MATERIALS AND METHODS

4.1 THE STUDY AREAS AND STATIONS

4.1.1 Gazi Bay

Gazi Bay, its position, morphological components, depth and sedimentary facies which are a result of the interplay of geomorphologic history, river discharge of water, sediment, tidal currents and waves and coastal processes are shown in Figure 4.1.1.1 which also indicate three parts of the bay. These parts are the marine dominated entrance area, the mixed energy area forming the central bay basin, and the river dominated area colonized largely by mangrove vegetation and (the Kinondo Creek etc).

The bay is situated 50km south of Mombasa and oriented in a north south direction. It is 7 km long and has a width of 4km in the central basin with a total area of about 30km^2. The mean depth at sea level is 3m. Two seasonal rivers Kidogweni River and Mkurumuji River arise from the coastal ranges of Shimba Hills debauch fresh water into the bay after draining an area of 30 and 164 km^2 and respectively. Kidogweni River enters the bay through the Kidogweni Creek while the Mkurumji River discharges directly into the central bay basin (mixed energy area) from the western side. During the IMSR and the IMLR season discharge 5.0 and 17.0m^{3}s^{-1} respectively as reported by Kitheka (1997).

Two tidal fluvial creeks, Kidogweni and Kinodo Creeks 5.0 and 2.5km long respectively, cut through the vegetation in the 'river dominated area' of the bay. The vegetations colonizing the bay are mangroves which occupying 10 km^2 of inter-tidal area all of which is inundated by the marine waters during the extreme HHWS tides.

Kidogweni tidal channel shows tidal meandering in the upper part of the creek and tidal sandbars where it enters the central bay basin. Sandy shores occur in the northwestern part of the central basin, while large parts of the inter-tidal area at the lower end of the river dominated area are extensive seagrass beds (see Hemmiga et al., 1999) and mud flat occur southwest of Kinodo tidal channel.

The central basin area, which can also be referred to, as 'backreef lagoon' is sheltered from ocean waves on its eastern side by the Charle Peninsula, the Charle Island and an extensive coral reef platform. Shallow tidal openings occur between Charle Island and the peninsula.

In the marine dominated part of the bay coral reef and extended coral plat forms as barriers. Inlet and wave cut opening area occur in the sea face coral barrier, which extends in a north-south direction as a continuation of the elongated Eastern Africa fringing reef.

In the literature review Chapter 3, Section 3.2.3.1 to 3.2.3.4 previous research work in Gazi Bay by Kruyt and van de Berg (1993) and Kitheka et al. (1997) was presented. It was established there that in the mangrove creek area the salinity range was 2 and 15 in the open part of the bay area the range was 31-33 for the during the rain season of 1993-1994. During the dry periods, however, salinity remained at 35. Hence a salinity gradient is evident during the wet period and measurable buoyancy exists, the salinity gradient, however, diminishes greatly during the dry period.

The temperature range for 1993-4 was found to fall in the range 25.5 -31.5 °C with the lowest value in August and highest value in December and the fluctuations could be as large as 2.5 °C. The tide was found to be mainly semi-diurnal.

During maximum water discharge from Mkurumuji River nutrient rates of 12 kg N day^{-1}, 40 kg N day^{-1}, and 30 kg N day^{-1} as ammonia, nitrate and phosphate respectively occurred (Ohowa, 1996). For Kidogweni River the values were 5, 10 and 9 kg N day^{-1}, however, they were much smaller for the dry period of very low freshwater discharge.

These earlier studies however did not involve time series measurements of tides and currents, thus more detailed information on tidal response, water exchange and further description of Gazi Bay was necessary. Thus seven hydrographic sampling net stations (I-VI) and two transects were established as indicated (Figure 4.1.1.1) along with three tide gauge stations (MT1-MT3) and one current meter station (RCM).
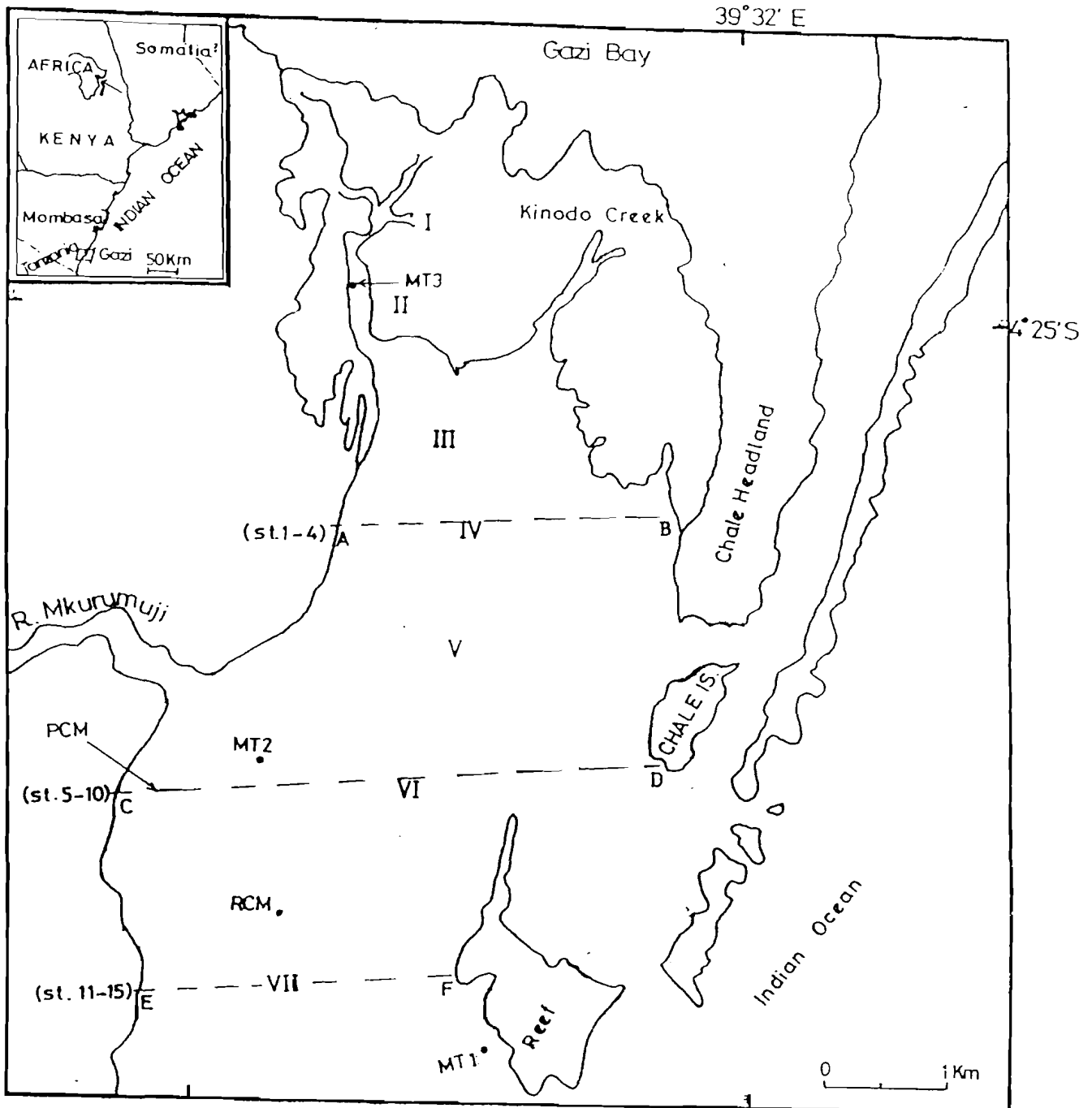
Figure 4.1.1.1 Gazi Bay oceanographic stations net (I-VII), two transects. tide gauge

stations, and one current meters stations (PCM and RCM).

4.1.2 Tudor Creek

Tudor Creek, which lies to the north of the island and the old Mombasa port where Fort Jesus and the KMFRI are situated, is one of the two inlets surrounding the Mombasa Island. The other is the Kilindini Harbour. The creek has a total length of 14km, and a surface area of 22km^2. It consists of the entrance area, the central area and inner parts. The entrance is a marine dominated, high-energy zone, with deep single sinuous inlet channel. The inlet has a length of 4km and width of 300m and a mean depth of 20m. The depth, however, is variable and occasionally scour holes (40- 50m) occur in parts of the inlet bends. The surface area of the inlet varies from 1.31 km^2 at low water spring tide (HWS) to 1.72 km^2. The inlet is connected to a central relatively shallow (5m-deep) basin, which has a width of 3-4km and is fringed by mangroves and mudflats. The central basin has an area of 6.37 km^2 and 22.35 km^2 at LWS and HWS respectively.

The basin is a mixed energy zone area that gradually grades into river influenced peripheral lagoons and small creeks both fringed by mangroves and mudflats. The mangrove forest takes up 8km^2 of the total area and has the two small creeks, Kombeni and Tsalu, which are 4.5 and 3km long respectively. The basin has an average depth of 5m during maximum high water, with a mean of 3m at MSL. The creeks and the basin form 80% of the total surface area of Tudor Creek. Tudor Creek receives fresh water discharge during the wet seasons of 8m^3 s^{-1} and 5m^3 s^{-1} from Kombeni and Tsalu Rivers, which open up to the two small creeks leading to the shallow central basin.

The six oceanographic sections (I-VI) established, together with current meters (RCM, PCM) and tide gauge stations (MT1-4) are all indicated in Figure 4.1.2.1. A weather station was also placed at KMFRI.

67
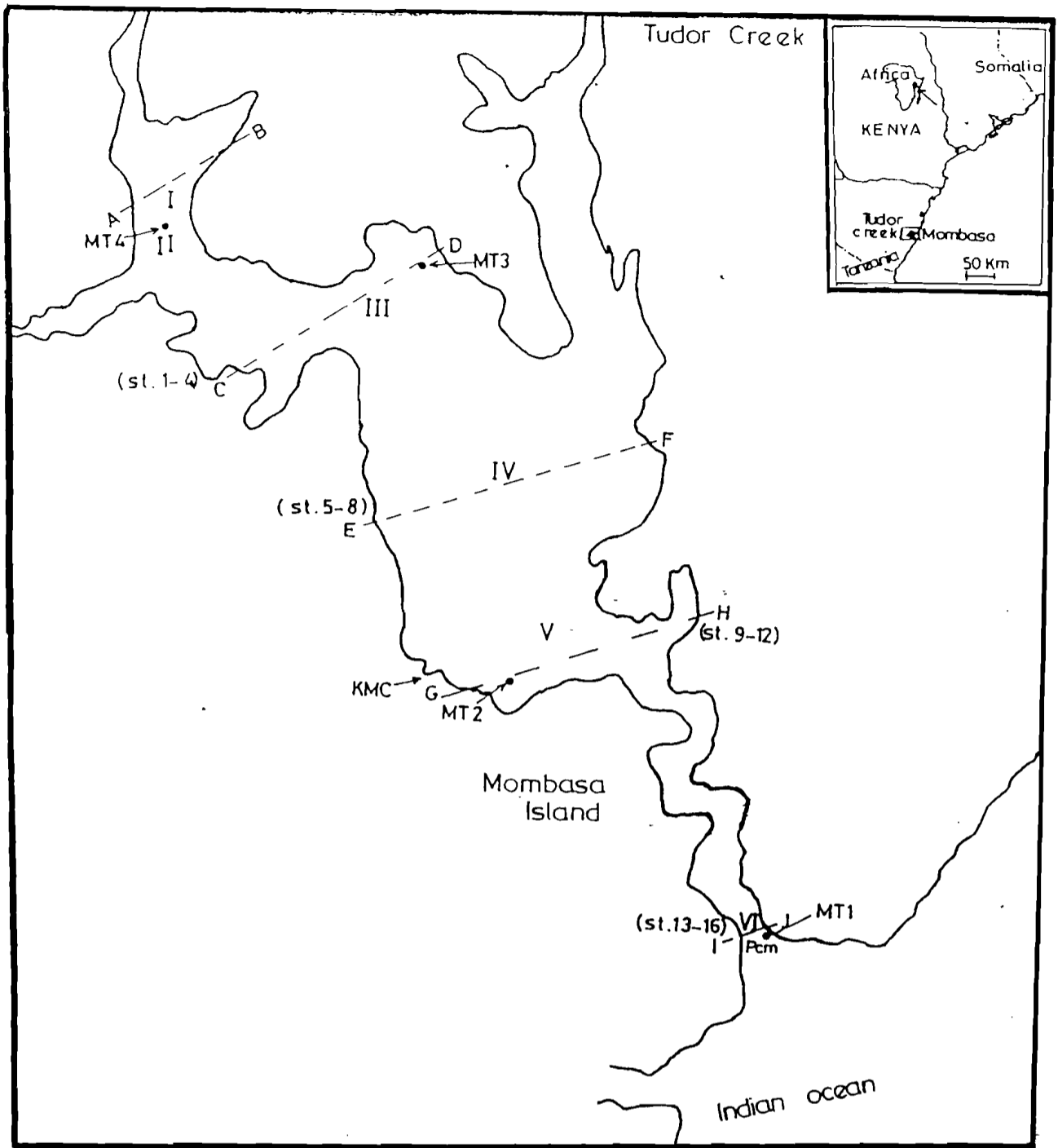
Figure 4.1.2.1 Tudor Creek oceanographic stations net (I-VI), two transects, tide gauge stations, and one current meters stations (PCM and RCM). Note also the weather mast station at position marked KMFRI.

Previous hydrography, currents and sea level studies were discussed in the literature review Chapter 3, Sections 3.2.3.1 to 3.2.3.4. Summarising the finding here, the highest mean monthly temperature (28-29°C) in the offshore water was observed in March and April; where as the lowest temperature of 24-25°C occurs in July-August for year 1975. Temperature fluctuations were as high as 2°C in the creek. The fresh-water runoff results in slightly lower density of the creek waters. The density distribution was found close to uniform with depth in the inshore and offshore water suggesting vertically well mixed. A salinity gradient was observed along the creek in wet periods, but seemed to disappear during the dry periods. Surface salinity was ranged between 33-34.6 during wet period and 35-35.7 during the dry periods.

The creek is dominated by tidal current close to $1ms^{-1}$(Norconsult, 1975). Kimaro (1987) found a clockwise eddy near KMFRI. Nutrients were high during the wet period (May-June) but low during the dry periods in general the creek can be classified as 'low nutrient estuary' of which nutrient range below 10-40µgat/l. The values during the rain season were higher than those found in the open waters of the western Indian Ocean which according to Smith and Cordisporti (1980) rarely exceed 5µg-at/l. The nutrient range 13-20µg at /l found by Smith and Cordisporti (1980) for the Somali upwelling region compared well with those of Tudor.

69

4.1.3 Kilifi Creek

Kilifi Creek is located 70 km north of Mombasa at 3° 35'S and 39 °40'E. The Morphological components of Kilifi Creek are illustrated in Figure 4.1.3.1. It is similar in shape to Tudor Creek also with two small creeks, 'Maya' and 'Vitengeni Creeks,' fringed with mangroves. Vitengeni Creek is 10km long; width varies from 0.5 to 3.5km, and is three times larger than Maya Creek. Two small seasonal rivers discharge through Vitengeni Creek into a wide inner basin. The basin although almost circular in shape can be divided into upper and lower reaches. The upper reaches have more fringing mangroves and peripheral lagoons than the lower reaches, which have high and steep banks. The rivers are Dzovuni and Vitengeni and have their origin in the coastal Islands. Sand and mud flats occur in at the mouth of each creek. There are no sea grasses in the upper reaches of the creek basin.

In total mangroves and mud flats cover an area of $8km^2$, whereas the surface area of the basin alone is $17km^2$ and including the two creeks is $25km^2$. The basin has mean depth of 7m at MSL. The basin is connected to the Indian Ocean through a 2km long and 300m wide inlet. The mean channel depth is 15m. The channel cuts through fringing coral platform, which is similar to that found at Tudor creek entrance with back-reef lagoons on either side. Numerous sea grasses occur at the bottom and in the small tidal channels that open to the ocean. Waves constantly break at the entrance.

Five sampling stations were made along the creek, and three locations selected for tide gauges. The stations (l-V) are shown in the Figure 4.1.3.1 as well as the location of the tide gauges MT1, MT2 and MT3 and the current meters PCM and RCM. Stations 1-4, 5-8, 9-11, and 12-15 were stations made across-the creek for salinity and temperature.

70

Letters A-G represent transects and also location where a few measurements using surface drifters were carried out.

No previous hydrographic studied for Kilifi Creek.
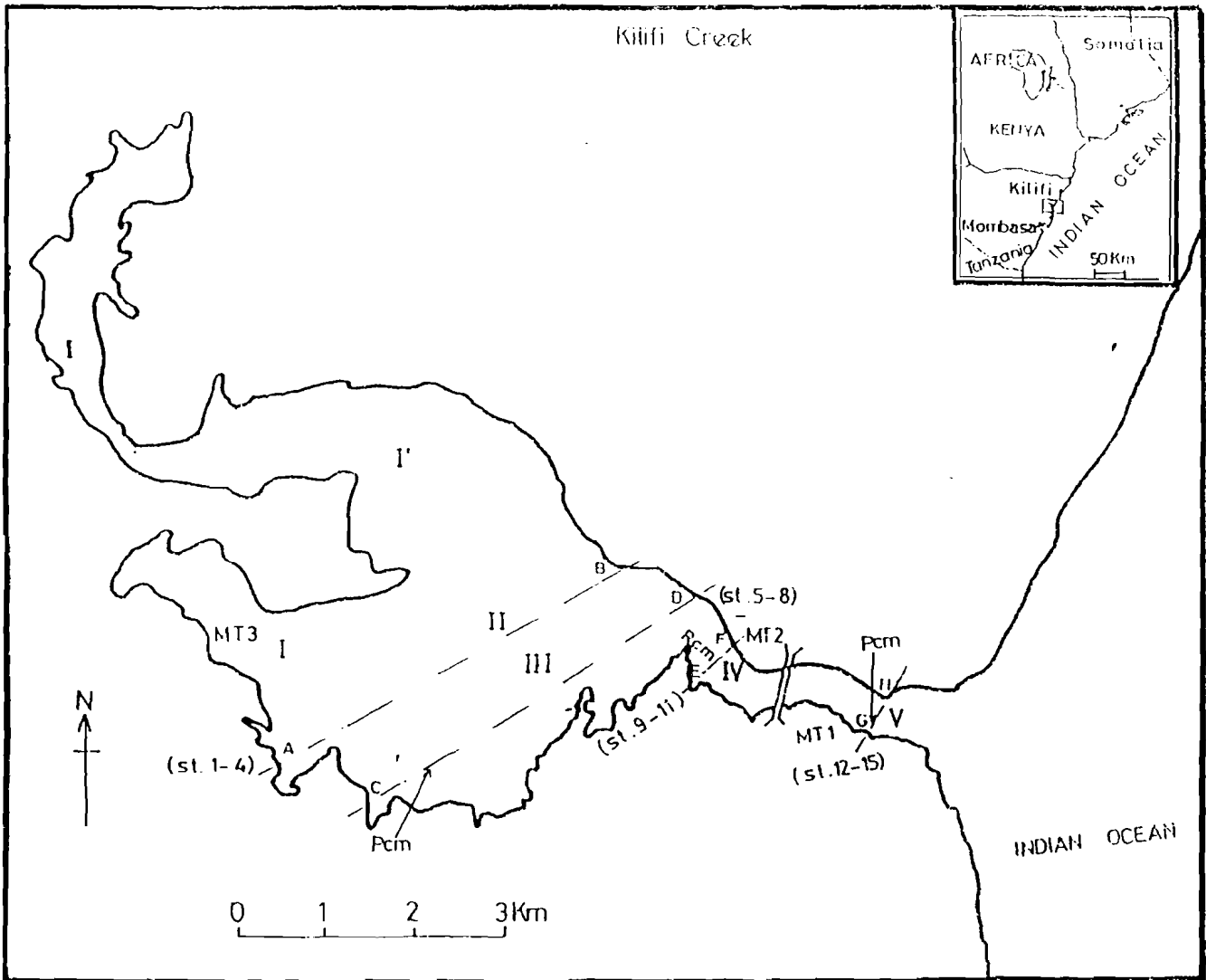
Figure 4.1.3.1 Kilifi Creek oceanographic stations (I-VI), sections, tide gauge and current meter stations (PCM and RCM) are indicated.

4.1.4 Meteorological stations

A weather mast, from which data for complete heat and radiation may be carried out, was placed at the Kenya Marine and Fisheries Research Institute (KMFRI) building, and located as shown in Figure 4.1.2.1.

4.1.5 Other stations and data sources

Other data sources include as mentioned, available oceanographic data from recent cruises, R.V.Tyro 1992-93, R.V. Dr. Fridjof Nansen 1982-83, and M.V. Kusi 1979 (see MONEX data 1980). Some sections, each with a number of oceanographic stations, were taken perpendicular to the coastline off the location of the study sites. The location of these transects and stations are shown in Figure 4.1.5.1.

Long-term sea level data is available from the Global Sea Level (GLOSS) stations of Mombasa, Lamu in Kenya (Figure 4.1.5.1) and Zanzibar further below in the in Tanzania (actual location not shown). Some of the tide gauges are solar powered and record sea level data at hourly intervals. Lamu station has telemetry arrangements that enable data to be transmitted via satellite to the University of Hawaii.

Nutrient stations were essentially two, one inside the creeks (bay) and the other at the entrance. Simultaneous series of stations for nutrient measurements were also available from other projects focusing especially at Gazi Bay. Other source of nutrient data was available from selected stations from the mentioned cruises (see in Chapter 6).

72
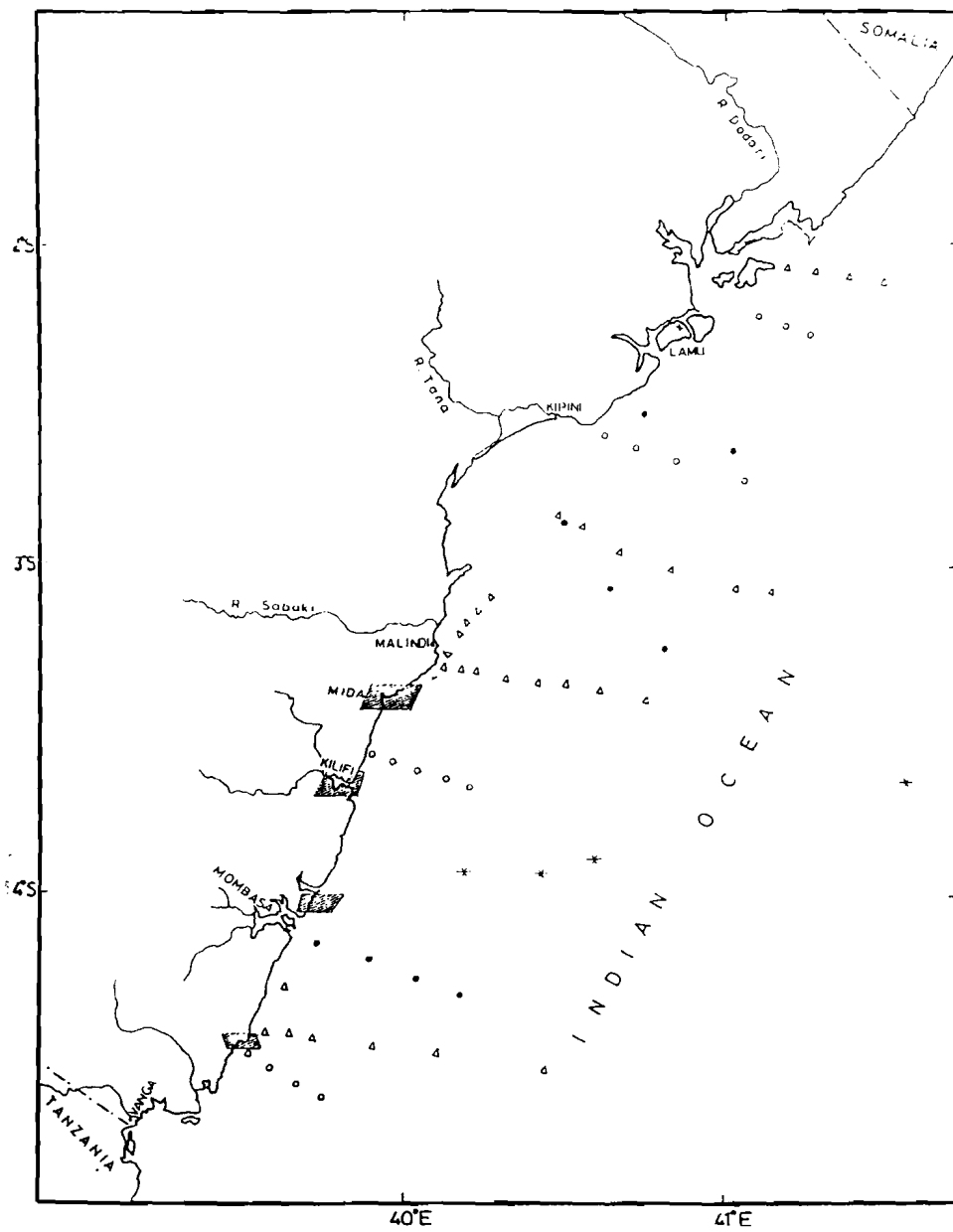
	R.V Tyro (1992-93)
.	M.V. Kusi (1979)
o	R.V. Dr. Fridjof Nansen (1982-1985)
*	RRS Charles Darwin (1966-87)

Figure 4.1.5.1 Oceanographic stations occupied during various historical cruises off Kenya coast.

4.2 INSTRUMENTATION

4.2.1 Instruments for oceanographic measurement

In this section instruments used and the parameters measured are presented and discussed. The basic equipment used in this study were, recording tide, recording current meter and temperature-salinity sensor for logging and for observations. In addition we used pendulum current meters for direct current measurements and a so-called weather station, which was equipped with several sensors for the studies of heat fluxes.

4.2.1.1 Portable tide gauge

The instruments used for sea level observations were tide gauges of the type Micro Tide from Coastal Leasing. These are portable self-contained pressure-observing instruments that can be programmed and deployed in water for periods up to a year if sampling is made once per hour. The instrument is shown in Figure 4.2.1.1. It measures sea level and temperature with an accuracy of ±0.015m and ±0.2 °C respectively. Data storage and batteries for providing power to the instrument are all inside a watertight metal tube (Figure 4.2.1.1). We had three instruments at hand. Instruments may have capacity for burst measurements where registration can be stored at intervals of 0.16 s, implying that ocean swells can be logged. This means that memory capacity has to be increased. For normal registration of tide, we set the storing to 10min or 5min intervals averaging over 2 min. This means that the instrument can be deployed for a minimum of 80 days. The tide gauges record total pressure in pounds per square inch (PSIA).

The pressure was converted to meters of water to sea level by subtracting the air pressure, and multiplying by the conversion factor of 0.689. However, correction for air pressure was not done as the air pressure is normally observed only a few of times per day. Instead we just averaged the series decreasing the observed values by the period mean. Thus, we might expect some smaller difference between results obtained from pressure gauges and data obtained from instruments measuring the actual sea level, where a full response of the air is expected. Wijeratine (2001) indicate that strong resonance phenomenon in the atmospheric pressure appear mainly as S_2 or S_1 components and may affect result from harmonic analysis. The amplitude of S_2 and S_1 is of the order of 1 and 2 cm respectively
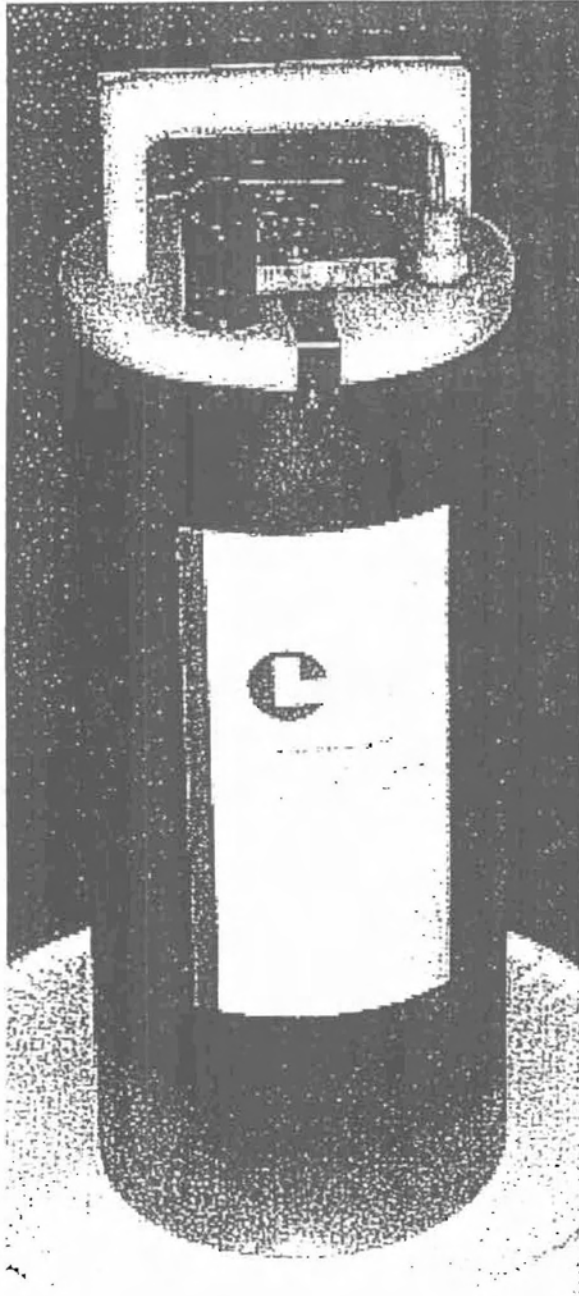
Figure 4.2.1.1. An example of the tide gauge used in this study.

4.2.1.2 Self recording current meter

The recording current meter (RCM) we used in this study was rotor current meter (SD6000 from Sensor data). This instrument has a memory for 6000 data sets of velocity, direction and temperature. It can be pre-set at time interval from 5-180 minutes. Thus, at an interval of 10min the sampling period is 40 days. The RCM is a complete acquisition system with an optical read out head and computer software and is powered by lithium batteries that last for two full periods. It can measure currents and temperature from 0 to $8ms^{-1}$ and -2 to 40 °C with an accuracy of ±2 cms^{-1} and ±0.2 °C respectively and $\pm5°$ on direction. With a small magnet the current meter can be switched on and off in the field. The computer program may be used to set sampling intervals, but also for downloading and basic treatment of data. The deployment is shown in Figure 4.2.1.2. A strong rope attached to a vinyl buoy (10kg) is used to keep the RCM upright whereas it is anchored by 20-30kg weights. Thus it can be done by hand in shallow inshore waters.

4.2.1.3 Pendulum current meter

The Pendulums Current Meter (PCM) is v-shaped vane. Several PCMs are usually assembled by attaching them to a rope at selected spacing in relation to required depths. Figure 4.2.1.3 illustrates an assembly of the PCM, deployed in a cross-section in the Tudor Creek inlet. Each vane is fitted with a gelatine filled casing to which is attached a magnet suspended on a thin cord. The gelatine casing is heated and the gelatine melted during deployment. The magnet indicates the north direction and is used to determine the direction of flow while the inclination of the cord gives the angle from which the current speed can be determined. The vane is oriented in the direction of the current while the

initially melted gelatine stiffens and the inclination of the cord and the magnet direction is 'frozen'. This takes place up to a temperature of 30-32 °C, for a maximum solution of gelatine, and occurs within 15min-1hr, depending on the surrounding temperatures and the original temperature of the gelatine solution.

The PCM performance is described and discussed by Cederlöf et al. (1995). It has accuracy of 2 cms^{-1} and ±5°, for current speed and direction. The PCMs were used to obtain a simultaneous picture of the flow across part of a cross-section. A deployment (except for the RCM) for pendulum is carried out in some few minutes. It can be recovered within 30 minutes once the gelatine is stiffened. Thus typical time for the above deployment is 1 hour, after which a new deployment can be done.

A portable echo sounder and a GPS-navigator were used for measuring depths and position in the study sites. Landmarks on cliff banks were also used for determining the position.
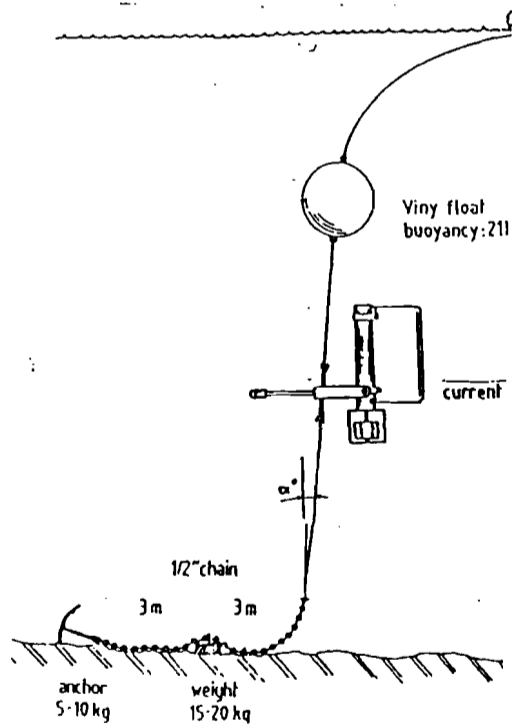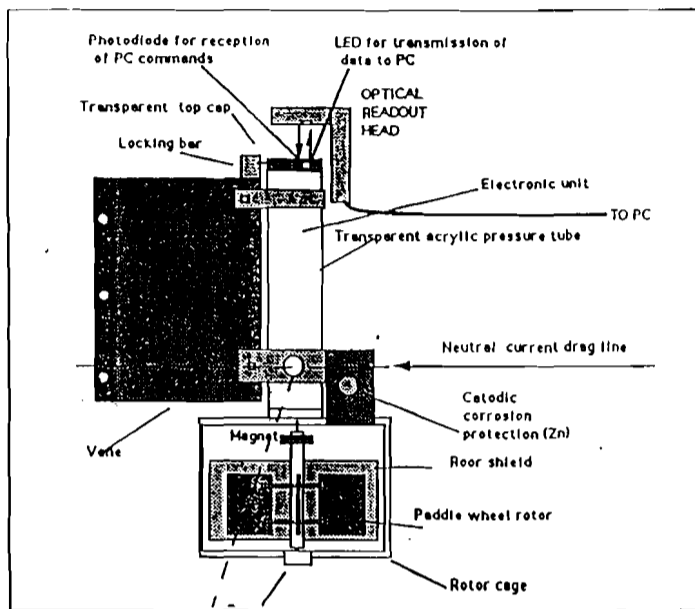
Figure 4.2.1.2 A SD-6000 RCM from Sensor data is shown in the upper panel with its design (electronic unit, paddle wheel rotor, magnet and vane). Lower panel shows a mooring arrangement.
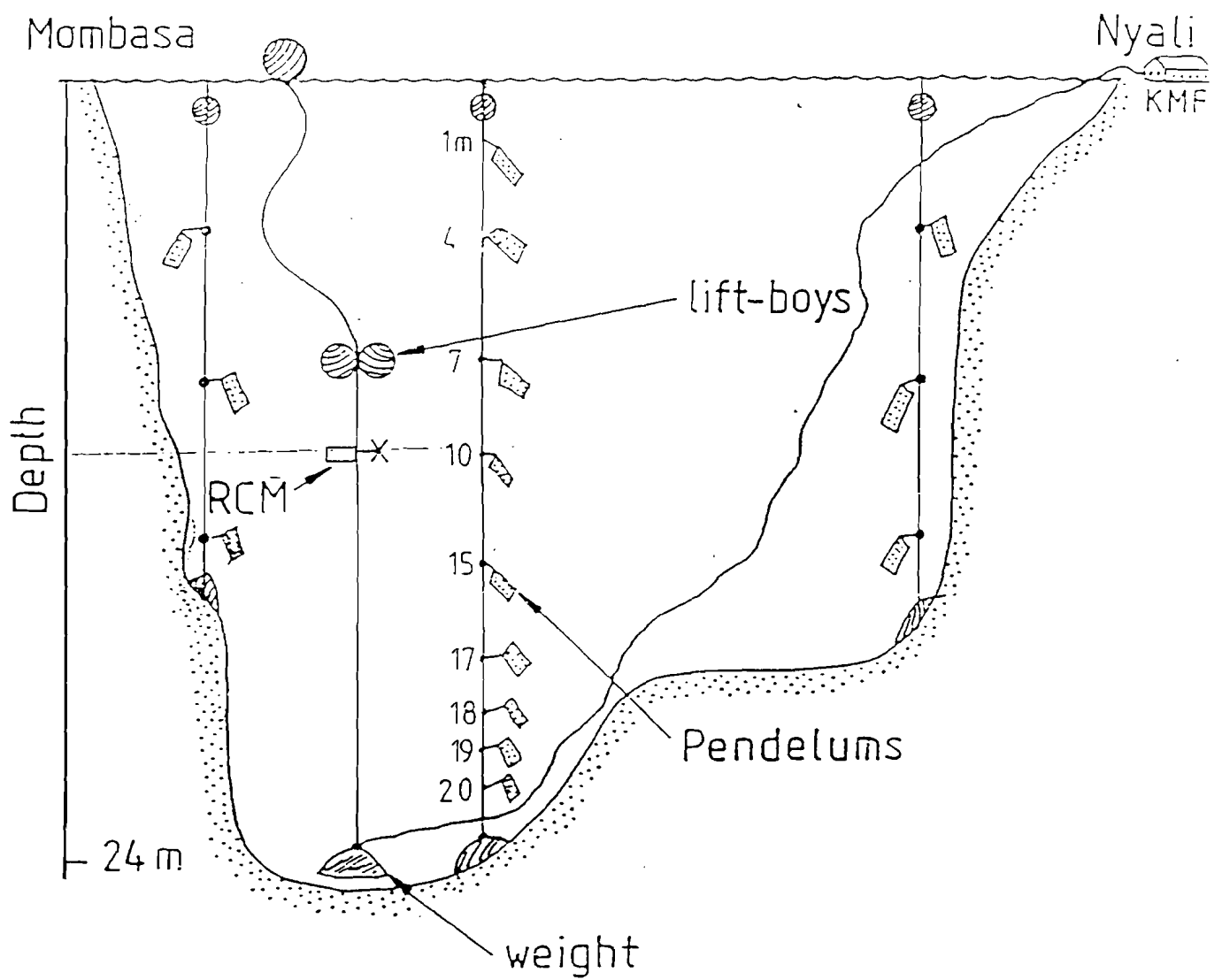
Figure 4.2.1.3 Deployment arrangement for Pendulum Current Meters at a cross-section in Station VI in Tudor Creek.

4.2.1.4 In situ salinity temperature sensor

Salinity and temperature measurements were carried out with a salinity-temperature (PST) sensor (Aanderaa 3210). It has an accuracy of 0.1 PUS, and temperature with 0.2°C. A display unit (Andrea 3515 was used for in situ observation (Figure 4.2.1.4). The same PST was also connected to the weather mast, where it was used for observations in one point during longer periods. The sensor, which actually measures conductivity and temperature, is developed for being mounted on current meter and for this later type of use, and not for vertical profiling. The performance for obtaining vertical profiles is not satisfactory because of slow temperature sensor. Thus, obtaining good data on profiling is also a matter of experience. There is also the general tendency of the PST sensor to give lower values after some weeks of continuous observations. This might be due to alga growth, whereas current cleaning of the sensor may help. However this type of problem seems to occur also when the instrument is positioned far below the phobic layer (Rydberg per.comm.).
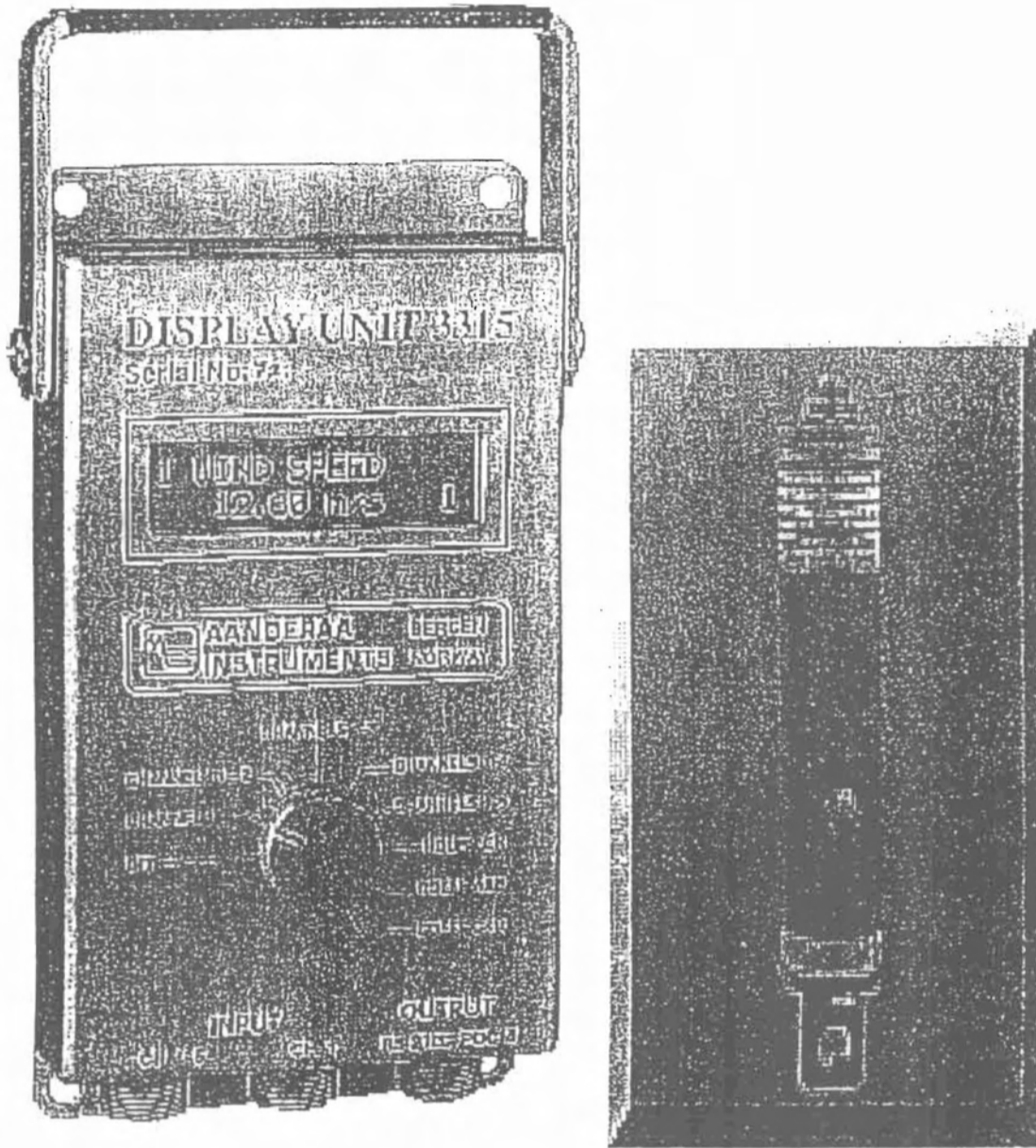
Figure 4.2.1.4 Shows device for salinity profiling and temperature measurements, with a Display Unit (Aanderaa 3515), and a salinity temperature sensor (ST-Sond 3210).

4.2.2 Instrument for meteorological measurements

4.2.2.1 Aanderaa weather mast

A weather mast of type Aanderaa Model AAWS 2700 was used for meteorological observations, particularly for radiation measurements. A weather mast similar to the one used in this study is shown in Figure 4.2.2.1 It can be equipped with 12 sensors, which is the upper limit for scanning unit, described further below. Range accuracy and resolution is show in Table 4.2.2.1.We used the following sensors:

Air temperature, the electrical thermostat uses the linear dependence of the electrical resistance on temperature. The sensing element, a film type platinum resistor is well insulated from other thermal influences, thus enhances the accuracy.

Relative humidity, where the probe, protected from the direct sunshine and radiation uses a polymer to sense the humidity. A Millipore filter protecting the sensor from atmospheric pollution needs to be replaced at intervals, depending on the pollution at the station.

Air pressure, where the sensor measures air pressure by the use of miniature monolithic silicon pressure transducers.

Sunshine duration, where the probe measures presence and duration of sunshine thus providing indirect information of the cloud cover. The sensor records the duration of solar radiation as long as there is a well-defined shadow from the *'shadow post'* at the top of the probe. Radiation intensity contrast created between the photodiodes, one under the shadow and other not under the shadow is a measure of sunshine duration. The sensor is reading once each pre-set sampling interval (giving either 0 or 1)

83

Net radiation, where the sensor measures both incoming solar radiation and the net infrared radiation. Reflection of the sunlight is not included, however, and therefore needs an extra sensor (see Mahongo. 1997). The upper surface of the radiation detector is exposed to radiation while the opposite surface is shielded from it. Exposed surface, depending on the heating or cooling, will emit or absorb radiation, thus generating a temperature difference between the two surfaces of the detector, which is a measure of the net radiation and recorded by the instrument.

Sun radiation, with an accuracy of $\pm$ 1%, and a resolution of 4 W m^{-2} was also used.

Wind direction, The sensor is pivoted with a lightweight wind vane and has housing with a compass sensing element, which follows the magnet on the vane, thus, giving the wind direction.

Wind speed, a three-cup rotor on an arm is fixed on the top of the housing by two ball bearings. Rotation of the magnet fixed on the lower arms end generates a magnetic field, which is sensed by a magneto-inductive switch and converted into an arithmetic mean of the wind regardless of pre-set interval (even the maximum speed (gust) can be logged.)).

Rainfall, The collecting funnel of the tipping bucket of the rain gauge has an orifice of 200 cm^2. Rainfall collected by the funnel is led into the bucket as equal sized droplets, each of which represents 0.2-mm rainfall. The number of droplets (pulses), within the pre-set sampling interval, gives total rainfall. In addition to the met parameters,

84

we also accordingly connected the salinity temperature sond, which was then equipped with a slightly different cable connection.

The sensors were connected to the scanning unit, by which the frequencies of observation (usually 20min) were set. The housing of the mast also included a battery and a Data Storage Unit (DSU). The instrument was run for periods of 1 to 3 months. Connecting the DSU to the Readout Unit and to a computer plus software gave the read out. Through the software the digital data were converted to engineering units.

Table 4.2.2.1. Sensor specification for the Aanderaa weather mast

Sensor	Range	Accuracy	Resolution
Rainfall	12 mm/min (Maximum)	± 2%	0.2 mm
Air temperature	-43 to 48°C	± 0.1%	0.1%
Sun radiation	± 2000 W m^{-2}	± 1%	4 W m^{-2}
Relative humidity	0 to 100%	± 2% RH	0.1%
Sunshine duration	-	-	1 minute
Wind direction	> 0.3 m s^{-1}	< ± 5°	-
Wind speed	Up to 79 m s^{-1}	± 0.2 m s^{-1}	-
Air pressure	920 -1080 hPa	± 0.2 hPa	0.2 hPa
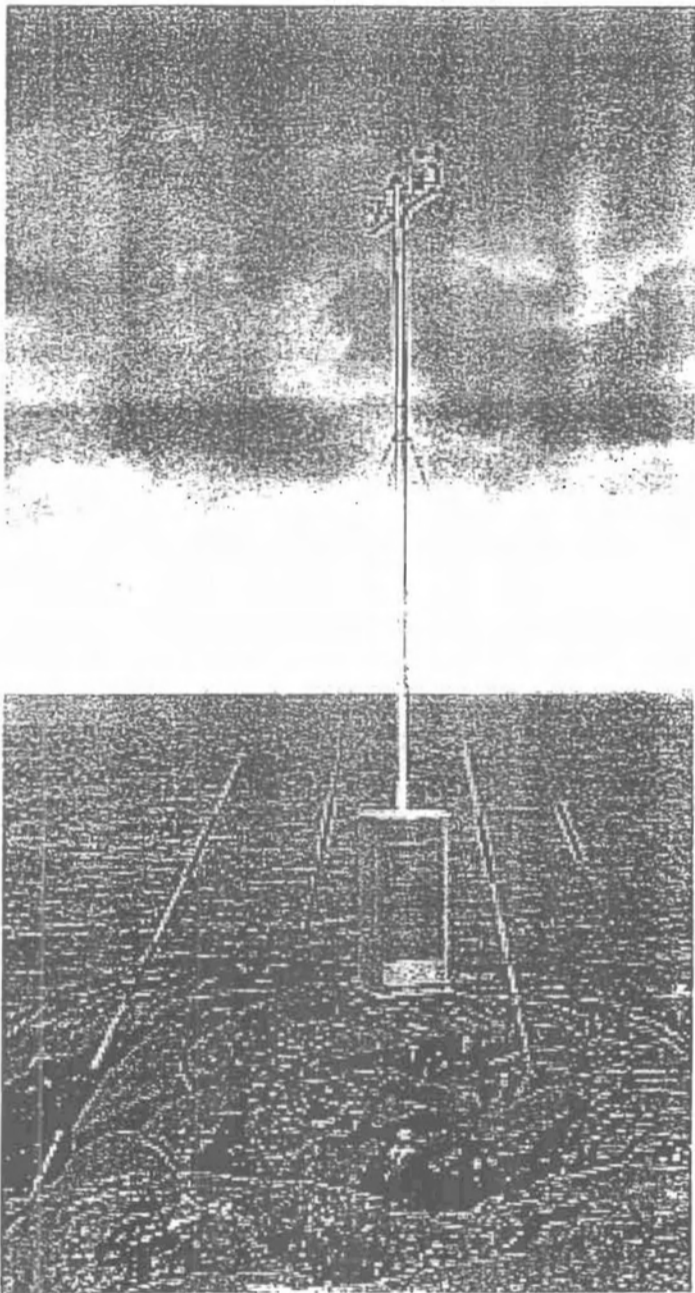
Figure 4.2.2.1 Aanderaa weather mast was used for collection of meteorological data at KMFRI (Tudor Creek).

4.3 MEASUREMENTS AND TREATMENT OF RAW DATA

4.3.1 Scope of measurements, available data and sampling schedules

The measurements included continuous recording of water heights (sea level measurements) and current measurements using the portable tide gauges and current meter (RCM) and the salinity device mentioned in Section 4.2. Spatial surveys included hydrographic measurements, salinity and temperature, nutrients, transparency and morpho-bathymetric surveys. In addition to the measurements data sets already available, and used in the thesis, include oceanographic data from recent cruises in Kenya offshore waters as earlier suggested and oceanic sea level data sets from three GLOSS-stations in the East Africa Bight. The meteorological data include continuous measurements using the Aanderaa weather mast described earlier and the available meteorological data sets from Kenya Meteorological Department. The data includes concurrent data as well as past data sets. These data sets are used as a supplement to those from Moi International Airport Meteorological Station (MIAMS). MIAMS was considered as representative station to the three study sites as it is central to Gazi Bay-Kilifi Creek coastal zone. MIAMS gives monthly mean values based on the arithmetic means of daily observations at 0600 and 1200hrs. Data from other relevant stations is cited as well. The measurements campaigns are made and data sets used in the in the context of the inter-monsoon long rain (IMLR season), the southeast monsoon (SEM season), the inter-monsoon short rain (IMSR season) and the northeast monsoon (NEM season). The schedule and activities for the measurement campaigns from 1994-99 are shown in Table 4.3.1.1. Measurements for each parameter are described in details in the caption.

87

Measurement from the weather mast, data from other coastal stations and the hydrographic surveys for each study site, the offshore oceanographic data and GLOSS sea level data sets are described. Some examples of raw data given are given in this section.

4.3.1.1 Field campaign- schedule for measurements and data assembling

In Table 4.3.1.1 focus has been given on the times during which observations were done. The real content of the observations is selective and does not indicate schedules in which equipment failed to work or so. Caution was exercised in identifying the locations for RCM and tide gauges in order to enhance security or minimize interference from fishermen. Each of these measurements is described below in separate headings.

Table 4.3.1.1. Dates, instrument and activity schedule for field measurements

	NEM				IMLR		SEM				IMSR	
	12	1	2	3	4	5	6	7	8	9	10	11
1994	GT/Micro, 22/12 ;22/1/95						TMicro-25-30 11, RCM				10-30/10	
1995	GSTN,R,PCM:3-4/1, 10-11/2 G/T-Micro 17th/3 ⇒ TSTN, PCM: 12-14/1, 2-4/3 KSTN, PCM:20-21/1,24-26/2				GSTN: 8-10 5 TSTN:22-24/5 KSTN:29-30 PCM		GSTN:6-7 7-11-14 8 ,TSTN 13- 14/7-17-18/9. KSTN:20-21.7-20- 26/8⇒G-T-Micro 22/6⇒24 7. 1⇒30/9, PCM				GSTN-7-8 9 TSTN:16-17/9 KSTN:23-24 9	
	ZML-TG & MD ⇒											
1996	GSTN:8-9/1-10-11/2 TSTN:17/2-7-8/3 KSTN-26-28/1, 15-17/2, 1-4/3, Micro-Calibrations				KSTN:19-29/5 KSTN:14/5 GSTN:3-4/5 TSTN:12-13/5 (PCM)		T-WM 14/6 ⇒⇒26 /8 GST:3-4/7,8-9/8 TSTN:10-11/7, 17-18/8 (PCM) TG & RCM-MTWAPA CREEK TG & RCM-BAMBURI LAGOON				GSTN:4-6/10 TSTN:11-12 10 KSTN:25-26/10	
	ZML-TG & MD ⇒											
1997	GSTN: 3-4/1, 9-10/2 TSTN:11-12/1, 17-18/3 KSTN:17-18/1, 26-27/3				GSTN:7-8/5 TSTN:15-16/5 KSTN:23-24/5		KRCM 11⇒17/7⇒ KSTN GST:4-5/7, 10-12/9 TSTN:13-14/7, 20-21 8				TST:8-9	
	ZML-TG & MD ⇒											
1998							T-MT 30/10-7/11					
	ZML-TG & MD ⇒											
1999							G-MT 25-30 9, GST					
	ZML-TG & MD ⇒											

Key: NEM: Northeast monsoon period, IMLR: Inter-monsoon long rain period. SEM: Southeast monsoon period and IMSR-Inter-monsoon short rain period. 1-12: months, and date e.g. 25/5 means 25th May RS-River station, GSTN-Gazi salinity temperature and nutrient measurements, TSTN-Tudor salinity temperature and nutrient measurements;

KSTN-Kilifi salinity temperature and nutrient measurements, RCM-current meter, PCM-Pendulum current meter. WM- weather mast. G T K-Micro-Gazi and Tudor Micro-tide deployment, ZML-TG: MD-Meteorological data from coastal stations. Zanzibar-Mombasa -Lamu tide gauges, D-Drifters.

4.3.1.2 Weather mast measurements

The first weather mast data were obtained for a period of 80 days (14 June- 28 August 1996, at the KMFRI station in Tudor Creek. Some of the records were not good for the period 9-28 August 1996. Some of the raw data records are shown for the period from 14 June- 8 August 1986 in Figures 4.3.1.1a-d, and include (a) wind speed (b) wind direction, (c) air pressure and (d) air temperature. Other meteorological data is taken up in detail from these records are presented in Section 5.2.2 together with theoretically computed radiation and turbulent fluxes.
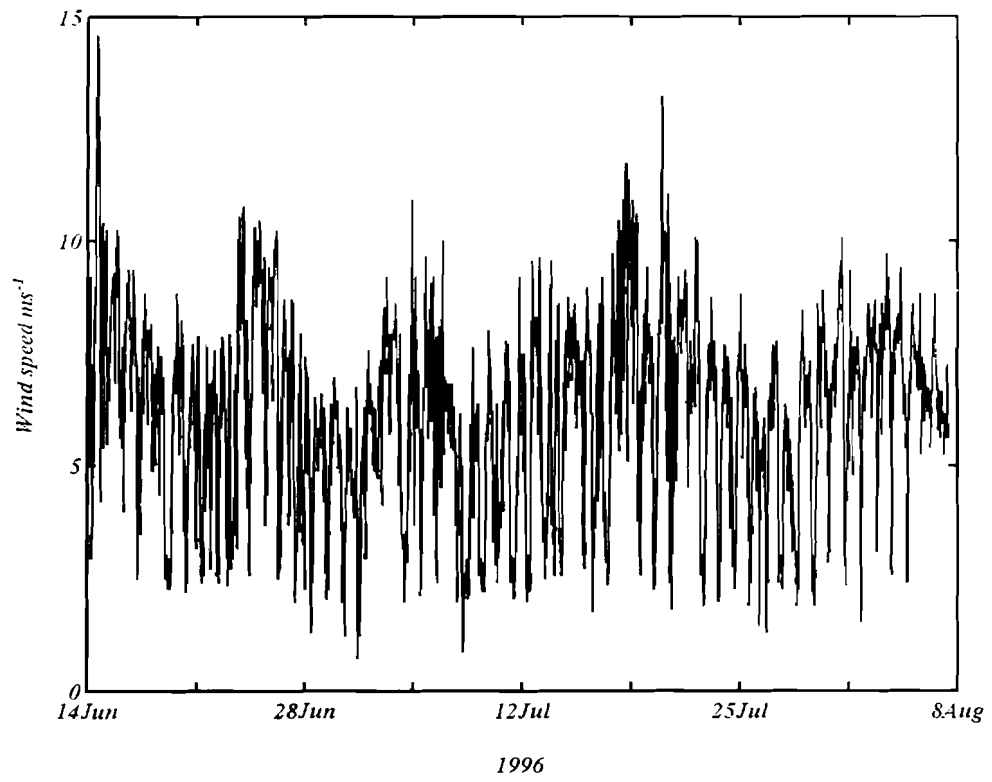
Figure 4.3.1.1a Wind speed from the weather station for the period 14 June to 8
August 1996.
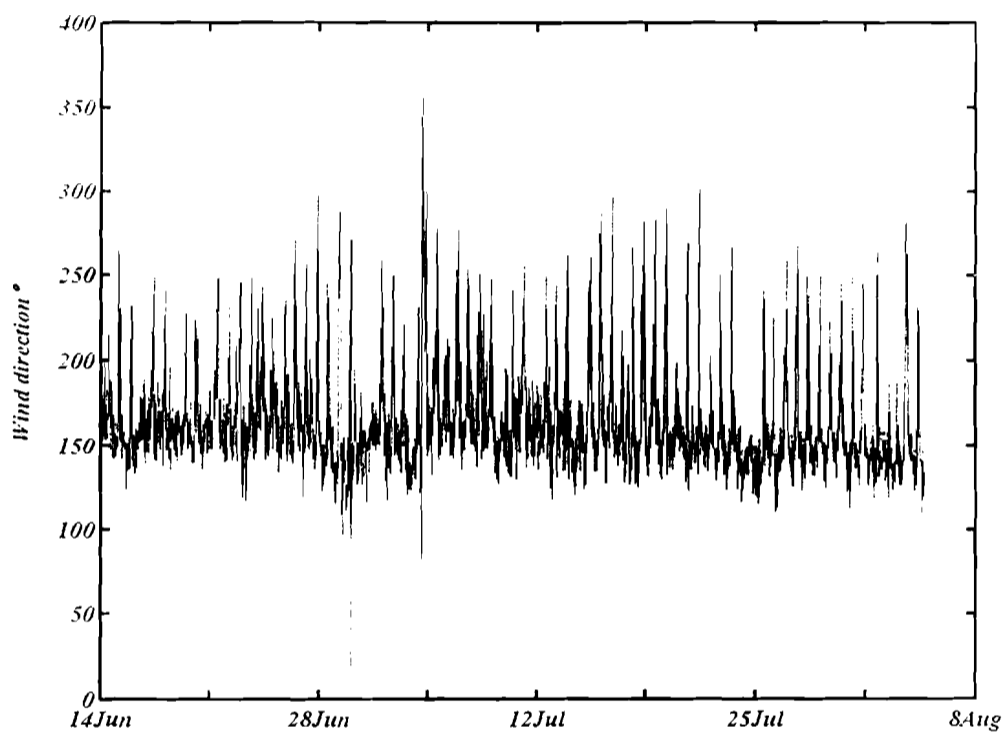
Figure 4.3.1.1b Wind direction from the weather station for the period 14 June - 8 August 1996.
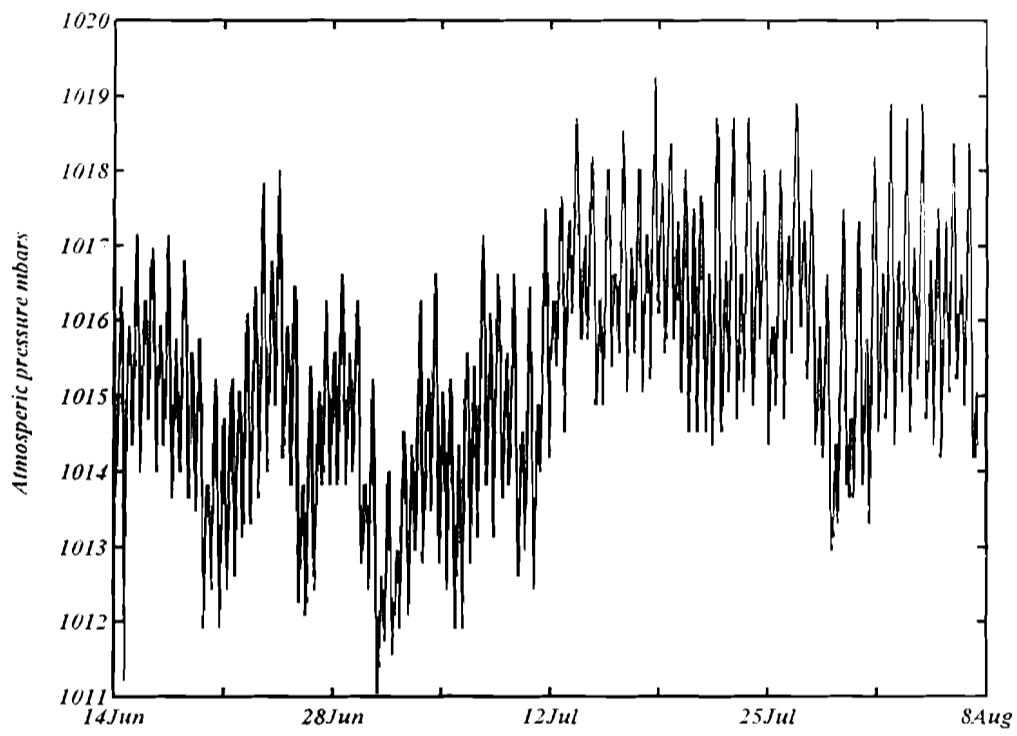
Figure 4.3.1.1c Air pressure measurements from the weather station for the period 14 June - 8 August 1999.
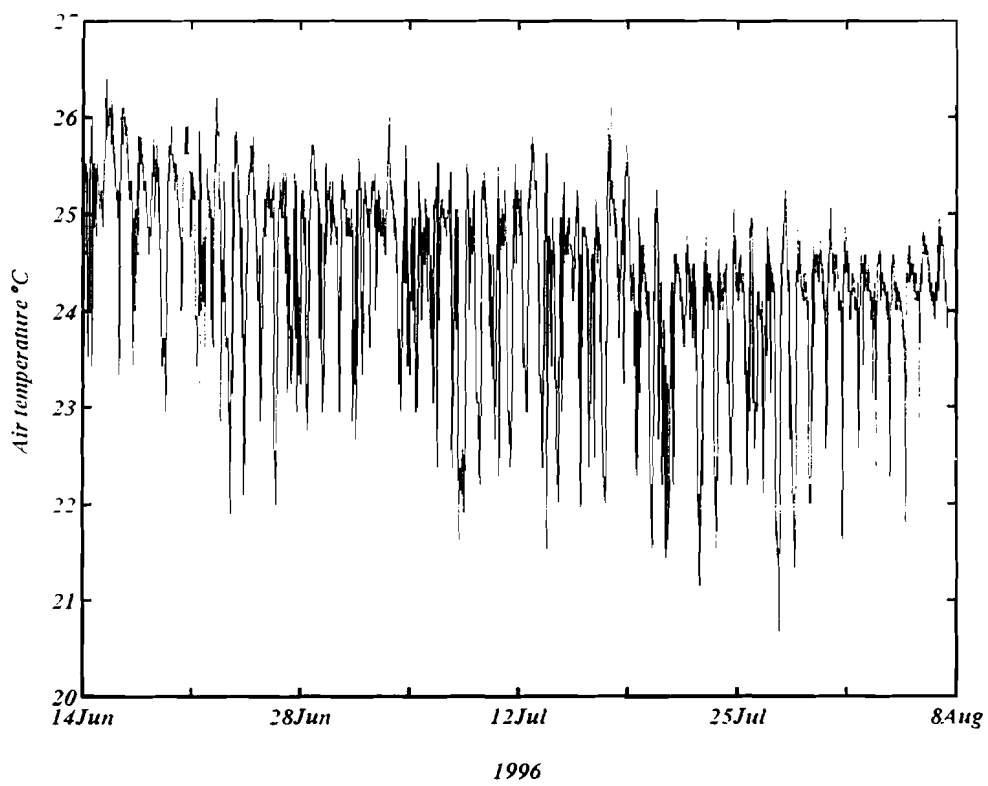
Figure 4.3.1.1d Air temperature from the weather station for the period 14 June - 8 August 1996.

4.3.1.3 Data from MIAMS and other coastal stations

In addition to MIAMS data that include monthly means of rainfall and evaporation for the duration (1994-1998), data from other relevant stations that include monthly means rainfall, evaporation and air-temperature is used. These include data set from Shimoni (41yrs), Musabweni for 19955-1998(43yrs), Ramisi for 1966-1998(32yrs), Kikoneni for 1972-1998 (26yrs) and Shimba Hills for 1975-1998 (23yrs), as well as for Malindi Airport for 1962- 1998 (36yrs). Records of measurements for 1994-1998 of the monthly average air pressure, wind, humidity, precipitation and air-temperature and evaporation; are further analysed and presented in Section 5.2.1.3 and 5.2.1.4.

4.3.1.4 River discharge, catchment- surface areas and bathymetry

In Gazi Bay the two main rivers are the Mkurumuji and the Kidogweni (Figure 4.3.1.4a). In Tudor Creek, there are the Kombeni and Tsalu Rivers (Figure 4.3.1.4b), and in Kilifi Creek, the Ndzovuni and the Vitengeni Rivers (Figure 4.3.1.4c). Of the rivers mentioned, only Mkurumuji River is gauged and has a sufficiently long observation period (covering 1967-1987) to be used for establishing relationships between rainfall, catchment area and river discharge. The average monthly discharge of the Mkurumuji River is shown in Table 4.3.2a. This is the only way by which discharge into the various study sites can be calculated for the years 1994-1998, when the rivers were gauged. The surface area of each study site was determined form resource maps and admiralty charts. The maps of the creeks were drawn to scale from topographic map (East Africa 1:50,000; Sheet 201/1, Series Y731, Edition 5-SK, 1973) and subdivided into small squares which were the counted off.
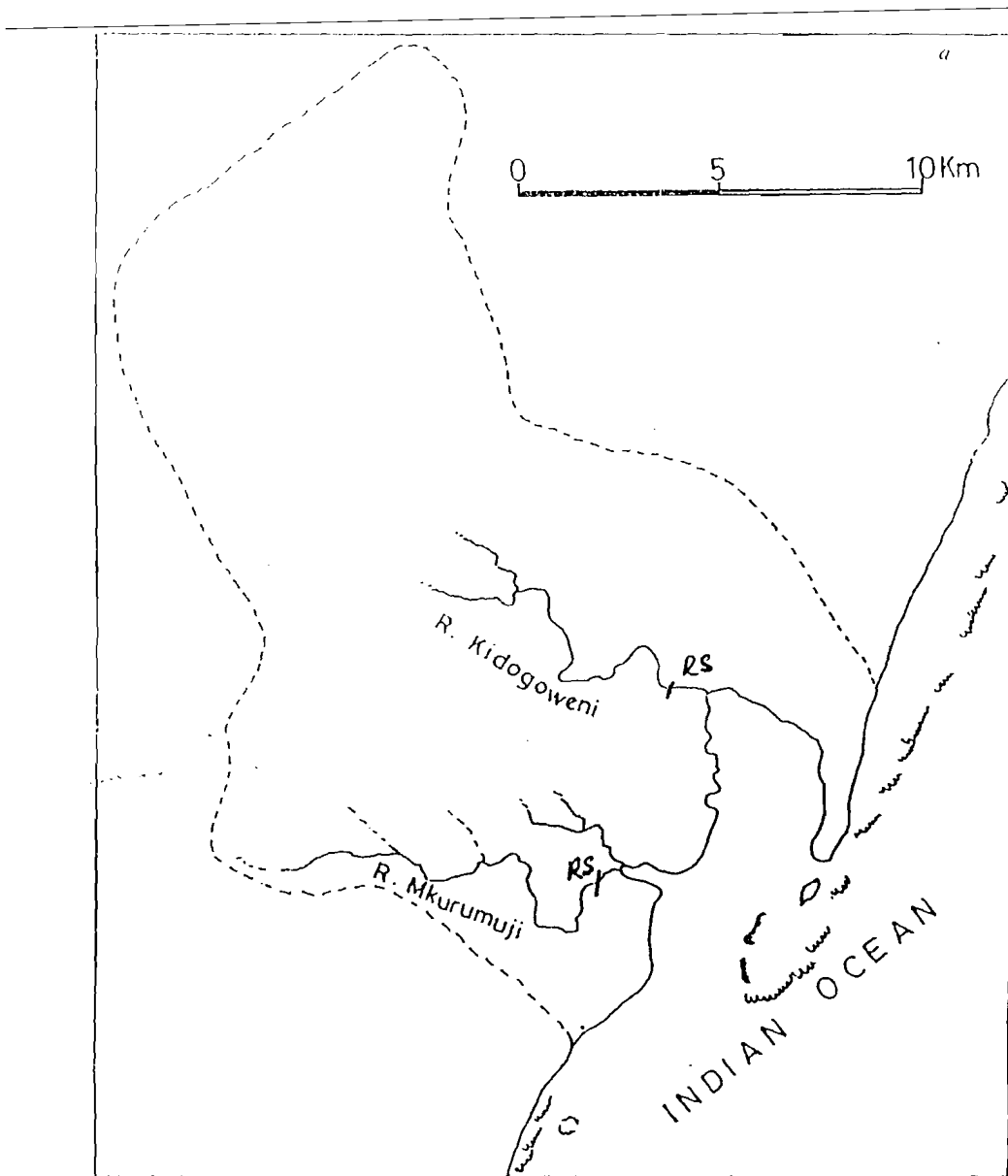
Figure 4.3.1.4a The catchment area (dotted lines) and rivers draining into Gazi Bay.
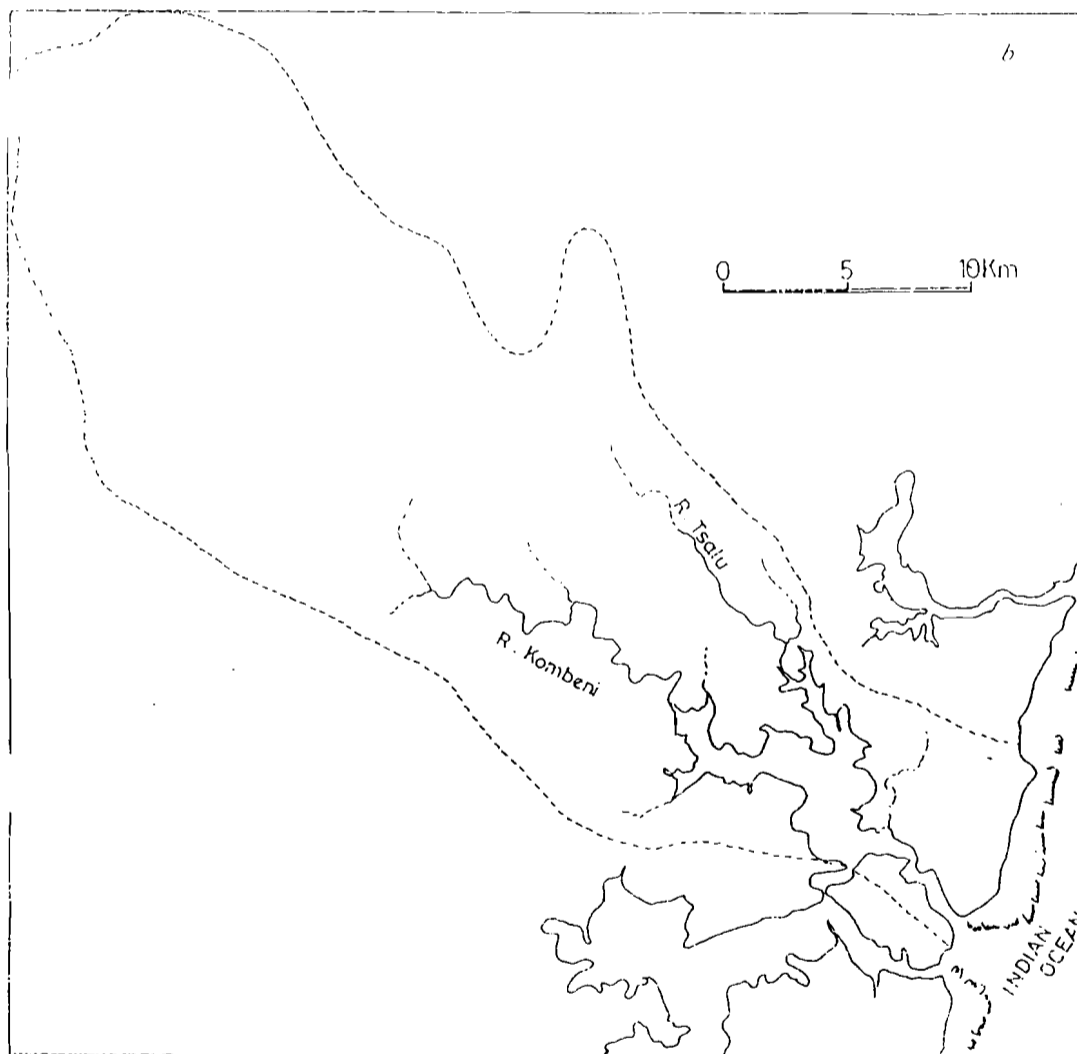
Figure 4.3.1.4b The catchment area (dotted lines) and rivers draining into Tudor

Creek.
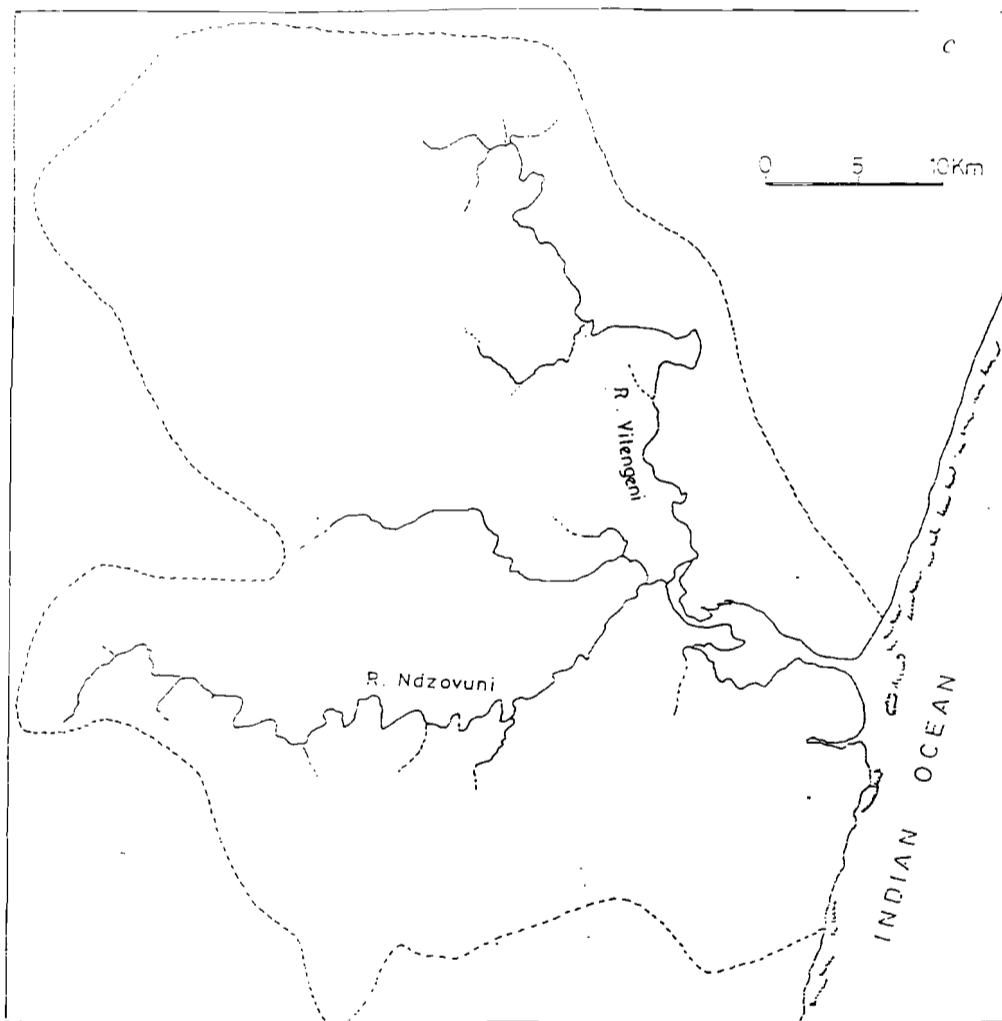
Figure 4.3.1.4c The catchment area (dotted lines) and rivers draining into Kilifi

Creek.

4.3.2 Hydrographic data of Gazi Bay

In Gazi Bay ventilation of the mangrove area occurs through the Kidogweni and Kinondo Creeks (see Figure 4.1.1.1). Kidogweni Creek was used for observations because it receives discharge from Kidogweni River. Hydrographic observations and bathymetric surveys were carried out during HWS, in five stations along the bay (Figure 4.1.1.1) using small boat. Stations II and I, both with a depth of about 5m, were located in the Kidogweni Creek. Station III and IV were located in the upper part of the bay and the mid- section of the bay respectively. Station V was located near the mouth of Mkurumuji River. The more oceanic stations VI and VII were located at the entrance and off the bay respectively (see Figure 4.1.1.1).

Pendulum and position of the current meter and the tide gauges deployments are shown in Figure 4.1.1.1 as locations marked MT1, MT2, MT3, RCM and PCM. Dates of measurements are given in Table 4.3.1.1. Each of these measurements is considered in Section 4.3.2.1. We describe the observations in some detail below.

4.3.2.1 Temperature and salinity measurements

Salinity and temperature were measured with the ST-sensor, at the surface, mid-depth and at the bottom three times in each monsoon season at stations I-VII. Sequential measurements were made at Stn IV where the cross-section was situated. We used a small speedboat with an outboard engine for sampling. It took us about 2 hours to cross the bay from the entrance of the bay to Kidogweni River including stops and sampling. These runs were carried out at spring and neap tides and during wet and dry seasons. Thus run started one hour before either high or low water at the channel entrance, and ended one hour after in the upper reaches of the Kindogweni.

A full 24 hours time series of salinity and temperature measurements was obtained during 1999, near the location of the RCM with a ST- sensor. Two examples of continuous temperature record obtained from tide-gauges located at MT2, and the RCM near the mouth of Mkurumuji River is shown in Figures 4.3.2.1a and 4.3.2.1b where the three panels show axis with (a) number of observation (b) days and (a) the actual dates of observation. Detail results of the temperature time series are taken up Section 5.3.1.1.
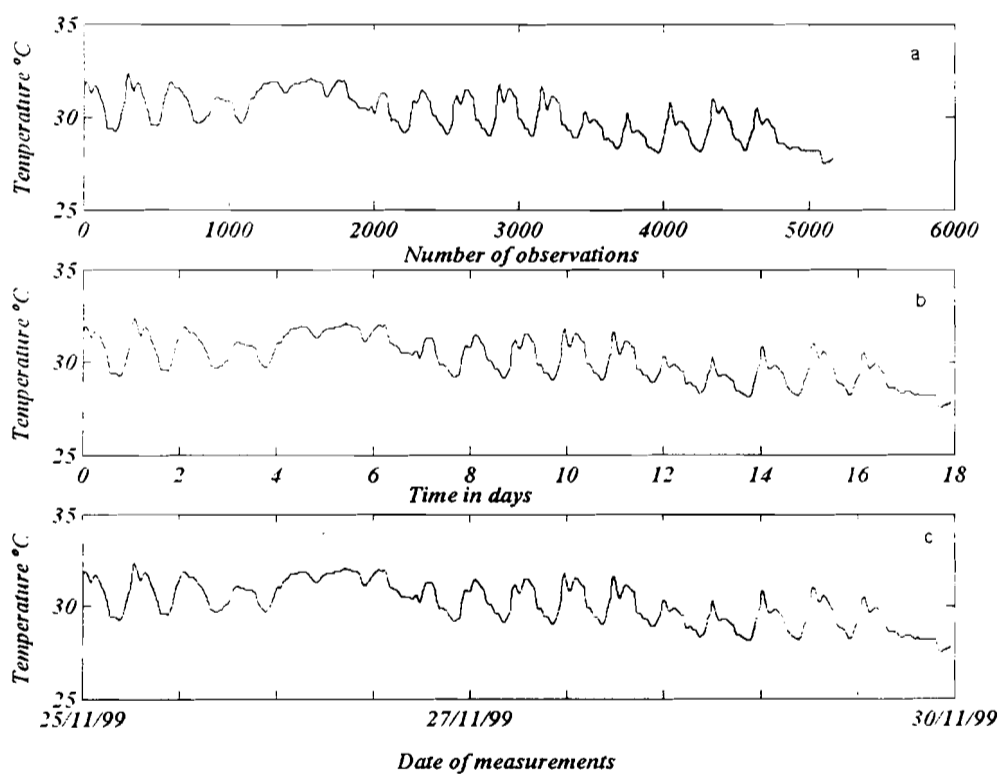
Figure 4.3.2.1a Example of continuous sea temperature measured at station (MT2) in Gazi Bay showing panel (a) temperature vs number of observation, panel (b) vs number of days panel (c) vs actual dates.
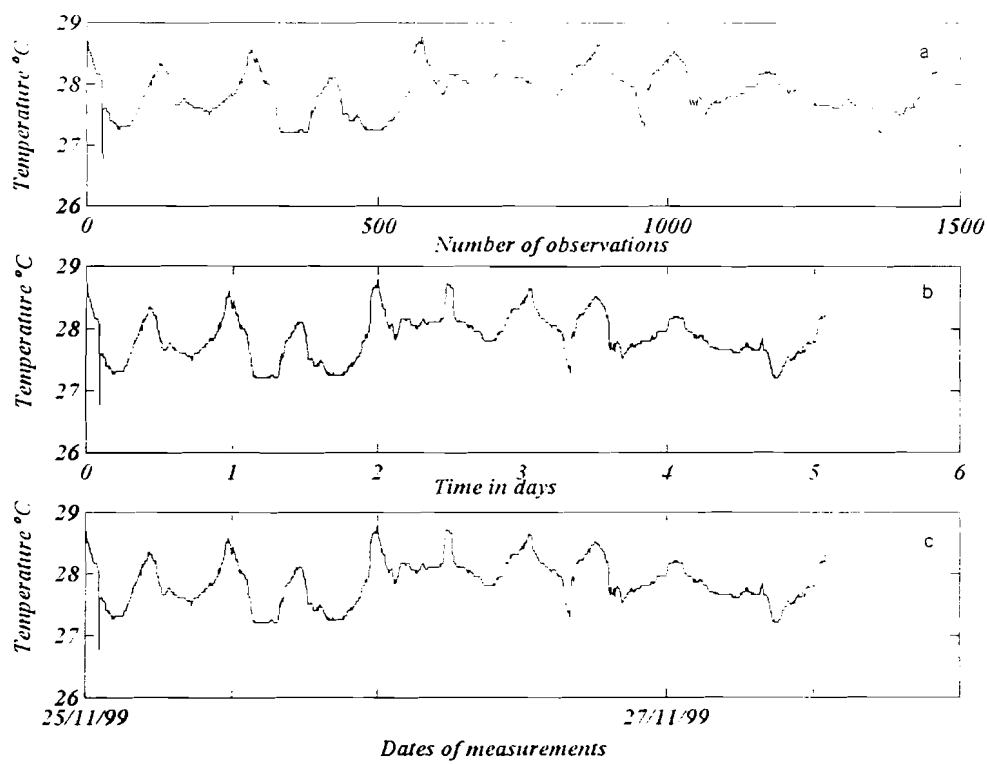
Figure 4.3.2.1b An example of continuous record of sea temperature measured by RCM near station MT2 in Gazi Bay showing panel (a) temperature vs number of observation, panel (b) vs number of days panel (c) vs actual dates.

4.3.2.2 Recording current measurements

Current measurements were also carried out using the Recording current meter (RCM), in the mid-channel area, near station IV from 11 November to 24 December 1999. A nylon rope to a 25-kg concrete block, using a submerged buoy, secured the deployed. Earlier longer deployments of mooring equipment were repeatedly unsuccessful due to logistics problems. Interference by fishermen with frequent loss of equipment but also instrument failures and seaweed in the rotor resulted in few good measurements in comparison with the larger efforts that were put in. An example of the raw data from the current meter showing the number of observations and magnitude of the current speed is shown (Figures 4.3.2.2). The current speed and direction are further analyzed in Chapter 5.
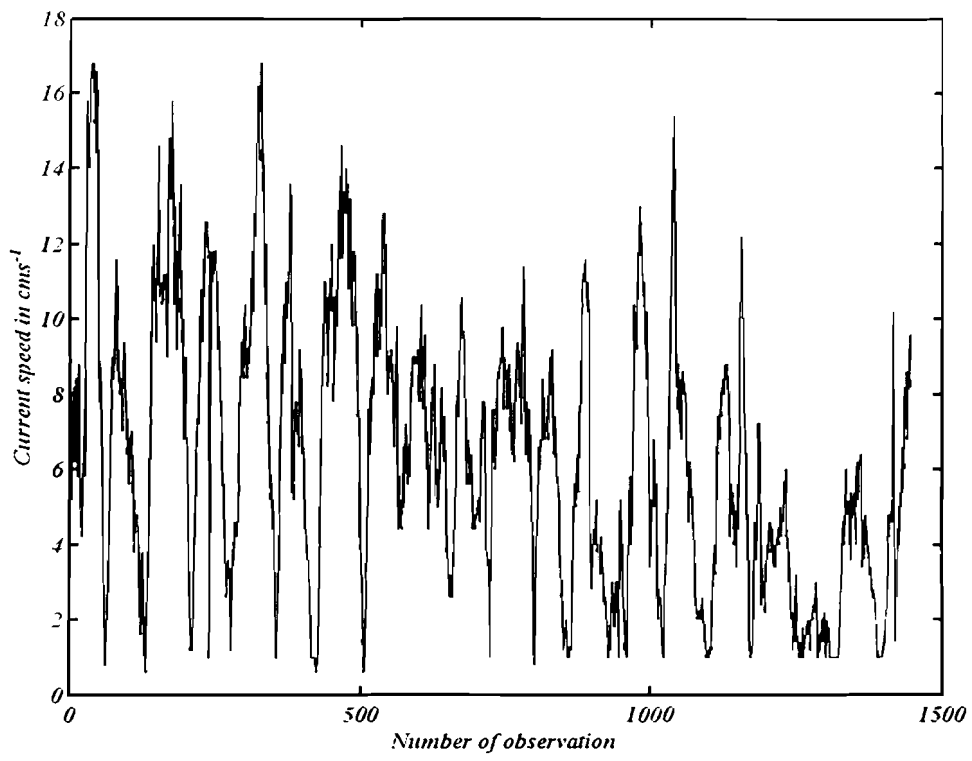
Figure 4.3.2.2 Current record measurements in Gazi Bay (location RCM, Figure
4.1.1.1) for 5 days period between 25-30 November 1999; 1500 observations at 5 min
interval.

4.3.2.3 Pendulum current measurements

Pendulum current meters were deployed along cross-section near KMFRI before high water. For the observations with PCM's, 2-5 pendulums were deployed depending on the total depth. For example, in the channel where the total depth was 10m, the pendulums were deployed and spaced at 1.5, 2.5, 4, 6.5, 9 meters. After 45 minutes the gelatin coagulated and the direction and the inclination was determined and current velocities read off a calibration graph. The cross-section drawn to scale using a combination of our own observation and chart data was used to obtain mean velocity perpendicular the section. Sub-divisions were made corresponding to the number of PCMs used. The expression given in Section 4.4.1.1 was then used to calculate the velocity perpendicular to the assigned area.

4.3.2.4 Sea level time series measurements

Tide gauges were deployed in Gazi Bay at stations MT1, MT2 and MT3 (Figure 4.1.1.1) during November 1999. The tide gauges were attached to a metal plate weighing about 25 kg. A diver placed them at convenient reef locations MT3 or hid them carefully in seaweed beds (MT1-2), to avoid thefts, which, during the earlier attempts, were a serious problem. The aim was to have a one-month series from all three tide gauges. However, the gauges worked for different duration, giving some short and some longer data sets. Two tide gauges were place in the Kidogweni Creek and the entrance channel at MT2 respectively and set to record simultaneously. MT1 had unreliable sea level data record, and therefore not used. MT2 worked from 11-30 November 1999. and good data set was available for 18 days, thus covering neap-spring period for both tide gauges. The

third gauge was deployed on the reef at MT3, however, the gauge was stolen but we got

it back. An example of sea level measurements (5min interval) is shown in Figure

4.3.2.3 in three panels. Panel (a) is the total untreated record and panel (b) and panel (c)

are treated. Statistical analysis, as well as harmonic and spectral analysis is presented in

Section 5.3.1.2, 5.4.1.2 and 5.4.1.2.
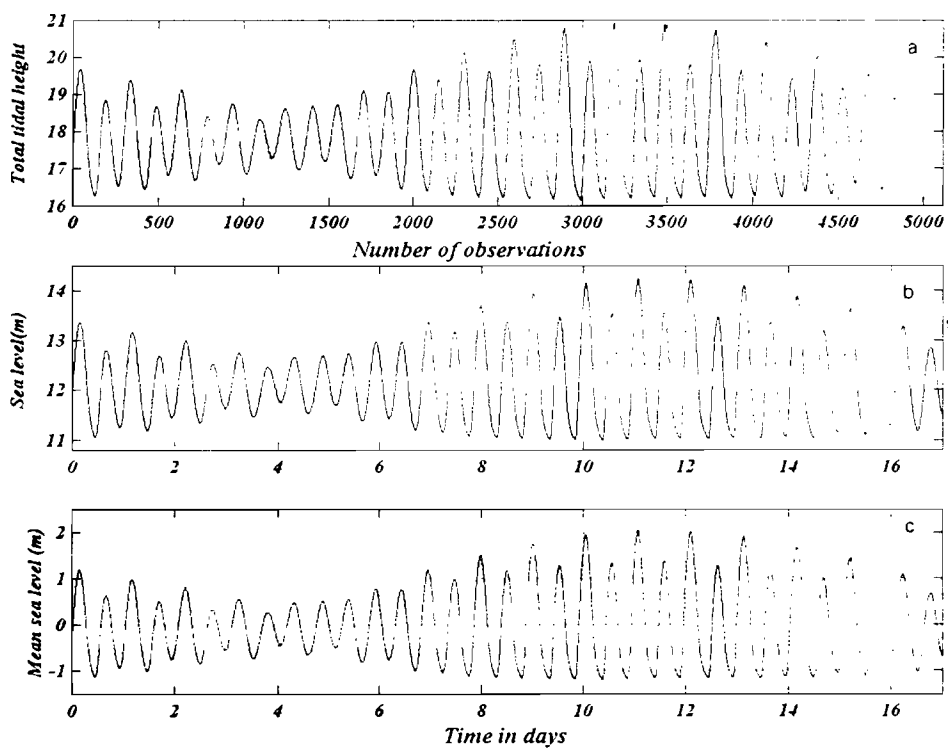
Figure 4.3.2.3 Example of sea level measurements carried on 13-30 November 1999 showing (panel (a)) raw record of sea level uncorrected for air pressure for 5000 observations at 5min interval for positions MT2 near Mkurumuji River. Note the amplitude rage 16-21m in panel (a). Panel (b) and panel (c) are treated records (see Chapter 5).

4.3.2.5 Nutrient measurements

Surface water samples were collected at stations I and V. They were stored in 250ml Nansen bottles and transported to the KMFRI laboratory for nutrient analysis. The analysis involved the determination of the concentrations of dissolved inorganic nutrients (nitrate-nitrite and phosphate) according to the methods of Parsons et al. (1984), or by the same methods but minor modifications (Ohowa at al., 1997) for use with a Technicon Autoanalyser II system. The measurement coincided with another project measuring the same parameters albeit more intensely. Basically, observations were carried out together with the ST-sensor campaigns from 1995-1997.

4.3.3 Hydrographic measurements in Tudor Creek

4.3.3.1 Spatial and temporal temperature and salinity

Tudor Creek has two main channels that are coupled to the Kombeni and Tsalu rivers. The larger Kombeni Creek or (channel) was selected for the study of salinity and temperature variability. Six stations were established, including cross-sections at Stn III and IV (Figure 4.1.2.1). Profiling measurements were carried out twice, with ST-sensor approximately twice during each monsoon stage from September 1995 to October 1999. Measurements were carried out using a speedboat during high and low slack water, usually from surface to bottom. Occasional measurements were made across the creek to ensure sufficient covering particularly where there were bends. Monthly mean temperature and salinity data are presented in Section 5.4.1.1.

Time series measurements of temperature and salinity were obtained concurrently with the meteorological measurements (see Section 4.2.1.1) by connecting a ST-sensor to

the weather mast. Temperature was also measured using three tide gauges as shown in the locations (Figure 4.1.2.1). That is at the entrance MT1, mid-reaches of the creek (near the old KMC) at position marked MT2 and in the upper reaches of the creek (Jomvu Kuu, MT4). An example of the creek temperature record in the three locations is shown in Figure 4.3.3.1 for data collected on 2-26 October 1998.

(Spatial salinity and temperature are shown in Table 4.3.3.2).
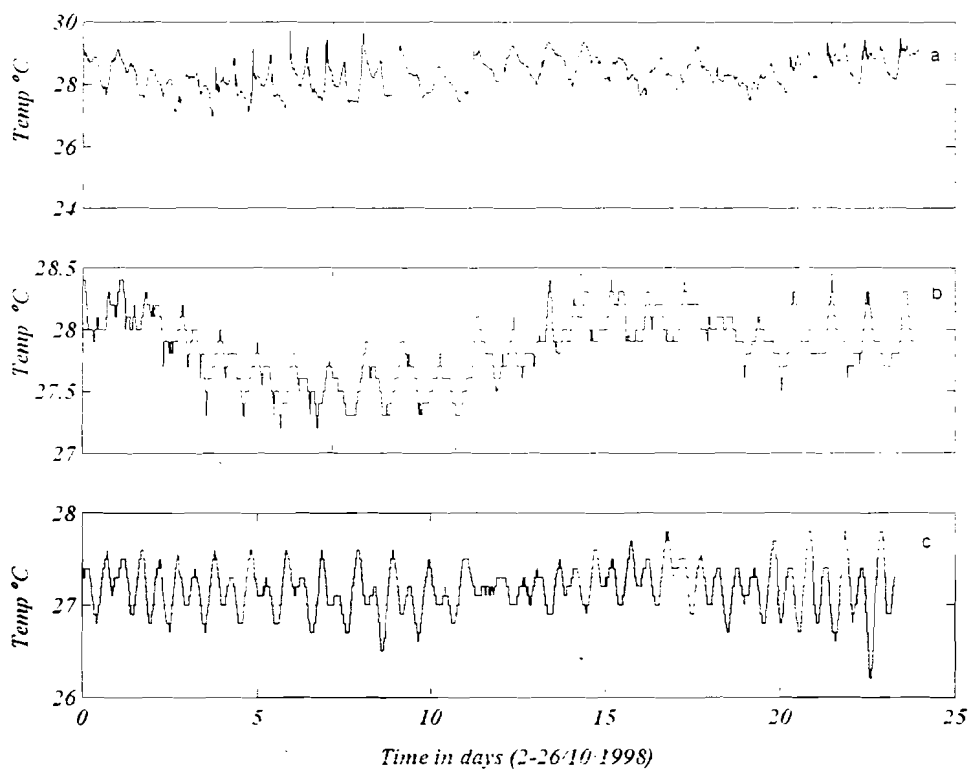
Figure 4.3.3.1 Example of creek temperature record. Panel (a) in the upper reaches of Tudor Creek (Jomvu Kuu MT4) panel (b) in the mind-reaches (near old KMC, MT2) and at the entrance (ocean) MT1 measured 2-26 October 1998.

4.3.3.2 Nutrient measurements

Two sets of three water samples for nitrate, nitrite and phosphate analysis were collected at the surface, mid-depth and near the bottom between station I-III, and VI (Figure 4.1.2.1). The results were averaged to obtain mean values for the inner part of the creek, and for the ocean near the entrance respectively. The mean values are shown in Table 5.4.3.2 together with results from the IMLR of Kazungu, 1989 for comparison.

4.3.3.3 Current measurements

Current meter measurements were carried out near KMFRI at the location indicated as by RCM (see Figure 4.1.2.1) at 10m at a total water depth of 25m. The observation was made from 26 June to 2 August 1996. The record contained 1029 observations, and measurements were carried out at 10minutes interval. Part of the time series measurements is shown in Figure 4.3.3.3. More processed records in sections 5.3.1.3; 5.4.1.3 and 5.5.1.3. Drifters or float drogues were deployed at several locations, during flood and ebb to determine tidal streams and tidal excursions. At flood the drifters were placed at station VI and for ebb in station III. The results are presented in Sections 5.3.1.3, 5.4.1.3 and 5.5.1.3.

The pendulum current meters were deployed along the cross-section VII shown in Figure 4.1.2.1. Measurements were carried out hour before slack water i.e. before the expected maximum ebb or flood velocities.

A procedure for calculating volume flux is given in Section 4.4, for instantaneous volume flux estimates. Worked up results from the PCM are presented in Table 5.3.1.3.

5.4.1.3 and 5.5.1.3 and the same measurements were applied in bottom profile to determination the characteristics of vertical velocity profile (Sections 4.4.6.2 and 5.6).
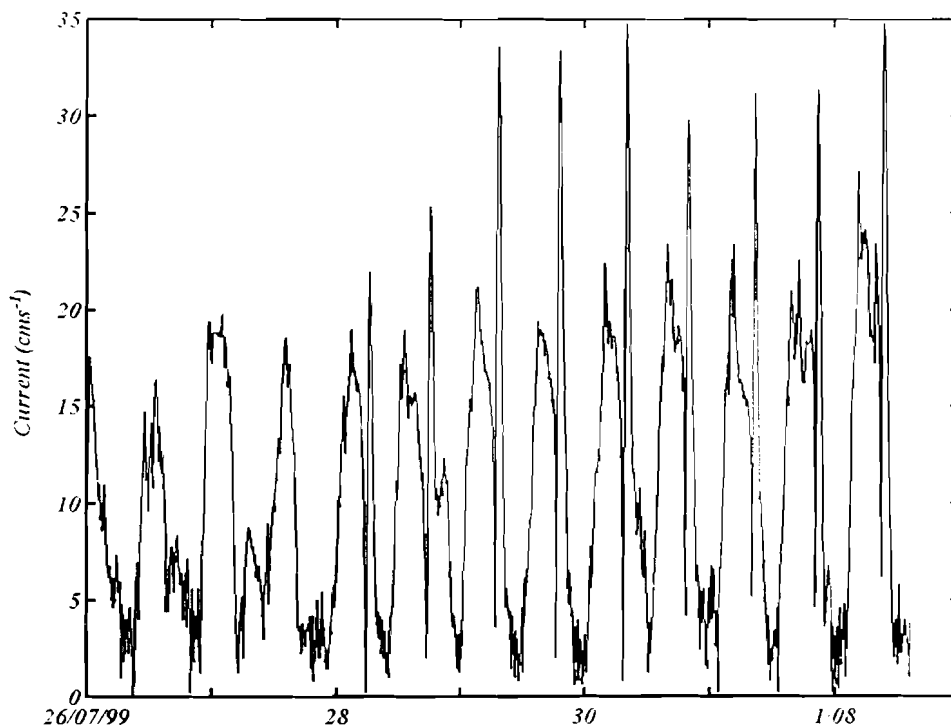
Figure 4.3.3.3 An example of current meter measurements near the KMFRI from 26 July to 2 August 1996. The current meter was placed at in mid-depth position at 10m in a total water depth of 25m.

4.3.3.4 Sea level measurements

The first tide gauge deployment was done at MT1, at the entrance (ocean) to the creek. The second MT2 in Tudor harbor near the old Kenya Meat Commission (KMC), which is in mid-channel position. The third MT3 gauge was placed at Jomvu Kuu, which is the inner end of the creek in January 1993. It was a disaster; thefts implied that the tide gauges at MT2 and MT3 were lost. The third tide gauge at location MT1 was recovered but the data were lost due to instrument corrosion. In November-December 1994 and march-April 1995 more tide gauges were moored at MT1 and at MT2. The raw data is shown in Figure 4.3.3.4a-c. Analyzed data is presented in Sections 5.3.1.2; 5.4.1.3, and 5.5.1.3. These records were ideal for harmonic analysis i.e. extraction of amplitudes and phases as well as for calculation of tidal fluxes which are carried out in Sections 5.3.2.1-2 and in 5.5.3.2.

Later in June 1995, another two tide-gauges were successfully deployed at MT1 and MT4 (Figure 4.4.1.) a position which was repeated in September 1995. In October - November 1998 three tide gauges were successively placed at positions MT1, MT2 and MT3 in an effort to compare the ocean tides with those far up in the estuary they worked successfully. Figure 4.3.3.4 shows, unprocessed sea level measurements for the three successful tide gauges starting at the same time i.e. on 1/10/1998. MT2 worked for 27 days, MT1 and MT3 for 30 days. The corresponding temperature record from the three tide gauges has been referred to in Section 4.3.3.1.
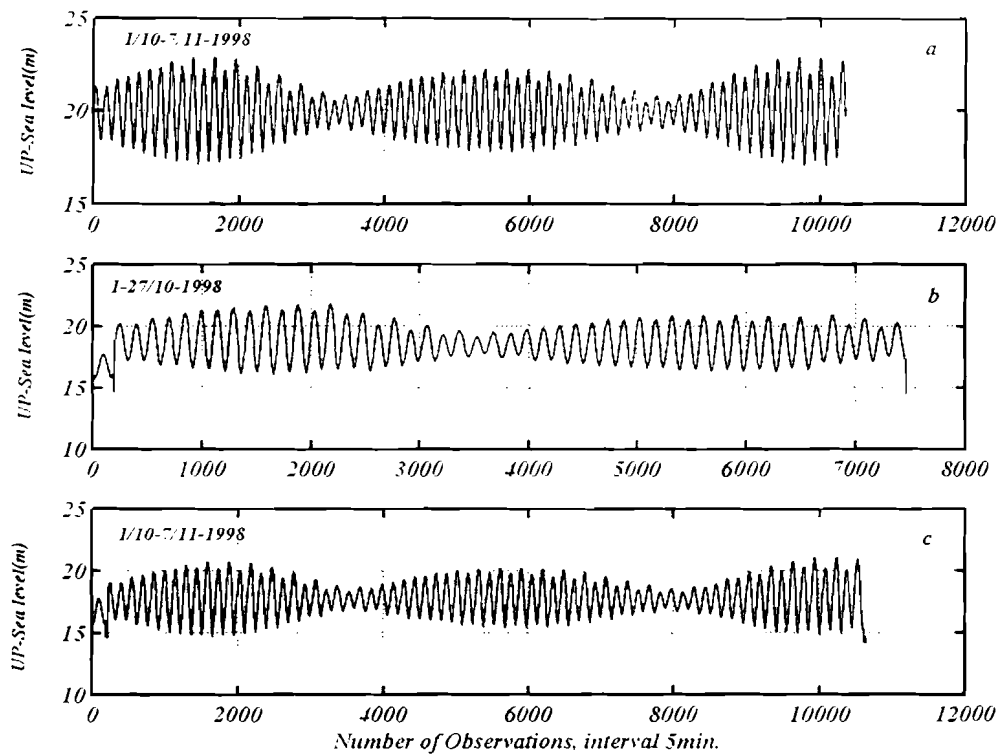
Figure 4.3.3.4 An example of unprocessed (UP) sea measurements carried out in (a) Tudor entrance (MT1), (b) Tudor harbor (MT2). (c) Jomvu Kuu (MT4), showing unprocessed (UP) sea level and the number of observations Oct-Nov 1998.

4.3.4 Hydrographic measurements in Kilifi Creek

4.3.4.1 Salinity and temperature variations

In Kilifi Creek, a lengthwise section with Stations I-VI (see Fig. 4.1.3.1) was selected. Station I is the innermost station, while VI is the ocean ward station. Two cross-sections C-D and G-H were selected, as shown in Figure 4.1.3.1.

Lengthwise salinity and temperature measurements were carried out from 1996-1998 in each four-monsoon stages defined in Section 1. Sampling was done during spring and neap slack water. The data were averaged monthly and station wise to obtain means of surface and bottom salinity and temperature. Mean values were determined for the inner basin, the mid-channel, and the entrance. Oceanic values were obtained from an oceanic station near the study site.
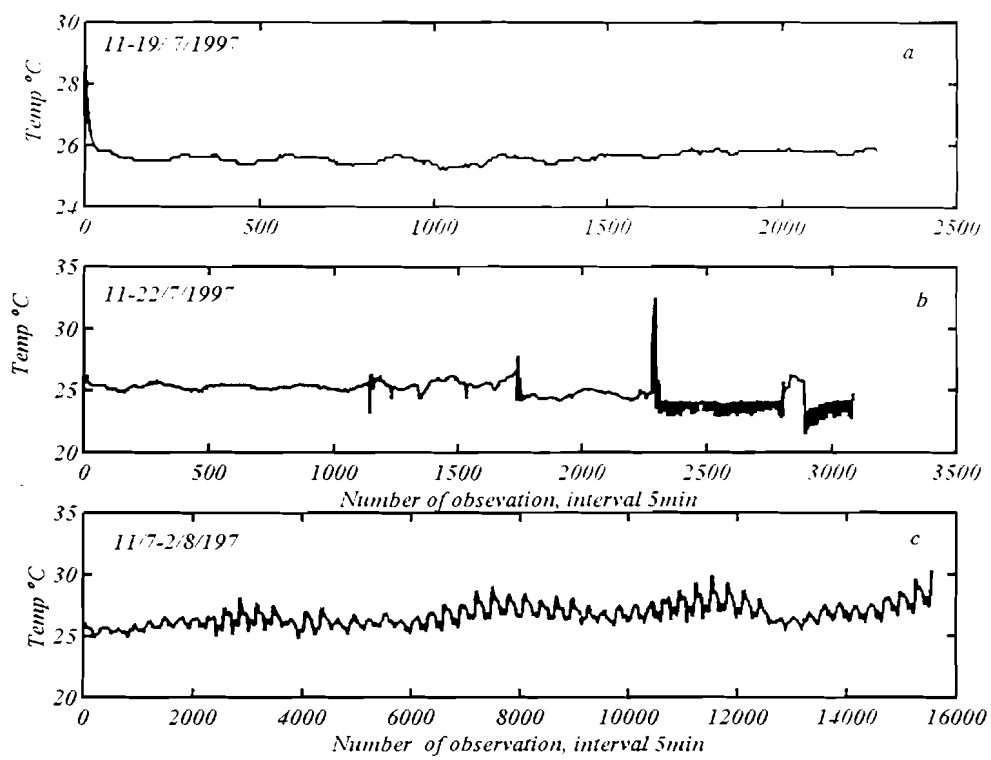
Figure 4.3.4.1 Examples of temperature data recorded for different duration, from the tide gauges and current meter in Kilifi Creek at (a) the entrance (MT1), (b) mid-channel (MT2) and (c) in upper reaches of the creek (MT3). Note data in panel (c) is most reliable.

4.3.4.2 Recording currents meter observations

A current meter deployment was done in the mid-channel area in July 1997. The aim was to collect simultaneous current and tide-gauges data for a period of two weeks. The current meter disappeared however and was not recovered until three months later, after notification by fishermen. It had worked from 11 July to 17 July 1997, and had 1800 observations (Figure 4.3.4.2a). An illustration of raw (300) measurements is shown for 11-12/7 /997 (Figure 4.3.4.2b) together with sea level data for the same period. Results showing record and direction are taken up in Chapter 5.
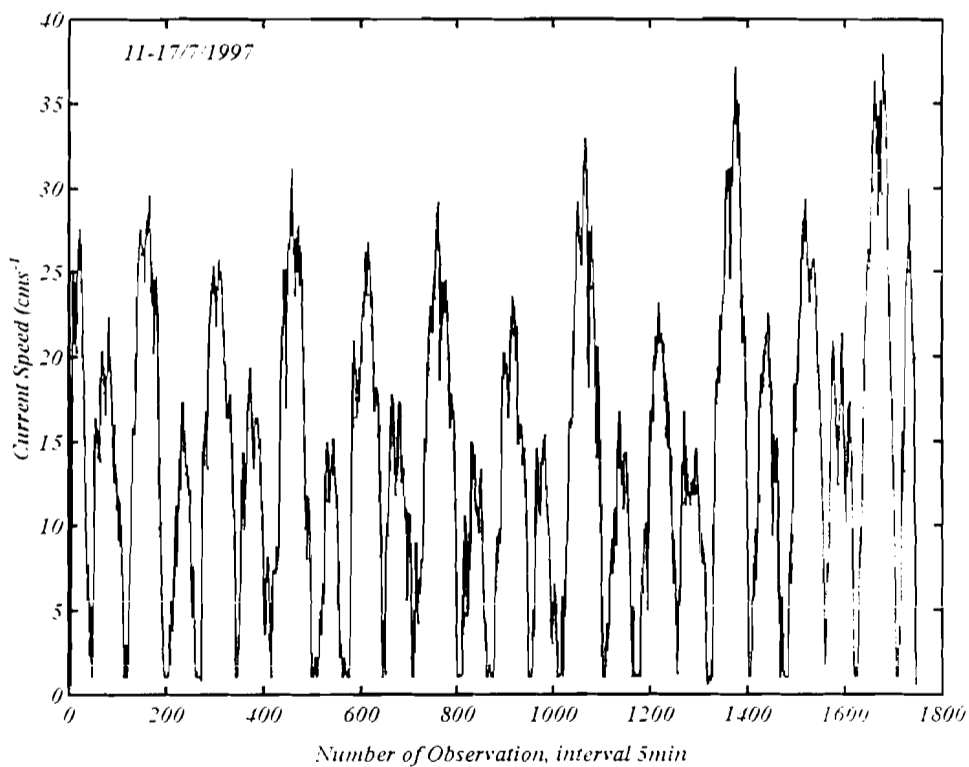
Figure 4.3.4.2a Current measurements (RCM) in mid-channel in Kilifi Creek, 5minutes interval (11-17 July (SEM) 1997).
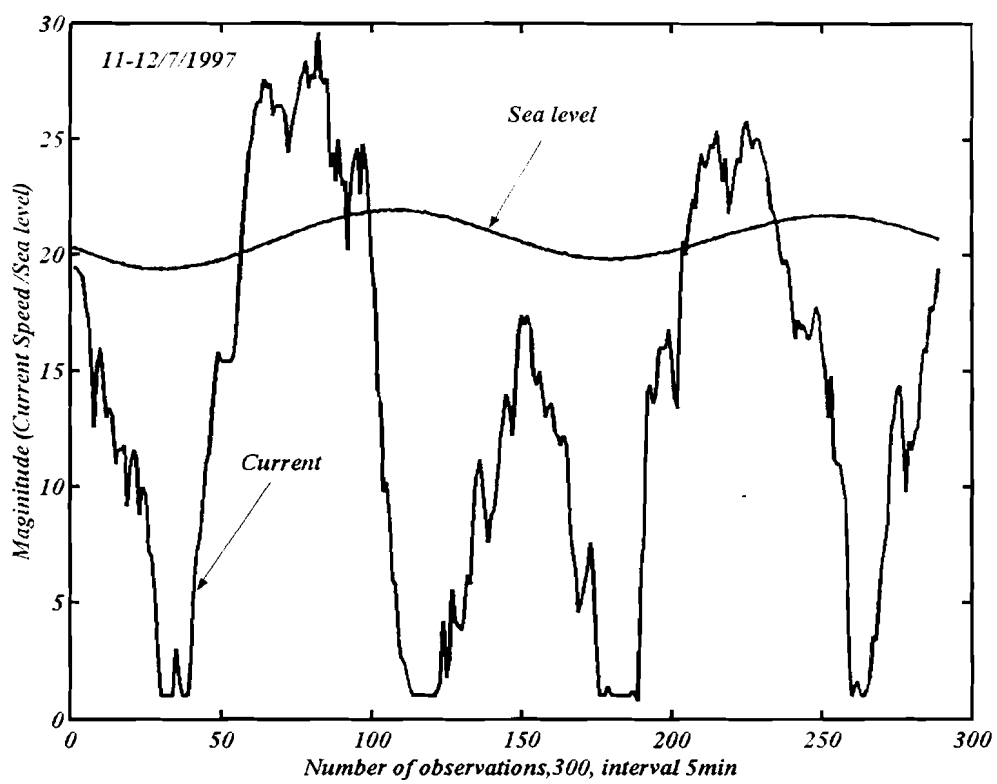
Figure 4.3.4.2b Example of current record plotted with sea level data for 300 observations from mid-channel in Kilifi Creek, 5minutes-interval form 11-12 July (SEM) 1977.

4.3.4.3 Sea level measurements

Three gauges were place at stations MT1-3 as in (Figure 4.1.3.1) in July-August 1997. MT1 was placed near the entrance, MT2 in the mid-channel area and MT3 within the creek. The tide-gauge within the bay worked for 52 days from 11 July-2 August, while MT1 on the oceanic side recorded from 7-22 July. Data from MT2 seemed unreliable; therefore they were not included in the analysis. The raw data from MT3 and MT1 is shown in Figure 4.3.4.3. Statistical and harmonic analysis were performed on the data.
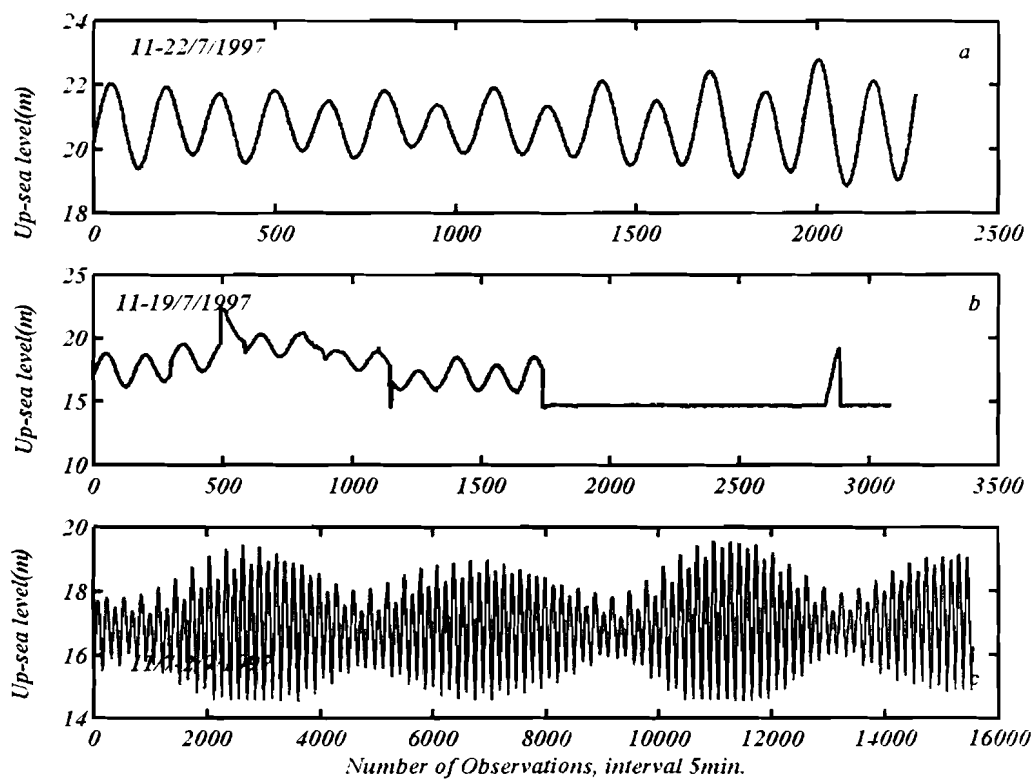
Figure 4.3.4.3 Sea level records from the tide gauge at (a) the location marked MT1, (b) measurements taken at MT2 (c) measurements were taken form 11-21 July 1997.

116

4.3.4.6 Nutrient measurements

Surface water samples were taken at stations II, III, and VI during the dry and wet periods at the time of measuring salinity and temperature (see section 4.3.6.1). They were analyzed for nutrients (nitrate, nitrite and phosphate) using the methods as described earlier. Results are presented in Section 5.

4.3.5 Available oceanographic data

4.3.5.1 Temperature, salinity, and nutrients

To gain more insight into the structure of the water that is exchange between the creeks and the ocean, it was thought advisable to consider the properties of Gazi-Kilifi offshore water. The Gazi-Kilifi offshore water can be considered to extends from the entrance areas of each of the three study sites as far oceanward as the limits of stations shown in Figure 4.1.5.1. These are the stations on transects occupied by R.V.Tyro (1992/1993); R.V.Dr. Fridjof Nansen (1982-85) and M.V.Kusi during the Monsoon Experiment (MONEX) of 1979 (see MONEX report, 1980) and bound south and north by a line drawn perpendicular to the coast 20 km to the north of each entrance. The stations and transects (Figure 4.1.5.1), are essentially those that appear south of Malindi. The oceanographic data include vertical salinity and temperature and nutrient (Silicate, phosphate, Nitrate, Nitrite and Oxygen) from surface to 2000m in some of the stations, particularly those occupied by R.V.Tyro. Since no oceanographic profiles are documented for the shelf or ocean water in this locality, the unpublished data offers superb opportunity for studying the offshore water structure visa vise 'creek-inshore water structure' (see Chapter 5). Data from surface to 300m is considered for salinity and

temperature contours. Data for May-June, and November –December from R.V. Dr. Fridjof Nansen, and mostly data from R.V.Tyro was used for vertical obtaining vertical profiles and water mass properties, particularly for those selected stations with depth up to 2000m (Chapter 6).

4.3.5.2 Oceanic current data

Several vertical profiles giving alongshore and across-shore current component and direction of the main current were measured during cruises by the M.V. Kusi (1979). R.V. Ujuzi also carried out some buoy studies and reported as Anonymous, 1980) and R.V. Tyro, (1992-3) near Tiwi south of Mombasa and close to Gazi Bay.

4.3.5.3 GLOSS Sea level data from Mombasa, Lamu and Zanzibar

Permanent tide gauge stations are measuring sea levels in Kilindini Harbor on the opposite side of Mombasa Island in relation to Tudor Creek, at Lamu about 250km north of Mombasa, and at Zanzibar 350km south of Mombasa. Almost continuously records of sea levels are available from 1994 and onwards. Only a few months of data are missing. In order to determine the seasonality of the sea level in the context of the monsoon forcing, data for the years 1995-1997 was examined. The results are presented in Section 5.4.2.3.

4.4 THEORIES AND ANALYSIS

Several different mechanisms may generate water exchange between the creeks and the ocean. They include, solar radiation, freshwater discharge into the creeks, salinity fluctuations, wind, waves, and tides as well as along shore current or coastal current along the entrance. For example, the tides are responsible for much of the short-term variability in the coastal sea level and currents variability. The variability of the meteorological and hydrographic parameters also affects the circulation. The sun radiation heat the upper layers of the ocean thereby changing the sea levels and affecting the currents, precipitation and evaporation add and remove water and affect both salinity and currents most clearly seen in estuarine circulation.

Changes in salinity and temperature affect the density through the equation of state $\rho = \rho_0(1 + \alpha T + \beta S)$. While density changes in turn affects the pressure force through the hydrostatic equation $P = \rho_0 + \rho g h$. The pressure in turn together with the winds through the equation of motion drives the circulation. Interaction with the surface water mixing create both barotropic and baroclinic motion. Salinity and temperature may vary with season in the offshore waters, thus offshore dynamics may create oceanographic conditions that force or introduce different water types in the creeks. One prominent part of our data analysis will involve offshore water structure determination to discern its seasonal implications on the water exchange or renewal in the creeks.

The outline of the analysis is as follows: In Section 4.4.1, heat budget and fluxes are established.

119

In Section 4.4.2, mechanisms driving water exchange such as fresh water, ambient circulation, and mixing are analysed and expression for volume fluxes and net water exchange given. In Section 4.4.3, water exchange generated by tide forcing is analysed and expressions given for the observed sea level, volume flux and net water exchange. Least square and harmonic analysis methods are also considered. One-dimension friction model for energy dissipation and a method to estimate friction coefficient are examined. Section 4.4.4 takes up flushing time determination. Two expressions one based on total volume flux and another on longitudinal diffusion are analysed.

4.4.1 Heat Budget and fluxes

4.4.1.1 Radiative fluxes

The heat that warms up the creek water usually originates in one way or the other from the sun and the amount of short-wave solar radiation that enters through the sea surface. Whereas the solar energy in the upper atmosphere that hits the surface perpendicular to the incident light is constant and the amount of energy that reaches the surface is possible to calculate if used with latitude and season (see Budyko, 1974). The amount that reaches the sea surface also depends on cloud cover, moistures and particles in the air. Various expressions have been devised (see below), with coefficients to correct for cloud cover. The surface albedo is another important factor, which also varies and influences the amount of solar energy that enters the ocean. However, the warming and cooling that occurs in the water column is a result of net gain or loss of heat energy through the air-water interface including advective gains or loss by the tidal circulation.

To a lesser extent gains and losses through exchanges with the bottom sediments also affect the heat balance of a particular (shallow) area. According to Smith (1985) conservation of heat equation requires:

$$\frac{\Delta H}{\Delta t} = A\left[(Q_S - Q_B) + (Q_H - Q_E) + Q_M + Q_A\right]$$

4.4.1

Where the term $\frac{\Delta H}{\Delta t}$ is the temporal change in total heat (Jm^{-3}) stored in the creek water column, A is the surface area, and QS $(Jm^{-2}s^{-1}$ or $Wm^{-2})$ is solar radiation entering through the sea surface. Q_B is the heat loss by the net outgoing long-wave radiation. Q_E is the net heat less through evaporation (the latent heat flux); Q_H is the sensible heat flux through the sea surface; Q_M is the conductive heat exchange with the sediment. The term Q_A finally represents advection or diffusive heat fluxes (i.e. the exchange of heat with the surrounding). The terms are illustrated in Figure 4.4.1. Fluxes entering the water body are positive while those directed away from it are negative. Sensible heat fluxes may have either direction, whereas Q_M will be omitted in this case.

The radiative fluxes Q_S and Q_B are the ones mostly likely to be changed considerably between the rain and dry seasons as they both vary inversely with cloud cover. They also depend on the sun altitude, which in turn depends on the latitude and season. Gas molecules in some bands also attenuate them e.g. H_2O, O_3 and CO_2 are all-important. There is no insolation at night. They are reflected during an overcast sky, insulating the creeks against radiation energy.

To get the net solar radiation for the insolation entering and thus heating the creek water several corrections need to be applies to the several expressions existing for the calculation of solar radiation (Miller, 1981 and Reed, 1976a, 1978).
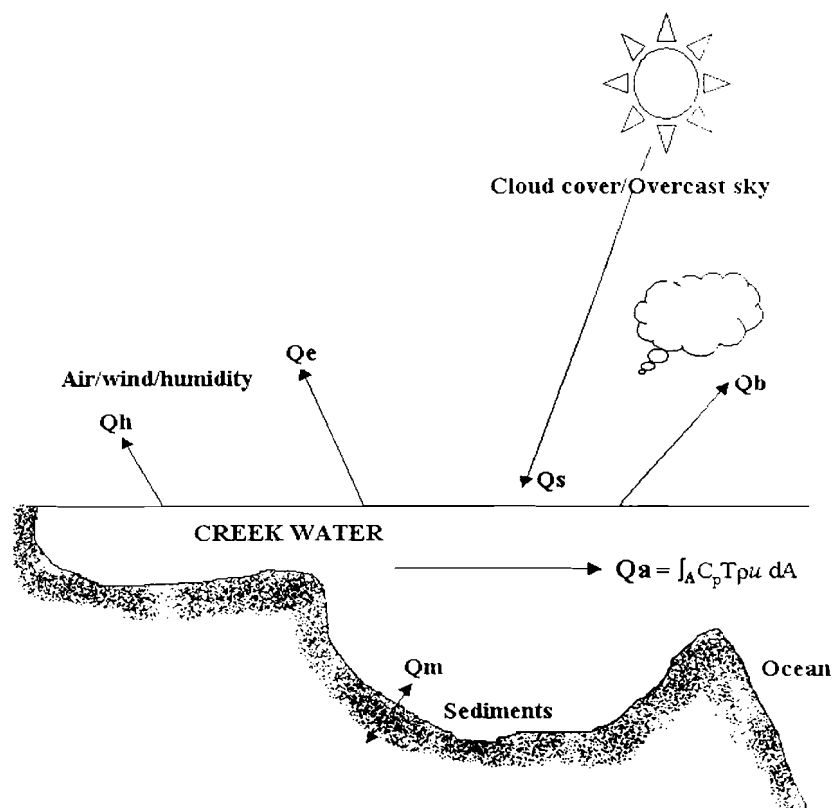
Figure 4.4.1 Schematic of various heat fluxes in the heat balance equation; fluxes entering the water body are positive while those directed away from it are negative.

The expressions require five corrections to the solar constant to account for; seasonal variation in the earth sun distance and the zenith angle at the latitude of study; sun angle, atmospheric turbidity, clouds, and surface reflectivity at the air-sea interface.

Estimate of the net short-wave solar radiation entering through the sea surface, Q_s

The net solar or short wave radiation is measured directly by the weather mast. However, it can be calculated as well. The equation calculating Q_s has been given several different expressions. Following Hill (1982),

$$Q_s = Q_o F (1-A)$$ 4.4.2

Here, Q_o is the clear-sky mean daily insolation, F is a cloud correction factor and; A is the sea surfaces albedo i.e. the ratio of incident to reflected sunlight.

For estimate of Q_o formula suggested by Reed (1977) is used:

$$Q_o = A_o + A_1 cos\phi + B_1 sin\phi + A_2 cos2\phi + B2sin2\phi$$

Where ϕ = (t-21) (2π/365), t is the time in Julian days. For the latitudes 20°S-40°N the coefficients are: A_o = -15.82+326.87cosL, A_1 = 9.63+192.44cos (L+π/2); B1 = -3.27+108.70sinL; A_2 = -0.64+7.80sin (L-π/4); B_2 = -0.50+14.42cos (L-π/36).

Reed (1977), gives F=1-0.62C+0.0019α, where α is the noon solar altitude and is given by $Sin\alpha = sinL sin\delta + cosL cos \delta$ (Mohanty et al., (1966)), L is the latitude of a place (degrees) and δ is the sun declination. δ = 23.87sin (2(t-82)/365 (Castro, 1994), where t is as above.

Q_o was estimated as from the sun radiation observed from the mast the expression given as $Q_oF = Q_s / (1-A)$, where the expression is approximately Q (1+A).

123

Estimates of Q_o shown in section in section 5.2.2.1, where the weather mast data is used

in the calculations and compared with the average annual value for insolation (Q_S).

Estimate of net long- wave back radiation

The net long-wave back radiation Q_B flux is calculated according to (Gill, 1982):

$$Q_B = \varepsilon \; \sigma \; T_s^4 \;(0.39\text{-}0.05\sqrt{e_a}) \;(1\text{-}0.6n_c^2) \qquad\qquad 4.4.3$$

Where $\sigma = 5.67*10^{-8}W^{-2}K^{-4}$ which expresses the black body emission from the surface

temperature T, reduced for water vapour and cloud cover. σ Is the Stefan-Boltzmann

constant, $\varepsilon \approx 0.985$ is the emissivity of the sea surface. ($^\circ$K) is the sea surface absolute

temperature in degrees Kelvin. n_c is the fraction of cloud and e_a is the vapour pressure of

the air. $e_a = e_s r/100$, r is the relative humidity observed with the mast data and e_s (mb) is

the saturation vapour pressure at the sea surface expressed as:

$e_s = 6.108e^{19.85}(1\text{-}T/T_o)$, where T is the sea surface temperature in $^\circ$K and T_o =273°K.

Castro et al. (1994) used the following expression to calculate the saturation vapour

pressure: e_s =0.98 [1+10^{-6}P (4.5+0.006Ts2)10$^\gamma$, P is the air pressure in (mb) and γ =

$(0.7859+0.03477T_s)/(1+0.00412T_s)$ of Q_B are shown in Section 5.2.2.1. Data are

compared to observed values of the net radiation and sun radiation as observed from the

most data. Q_{net} =Q_s (1+A)-Q_B, so Q_{net} must be reduced by Q_{sunrad}.

4.4.1.2 Turbulent heat fluxes

The expression for sensible heat fluxes used here is the one given (see Gill 1982)

by:

$$Q_H = \rho \; C_{pa} \; C_h v_a \; (T_s\text{-}T_a) \qquad\qquad 4.4.4$$

ρ_a is the air density, $C_{pa} \approx 1000Jkg^{-1} K^{-1}$ is the heat capacity of air. Gill (1982) suggested $C_h =0.83x10^{-3}$ is the heat transfer coefficient. v_a (ms^{-1}) is wind velocity, T_s (^oC) is the sea surface temperature and T_a (^oC) is the air temperature. The air and the sea surface temperature are those from the met mast and the ST-sensor. The results of these estimates are given in Section 5.2.2.2 of the result Chapter.

Estimate of net heat lost through evaporation

Estimates of net heat loss through evaporation (E) were done from wind and humidity measurements according to the expression:

$El_v = Q_E$

Where,

$Q_E = L_v \rho_a C_e v_a (q_s - q_a)$ 4.4.5

$\rho_a = (3.4838x10-3)P/T_v+273.16)$

Where P is the air pressure in (mb) and T_v is the virtual air temperature, given by:

$T_v = \{(T_a+273.16)[1+0.608 q_a]\}-273.16$, C_e is the exchange coefficient for water vapor (Stanton number S), and together with C_h, (Dalton number) is not known. We used

$C_e = C_h$ $(=0.83x10^{-3})$. Here q_a is the specific humidity of air (mass of water per unit mass of air) at the standard level and q_s is the saturation specific humidity at the sea surface temperature. Gill (1982) has given this as:

$q_a =(0.62197)$ e_a $/(P-0.378e_a)$, $q_s=(0.6219)$ e_s $/(P-0.378e_s)$. L is the latent heat of evaporation, and C_{pa} is the specific heat of air at constant pressure they are both given by Blanc (1985). Lv=4.1868 (597.31-0.56525 T_a).

$C_{pa} = 1004.6(1+0.8375 \; q_a)$. The evaporation also is the term in the net fresh water supply to an estuary (see Section 5.2.1.3). Thus the calculation of E is used there as well. Estimates of Q_E are given in Section 5.2.2.2.

4.4.1.3 Heat flux

Cederlöf et al. (1995) in estimating the instantaneous heat flux Q_A through a cross section in Chwaka Bay they used the expression

$$Q_A = \rho C_p \frac{d(A_h h_t T_t)}{dt} \qquad\qquad 4.4.6$$

A_h is the change of bay area with sea level height, determined from hypsographic curve of individual study area, which gives the change of area of the creek with tidal amplitude, while h_t is the sea level time series data. The expression $\dfrac{d(A_h h_t)}{dt}$, which is easily recognisable in the right hard terms of the expression 4.4.6, is volume flux across a transverse section at the entrance station (e.g. Section 5.3.3.3), ρ is the sea water density (ρ =1026 kg m^{-3}), C_p is the specific heat (i.e. the amount of heat required to raise the temperature of 1kg of water by 1°C) which is 4.186 kg^{-1} °C^{-1}). The results are given in Section 5.3.4, 5.4.4 and 5.5.4.

In addition, the calculation of heat balances (say on the monsoon scale) (Q_{max}) is

$$Q_{max} = A_s \eta_o(t) \Delta T \qquad\qquad 4.4.7$$

Where A_s is the mean surface area of the creek (bay), η_o is the mean oceanic sea level from long-term data series. ΔT is the change in mean spatial temperature in the creek from one monsoon season to the next. Methods for the estimate of long term exchange

rates are rare because of the difficulties of evaluating all the right had terms in the heat equation. Since the increase and decrease of the observed temperature is proportional to the amount of heat generated in the water column by solar radiation absorbed in it, the increase in temperature in a given column of water calculated by rewriting the above expression;

$$\Delta T = \frac{\Delta Q}{mC_p}$$
4.4.8

Where, ΔT is the temperature increase, ΔQ is the energy absorbed in kJ, m is the mass of the water, C_p is the specific heat. An empirical absorption profile (Woods and Barkman, 1986) for shallow water for shallow mixed layers can be employed in this calculation to find the proportion of incoming solar radiation absorbed in each creek.

4.4.2 Water exchange due to fresh water, current and wind

4.4.2.1 Fresh water induced exchange and volume flux

Water and salt balance in the study are will be used to determine the water exchange. A more detailed theoretical derivation of salt balance by integration along the length (L) of the creek, indicating that in a steady state advection equals turbulent diffusion is given by Prichard (1954, 1956). A brief summary is, however given below, where theoretical analyses on salt balance for a typical creek using the Knudsen equations, which take into, account the equation of continuity and conservation of volume are considered (Chapter 5).

Figure 4.4.2 is a sketch to of a vertical longitudinal section on water exchange. The continuity equation for salt within the creek basin can be written as:

$$\frac{d}{dt}(VS_i) = Q_oS_o - Q_iS_i \qquad\qquad 4.4.10$$

Where Q_o is inflow of oceanic water within the creek with salinity S_o.

Q. Q_i is the outflow of the creek water with salinity S_i.

V is the volume of water with salinity S_i.

Assuming that the volume, V, is constant, which holds when averaged over long periods.
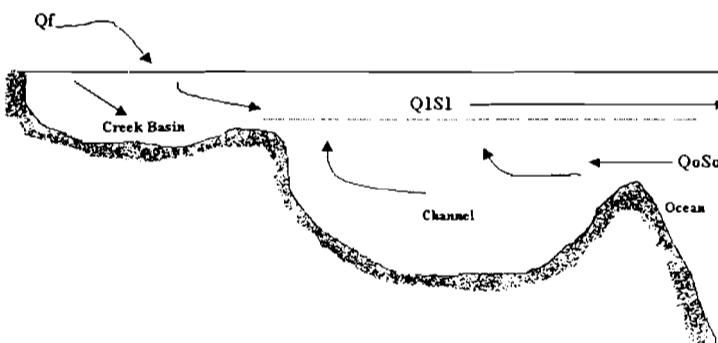
Figure 4.4.2 Schematic showing water balance in a typical creek.

Equation 4.4.10 can be written as

$$V\frac{dS_i}{dt} = Q_oS_o - Q_iS_i \qquad\qquad 4.4.11$$

Conservation of volume gives,

$$Q_i = Q_o + Q_f \qquad\qquad 4.4.12$$

Where, $Q_f = Q_r + (Q_p - Q_e)$ is the net fresh water supply to the creek, and

Q$_r$ is the fresh water discharge into the creek.

Q$_p$ is the precipitation over the lagoon.

Q$_e$ is the evaporation (and evapo-transpiration) from the creek surface.

Thus,

$$V\frac{dS_i}{dt} = Q_o S_o - (Q_o + Q_f)S_i \qquad\qquad 4.4.13$$

Equation (4.4.13) can be written as

$$Q_o = \frac{V\dfrac{dS_i}{dt} + Q_f S_i}{S_o - S_i} \qquad\qquad 4.4.14$$

From equation 4.4.13 water exchange generated by fresh water in the creek and salinity difference can be calculated. (Note the calculation requires knowledge of evaporation and precipitation and river input as well as salinity differences).

Further, the expression given by Eq. 4.4.13 can be cast into tidal range by

$Q_r = Q_e * A_c/T.\rho(=1000)$, $Q_r = A_s * V_F$ where $V_F = (4/3)(\pi/2)(A_s/A_c)(2\eta)$. \qquad 4.4.15

4.4.2.2 Observed current expression for volume flux

From theoretical point of view current meter measurements give a record of the tidally varying current, with sinusoidal signature. The signal obtained is a composite of different flows and can theoretically be decomposed. This is expressed into the steady flow and the time varying motion and into turbulent part as

$$u = \langle u \rangle + U + u' \qquad\qquad 4.4.16$$

where $\langle u \rangle$ is the mean over the time period of study. U is the sinusoidal ebb and flood tide and u' is the non-steady, non-periodic residual.

$$U = \sum_i A_i \sin(\omega_i t + \phi_i) \qquad\qquad 4.4.17$$

Where A is the amplitude of the ith constituent, ω the angular frequency and ϕ is the phase angle.

Expressions and results arising from decomposition of Eq. 4.4.17 are given in Sections 5.3.2.2, 5.4.2.2 and 5.5.2.2.

To analyze PCM measurements the cross-sections are divided into e.g.8 subsections, i.e. one for each PCM observation. The mean velocity (u_i) perpendicular to the cross-section (i.e. the velocity along the channel) the magnitude of the observed velocity (V_i) and its direction (θ) and the direction (β) of the cross-section from the E-W is expressed as

$$u_i = V_i \cos(\theta + \beta)$$

The mean velocity is obtained from cross-sections using the expression:

$$U_i = U_o \cos(\alpha + \beta) \qquad\qquad 4.4.18$$

Where U_i = the velocity perpendicular to the assigned area; U_o = the observed current speed; α is the direction of observed velocity; β is deviation of the cross-section from east-west direction. The mean velocity is determined from the measurement according to

$$U_m = \frac{1}{8} \sum_{i=1}^{n} U_i \qquad\qquad 4.4.19$$

130

4.4.2.3 Theoretical current, given by area and tidal range

Sverdup et al. (1942) expressed the average current in relation to some of the tidal wave characteristics, tidal range and tidal period as

$$U_{Av} = \left(\frac{A_b x T_r}{A_c} \right) x \left(\frac{1}{0.5T} \right) \qquad\qquad 4.4.20$$

Where U_{Av} is the average velocity, A_c is the cross-section area, A_b is the basin area upstream of the cross-section, T_r is the tidal range and T is the tidal period in seconds. The tidal prism (P) or the inter-tidal volume is given by $(A_b x T_r)$ in this expression.

The maximum velocity during the flood tide would be $\pi/2$ times the average velocity and would be 4/3 times greater at the center of the channel than at the periphery. Consequently, the maximum velocities on the flood tide would be

$$U_{Max} = \frac{4}{3} x \frac{\pi}{2} x \frac{A_b x T_r}{A_c} x \frac{1}{(0.5T)} \qquad\qquad 4.4.21$$

where U_{max} ms^{-1} is the maximum velocities and the variables are as in Eq.4.4.19. The above are referred to as barotropic currents and they represent the lowest order of response of the bay to remote (coastal sea level) forcing, with inflow corresponding to a rise in sea level and vice versa.

4.4.2.4 Water exchange related to ambient circulation mode

In the sketch (Figure 4.4.3a-b) which illustrates a typical creek (a) plan view and (b) longitudinal section, U denoted the current along the entrance of the creek. A current flowing along the entrance as shown may spread its motion into the creeks and generate

circulation in the creek. Assuming water flows into the creek on one side and out on the other as illustrated in Figure 4.4.3a, water exchange is given by the expression

$$Q = \alpha h \frac{B}{2} U$$

4.4.22

where Q is the volume flux induced by the current and α is a constant describing the topography, $0<\alpha<1$(cf. Söderkvist 1997), α can be taken as equal to 1. With fixed topography and the close proximity of the coastal flow at the entrance the flow into the creeks changes linearly with the along shore velocity. This is probably more applicable in Gazi Bay where the channel entrance channel is aligned almost North-south direction and considerable flow may get into the bay over the fringing reef (Section 5.3.2-3).

Another approach is to consider the net onshore-offshore component of the particle motion off the entrance, computed from tidal prism, assuming that the flow of unit width perpendicular to the entrance with a period T and the height H enters a tidal prism of volume (DH) in time $0.5T$.

The average onshore-offshore velocity may be expressed as:

$$U_T = \frac{2DH}{Td}$$

4.4.23

Where D is the distance from the shoreline to the shelf slope; H is the mean tidal range d is the mixing layer thickness. This is considered in Sections 5.4.2-3, and 5.5.2-3).

4.4.2.5 Water exchange due to wind and mixing processes

The type of horizontal circulation expected due to wind forcing in is also shown in Figure 4.4.3a.
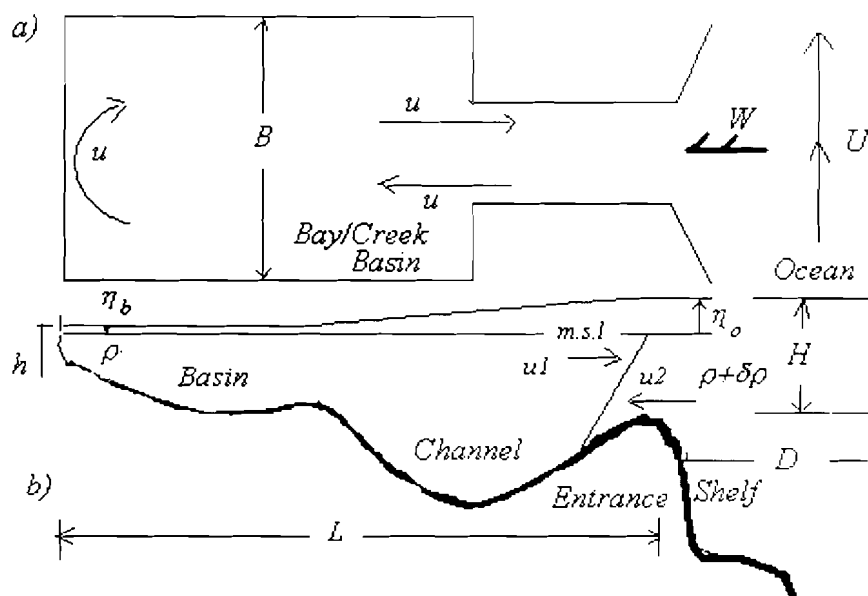
Figure 4.4.3 Sketch showing different circulation types in a typical creek. Panel (a) shows horizontal circulation and panel (b) two-layer circulation.

L -and B- are the length and the width of the creek. h- is the depth of the creek. H -is the depth outside the creek. u- is the velocity. ρ- is the standard density of water and $\delta\rho$- is the density difference η_o and η_b are the ocean and the creek sea levels respectively.

L, B, and h, W are as indicated in the caption. When the wind (W) starts to blow over the sea surface, water moves with a velocity u in the direction of the wind. The wind

velocity component perpendicular to the entrance of the bay generates water exchange in the creek. Assuming a balance between wind stress and bottom friction, and applying a quadratic drag force and excluding pressure gradients, the momentum equation can be is expresses as:

$$\frac{\partial u}{\partial t} = \sqrt{\left(\frac{\rho_a C_d W^2}{\rho_o}\right)} - C_{db} u^2$$

Application of steady state condition since the creek is shallow and the surface current quickly responds to changes in direction and strength of the wind. Taking x-axis as directed into the creek and assuming that the in and out flows are occupied by equal cross sectional area, the water exchange due to wind is given by

$$Q_W = \frac{Bh}{2} W \cos(\varphi) \sqrt{\left(\frac{\rho_a C_d}{\rho_o C_{db}}\right)} \qquad \qquad 4.4.24$$

The expression is similar to that given by Anderson and Rahm, (1986), where the angle φ is set to zero when the wind is directed into the bay and 180° when the wind is directed out of the bay.

Monsoon related- mixing processes

On seasonal and annual scales fresh water in combination with mixing processes, (and Kelvin waves!) drive various modes of gravitational circulation; generate residue currents that in turn drive water exchange on 'monsoon time scales'. Inter-seasonal salinity and temperature structure when analyzed can be used to infer modes of water exchange during different monsoon seasons.

Mixing process can result in onshore -offshore residual currents at the entrance and along the axis of the creeks, erode the thermocline; and transport various oceanic water masses into the creeks thereby indirectly generating water exchange. Without delving deep into buoyancy derivation a measure of the effectiveness of the wind or tidal mixing can be expresses in terms of the buoyancy flux (N) and wind (W) through the expression

$$\frac{N}{\omega_*^3}$$

$$N = \frac{g\alpha Q}{\rho_w c_p} \qquad\qquad 4.4.25$$

Where α is the volume expansion coefficient of water, ρ_w is the density of water, is the specific heat of water and Q is the heat flux. Wind enters through the expression

$\omega_* = \sqrt{\left(\tau\big/\rho_w\right)}$ or $\omega_*^2 = \rho_a k_s W^2 \big/ \rho_w$, where k_s is the friction coefficient taken equal to

1.5×10^{-3}.

$\dfrac{N}{\omega_*^3}$ has the dimensions of 1/length and when multiplied by a depth h is equal to the

energy input required to mix the water completely over the depth h,

$(= \rho_w Nh\big/2$) divided by a quantity equal proportional to the rate of turbulent energy production by the stress (James, 1980).

Starting with the assumption of well mixed or stratified layer the expression

$$Nh_1 \big/ \omega_*^3 \qquad\qquad 4.4.26$$

135

Where h_l is the depth of the mixed layer expression 4.4.26 can be used to indicate whether the thermocline is eroded provided a critical value is established. These expressions are applied in the section dealing with the thermocline (Section 6 and eventually in the discussion Chapter 7).

4.4.4 Water exchange generated by tide

4.4.4.1 Tidal wave analysis

Creeks considered in this thesis are essentially each a tidal channel of variable depths and marginally decreasing depth towards the inner mangrove-fringe basins. Redfield (1950) considered tidal waves in channels. He applied his theory on tidal wave traveling in straight parallel-sided channels of constant depth. Hunt (1964) considered the case of channel of varying depth and tapering sides. Here, tidal wave is theoretically analyzed without including the shoaling.

The equation of a wave subject to linear friction travelling along the x-axis in the positive x-direction is given by, for example, Bowden (1983) as

$$\eta = A_o e^{-\mu x} \cos(\omega t - \kappa x) \qquad\qquad 4\ 4.27$$

where η is the elevation of the sea surface relative to the equilibrium (mean sea level). A_o is the maximum elevation at $x = 0$. μ is a damping coefficient with units of (wavelengths)[-1].That means the amplitude falls by e^{-1} for every wavelength travelled in the creek channel, k is the wave number (2π/wavelength), ω the angular frequency (2π/period) and t is the time.

136

Similarly the current velocity in the wave field defined by Eq. 4.4.27 is

$$u = Ue^{-\mu x} \cos(\omega t - kx + a)$$ 　　　　　　　4.4.28

where the terms are as in Eq.4.4.27. If h is the mean water depth then

$$U = \frac{\omega A_o}{\left[h(\mu^2 + k^2)^{1/2}\right]}$$ 　　　　　　　4.4.29

The phase by which the current leads the elevation is

$$a = \tan^{-1} \mu / k$$ 　　　　　　　4.4.30

Thus theoretically, Eq.4.4.27 and 4.4.28 represent the sea level and the current measured at various locations, U is the total current (Eq. 4.4.29). The damping coefficient for the tidal wave can be estimated from the tidal analysis of the sea level or current measurements. Theoretically maximum transport in the tidal wave can be estimated from $u_o h$ and compared to the transport observed from the current meters for each creek.

Since both current meter and tide gauge are used tidal energy for each creek can be determined from tidal characteristics as

$$E = \frac{1}{2} \rho g \eta_o u_o \cos\varphi$$ 　　　　　　　4.4.40

where E is the energy flux in $Jm^{-2}s^{-1}$, η_o is the tidal elevation amplitude, μ_o is the tidal current amplitude and φ is the phase difference between currents and elevations. The energy flux is maximum in a progressive wave for which $\varphi = 0$, and zero in a standing wave for which $\varphi = 90°$, the calculation is performed in Sections 5.3.2.3, 5.4.2.3, and 5.5.2.3, where the harmonics of the sea level and current are examined using the least squire and spectral analysis.

137

The rate of energy dissipation can be used to derive value for quadratic friction coefficient, c_D, usually used in the numerical models of the tide. The average rate of energy dissipation, over a tidal cycle, by bottom stresses over creek area A is

$$E = \left(\frac{4}{3}\pi\right)c_D\rho\overline{u_o^3}A \qquad\qquad 4.4.41$$

where E is as in Eq. 4.4.40, u_o^3 is the spatial average of the cube of the depth mean current amplitude in the region (this is difficult to measure, best that can be done if this work is to cube the mean current measurements taken at mid-channel depth). Further, brief theoretic analyses on one-dimension friction model follow in Section 4.4.4.5.

4.4.4.2 Observed sea level expression for volume flux

Hourly tidal discharge can be calculated using tidal hypsometric flow model

$$q_t = \frac{dV}{dt} = \frac{\partial l}{\partial t}(A(h)*h) = \frac{d}{dt}(Ah) \qquad\qquad 4.4.42$$

(Boon, 1975) where V is the volume of the cross-section at the entrance, the volume flux (q_t) is the instantaneous cross-sectional discharge, and A is the upstream (horizontal) area A of the mangrove-creek basin inundated by water when the tidal elevation is h (t). Eq.4.4.42, is based on flow continuity and was developed by Eiser and Kjerfve (1986).

The idea is to calculate horizontal area at various sections of the creek, by dividing the creek into smaller areas or grid then calculating the area of each section and summing them up to get the total area of the bay.

If simultaneous sea level measurements (h) of several stations of the water bodies are

available, $q = \sum_{i=1}^{n} A_i \frac{dh_i}{dt}$ 4.4.43

In this study, simultaneous sea level measurements from several stations were scarce. Thus the instantaneous volume flux was calculated using one set of tidal measurements at the entrance of each study site. Hence, Eq. 4.4.42 equates the instantaneous inlet discharge (left hand term) to the volumetric flow (right hand term) through the inlet water surface rise or fall needed to balance that flow. It was gives an accurate record of the creek surface elevation time-history used to calculate the instantaneous inlet discharge and velocity (Section 5.3.2, 5.4.2 and 5.4.2), on the assumption that the creek surface remains horizontal as it oscillates. Integration of the above volume fluxes expression gives volume fluxes for flood and ebb period as well as results (Section 5.3.3.3, 5.4.3.3 and 5.5.3.3).

4.4.4.3 Theory on harmonic analysis and tidal classification

Time series measurements such as the sea level and current are subjected to harmonic analysis, which is a method for extracting amplitudes, primary harmonic constituents, phases and their compound tides. Constituents are used to determine the propagation speed of the tide, determine the degree of tidal asymmetry, and calculate phase differences. They can also be used to reconstruct the original tidal signal or to predict tidal water levels and currents.

The analysis is based on the" Method of Least Squires" which involves fitting a set of cosine (or sine) curves with given frequencies, varying amplitudes and phases, and

minimising the sum of deviations from the original curve. In Eq 4.4.27, analysis was given of a tidal wave. However, combinations of sine and cosine functions can be used as under (Eq.4.4.44). Time series measurements is a set of data points whose parts can be expressed by trigonometric series with the specific frequencies ω_k varying its amplitude and phase and written in the form (cf. Cederlöf, 1995).

$$\varsigma(t) = \left(a_k \cos\omega_k t + \sin\omega_k t\right) \qquad\qquad 4.4.44$$

According to the least-square fitting, the minimum of the function F where z_n are the observed values at times t_n is determined,

$$F(a,b) = \sum_{n=1}^{N}\left(z_n - \sum_{K=1}^{n}\left(a_k \cos\omega_k t_n + b_k \sin\omega_k t_n\right)\right)^2 = \min \qquad\qquad 4.4.45$$

The minimum values of the function F is obtained by putting the partial derivatives of F with respect to all the components a_i and b_i of the vectors a and b equal to zero.

$$\frac{\partial F}{\partial a_i} = 0$$
$$\qquad\qquad \text{for } i = 1,2,\ldots\ldots\ldots K \qquad\qquad 4.4.46$$
$$\frac{\partial F}{\partial b_i} = 0$$

Partial derivatives of the expression 4.4.45 constitute a linear algebraic system of two equations with two unknowns a and b,

$$\sum_{k=1}^{K} a_k \sum_{n=1}^{N} \cos\omega_i t_n + \sum_{k=1}^{K} b_k \sum_{n=1}^{N} \cos\omega_i t_n = \sum_{n=1}^{N} z_n \cos\omega_i t_n$$

$$\sum_{k=1}^{K} a_k \sum_{n=1}^{N} \sin\omega_i t_n + \sum_{k=1}^{K} b_k \sum_{n=1}^{N} \sin\omega_i t_n = \sum_{n=1}^{N} z_n \sin\omega_i t_n$$

4.4.47

These two equations (4.4.47) can be simplified by introducing the matrices C, S, X, and the vector c and s,

$$\sum_{k=1}^{K} a_k c_{ik} + \sum_{k=1}^{K} b_k x_{ik} = c_i$$

$$\sum_{k=1}^{K} a_k x_{ik} + \sum_{k=1}^{K} b_k s_{ik} = s_i$$

4.4.48

The expression 4.4.48 can be put into compact matrix notation according to,

$$M \times x = m$$

$$\begin{pmatrix} C & X \\ X^T & S \end{pmatrix} \begin{pmatrix} a \\ b \end{pmatrix} = \begin{pmatrix} c \\ s \end{pmatrix}$$

4.4.49

The expression 4.4.49 is a system of 2K equations with 2K unknowns a_l through a_K and b_l through b_K. The solution is,

$$A = \sqrt{\left(a^2 + b^2\right)}$$

4.4.50

141

$$\tau = a \tan\left(\frac{b}{a}\right)$$ 4.4.51

Where A is amplitude and τ is phase lag.

A Programme written in matlab, using the above functions to analyze and runs with a set of tidal periods for various tidal components and returns periods, amplitude and phase angle (cf. Cederlöf, 1995).

Classification is given by the ratio between major diurnal and the semi-diurnal constituents (Courtier 1933) according to the form number (F).

$$F = \frac{(K_1 + O_1)}{(M_2 + S_2)_1}$$ 4.4.52

where the coefficients are for four major astronomical components namely M_2, S_2 (semi-diurnal), K_1 (diurnal) and O_1 (diurnal). The results for this analysis are given for example in Section 5.3.2.3.

Results obtained are presented in Sections 5.3.3.3, 5.4.3.3 and 5.5.3.3.

4.4.4.4 Spectral Analysis

Spectral analysis is a method used to calculate phase and the propagation of the tidal signal between sites and is useful when harmonic cannot be effectively determined. Unlike harmonic analysis it does not use predetermined tidal frequencies to determine the frequencies, which are in the data. In spectral analysis the cosine function is determined numerically from the original data, and the cosine function is then used to reconstruct the original data. The power density (PSD), one outcome of this method is used. The PSD shows the magnitude of each cosine term in the summation series. The analysis is done

142

through matlab Programme to obtain fine wave spectrum (specific peaks) with the broad

energy spectrum band filtered out. The results are shown following those of tidal analysis

(Sections 5.3.2.3 and 5.5.2.4).

4.4.4.5 Friction model for tidal energy dissipation

Consider the schematic a creek basin with a surface area A_L connected to the

ocean by a narrow channel of length L, depth h, and width w, ξ_o and ξ_L are water levels in

the creek and the ocean (cf Fig. 4.4.4.3a-b). Assumption of dynamic balance in the

channel between local acceleration, pressure gradient and bottom allows for the

expression

$$\frac{\partial \xi}{\partial x} = -\frac{1}{g}\frac{\partial u}{\partial t} + \frac{F_b}{g\rho h} \qquad\qquad 4.4.53$$

Where positive flow is along the x-axis into the creek and where the tidal level $\partial \xi$ is

ignored compared with the mean depth h of the water in the channel. ρ is the density of

the sea water; A_L, L and w are assumed not to depend of the tidal level, requirements.

Application of the linear law of friction gives,

$$F_b = -\kappa \rho U \qquad\qquad 4.4.54$$

(This can also be written as $F_b = -\kappa \rho \mid U_b \mid U_b$. Where κ is a dimensionless constant).

Application of continuity equation results in

$$A_L \frac{\partial \xi_L}{\partial t} = whU \qquad\qquad 4.4.55$$

Substituting into (4.4.54) for U and into (4.4.53) for F_b give

$$\frac{\partial \xi}{\partial x} = -\frac{L}{g}\left(\frac{A_L}{wh}\right)\left(\frac{\partial \xi^2}{\partial t^2}\right) - \left(\kappa \frac{A_L}{gwh^2}\right)\left(\frac{\partial \xi_L}{\partial t}\right) \qquad 4.4.56$$

If κ, w and h are assumed not to depend on y, then by integration along the channel

$$g\xi_o = g\xi_L + \left[\frac{\kappa A_L L}{gwh}\left(\frac{\partial \xi_L}{\partial t}\right) + \left(\frac{A_L L}{wh}\right)\left(\frac{\partial \xi^2_L}{\partial t^2}\right)\right] \qquad 4.4.57$$

Suppose that the creek is driven by a harmonic variation of ocean level, for example M_2,

then ξ_o =Hcos(σt), where σ=2π/T, the solution of equation (4.4.55) is:

ξ_L = αHcos (σt-θ), Where, α=(ϕ2+μ2$)^{-1/2}$; θ = arc tan (μ/ϕ) and

$$\phi = \left[1 - \left(\frac{A_L L \sigma^2}{whg}\right)\right] \text{ and } \mu = \left(\frac{\kappa A_{L\sigma}}{wh^2 g}\right) \qquad 4.4.58$$

The above solution represents a damped oscillation (cf Eq.4.4.27) with a phase lag. The

average rate of energy dissipation due to the work done against the channel friction over

a tide cycle of M_2 is computed using the expression

$$E_{Loss} = \frac{\sigma}{2\pi} \int_0^{\frac{2\pi}{\sigma}} F_b wUL \partial t$$

Substituting F_b from (4.4.54) and U from (4.4.55), the rate of energy loss is

$$E_{loss} = \frac{A_L L \sigma^2 \kappa_\rho H^2}{2h^2 W} \qquad 4.4.59$$

Pugh (1979) used equation similar to (Eq.4.4.59) to calculate the rate of energy loss in an

atoll system. Eq. 4.4.41 and 4.4.59 both are for tidal energy loss determination but apply

different parameters.

Substituting into (4.4.54) for U and into (4.4.53) for F_b give

$$\frac{\partial \xi}{\partial x} = -\frac{L}{g}\left(\frac{A_L}{wh}\right)\left(\frac{\partial \xi^2}{\partial t^2}\right) - \left(\kappa \frac{A_L}{gwh^2}\right)\left(\frac{\partial \xi_L}{\partial t}\right) \qquad 4.4.56$$

If κ, w and h are assumed not to depend on y, then by integration along the channel

$$g\xi_o = g\xi_L + \left[\frac{\kappa A_L L}{gwh}\left(\frac{\partial \xi_L}{\partial t}\right) + \left(\frac{A_L L}{wh}\right)\left(\frac{\partial \xi^2_L}{\partial t^2}\right)\right] \qquad 4.4.57$$

Suppose that the creek is driven by a harmonic variation of ocean level, for example M_2, then $\xi_o = H\cos(\sigma t)$,   where $\sigma = 2\pi/T$, the solution of equation (4.4.55) is:

$\xi_L = \alpha H\cos(\sigma t-\theta)$, Where, $\alpha = (\phi 2 + \mu 2)^{-1/2}$; θ = arc tan (μ/ϕ) and

$$\phi = \left[1 - \left(\frac{A_L L\sigma^2}{whg}\right)\right] \text{ and } \mu = \left(\frac{\kappa A_{L\sigma}}{wh^2 g}\right) \qquad 4.4.58$$

The above solution represents a damped oscillation (cf Eq.4.4.27) with a phase lag. The average rate of energy dissipation due to the work done against the channel friction over a tide cycle of M_2 is computed using the expression

$$E_{Loss} = \frac{\sigma}{2\pi} \int_0^{\frac{2\pi}{\sigma}} F_b wUL\partial t$$

Substituting F_b from (4.4.54) and U from (4.4.55), the rate of energy loss is

$$E_{loss} = \frac{A_L L\sigma^2 \kappa_p H^2}{2h^2 W} \qquad 4.4.59$$

Pugh (1979) used equation similar to (Eq.4.4.59) to calculate the rate of energy loss in an atoll system. Eq. 4.4.41 and 4.4.59 both are for tidal energy loss determination but apply different parameters.

144

4.4.5 Flushing time and residence time determination

4.4.5.1 Fraction of the fresh water concentration

Flushing time

There are several methods of calculating water exchange or flushing time.

Frequently the flushing time is referred to as the e-folding time, defined as the time

required to decrease the volume of water in the bay to e^{-1} (about 37%) of its original

volume, where e is the base of natural logarithms.

A traditional method, used for the estimates of the residence time or the *flushing*

time method is given by the expression

$$F = \frac{\left\{\left(1 - \frac{S_b}{S_o}\right)V_b\right\}}{R} \qquad 4.4.60$$

where (S_b) is the mean salinity in the inner shallow basins in the creek. S_o is the salinity

of undiluted seawater or can be taken as the salinity of the ocean entering the bottom of

the inlet. R is the volume of the river discharge that is the monthly mean fresh water input

to the creek. V_b is the mean volume of water in the creek, which is the volume of the

creek at mean high tide.

The Residence time

The residence time (T_r) is given by

$$T_{res} = \frac{V}{Q_{max}} \qquad 4.4.61$$

where Q_o is inflow of oceanic water within the creek with salinity S_o. Q_i is the outflow of the creek water with salinity S_i. V is the volume of water with salinity S_i, and Q_{max} = max (Q_o, Q_i). This expression arises from Eq. 4.4.11.

4.4.5.2 'Large-scale-flushing time' method

The seasonal rivers in the study area usually dry up, during the dry season. For dry periods, a flushing time expression developed by Wolanski et al. (1990) in his studies in mangrove creek systems can be applied with minor alteration. The expression is given as

$$A_t E_t S = B A_c \frac{dS}{dx} \qquad\qquad 4.4.62$$

Where S is the salinity, x is the distance from the entrance to the mouth the creek. E_t is the evapo-transpiration rate and A_c the main cross-section area. A_t is the surface area of the inter-tidal swamp (mangrove area including mud flats).

$$B = \frac{A}{1+\varepsilon} + \varepsilon U_o a^2 \frac{T}{48}(1+\varepsilon) \qquad\qquad 4.4.63$$

$2T$ is the tidal period, A is the longitudinal eddy diffusion coefficient in the stream, ε is the ratio of the volume in the lateral embayment, U_o is the peak tidal current, and B is a mean range is $50\text{-}150 m^2 s^{-1}$ (Ridd et al., 1990).

B can be assumed to fall between the mean range, suggesting that the key variables are the areas, salinity and evaporation and B can be assumed equal to $100 m^2 s^{-1}$ since the creeks are similar to those considered by Wolanski et al. (1990) and Okubo (1973). That is the creeks considered in this work have side swamps fringed with

mangroves, which trap water and enhance lateral trapping (Okubo 1973). When water

moves into the embayment from the main tidal channel during flood a fraction of it ends

up trapped in the swamps. At ebb tide the trapped mass of water returns to the main

channel and mixes with the ambient water, thus enhancing mixing.

Residence time is expressed as

$$T_{res} = L^2 \big/ B \qquad\qquad\qquad 4.4.64$$

where L is the length of the creek. B can be computed from es 4.4.62 instead of Eq.

4.4.63, assuming that the other parameters in Eq. 4.4.62 are known. And the salinity is

taken as mean values in the creek and at the entrance. These other parameters can be

estimated and are typical to each study area. The method is referred in this thesis as

'large-scale-flushing time'. This is because the salinity in the creek could be driven by

other large-scale modes of water exchange. Such modes are, for example, the invasion of

low or high salinity water from the ocean, evaporation, river input and Kelvin wave

events (The corresponding ratio of the mixed layer depth in NEM to that of SEM can be

used as an addition constant to modulate B in Eq.4.4.62. This method is applied in

Sections 5.3.3.4, 5.4.3.4 and 5.5.3.4.

4.4.6 Bottom layer friction and energy dissipation

4.4.6.1 Drag coefficient

When the co-ordinates to be x-positive along the channel of the creek and y axis

in the transverse direction, then the equation of motion for the creek reduces to balance

between pressure (P) and friction (F) against the creek bottom (Stigebrandt, 1980). The

sea level drop between the open ocean and the inner part of the creek gives the net

longitudinal pressure gradient along the creek, which is balanced by the friction. The difference in sea level (Δh) is then given by subtracting the mean oceanic sea level, given by the tide gauge at oceanic side, from the mean sea level inside the creek given by the inner tide gauge. The equation of motion reduces to:

$$P = A\rho g\Delta h$$

$$F = WL\tau_b$$

where A is the vertical cross-section area $(A=B.H)$ where B is width and H is depth. ρ is density. g is acceleration due to gravity. W is the length of the wetted parameter of the cross sectional area, $(B+2H)\approx W$, and L is the length of the creek. τ_b is the bottom friction, which is parameterized by the drag coefficient C_d according to a quadratic friction law,

$$\tau_b = \rho C_d U^2$$

where U is the mean longitudinal velocity. From the balance of the pressure and friction forces the drag coefficient is computed the following expression,

$$C_d = \frac{g\Delta hA}{LU^2W} \qquad\qquad 4.4.65$$

In theory one can calculate the friction coefficient in this manner. Note, the mean current U, is obtained by dividing the mean out flow Q from the creek by the cross-section area (A). That is U= Q/A where U is from RCM or PCM. Note also the average tidal current can be computed theoretically.

4.4.6.2 Friction velocity and boundary layer

Moving water in contact with seabed slows down at the water bottom interface while above the interface the flow is faster. The mechanism produces is responsible for friction drag and velocity shear (friction velocity). The flow also produces disturbance turbulence mixing around bottom objects (roughness elements). The velocity profile is asymptotic close to the bottom and obeys, and for well mixed water layers, it obeys what is known as "the law of the wall" or the *von Karman-Prandtl* equation, given by the expression:

$$u = u^* \left(\frac{1}{k} \ln \frac{z}{z_o} + lR_i \right),$$
4.4.66

$u^* = (\tau_o/\rho)1/2$, z_o relates the hydrodynamic roughness of the seabed to the $\kappa=0.4$ is the roughness length. Dyer (1986) has shown that the bed shear stress (τ_o) is proportional to the squire of the current in the boundary layer. That is $\tau_o= C_d u^2$, $l \approx 5$ is a constant. Ri is the gradient Richardson number that is depended on turbulent mixing, thus it can be written as z/L where L is the Monin-Obukov length.

The mean value for U was measured in the main channel of Tudor and Gazi Creeks, and u^* estimated and together with roughness height z_o (See Appendix C).

CHAPTER FIVE

RESULTS OF METEOROLOGY, HYDROGRAPHY, CURRENT, TIDES AND WATER EXCHANGE

5.1 COASTAL METEOROLOGY

Two data sets were obtained. The first data set was from the creek-weather mast station located in Tudor Creek and covered the SEM and IMSR season and therefore this data set did not cover a full year. The second data set was the monthly average data from the coastal stations in Kwale, Mombasa and Kilifi districts. Results for each of these stations are presented separately. From these data set magnitudes of the meteorological forcing factors are analyzed.

5.1.1 Statistical results from the creek-weather mast station

The data from the creek -weather mast covered a period of 80 days from 14 June to 28 August 1996. The raw data records obtained were shown in Section 4.3.1.2 (Figure 4.3.1.1a-d. Table 5.1.1 shows a summary of statistical results for the seven of parameters.

(The data records of Figures 4.3.1.1a-d were filtered; with same filter all of then to remove spikes and to obtain clear variations).

Figure 5.1.1-1-3 depicts fluctuations in not so clearly seen before in the unfiltered data Figures 4.3.1.a-d. For the variation of atmospheric pressure, wind speed and direction the results are shown in by arrow Figure 5.1.1.2. Observing atmospheric pressure, the ranges are 1010.0 –1019.2mb, with a mean of 1015.3mb. In the last week of June the pressure is at 1012mb then increases to 1015.5mb before decreasing by 2.5mb,

then increasing, around 12 July it was almost steady at 1016mb, followed by a shift to

1013.5mb, between day 25 and 8August. Although no evidence of strong correlation of

between parameters in Figure 5.1.1.1-3, at least comparisons can be made.

Table 5.1.1.1 Statistical results from the weather mast, data set of 14 Jun-8Aug 1996, Tudor Creek (KFMRI).

WEATHER MAST STATISTICS							
Statistics	W/Spd Ms^{-1}	W/Dir	A/psr mbars	A/temp ^{o}C	R/Hdity %	S/Rad Wm^{-2}	N/Rad Wm^{-2}
Max	14.6	356.1	1019.2	26.78	88.6	1270.4	1061.0
Min	0.4	18.1	1010.0	20.68	46.3	-34.9	-67.9
Mean	6.0	164.0	1014.8	24.36	75.6	241.7	179.5
Standard Deviation	2.1	30.1	1.70	0.99	4.8	344.6	292.6

Probably a prominent feature is the strong fluctuations of 160-190° from the end of June

and including the first three weeks in July. These fluctuations are probably caused by the

slight increase in air pressure. It appears that as the air pressure increases the wind

responds by rapid fluctuations and slightly increased in speed (e.g. shown by arrows).
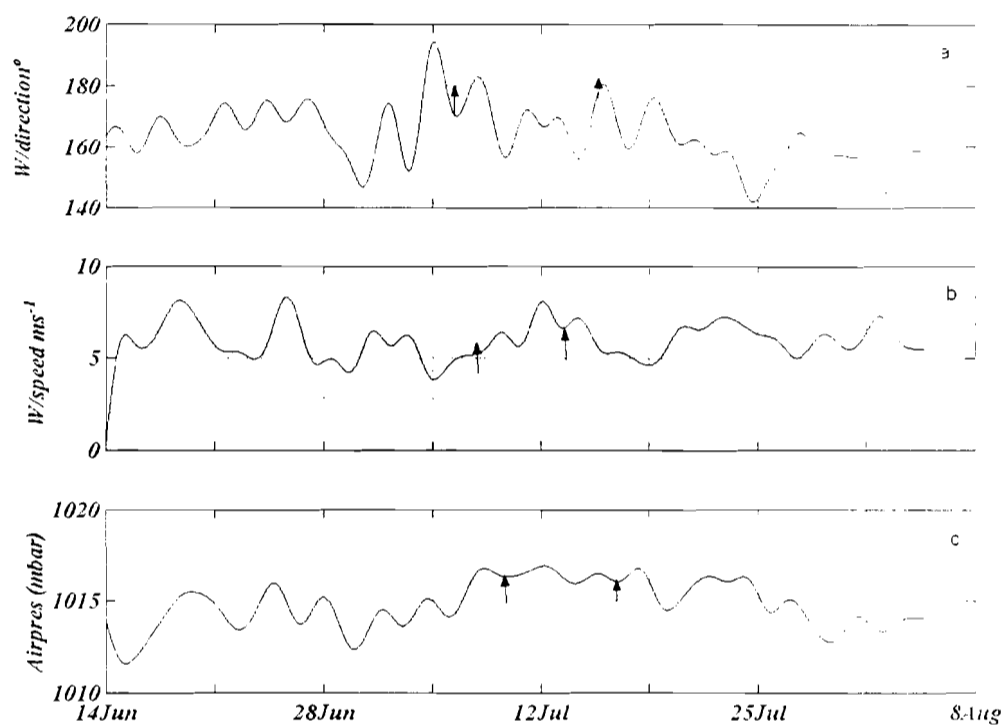
Figure 5.1.1.1 Fluctuation of (a) wind direction (b) wind speed and (c) air pressure, 14Jun-8Aug 1996. Note arrows, the air pressure increases wind speed and cause wind direction to increase and fluctuate.

The variation of air temperature and humidity, from weather mast. are also shown in Figure 5.1.1.2 panel (a) and (b). Evaporation increases slightly in July: the maximum values were 206.4mm, mean of 118.1mm, minimum of 74mm and standard deviation of 27mm. For this part of SEM evaporation rates are 0.2 - 0.56mm/day (2.1-6.5×10^{-9} m s^{-1}) and a mean value of 3.2 mm/day or 3.7×10^{-9} m s^{-1}. In Section 5.1.2 evaporation rate from long-term data is also computed and compared with these values.

152

A comparison of wind speed, air temperature and sun radiation is shown in Figure 5.1
1.3. Both solar radiation and temperature decrease up to the end of June. In July solar
radiation from values close to 200 Wm^{-2} to almost constant value equal to 300 Wm^{-2}, and
temperature remain constant at 24°C.
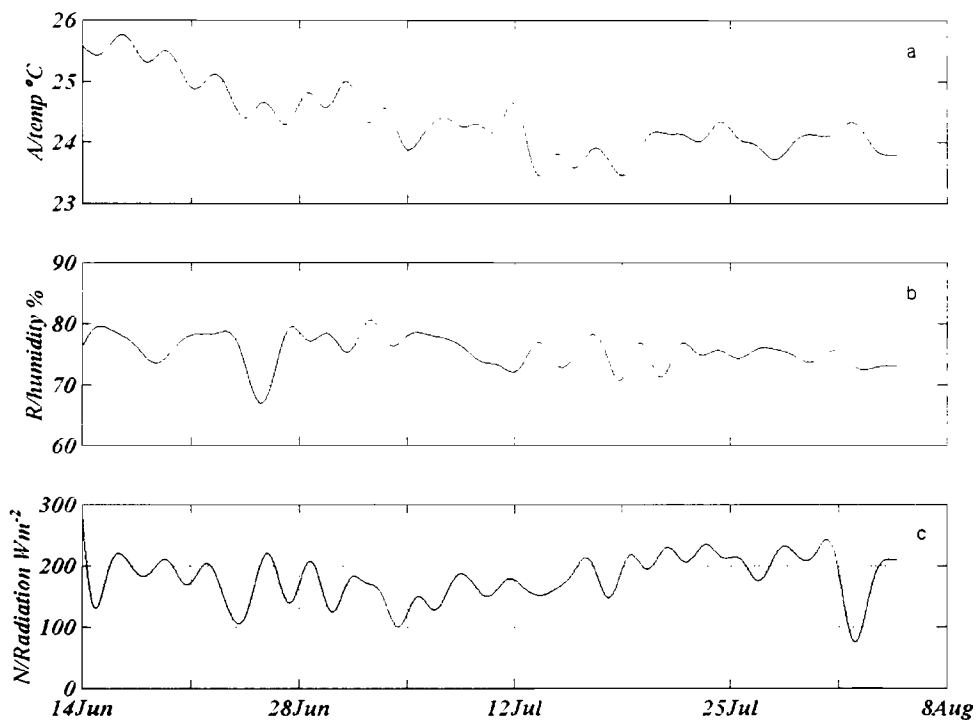
**Figure 5.1.1.2 Fluctuation in (a) temperature of (b) relative humidity and (c) net
solar radiation, 14 Jun-8Aug 1996. Note decreasing air-temperature**

Wind blew from southeasterly, between 145° and 200°, with a mean direction
cantered at 164°.The speed fluctuated between 2ms^{-1} and 14.8ms^{-1} with a mean of 6ms^{-1}.

The winds tend to become more southerly in July with higher fluctuation as the

temperature and solar heating approach almost steady values. These changes are probably associated with decreasing cloud cover and increasingly cooler Ocean during this part of the year. Pronounced wind fluctuations daily and weekly fluctuations are evident as well as fortnightly fluctuations are also evident.
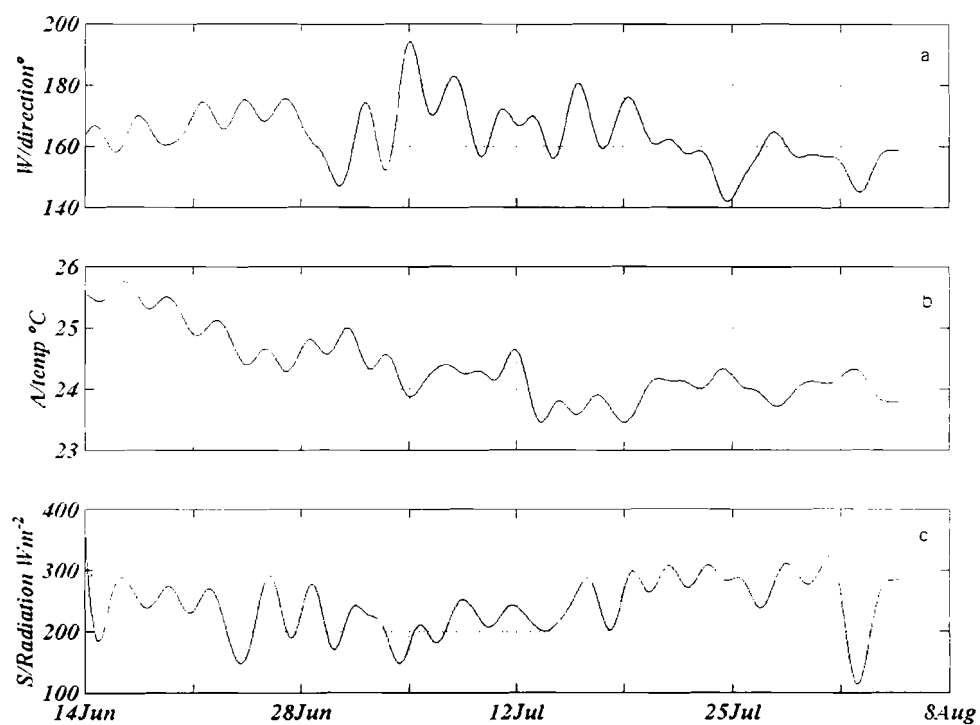
Figure 5.1.1.3 Fluctuation in (a) Wind direction (b) Air-temperature (c) solar radiation, 14 Jun-8Aug 1996.

Figure 5.1.1.3 also show steady decrease and 2-3 day fluctuations in addition diurnal variations and the fortnightly ones. Diurnal fluctuations are also present in wind direction.

5.1.2 Statistical results from coastal weather stations

Annual monthly means values

Annual monthly mean values for atmospheric pressure are shown in Figure 5.1.2.1 for MIAMS. Maximum atmospheric pressure (1015.3mb) occurs during SEM season and minimum (1011.9mb) in NEM season in the months of July and March respectively. During the IMSR season the pressure remain high but decreases by 2mb during the long rain season. Diurnal pattern is also evident in results from the weather mast and the annual records from the coastal stations. They indicate variation in the sea breeze. Mornings reveal higher air pressure values than the afternoons throughout the season. The difference in morning and the after noon air-pressure is 2mb between June and October, the difference increase and reach a maximum of 4mb in February.

These results indicate that morning air exerts more pressure than the afternoon air. Similarly the results suggest that during SEM season the air mass, which is blow by the southeast winds, is heavier than in NEM season.

Wind speed range is $0.6\text{-}4.6\text{ms}^{-1}$ in the morning at 0600 with a mean of 3.1m s^{-1} in the afternoon at 1200; the range is $4.9\text{-}6.0\text{ms}^{-1}$ with a mean of 5.6ms^{-1}, which is 56% of the value in the morning (Figure 5.1.2.2). Hence, daily fluctuations are clearly seen in the figure where the afternoon winds are slightly of larger magnitude than the morning winds. Seasonal fluctuation is also evident as can be seen by the months characterizing the each season.

During SEM season the maximum wind is 6.0ms^{-1}. The morning winds are lower during the NEM season with a mean of 2.6ms^{-1} while in the afternoon the speed is highest with a value of 5.7 m s^{-1}. Between March and April the wind increases rapidly to 4.1 m s^{-1} and reach maximum values in July-August before decreasing slightly thereafter.
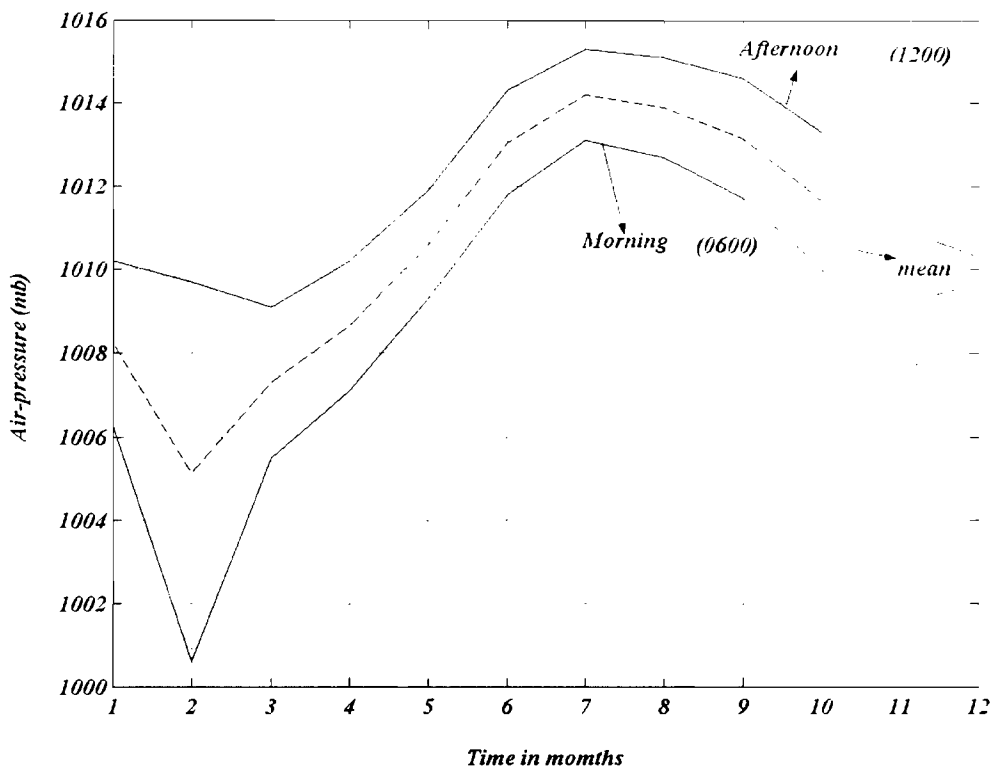
Figure 5.1.2.1 Annual monthly mean air pressure, in Mombasa, 1995-1998

Thus wind is slightly stronger in the SEM season than in NEM season for this part of the Kenyan coast. The wind decreases to a mean value of 2ms^{-1} in the LMSR. The direction fluctuates be 130° to 250 °C. Mostly the wind blew from southern direction.

Maximum and minimum temperatures depicted in Figure 5.1.2.3, shows the fluctuation of air temperature that further confirm the suggestion the suggested arrival of cool air mass as described above. The minimum temperature fluctuates between 18 and 20.8°C with a mean value of 19.5°C. The mean minimum temperature range is 21-25°C, with a mean high temperature value of 23.5°C in March.
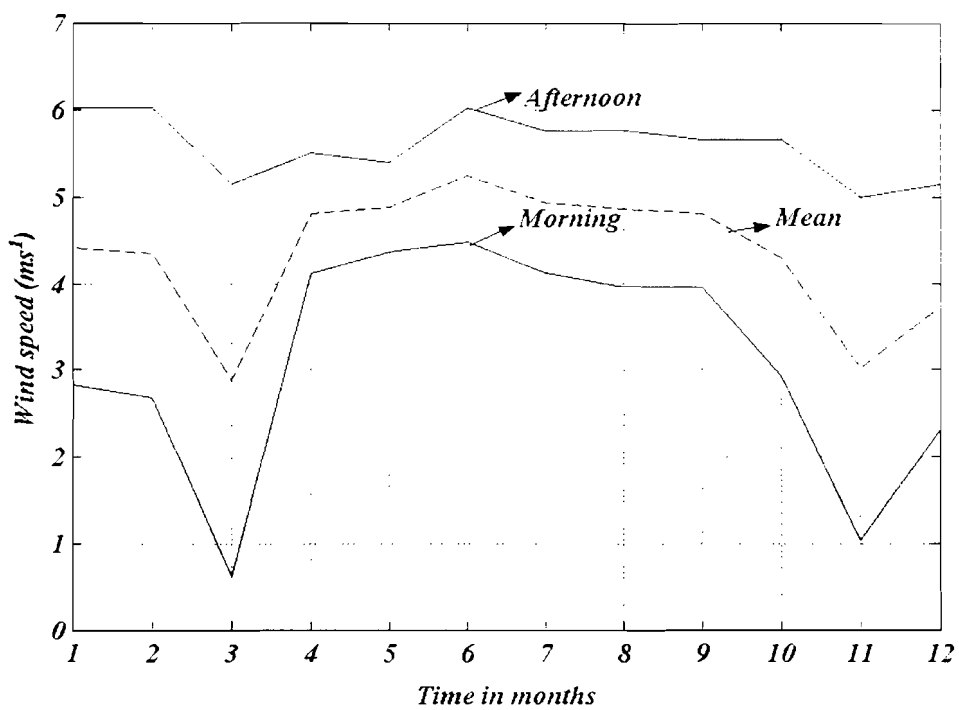
Figure 5.1.2.2 Typical monthly mean wind speed from MIAMS (1996-1997)

The mean, low maximum air temperature of 27.8°C occurs in August. The maximum air temperature range is 31-33.5°C with a mean maximum of 32.7°C in February. The variation in air temperature strongly indicates the atmosphere begins loosing heat immediately following the onset of Southeast wind in mid-may and

157

continues to do so for about 5 months from April-to August, after which the atmosphere gradually gains heat until a maximum of 30.5°C is reached in February-March. When maximum and the minimum temperature are combined, the resulting maximum temperature is 29.5°C and the lowest 25°C (Figure 5.1.2.3).
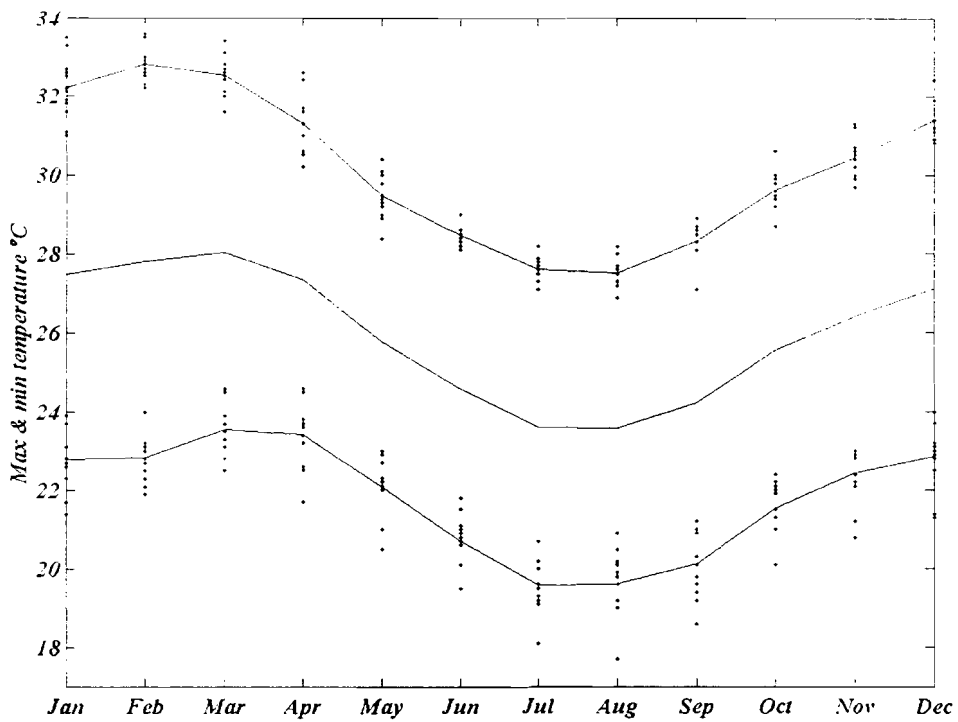
Figure 5.1.2.3 Monthly mean maximum and minimum temperature, MIAMS (1987-1997).

Note that the weather mast data was collected in June-August; Figure 5.1.2.3 confirms the decreased trend observed from the weather mast record during the entire period of measurements, although there short-term fluctuations were apparent.

The decreasing temperatures suggest cooling of creek water as well. Hence during this period the creeks loose heat.

Humidity is lowest during in March at the end of NEM season, but increases rapidly in April to a maximum of morning maximum of 85 in May, and 72 in the afternoon. In general humidity is higher in SEM than in NEM season
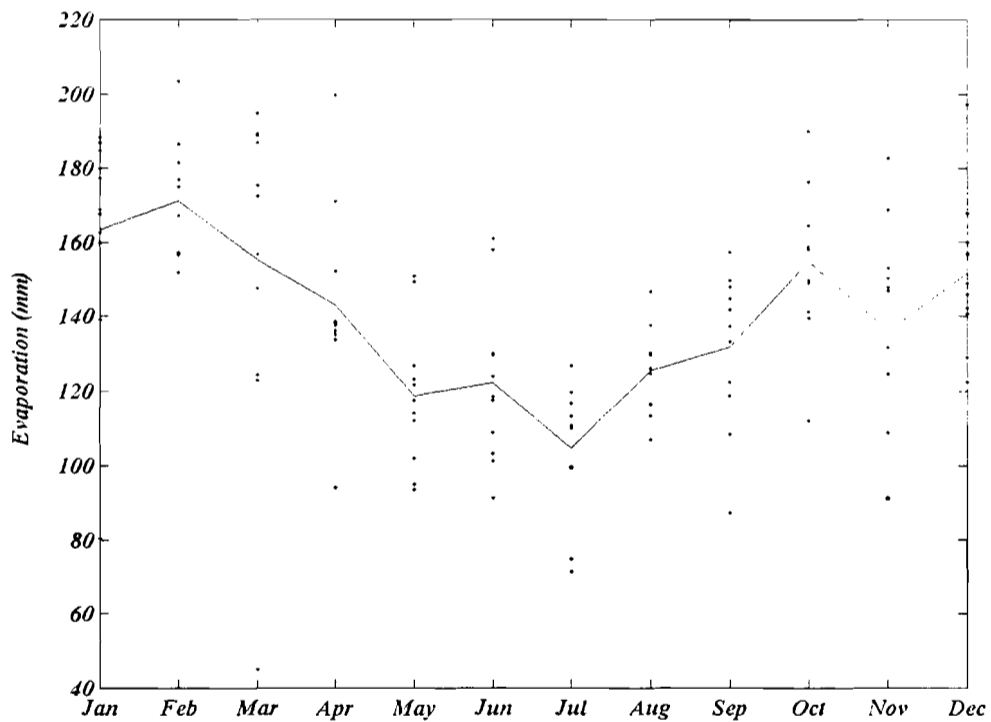
Figure 5.1.2.4 Mean monthly evaporation for the period long-term (1987-1997, evaporation from MIAMS (Source: KMD).

Evaporation shows seasonality with high and low values in different months. Maximum value of 203.4mm occurs in January, minimum value is 126.7mm in July ((Figure 5.1.2 4.). The mean evaporation is 175mm with standard deviation of 25.2mm.

The maximum values are close to those observed with the weather mast the minimum, however, the mean differ from this long-term results by 53mm and 57mm respectively. The evaporation rates obtained from this long-term data, the evaporation rates rage is 0.35-0.6 mm/ day (4 - 6x10^{-9} m s^{-1}) and mean value of 0.48 mm / day (5.6x10^{-9} m s^{-1}).

5.1.3 Statistical results on rainfall and fresh water discharge

Rainfall

As mentioned earlier we consider the synthesis of the mean monthly meteorological data that is available in the coastal. Such data include the precipitation results from Shimoni (SM), Longer meteorological data series (1957-1998) from Musabweni (43yrs), Ramisi (32yrs), Kikoneni (26yrs) and Shimba Hills (23yrs), and additional precipitation obtained from Mombasa and Moi Airport meteorological station. There is a variation of rainfall from one area to another. Shimoni, is the station closest than the other four to the sea and appear to receive greatest amount of rainfall. Each data set shows that the mean rainfall was highest in April-May with mean value range of 200-350 for the five stations considered. For the coastal stations from south to north i.e. Shimoni, Mombasa and Malindi corresponding to Gazi Bay, Tudor Creek and Kilifi Creek respectively, indicate a rainfall variation along the coastal stations with a northward decrease in rainfall. There is also variation in the amount of rain in each station in Kwale. Cumulative rainfall (Figure 5.1.3.1) in Shimoni suggests that maximum rainfall does not always fall in May. Unusual peaks do occur in March as well as in August.

These are probably influenced by trade wind rainfall, which occurs in Tanzania or topographic influence of the southern coastal highland characterised by Murima, Dzombo and Shimba hills.

The typical bimodal characteristic of rainfall is clearly revealed in 10 years data (1987-97) which also mirrors seasonality (Figure 5.1.3.1). Clearly. in normally years, least amount of rainfall occurs in January-February and September. High rainfall is in April-June with maximum in May. The rain decrease steadily from June to September and increase thereafter in October-November before the trend repeat.
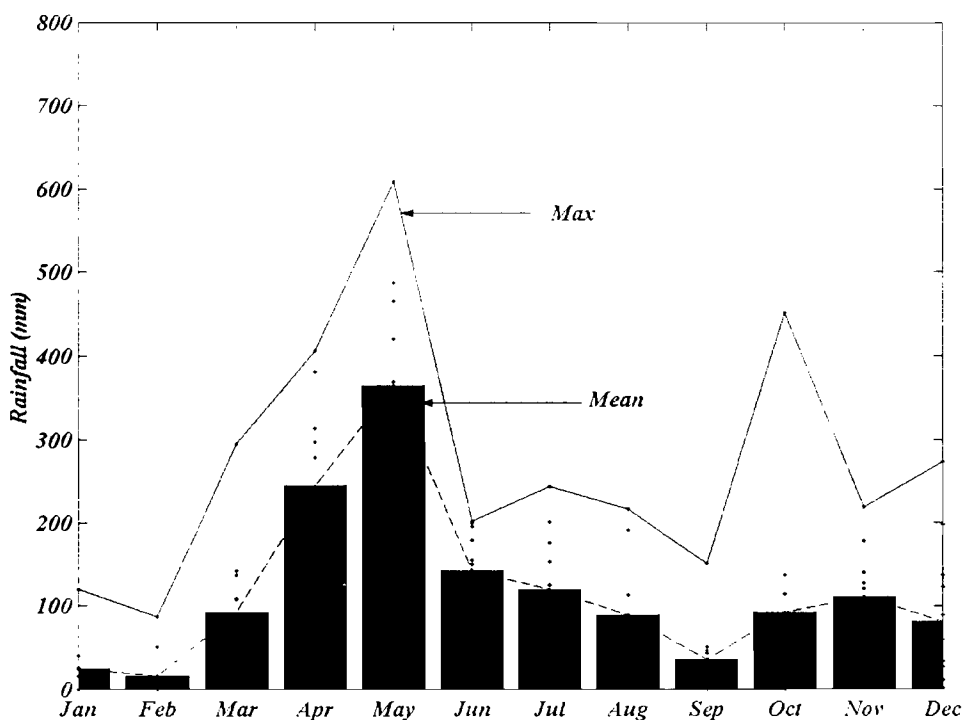
Figure 5.1.3.1 Cumulative rainfall for Shimoni Area (near Gazi Bay) observation from 1987 to 1997, Note the bimodal characteristics of the rainfall.

The rainfall for the three years of study 1995, 1996 and 1997 along those of 1972 to 1994 (dotted) is shown in Figure 5.1.3.2, which was not plotted with the data in Figure 5.1.3.1 so as to show the rainfall during the extraordinarily wet year. Total annual rainfall ranged from 800 mm to 2175 mm. Shimoni had a total average of 1410 mm, which is about 4mm/day of rainfall. MIAMS had an average of 1145 mm and about 3mm/day of rainfall. The highest rainfall fell in May 1996. The year with extra-ordinary rainfall was 1997 when the highest record of a total rainfall of 2175 mm was recorded. This year was referred to as the 'El-Nino year' in Kenya. In September-October the daily mean rainfall of 826 mm was recorded in October that year, and was still higher than the usual amount of rainfall by the end of the year and in the earlier part of 1998 (not shown). The curve showing the mean rainfall is also indicated in the Figure 5.1.3.2. MIAMS had a mean of 300 mm in May and about the same value in October. The data show that in May the rainfall was higher in Gazi area than in Tudor area although it tended to be vice versa in October.

From the mean curve shown in Figure5.1.3.2 the daily precipitation values can be obtained for each monsoon period.
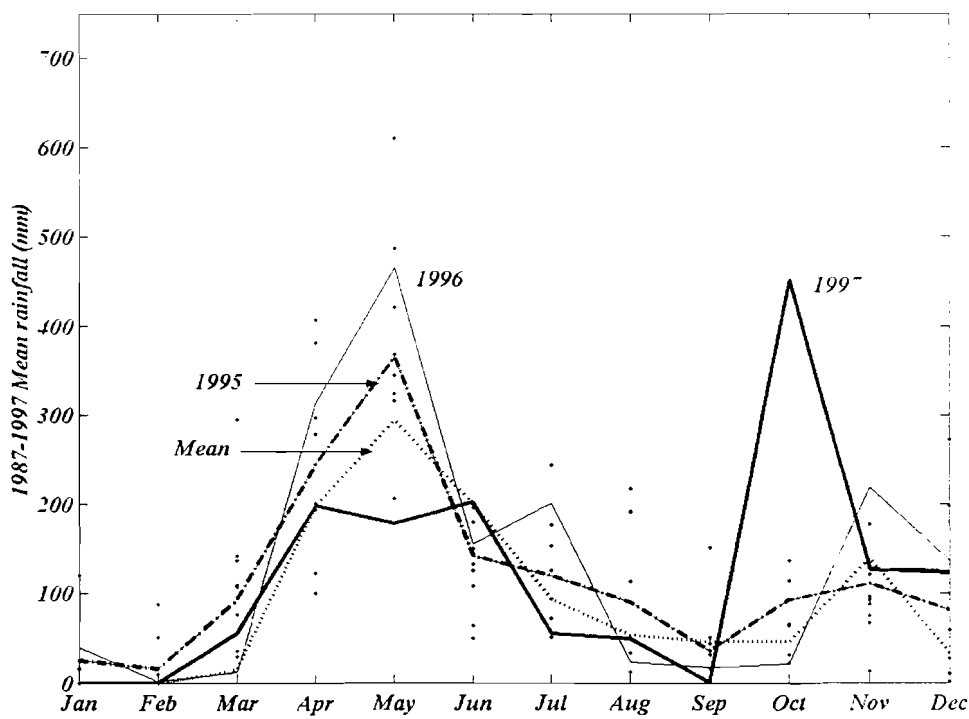
Figure 5.1.3.2 Depicts rainfalls for 1972-1997 with emphasis on 1995, 1996 and 1997 so as to highlight the extraordinary rains at end of the SEM-season in 1997.

River discharge

Several rivers and streams enter each of the study area, some of them carrying water only in the rains seasons. The main rivers and the corresponding catchment were shown in Figures 4.3.1.4a-c. Of the three watershed of the study area Kilifi Creek has the largest while Gazi Bay has the smallest. For Gazi Bay the two main rivers as mentioned earlier are the Mkurumuji River and the Kidogweni River. In Tudor Creek, are the Kombeni and Tsalu Rivers, and for Kilifi Creek, Nzovuni and Vitengeni Rivers. Of the

163

observations period covering a period of 1967-1987. The average monthly flows of the Mkurumuji River are summarized in Table 5.1.3.1. The estimates for the discharge values from the two rivers into Gazi Bay are shown in Figure 5.1.3.6. The discharge range is 0.16-4.0x 10^5 m^3/day. The highest discharge is in the IMLR season with a peak discharge in May of 4.0 x 10^5 m^3/day and a mean of about 2.2 x 10^5m^3/day. In the IMSR. NEM and SEM seasons the mean discharges are about 0.7 x 10^5 m^3/day, 0.4 x 10^5 m^3/day, and 0.8 x 10^5 m^3/day respectively.

Table 5.1.3.1 Discharge from Mkurumuji River 1966-1987

Mkurumuji river discharge (m^{3}s^{-1}) from 1966-1987											
Yrs	NEM				IMLR		SEM			IMSR		
	Jan	Feb	Mar	Apr	May	Jun	Jul	Aug	Sept	Oct	Nov	Dec
66-77	0.30	0.29	0.08	0.51	0.95	0.56	0.14	0.09	0.05	0.19	0.45	0.30
78-80	0.05	0.04	0.03	0.20	1.18	1.59	0.04	0.27	0.05	0.25	0.35	0.30
81-87	0.06	0.07	0.08	0.07	2.51	1.48	0.48	0.19	0.26	0.22	0.25	0.30
Total	0.41	0.40	0.19	0.78	4.64	3.62	0.66	0.55	0.36	0.66	1.05	0.90
Mean	0.14	0.13	0.06	0.26	1.55	1.21	0.22	0.18	0.12	0.22	0.35	0.30

It should be noted that discharge measurements are not easy to obtain and therefore effort was made to obtain other sources of information. For example Kitheka givers order for discharge of river Mkurumuji and Kidogweni to be of the order 4 x 10^5

164

m^{3}day^{-1} and a mean discharge of order 2×10^5 m^{3}day^{-1}, respectively, which agrees closely with the above results, he further points out that the maximum discharge can reach 17m^{3}s^{-1}.
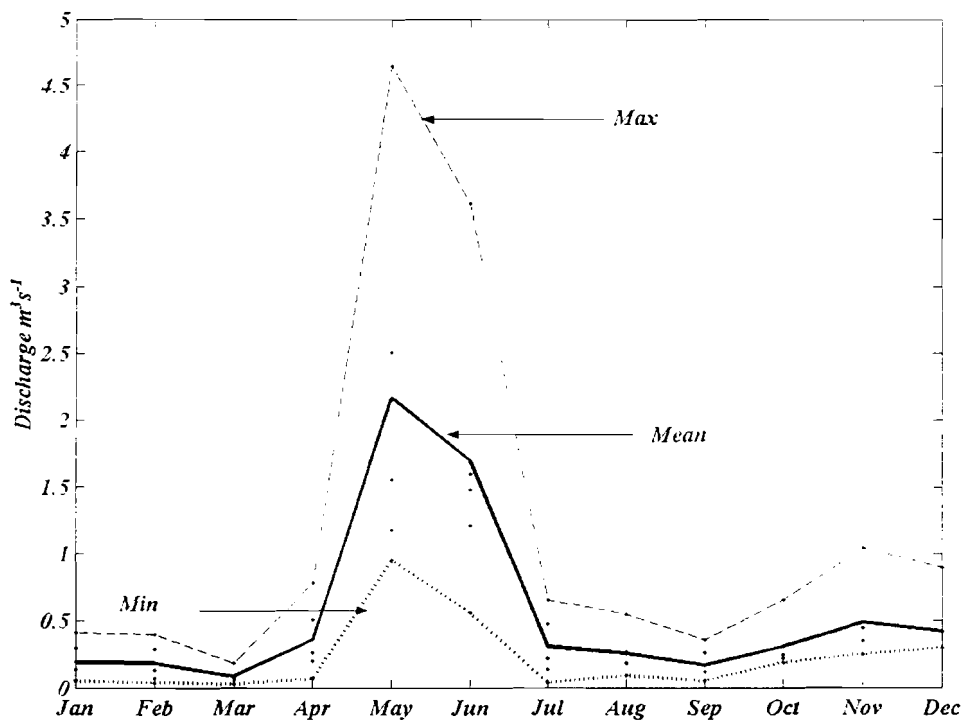
Figure 5.1.3.6 Typical discharge from Mkurumuji and Kombeni Rivers.

For the eestimate of river discharge where the rivers are not gauged, the long-period discharge is used to calibrate the river discharge into the Tudor and Kilifi creeks. By noting that the long-term discharge into Gazi Bay is of order 4×10^5 m^{3}day^{-1} and assuming the precipitation in the catchment enter the bay flows 'non-retention' the discharge would be 10×10^5 m^{3}day^{-1} for the annual average of 4mm/day rainfall.

This means that only 40% is able to reach the creek. 60% is lost. Tudor Creek catchment area is twice as much Gazi Bay catchment area, leading to only 20% reaching the creek basin. For Kilifi catchment area that is 7 times as large, only about 6% reach the creek basin as the river input (this assumption is used later when Knudsen model is applied to estimate water exchange).

Combined discharge into Gazi Bay, Tudor Creek and Kilifi Creek are also shown in Figure 5.1.3.7 (the source of data, Norconsult, 1975). The discharge into Kilifi is can also be taken as similar to discharge from Lwandani River discharging into Mtwapa Creek. The discharges are assumed as typical monthly values for the study areas. Figure 5.1.3.8 is discharge due to precipitation on the surface of Kilifi Creek (area=21km^2). The observed northward decrease in discharge into the study sites i.e. from Gazi Bay to Kilifi Creek is reminiscent of diminishing rainfall. More precipitation occurs in the south than in the north coast. There is also a tendency of the rain to start earlier as March-April in the northern part of the coast, making discharge appear more in April than in May.
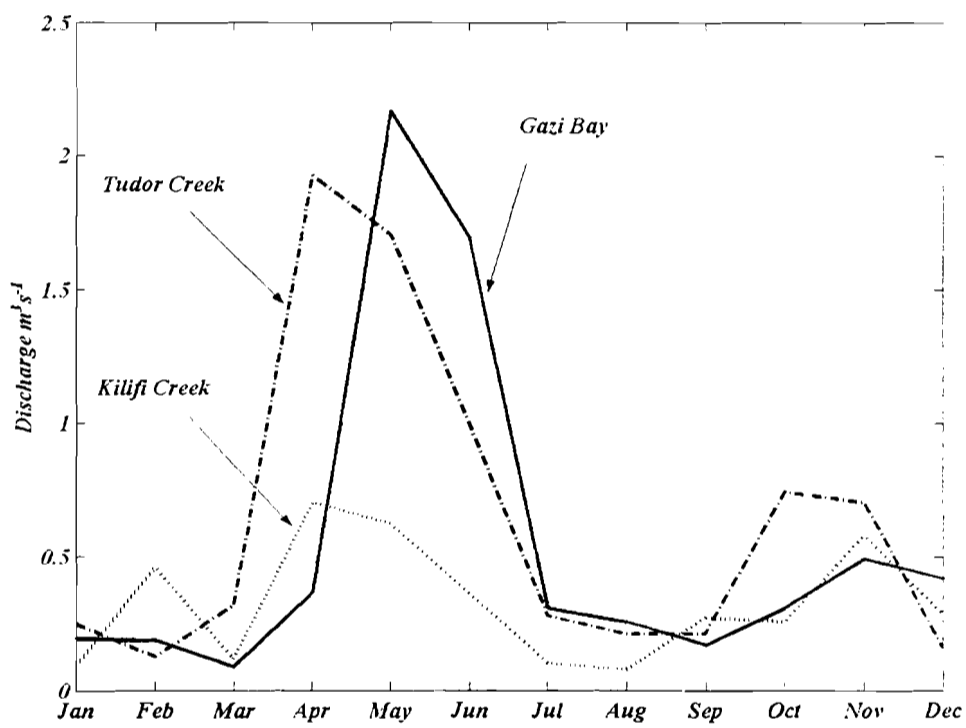
Figure 5.1.3.7 Typical river discharges into Gazi Bay, Tudor and Kilifi Creeks
(Source, KMD and Norconsult, 1975).

167
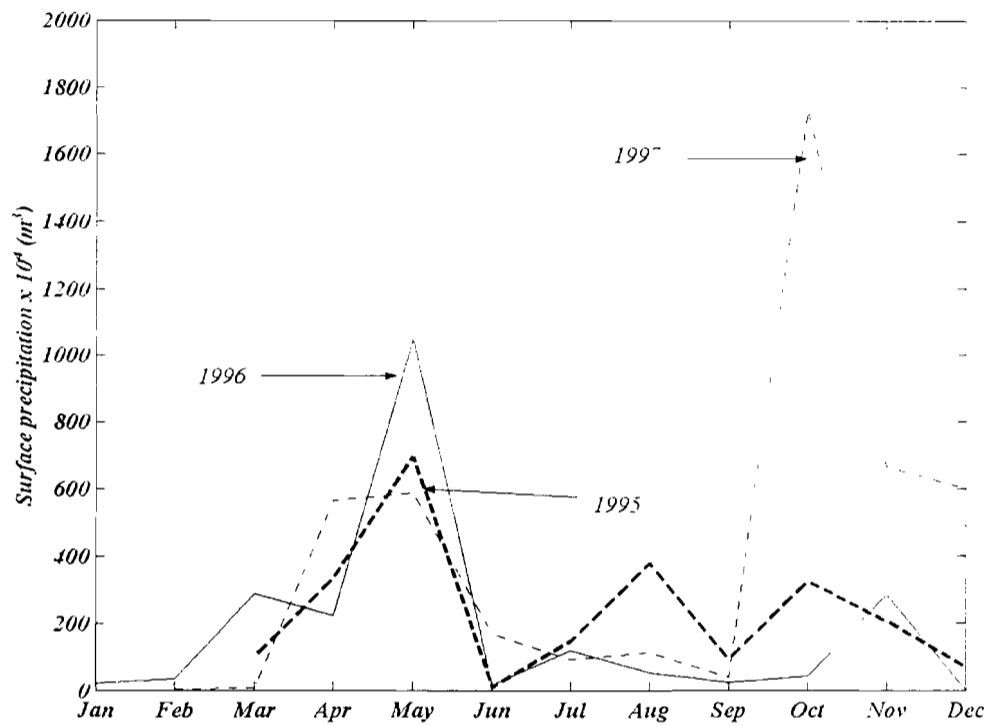
Figure 5.1.3.8 Discharge due to precipitation over the catchment area and the surface area of Kilifi Creek, for 1995, 1996 and 1997.

Estimates of evaporation

From the water exchange theory (Section 4.4.1), it is seen that fresh water input into the bay is required and also evaporation flux. Evaporation rate (Qe) which is defined as the mass of water evaporated per unit time(mm/day), was calculated using the meteorological data and the equation suggested by Gill (1982).

$$Q_e = \rho_a C_e w(q_s - q_a)$$

where Q_e = the evaporation (mm/day), ρ_a = density of air (Kg/m^3) w = wind speed (m/s)

q_s =specific humidity at the sea surface (Kg/m^3) q_a = Specific humidity at standard level

(kg/m^3) C_e= 1.5 x10^{-3} is a dimensionless coefficient called Dalton number.

Figure 5.1.3.9 shows the difference between the air and sea temperature in Tudor Creek during the time the weather mast was used.
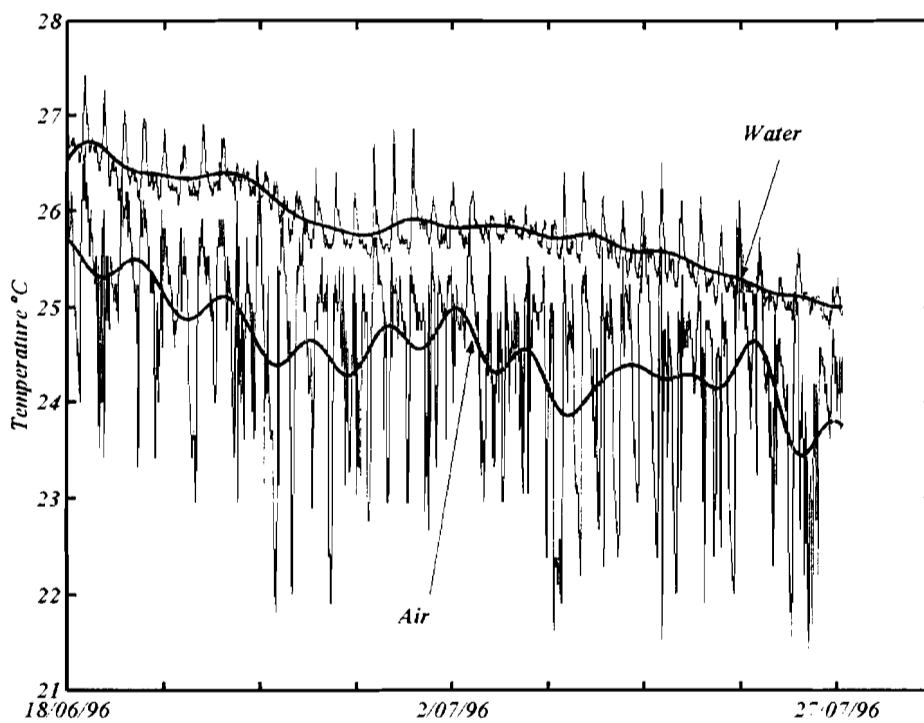
Figure 5.1.3.9 Illustrating the relationship between the air and sea temperature in the Tudor Creek for the period 18/06-27/07/1996.

Q_P and Q_e represent represents precipitation and evaporation respectively. The mean rainfall calculated from measurements in the available meteorological stations was used (and was assumed homogeneous for the three study sites). T= 86400sec, ρ = Density of freshwater taken as 1000Kg/m^3 in the creek (bay). A_s= Surface area, A_c= Cross section area and η=Average tidal range calculated in Section 5.3.3.3.

For q_R the mean values obtained for Mkurumuji River (Figure5.1.3.6), and predicted values for Kombeni and Tsalu Rivers are used.

To obtain q_R, q_E and q_P for short periods. Direct river discharge q_R was obtained from river flow (velocity) and cross-section. Precipitation (q_P) for short period was obtained by multiplying the mean rainfall with the sum of the catchment area and the creek or bay surface area.

To obtain q_R for long period, (inter-seasonal period) e.g. SEM dry (July to November), mean values of river discharge for the period in question were determined. This was also calculated from evaporation using the above expression. To get river discharge the land catchment area, excluding the bay-creek surface areas multiplied by amount by mean annual rainfall minus the same area multiplied by evaporation gave us an estimate of the runoff and river discharge into the bay.

5.2 ESTIMATES OF RADIATION AND HEAT FLUX

5.2.1 Radiative fluxes

The radiative fluxes are Q_S ($Jm^{-2}s^{-1}$ or Wm^{-2}) solar radiation entering through the sea surface and Q_B, which is the heat loss by the net outgoing long-wave radiation. Figure 5.2.1 shows the variation of the net out going radiation obtained from the weather mast in Tudor Creek for June-August 1996. The figure shows clearly fluctuations for the 55 days record and is probably caused by molecules in some bands e.g. H_2O, O_3 and CO_2. There is no insolation at night. They are reflected during an overcast sky, insulating the creeks against radiation energy. The calculated values range from –342.7 to175.6 Wm^{-2} with a mean of –57.5 Wm^{-2}.
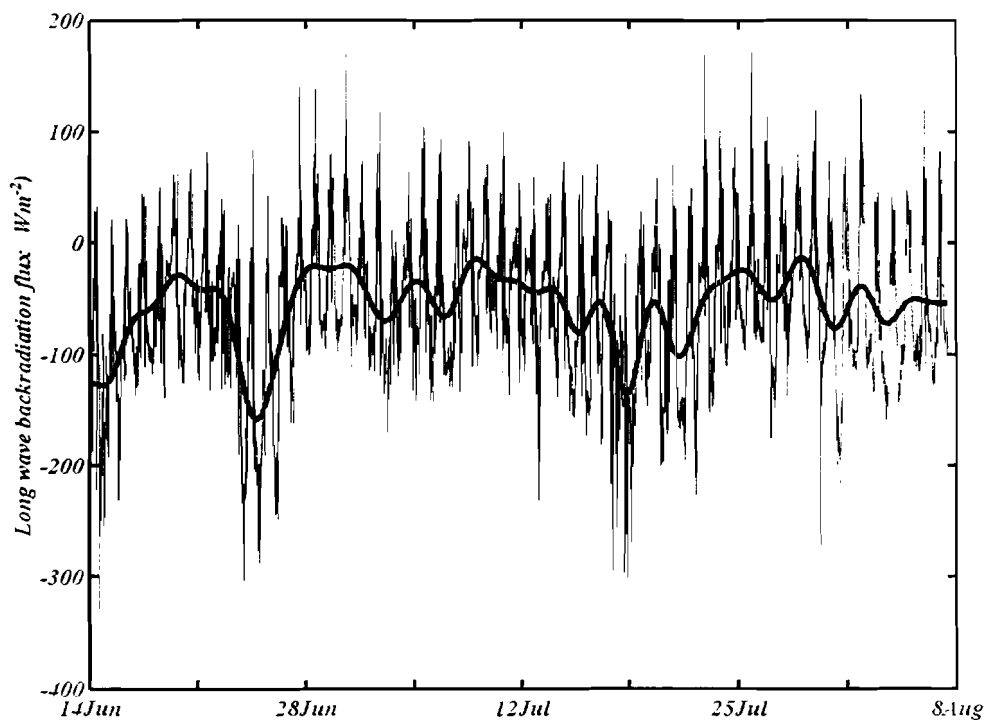
Figure 5.2.1 Back radiation from Tudor Creek weather mast station, June-August 1996.

171
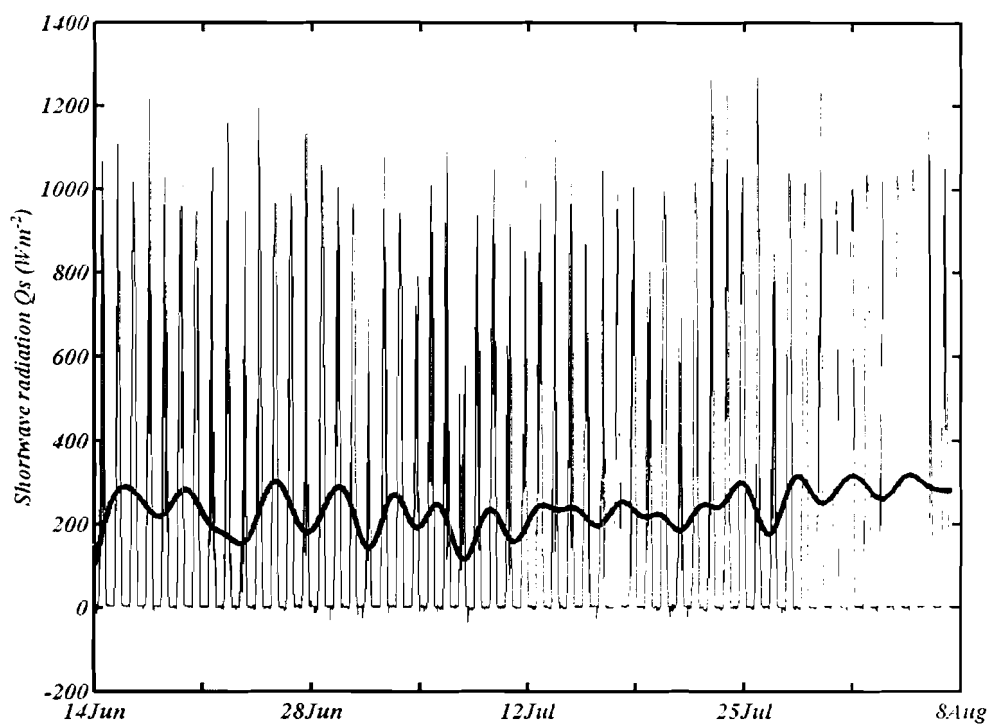
Figure 5.2.2 Solar radiation from Tudor Creek weather mast station, June-August 1996.

For the solar radiation shown in Figure 5.2.2, the maximum radiation is 1270 Wm^{-2}, with a mean of 235.5Wm^{-2}, and a standard deviation of 338 Wm^{-2}.

172
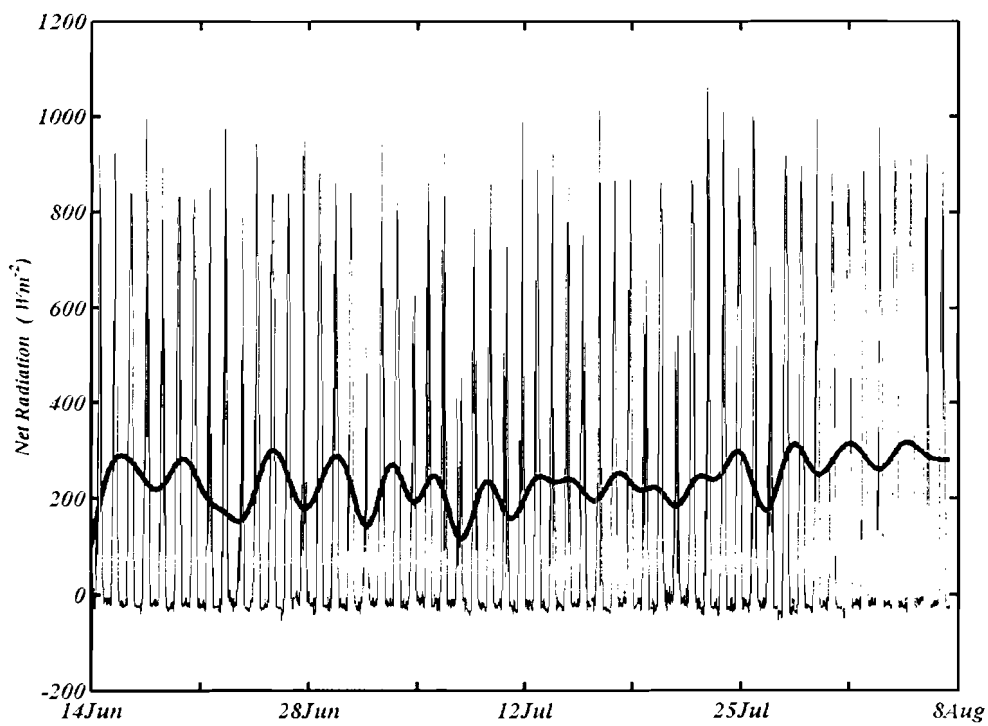
Figure 5.2.3 Net radiation from Tudor Creek weather mast station, June –August 1996.

The net radiation (Figure 5.2.3) varies from a maximum value of $1061\mathrm{Wm}^{-2}$ and minimum of $-68\ \mathrm{Wm}^{-2}$ and mean value of $175\ \mathrm{Wm}^{-2}$.

The values for the Q Atmosphere (or the total heat flux through the sea surface) range from a maximum of 1330.6 Wm^{-2} and a minimum of -620.7 Wm^{-2} with a mean of 70 Wm^{-2}.
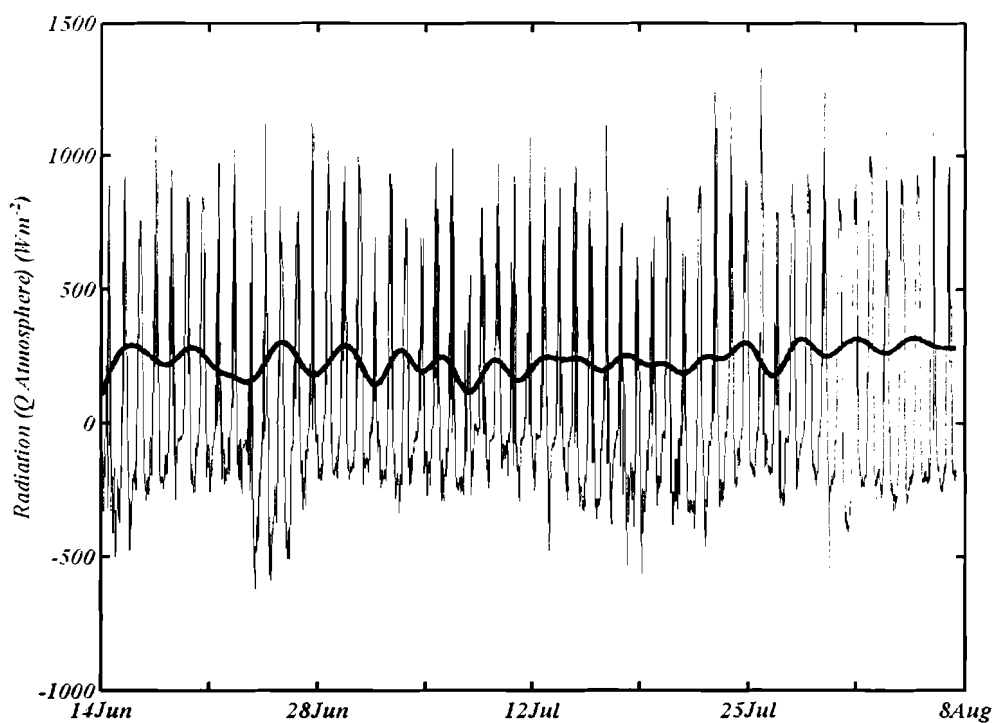
Figure 5.2.4a Solar Radiation (Q Atmosphere) from weather mast for the period, June –August 1996.

The net surface heat flux (Q_N) is the addition of the net solar (or short-wave) radiation Q_S, the net long-wave or back-radiation (Q_B)and the evaporative or latent heat flux (Q_E) and the sensible heat flux (Q_H) as noted in Eq.4.4.1.

Typical radiation measurements for the coastal area (Mombasa and Malindi) are shown in Figure 5.2.4b-c as well as sunshine and cloud cover.

The results of solar radiation shown in Figure 5.2.4b when compared with observation from the weather mast show radiation of similar magnitude, i.e. close to the mean range 180-200Wm^{-2}, shown in the figure, for the SEM season.
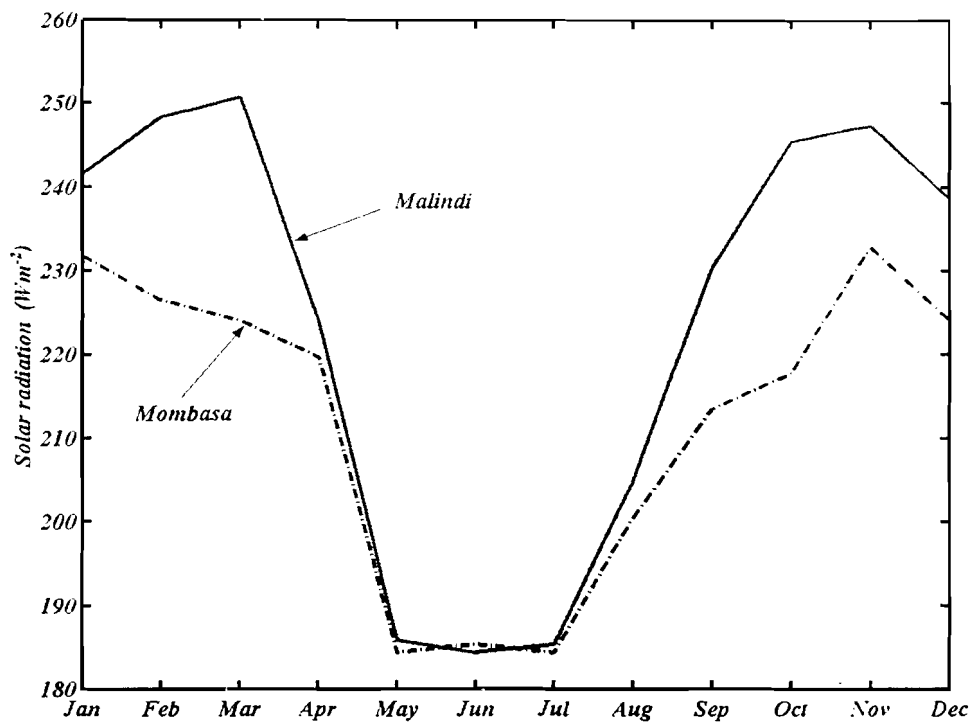
Figure 5.2.4b Typical monthly variation of solar radiation flux in Mombasa and Malindi (Data source, KMD).

The highest values fall within the range 260-280 Wm^{-2}. Solar radiation plummets to low and minimum values (less than 190 Wm^{-2}) from early march, probably due to invasion of clouds over the area; this is confirmed by Figure 5.2.4c where fluctuation in cloud cover is shown.
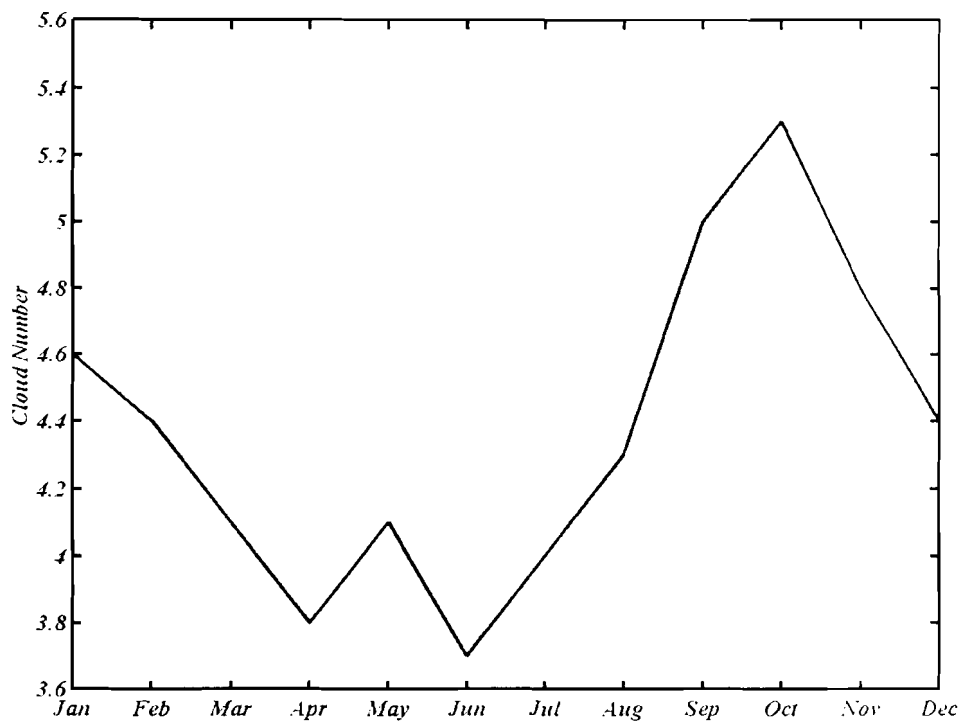
Figure 5.2.4c Monthly cloud cover variation within the year in the coastal area (Data source KMD).

5.2.2 Turbulent fluxes

Figure 5.2.5 shows the fluctuation of the sensible heat flux (Q_H). Maximum value is 75.5 Wm^{-2}, minimum –8.4 Wm^{-2} and a mean of 10.5Wm^{-2}.
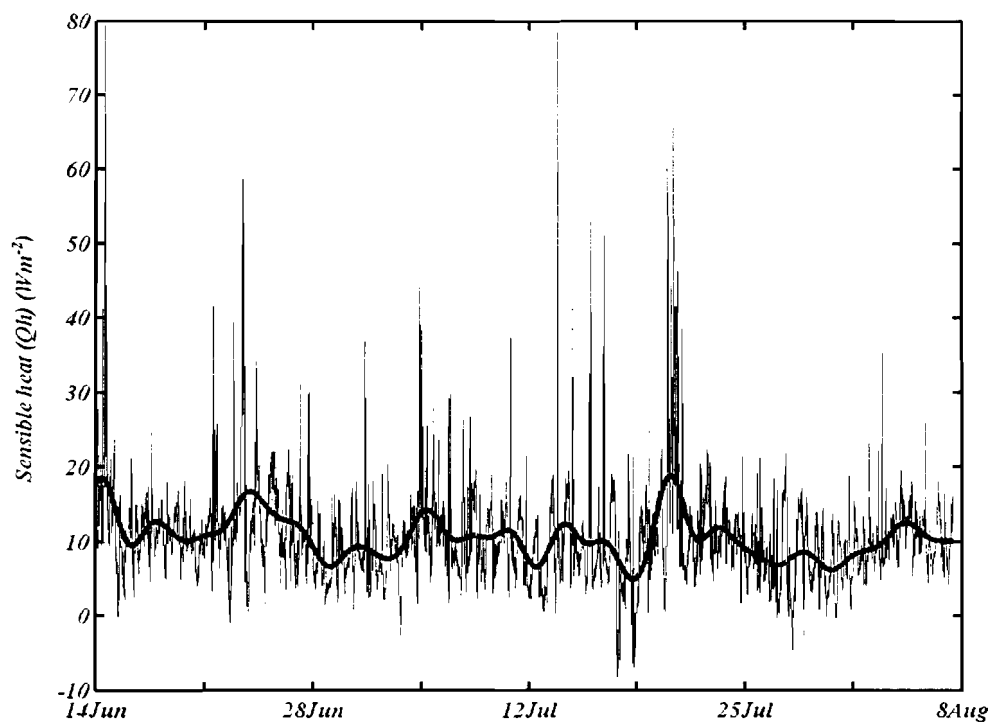
Figure 5.2.5 Fluctuations of sensible heat from weather mast at Tudor Creek June-August 1966.

The values for evaporative heat flux ranged form a maximum of 431Wm^{-2} to a minimum of 13Wm^{-2} with a mean of 118Wm^{-2} (Figure 5.2.6).
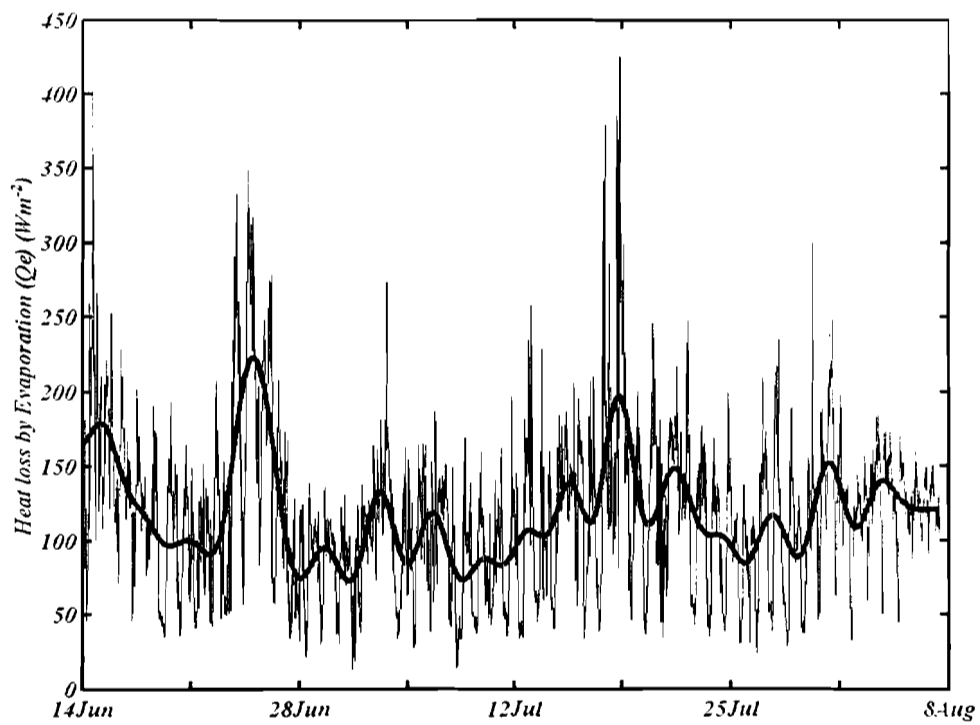
Figure 5.2.6 Fluctuation in evaporative flux. Note flux variation due to evaporation (Qe), June-August 1966.

5.3 GAZI BAY

5.3.1 HYDROGRPHY

Data from tide gauge, current meter, salinity surveys and other water properties

(e.g. nutrients and turbidity) are used to examine the hydrographic variability in Gazi

Bay, in times scales of a day, 14 days and longer. First, the 18-day long temperature

series is analyzed for response to tidal and solar forcing. Temperature variability

associated with neap and spring tidal periods are identified and compared. Forcing related

to tide is inherently associated with tidal currents; hence effects of the flow dynamics on

the temperature are analyzed by examining the tidal currents for the same period of

measurements. It is found that besides tidal and solar forcing morphology of the bay

could be playing a crucial role in enhancing thermal response during neap low water and

spring high water. In addition, the structure of the ocean water exchanged with the bay,

particularly during the peak of fresh water input is examined.

5.3.1.1 Bay temperature fluctuations

Figures 4.3.2.1a and 4.3.2.1b, show temperature observed for different days in November

1999, from the tide gauges and current meter located at position indicated by MT2 and

RCM. The two data sets have different duration. Statistical values of these parameters

over the entire record of each instrument are show in Table 5.3.1.

Table 5.3.1 Statistical values of temperature for the tide gauge (MT2) and current meter (RCM) over the entire period of measurements.

	MT2 Temp °C (18-days)			RCM Temp °C (5-days)		
	Max	Max	Mean	Max	Mean	Min
Total	32.4	28.8	27.8	28.8	27.8	26.7
Neap	31.1	-------	29.7	-------	-------	-------
Spring	31.8	29.6	27.5	-------	-------	-------
Two day event around low water neap day-4				32.1	31.6	31.0
Two day event around high water spring day -13				30.3	29.1	28.1

General decreasing trend in temperature from maximum value of 32.4°C to a minimum value of 27.8°C, with a mean of 30.2°C and a range of about 4.6°C is evident in Figures 5.3.1.1 top panel. Fluctuation related to neap and spring events are identified as the small and relatively more pronounced fluctuations in the top panel and centered on the 17 and 25 day respectively, and corresponding to the similar days in the lower panel of the same

figure. The gradually decreasing trend in temperature is attributed to fortnightly effect of the tide and probably has its source in larger amount of cooler oceanic water that enters the bay during spring than neap.
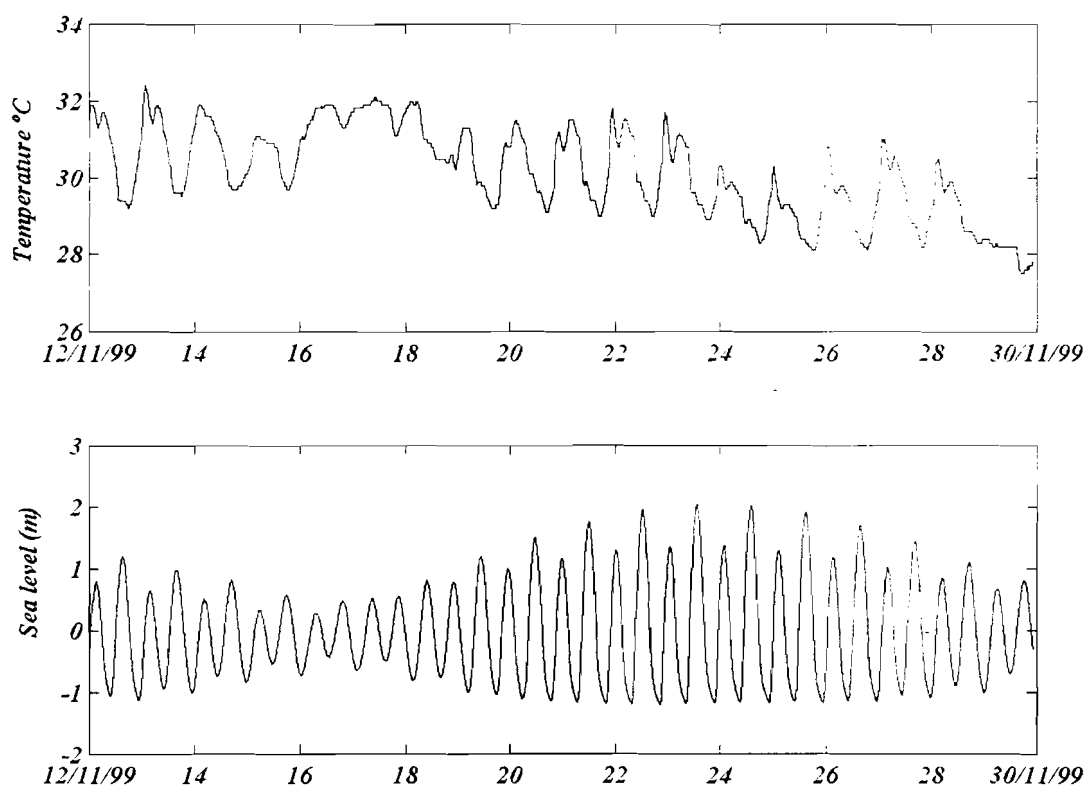
Figure 5.3.1.1 Temperature (top panel) and sea level (lower panel) fluctuations in Gazi Bay at station MT2 for a period of 18 days from 12-30/11/1999 during the Northeast monsoon season (NEM).

In Figure 5.3.1.2, temperature fluctuations in neap and spring are compared in the four panels of the figure. The results illustrate clearly that the temperature is higher in neap than in spring. Daily fluctuations are also evident; however, more details are given when temperature and current are plotted together (see Figure 5.3.1.6). Interesting thermal events seem to occur for 2-3 days around low water neap centered on day 16-18 and during high water spring centers on the day 22-26. The statistical analysis of the two events is also given in Table 5.3.1. The two events seem to occur around the height of each tidal stage as can be noted by careful examination of temperature during spring tide (Figure 5.3.1.1 top panel) on day 12-13.

The event around neap (day 16-18) indicates elevated temperature with maximum value of 32.1°C and a mean of 31.6°C, about 2°C over the mean of the first seven days. The spring maximum temperature is 31.8°C, with a mean of 30.3°C. During this neap 'thermal upwelling' event the range of temperature fluctuation is reduced by 70% of its spring value. More over, the results show that the temperature difference between high water slack and low water slack is 1°C, which is three times lower to than the spring value of 3 °C (Table 5.3.1).

182
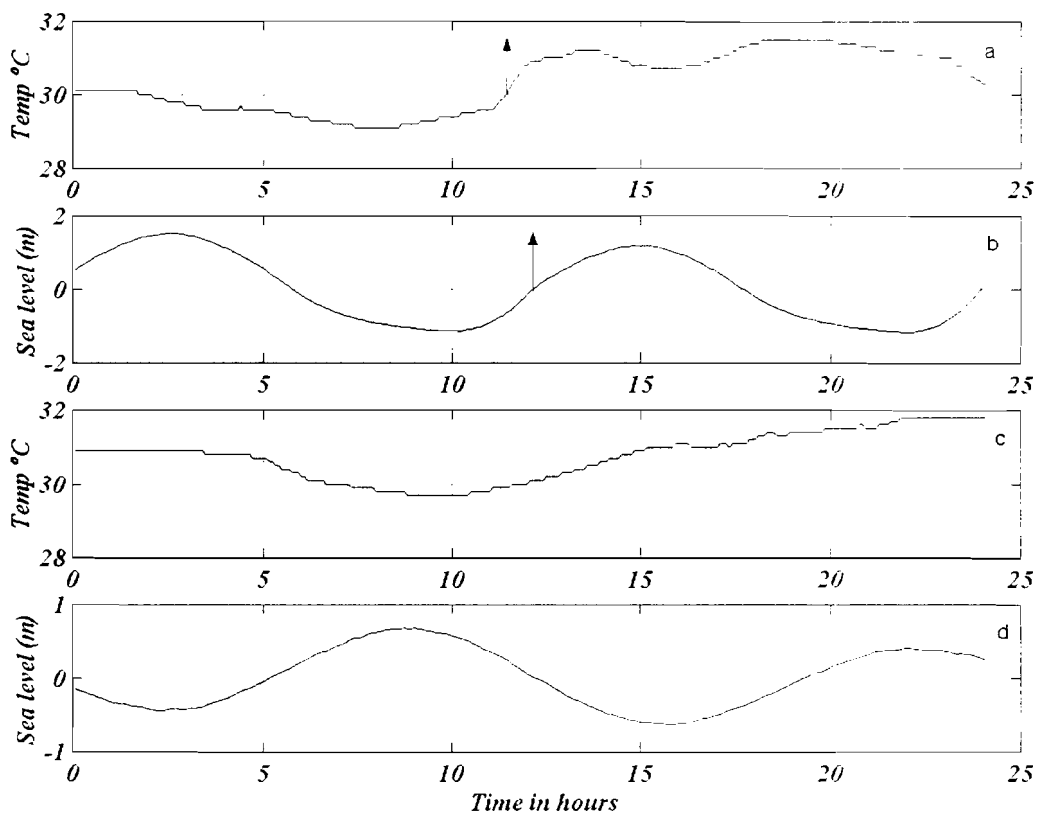
Figure 5.3.1.2 Panels illustrating range of temperature (a-b) sea level (b-d) during spring and neap around day 17 and day 25 from Figure 5.3.1.1.

The elevated temperature and diminution of range of temperature fluctuation during neap is evidence of enhanced solar heating and reduction in tidal excursion. This is probably caused first by direct solar heating of bay water and the inter-tidal area exposed at low water, followed by combined heating of the water by solar and the heated inter-tidal area during the flood period. Incidentally this seems to produce an overwhelming thermal forcing and elevates the temperature considerably. The diminution of the range of

183

fluctuations is probably an indication of short tidal excursion and hence reduced movement of warm water in the bay.

Around day 23-25, the temperature decreases by about $1^{\circ}C$ from the spring maximum of $31.8^{\circ}C$, and a reduction of the range of fluctuation by 30% occurs. Unlike, in the neap event, the phenomenon that lowers the temperature is probably evapo-transpiration which cools the water coupled with the cooling effect induce by the large canopy of mangrove forest. The reason for the small reduction in the range of temperature fluctuation is, again, suggested as caused by diminution of in tidal excursion. This time however, it probably occurs when tidal flow at high water spring is subjected to the friction in the mangrove area. The tidal range is greater in spring (2.8m) than in neap (1.2m), consequently fast currents and large tidal prism ensure spreading of water further into the mangrove areas, where it encounters increasing drag force from the roots and trunks of the vegetation, this can essentially be regarded as morphological forcing.

Daily fluctuations

The daily fluctuation for temperature in neap and spring are shown for one-day cycle in Figure 5.3.1.4. Two spikes of different duration observed in spring however, are not evident in neap for reasons stated earlier. For this particular day there was no simultaneous current observations made, however, the thermal response dynamics from day to day in the bay is further illustrated by analysis of the two forcing parameters, tide and current, for a period just before neap (see Figures 5.3.1.5-6).

Tidal response signature is again evident in the temperature series and elevation

of temperature during the day.
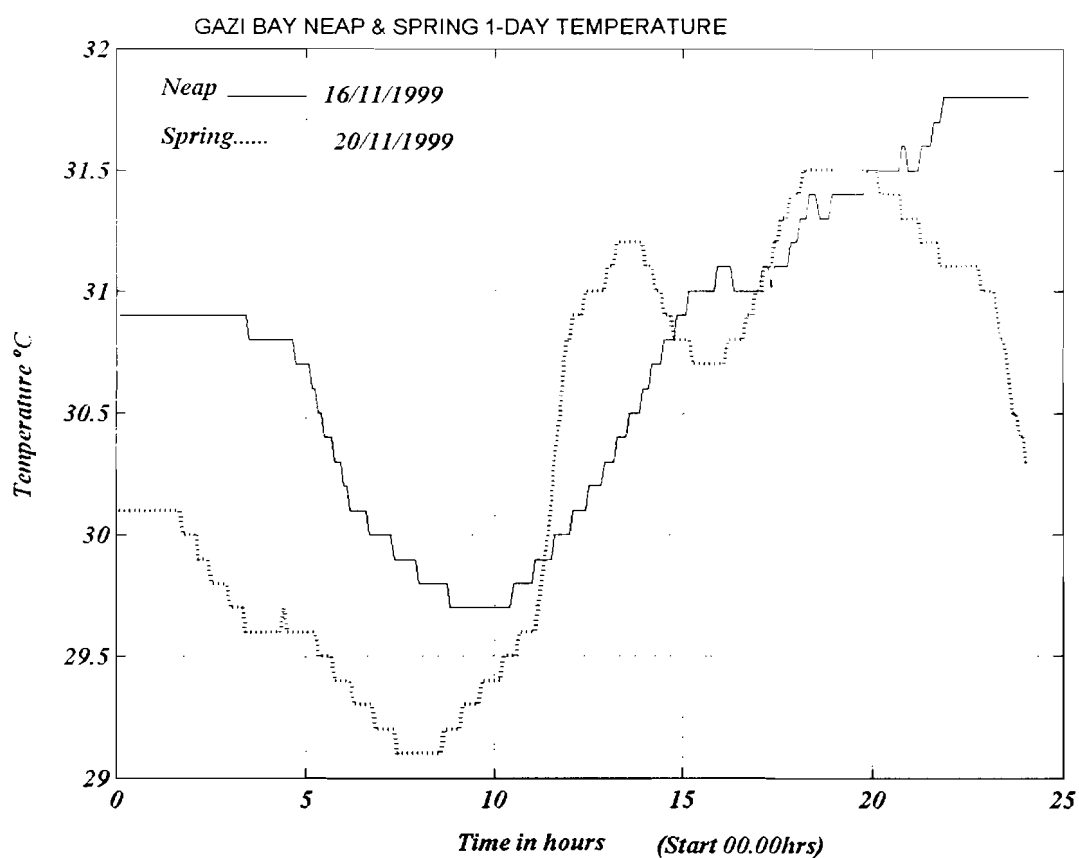
Figure 5.3.1.4 Comparison of neap and spring temperatures for one day in each period. Note the two spikes in spring and the cooling effect of flood tide just after the first spike and the elevated temperatures in neap.

The upper panel (a) indicating temperature in shallow water (2m) reflects high temperature and high range of temperature fluctuations than panel (c) representing temperature at 10m-depth in the channel. The results demonstrate that the range of temperature fluctuation ($3^{\circ}C$) is higher in the shallow areas and than in the deeper part of the bay.

GAZI BAY MT2 & RCM
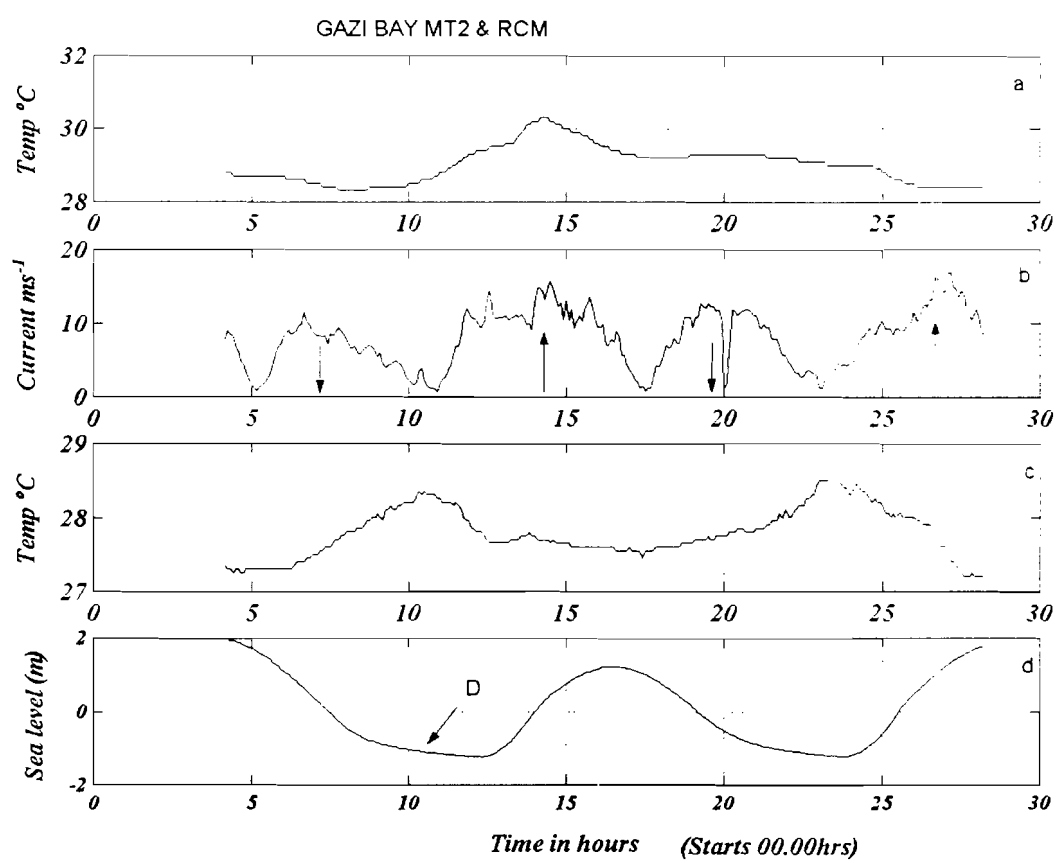
Figure 5.3.1.5 Composite illustration of (a) temperature in Gazi Bay at a depth of
2m, (b) tidal current at 10m depth, and sea level. Up and down arrow indicate flood
and ebb currents respectively. Note D in the lower panel indicating 'distortion'
hydraulic or morphological effect on sea level.

Further detailed examination of Figure 5.3.1.5a-d and Figure 5.3.1.5a-c reveal that
the temperature of water in the deeper part of the channel increases between 5-10hrs,
illustrating warming up of water during ebb. However, at the same time the water in the

bay gradually cools to a minimum temperature at 8hrs. This suggests that the warm water is not from the bay at this time. A plausible explanation of this warming up at deeper water is the local wind forcing. At night the sea is warmer than the ocean, the resulting offshore winds drive previously heated and trapped water in the bay out into the channel and farther offshore as a thermal plume. The presence of this plume having reached the entrance location during the ebb warms up the deeper water in the channel. This is well noticed in the earlier part of neap when the water tends to be trapped in the lower part of the bay and resulting in elevated temperatures at 10m (Figure not shown).

Solar heating can be expected to be weak in the morning when the sun is still at low angle. This results in local cooling of the inner part of the bay by the wind, which overwhelms heating effect. During the low water slack (10hrs) the temperatures reach maximum value of 28.3°C, and the bay by this time has warmed up due to sun heating. The winds probably weaken and begin to change direction at about this time. Without the hydraulic (or morphological) effect the sea level would not have a distortion (Figure 5.3.1.5) lower panel and would not be delayed before reaching minimum. The wind change, and the morphological influence probably give rise to an earlier flooding of the bay, the current leads the tide by 1.5hrs, as can be seen by comparing the flood current and the tide. This earlier flooding has insignificant cooling effect on the bay, however, as the time progresses the bay temperature increases rapidly. A maximum value of 30.2°C is reached at 14hrs.

The maximum temperature occurs just before the tide catches up with the flood current. The current accelerates at the turn of the tide and probably at the onset of onshore winds and drive Cooler Ocean water into the bay bringing the temperature down by about $1^\circ C$.

GAZI BAY MT2 & RCM
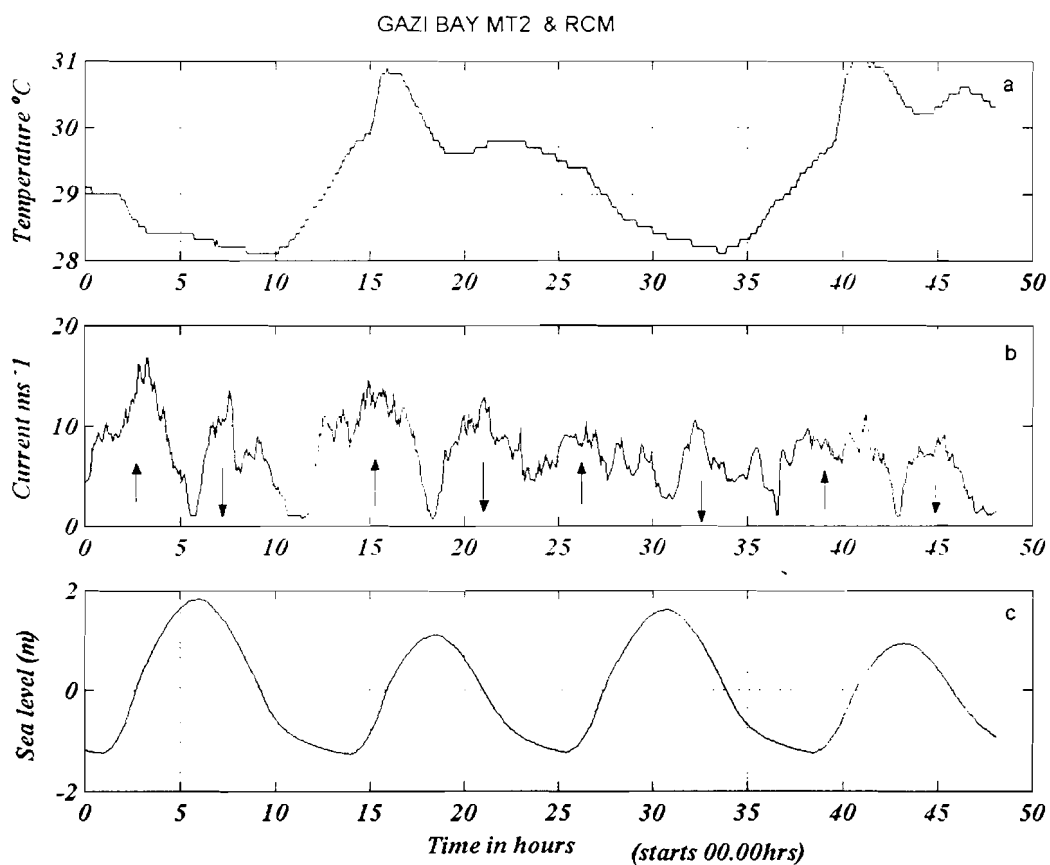
Figure 5.3.1.6 Temperature (a) current (b) and sea level (c) from Gazi Bay for two days (26-28/11/1999) during the NEM season. Note the daily fluctuation.

Solar forcing still continues after peaking at 14hrs, and at the turn of tide. When current reversed volume of water in the bay and depth decreases, and consequently leading to enhanced heating. This probably is the cause of the temperature increase observed as the

188

second spike clearly seen earlier in Figure 5.3.1.5, but barely noticeable in Figure 5.3.1.6. It should be noted that the first spike could sometimes have lower amplitude than the second, particularly when clouds, present in morning hours, reduce solar heating. It is clear also that ebb tide bring warm water into the channel and result in elevated temperature there with highest temperature occurring again at low water slack. As the sun inclines in the evening heating continues, intensity diminishes resulting in gradual decrease in temperature. With the cessation of solar heating the water in the bay and the channel cools. At night the offshore winds sets in and the process repeats.

Long-term seasonal variability

The temperature varies slightly from year to year. Slightly higher temperatures were recorded in 1997-1998 in 1995-1996. There are no large temperature fluctuations, between stations I-VII in Gazi Bay both for the surface water and bottom water.

Temperature variations occur from one season to the other. In the IMLR season, the temperature ranged from 30.5 to $27.5^{\circ}C$ a difference of $3^{\circ}C$. During the dry season, the range was from 29.4 to $33.7^{\circ}C$ a difference of $4.4^{\circ}C$. Lengthwise, throughout the season the surface to bottom the values were close to the range 27.9 to $28.7^{\circ}C$. This indicated that the water in the bay remained almost at the same temperature with no significant vertical temperature differences. Diurnal measurements revealed flooding tide introduced slightly cooler water from the ocean. While during ebb warmer water from upper bay area was found in the lower part of the bay.

5.3.1.2 Bay salinity fluctuations

24-hr salinity observations of 25-26 November 1999 are shown in Table 5.3.1.2 along with the observations made during neap and spring. Averages of salinity and temperature data collected hourly in surface and bed salinity at station III indicate higher salinity values and lower temperature in spring than in neap (Table 5.3.1.2). This is evidence that spring introduces high salinity and cooler water in the bay than neap. Figure 5.3.1.7 also shows salinity and temperature change from Station I to Station VI (Figure 4.1.1.1).

Table 5.3.1.2 Salinity and temperature during 24-hours (one day), neap and spring measured at station MT2 during the Northeast monsoon season (NEM).

PERIOD	PARAMETER					
1999	Salinity			Temperature		
	Max	mean	min	Max	mean	min
Day 25-26	35.05	33.14	30.51	35.05	33.14	30.51
Neap	33.89	33.65	31.34	31.5	30.54	28.21
Spring	35.25	34.93	32.14	30.8	28.92	27.82

The results indicate that relatively lower salinity and temperature occur during ebb in the morning hours (5-10h) with the lowest values occurring during lowest ebb

period. During flood tide the salinity increases and reaches maximum values in high slack

water. The creek water begins to warm up at about 10h, increases rapidly between 12 and

15h to a maximum temperature of about 30°C, due to solar heating before cooling

slightly due to invasions into the creek of the cooler oceanic water at maximum flood.
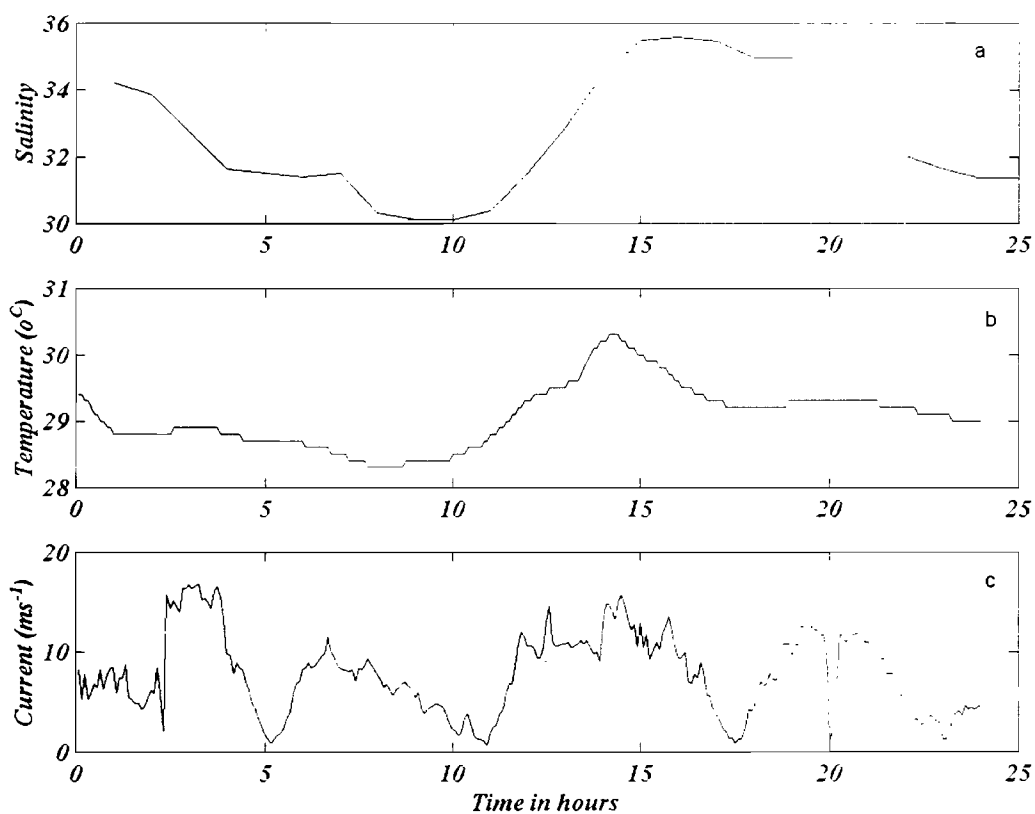
Figure 5.3.1.7 Example of daily fluctuation in (a) salinity, (b) temperature and (c) current in Gazi Bay on 25-26/11/1999.

Salinity taken along the bay indicate slight reduction in the surface salinity during

neap period, whereas the mid-depth salinity (not shown) and bed salinity remain high.

The reduction in salinity is most likely caused by brackish water from Mkurumuji River.

As the ocean water withdraws, it is replaced by water from the upper part of the creek. In addition, it should be noted that the small tidal excursion and slow currents in neap imply lower rate of mixing than during spring. More over the reduction in salinity is a consequence of coincidence of weak vertical mixing during the neap-tide period compounded by the brackish water of lower salinity at that time. As the current speeds increase in spring the surface salinity increases. This is partly caused by brackish water flushing from rivers Kidogweni and Mkurumuji, and partly because of increased mixing with the bottom water. The stratification (the difference in salinity between bottom and surface waters) becomes very small over the spring tide.
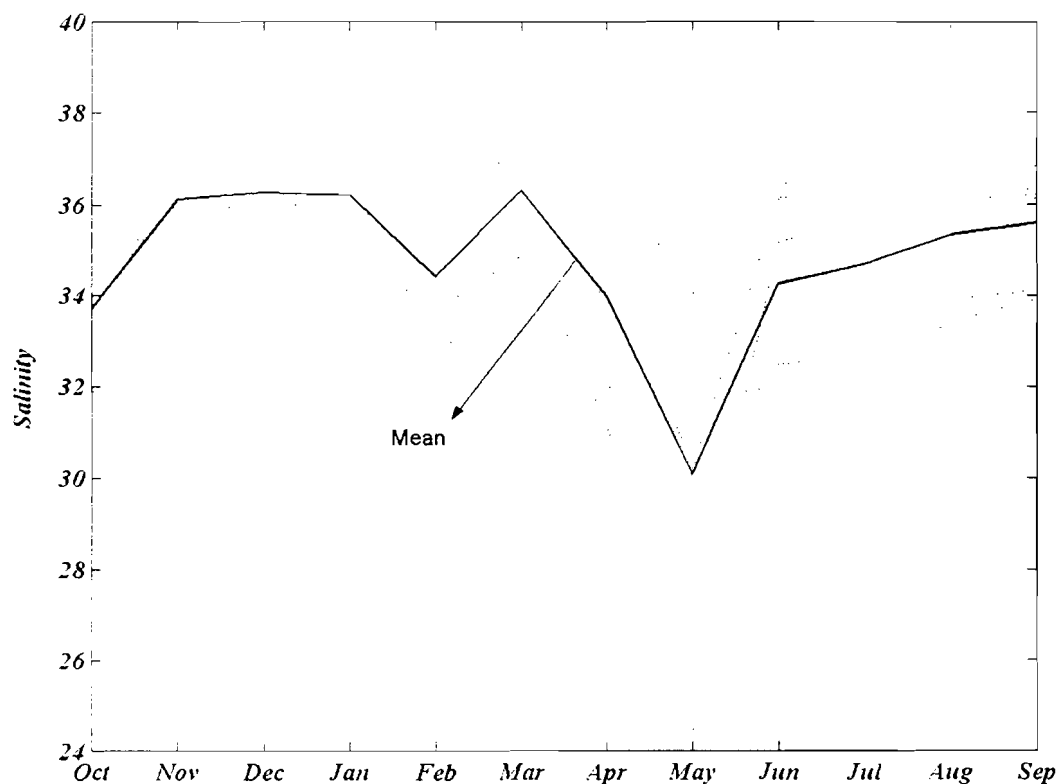
Figure 5.3.1.8 Mean monthly salinity covering the period 1996-97. Note lower salinity in February-March and insignificant salinity in November.

The salinity figure confirms the low salinity in IMLR and IMSR seasons. However, lowering of salinity before the start of the rain period suggest another non-local source of low salinity (see later) (probably arising from mechanisms related to the upwelling of the Kelvin waves in April-May and October-November along the East Africa Bight (Section 5.3.5.3). The maximum value of 29.2°C and 36.8 are found in January February (NEM) and the minimum values of 24°C and 33 just before and during the rain season.

During the wet season, the salinity ranged from 32.58 to 28.73 a difference of about 3.84. In the dry season, salinity was found to range from 34.37 to 35.95 a difference of 1.58; Surface salinity was found to vary from 30.22 to 34.59 and bottom from 34.72 to 35.47 at some localities bottom salinity was lower than the surface salinity. The result shows that water potentially likely to be exchanged with the bay is from 0-5m and with salinity of 35.35. At depth 10-50m-depth range salinity remains almost constant at 35.35, but higher than ocean. These results point to increased effects of evaporation due to increased solar radiation. The low salinity water is probably a part of low salinity water mass found at depths 200-400m (we will return to this in discussion).

5.3.1.3 Bay nutrients and other properties

Brief results on seasonal nutrient characteristics of Gazi Bay are presented here. More detailed studies on nutrients in the Bay can be found from the work of Hemminga et al. (1994) and Mwashote (1996). Also in Section 6.4.1m some additional nutrient information form inshore waters is presented for comparison with offshore.

Table 5.3.1.3 Nutrient characteristics in each season from station 1-VII, 1995-1996.

PERIOD	SITE		NUTRIENTS			
1995-1996		NH_4-N $(\mu MN)x10^{-2}$	NO_2-N $(\mu MN)x10^{-2}$	NO_3-N $(\mu MN)x10^{-2}$	PO_4-P $(\mu MP) x10^{-2}$	$Si(OH)_4$-Si $(\mu MP) x10^{-2}$
IMLR	I-III	40-150	70-250	100-990	20-30	
	VI-VII	30-140	50-150	400-1150*	20-30	
SEM	I-III	30-80	60-80	100-220	10-40	
	VI-VII	25-100	20-100	29-350	20-30	
IMSR	I-III	70-460*	10-40	38-70	60-100	
	VI-VII	10-60	5-60	42-110	5-90	
NEM	I-III	30-80	10-30	35-100	10-150	
	VI-VII	20-60	10-20	28-62	15-90	

Table 5.3.1.3 shows Nitrite, Nitrate, Phosphate concentrations in the bay in ranges. The range of nutrient from the mangrove-creek area is represented as from Station I-III. The second range VI-VII covers the entrance area. In IMLR Nitrite occur 56%. and Nitrate 72% of their total annual value. Other slightly greater concentration, NH_4 and PO_4, occur during the IMSR season of 37% and 20% respectively.

194

Further analysis reveals that more than 42% of the IMLR-Nitrate concentration occurs in the lower reaches of the bay (VI-VII) and high nutrient concentration in the upper bay area. They can be attributed to the discharge from rivers Mkurumuji and Kidogweni both of which according, as we saw in Table 5.1.3(a) have a fresh water supply of the order 4 m^3day^{-1} and 2 $x10^5m^3day^{-1}$ respectively during the rain season. (It is difficult to get good measurements of water discharge in these river systems because of lack of proper gauging).

Turbidity

The plume from River Mkurumuji was used briefly as a tracer during most the IMLR and IMSR seasons. It was observed the plume form the river moved right into the northeastward and across the bay to the Kinodo Creek (Figure 4.1.1.1) some of the water was trapped in the mangroves in the lower part of the creek. Part of the plume moved along the eastern part of the bay after making a clockwise turn. This confirmed that the water circulated clockwise during flooding stage. During ebb the plume near the Kinodo Creek migrated toward a secondary opening between the Peninsula and Charle Island. While toward end of ebb the main part of the plume migrated into the entrance channel area but after spreading brackish water in the entire central part of the bay. This movement of water in the bay as a strong implication to the sediment distribution and sea grass vegetation within the bay. During the two tidal stages sediment re-suspension occurred mostly near the mouth of the river and on the side of Kinodo Creek.

195

5.3.2 Sea level, currents and tidal analysis

5.3.2.1 Sea level

Figure 5.3.2.1 is a graphical representation of the rise and fall of the tide, which slightly looks like a cosine curve. This is a tidal curve of sea level time series of 12-30 November 1999 (18 days) for the tide gauge located at position MT2 in Gazi Bay (Figure 4.1.1.1). Similar time series was presented in Section 5.3.1.1 to aid interpretation of the temperature fluctuations there (see Figures 5.3.1.1-3). In this section we examine the sea level in detail. The top panel of the Figure 5.3.2.1a shows sea level time series with air pressure removed; whereas the lower panel (Figure 5.3.2.1b) the mean has been removed.

As we observed earlier, the neap and the spring periods with a series of low and high amplitudes respectively are centered on day 17 and day 25. The successive amplitudes are not equal. The tide nearly repeats itself once every lunar day, (24h and 50min), which is the time it takes a point on the earth to rotate back to the same position relative to the moon during each revolution. The daily rhythm of the tide cycle is given by the lunar day and not by the solar day of 24h.
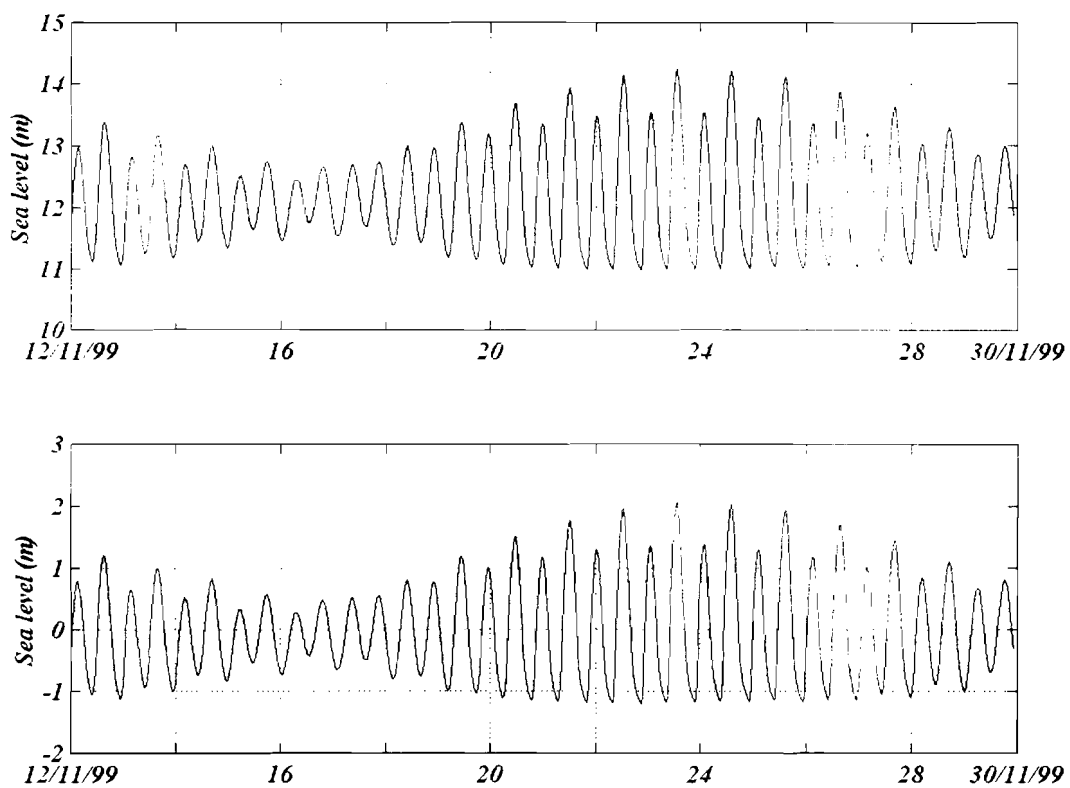
Figure 5.3.2.1 Sea level record from Gazi Bay Position MT2 for the 18 days, 12-30 November 1999, (a) with atmospheric pressure removed (b) mean removed.

Consequently, the times of high are roughly 50min later from one solar day to the next. Careful examination of the tidal curves reveals interesting features. The difference in height between the higher high water level and the lower low water is not equal, this is more pronounced at spring period when the fluctuations are largest, as can be seen by examining the top part of the curves. This is the diurnal inequality. The lower part of the spring period the inequality has been removed and the curve slightly distorted, this is the

effect of shallow water that give rise to shallow water tides (see Section 5.3.2.3). During neap the inequality is still observed particularly in the lower parts of the curve, indicating that the effect felt during spring low water is less felt during neap. However, inequality is removed at the top during two to three cycles in neap; this has something to do with thermal influence as we saw earlier. The tidal amplitudes during neap are reduced by almost 30% of their spring values. There is also the diurnal inequality between lower low water and higher low water and a daily inequality in the time intervals between pairs of high tides.
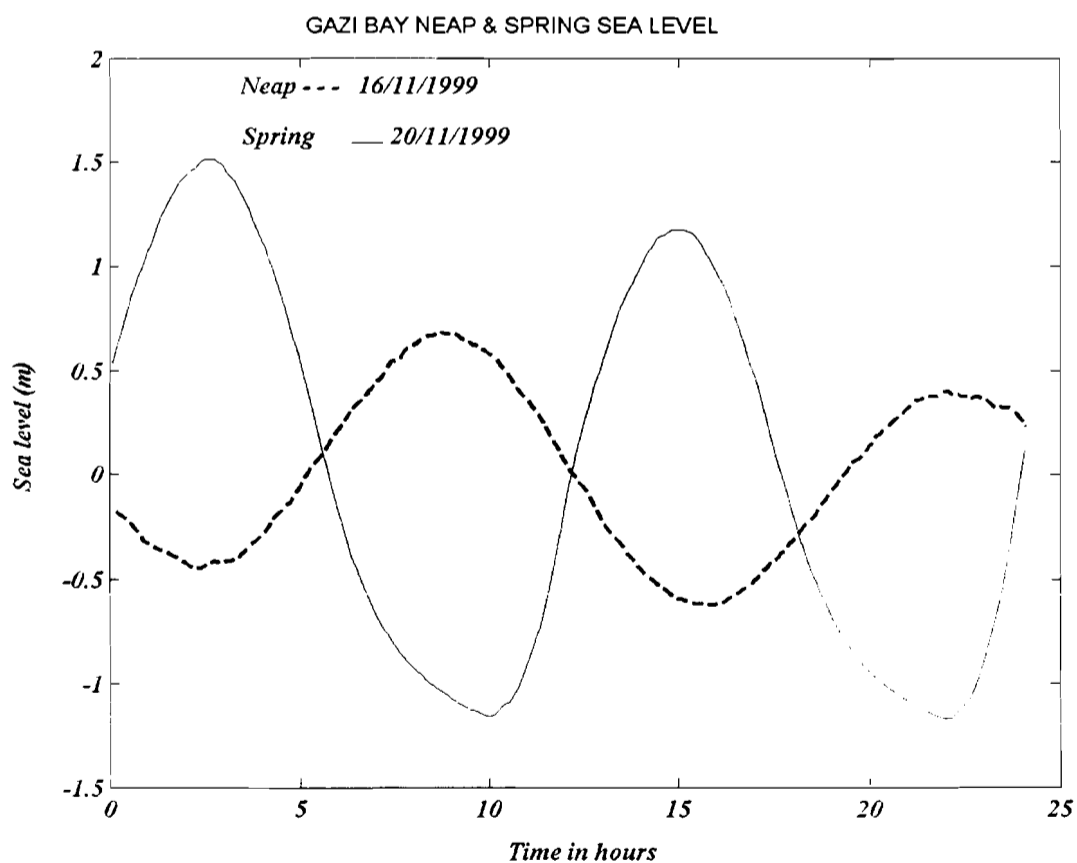
Figure 5.3.2.2 Tidal ranges during a day in neap (16/11/99) and spring (20/11/99) periods from tide gauge in Gazi Bay.

198

Figure 5.3.2.2 is a sample of the sea level record of one day plotted for both neap and spring periods. Two cycles (low and high) per day of which also reflect slight inequality, this suggest that in Gazi Bay the tides can be classified as mixed, mainly semidiurnal. We examine further the harmonic constituents that might be influencing the inequality in Section 5.3.2.3 under tidal and spectral analysis. From Figure 5.3.2.2 the tidal range (the difference in depth between high and low water) estimate give neap tidal rage value of 1.01m, where as the spring range is 2.8m hence, the spring tidal range is much higher than the neap tidal range.

A difference in tidal range during any particular day with the range changing progressively from one day to the next is also evident. The cyclic period has a period of about 2wk (14 days) during which the high tide becomes continuously higher and the low tide continuously lower for about 7 days. The role reverses, higher tide becomes lower and lower tides become higher for about the next 7 days. This is the fortnightly cycle that modulates the neap and spring. We also note that the tides do not repeat exactly after 14 days and would not do so even for a longer period. However, were our records several months long we would observe the tide closely repeat every 29.53 days. The inequality is most pronounced when the moon is farthest north of the earth's equator (tropical tides), but it is almost non-existent when the moon is directly above the equator (the equatorial tides). Both tropical and equatorial tides occur semimonthly. The tropical tide has a tendency to increase the diurnal range. When the moon is nearest to the earth (perigee) and when the tide becomes exceptional strong and vise versa, this gives rise to inequality termed monthly inequality. There are also exceptionally strong tides that occur in a year.

The inequality relationships, and various tidal ranges and age are examined in Section 5.3.3.3.

The development of time asymmetry in the tide is illustrated. The leading edge of the flood tide becomes steeper with short time duration to attain maximum amplitude; whereas the trailing edge-the ebb tide becomes flatter and takes longer than the flooding tide to reach its lowest level (Figure 5.3.2.2). The observed tidal asymmetry leads to extremely important variations in the bay tidal processes. The most obvious of the processes is the decrease and increase in flood tide and ebb tide duration respectively and consequently the flood and ebb currents. During spring the flood tide and ebb tide duration is about 4-4.7hrs and 7-8.4hrs respectively. That is the ebb duration is almost twice as the flood duration. For the neap period the flood tide duration is 6.1hrs, whereas the ebb duration was 6.4hrs. Hence, for neap the duration is almost equal and suggests insignificant tidal asymmetry. We conclude that, the asymmetry was more pronounced in spring period than in neap. The asymmetric difference is a consequence of depth, waveform velocity at crest and trough and topographical influences.

Phase inequalities, which are the variations in the tides or tidal streams due to changes in the phase of the moon, are given with tidal constituents in terms of degrees. Phase is the amount by which a particular cycle, such as harmonic constituent, progresses from specified origin, usually expressed in angular measure. Phases of the moon are the various appearances of the Moon during different parts of the synodical month. The cycle begins with *new moon* and the visible part of the waxing Moon increases in size during the first half of the cycle until *full moon* appears, after which the visible part of the

waning moon decreases for the remainder of the cycle. *First quarter* occurs when the Moon is at the east quadrature, *last quarter* when the Moon is in the west quadrature.

5.3.2.2 Currents

In the theory Section 4.4.2.2 various mechanisms generating current were analysed. The effort in that section was to find an average current that when multiplied with the cross-section area would give volume flux. In Section 5.3.1.1 some current results to support some observations of features there were also shown. In this section result of current measurements, the amplitude variations, maximum and mean values, direction and flow asymmetry, and time after high water calculations are presented.

It should be noted, however, that obtaining current data was much more difficult than obtaining sea level data. Moorings were necessary and were at risk from boats and fishermen. The complex topography and sometimes-high reef density made it difficult to select suitable sites. In fact because of channeling of the currents, two current meters a few meters apart at the entrance, one in the channel and one at the peripheral lagoon waters, may measure very different tidal currents. It is open to question if unbiased or representative tidal data can be obtained. To ensure good representative data effort was made to place the current meter at the center of the channel and in mid-position as possible. Due to the geomorphology of a basin, for instance, the bay and cross-section area influence the flow results in currents whose average and maximum values could be above that measured by those observed.

Figure 5.3.2.3a is a presentation of tidal current and direction time series of 5 days duration, obtained from the mid-position of Gazi Bay entrance channel, starting at

201

01.09hrs on 25/11/99 and ending at 01.29hrs on 30/11/99. The measurements were taken close to the height of spring and ended close to neap. The curve shows current variation in amplitude and magnitude with time. The current varies from a maximum value of 16.8±4.04 cms^{-1} in the first day of measurement and decrease to amplitude of 3 cms^{-1} in the 4-5 day.
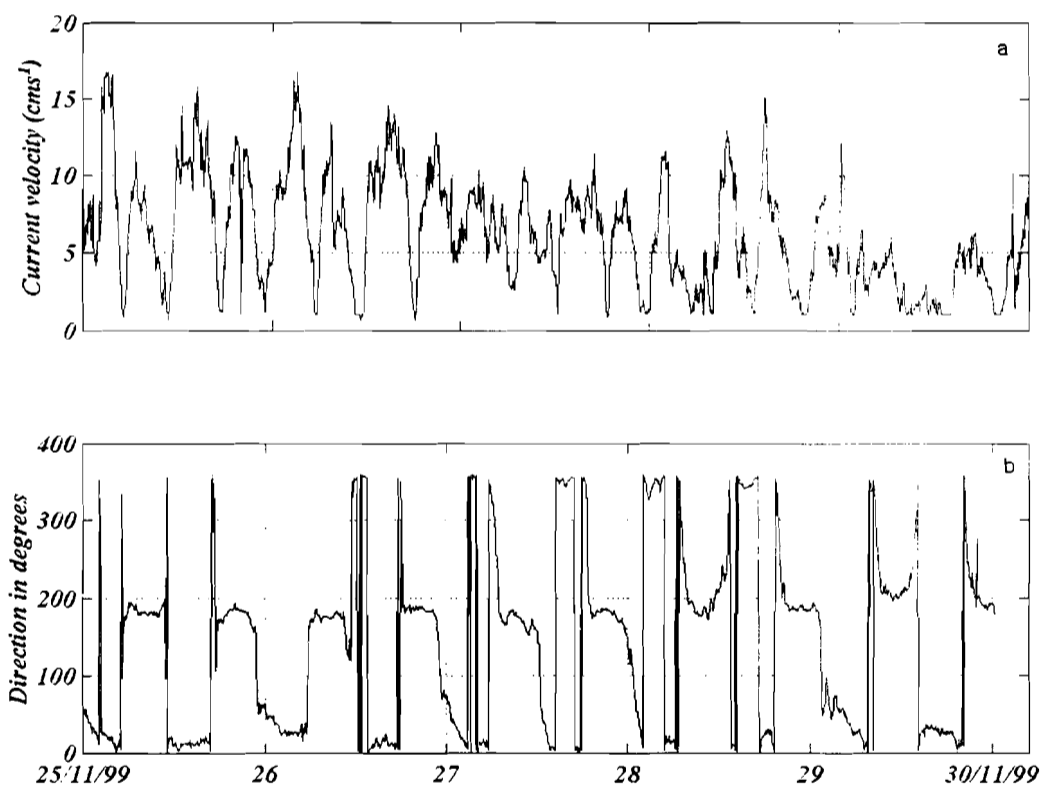
Figure 5.3.2.3 Example of (a) current (b) current direction time series from Gazi Bay entrance from 25-30 November 1999.

The mean current over the entire period of data was 6.2 ±3.6cms^{-1} and minimum 0.6 cms^{-1}. Hence, in spring the current are higher than in neap with value of 14-15 cms^{-1} and 5- 6 cms^{-1} respectively.

1462 measurements spurning a period of 5 days are analyzed, and despite the short length of the data the currents clearly indicate semidiurnal as well as diurnal and fortnightly spring neap variations. Figure 5.3.2.3b illustrates speed (cms^{-1}) versus direction (degrees) for the 25-30/11/1999 data, note also the direction asymmetry.
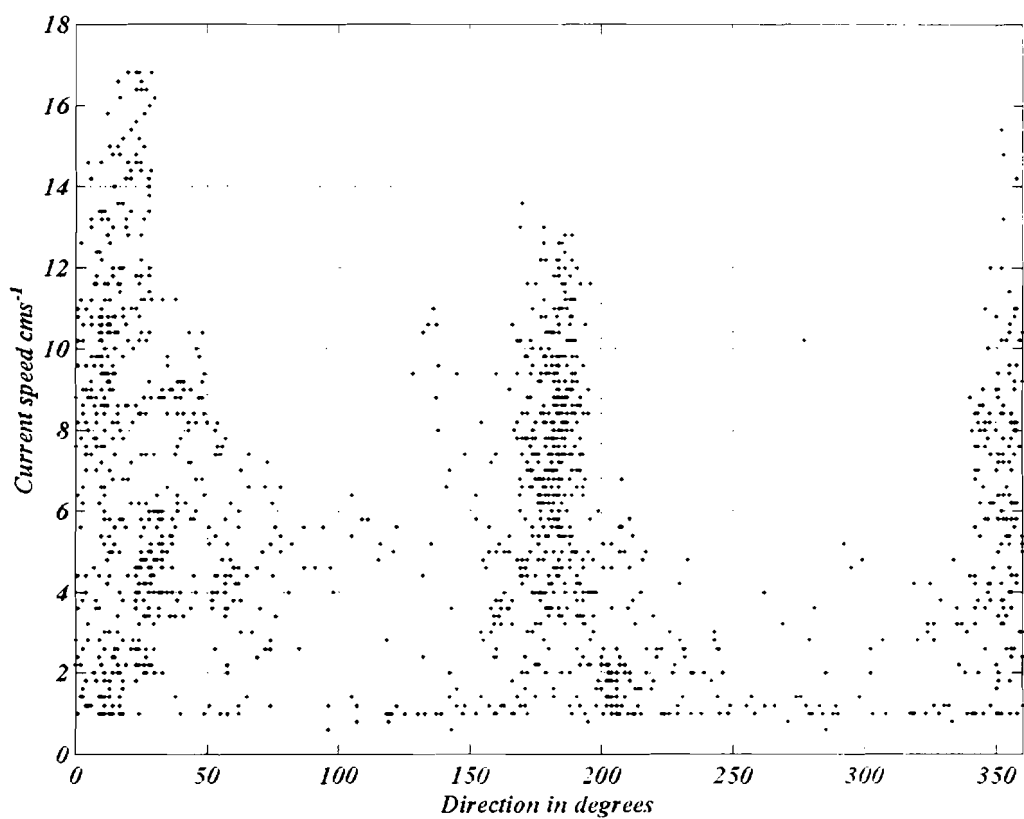
Figure 5.3.2.3c Speed versus direction indicating the main flow of water exchanged between the bay and the ocean for the period 25-30/11/1999.

Current speed and direction are presented in Figure 5.3.2.3c, which confirm the water into and out of the bay flow in a north-south direction. Predominant maximum

bay-ward flow tending to be directed 360- 20°N. The ocean-ward flow occurs in the range of 165-195 degrees. The clusters of dots towards the base and in between the two predominant directions indicate the effect of wind in the bay. Another feature that is clearly demonstrated by Figure 5.3.2.3c is the effect of wind on the direction of flow. Usually as the tide turns clockwise from flood direction (360-20 °N) to ebb (165-195 °S degrees) we expect the direction to switch as for example, illustrated by events marked (1) at day 2-3 (Figure 5.3.2.3d).
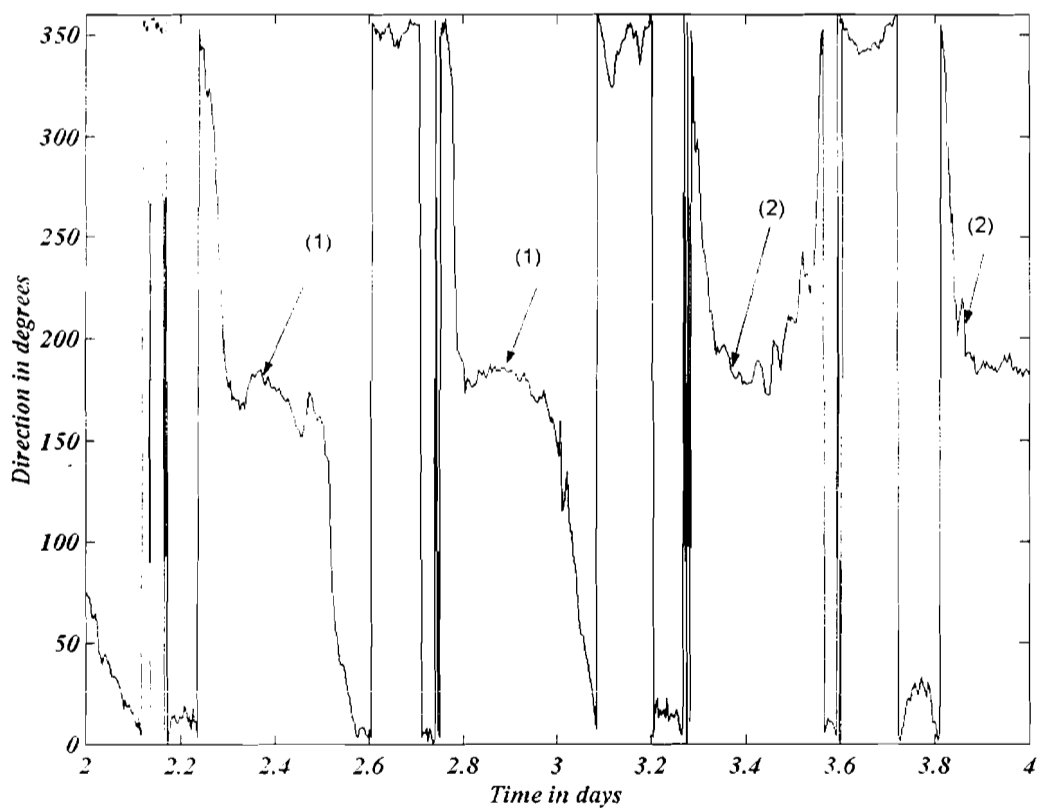
Figure 5.3.2.3d Illustration of the direction asymmetry in the flooding and ebbing phases of the bay water.

However, this is not always the case as can be seen by events marked (2), which shows that the reverse can also occur. This direction asymmetry is probability associated with the wind at the residence time of the water between the upper mangrove areas and the lower coral-fringed entrance area. Most likely the discharge is not entirely through where the current meter was located. Depending on the wind direction, the water might escape over and through one or so small openings in the eastern part of the bay.
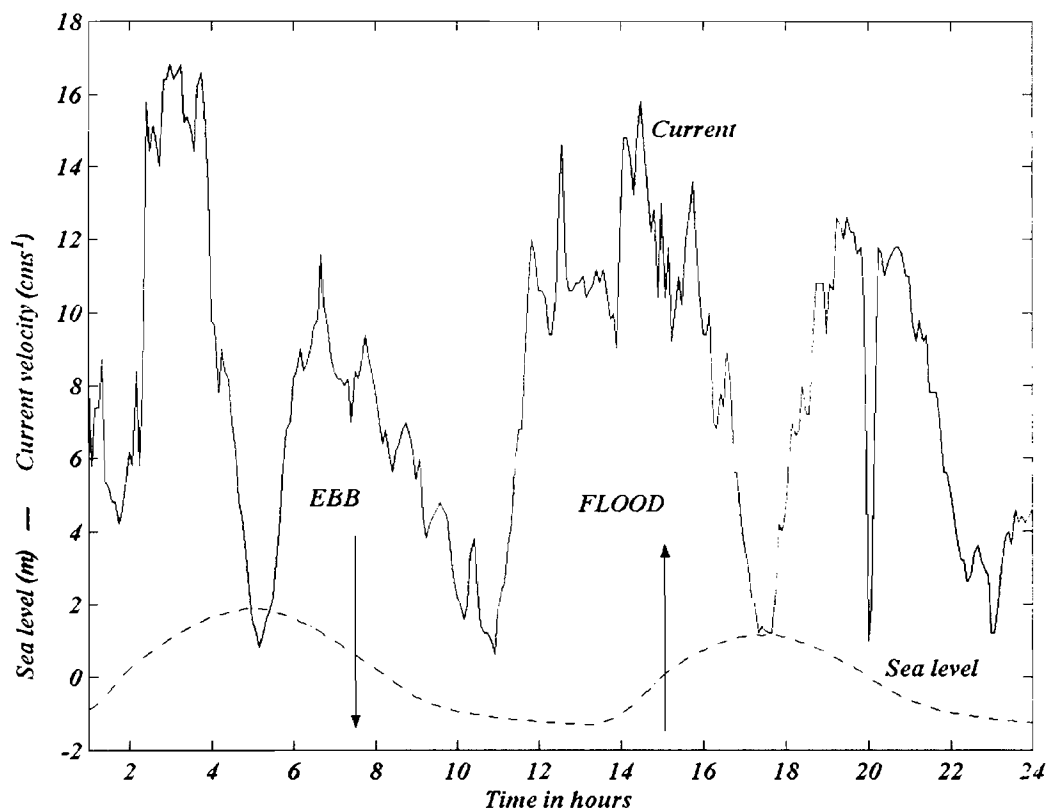
Figure 5.3.2.4 Example of current velocity-tidal stage relationship from Gazi Bay, for 24 hours for measurements started at 25-26/11/99 starting 00.15hrs.

The implication of this would be the a situation where the bay appears to receive more flood water than it discharges through the main channel to the western lower end

where the current meter was placed, thus also enhancing flow asymmetry. We infer that some discharge asymmetry on the account of wind and morphology of the bay is strongly indicated. More prominently, the preceding events of the current time series can perhaps best be presented by considering both current and the tide at the same time.

Figure 5.3.2.4 illustrates velocity-tide stage relationship from 25/11/99 starting at 00.10hrs and ending on 27/11/99 at 0.0.20hrs. Up-arrow indicates the flood tide/ flood current and down-arrow the ebb tide/ ebb current.

Further evidence is seen in Table 5.3.2.1 depicting the duration and magnitudes of ebb-flood currents and tides for six consecutive tidal phases.

Table 5.3.2.1 Illustration of ebb dominance for six tidal phases from 25-26/11/1999, in Gazi Bay.

Appx. hours range	Phase	Current Duration hrs	Tide Duration hrs	Max Current cms^{-1}	Min Current cms^{-1}
5-10	Ebb	5.8	8.4	11.6	0.6
11-17	Flood	6.5	4	15.7	1.3
18-23	Ebb	5.4	6.8	12.5	1.0
24-29	Flood	6	4.5	16.8	0.9
30-35	Ebb	5.3	8.1	13.6	0.9
36-43	Flood	6.8	4.2	14.6	0.6
Average	Ebb	5.5	7.8	12.6	0.8
Average	Flood	6.4	4.2	15.7	0.9

where the current meter was placed, thus also enhancing flow asymmetry. We infer that some discharge asymmetry on the account of wind and morphology of the bay is strongly indicated. More prominently, the preceding events of the current time series can perhaps best be presented by considering both current and the tide at the same time.

Figure 5.3.2.4 illustrates velocity-tide stage relationship from 25/11/99 starting at 00.10hrs and ending on 27/11/99 at 0.0.20hrs. Up-arrow indicates the flood tide/ flood current and down-arrow the ebb tide/ ebb current.

Further evidence is seen in Table 5.3.2.1 depicting the duration and magnitudes of ebb-flood currents and tides for six consecutive tidal phases.

Table 5.3.2.1 Illustration of ebb dominance for six tidal phases from 25-26/11/1999, in Gazi Bay.

Appx. hours range	Phase	Current Duration hrs	Tide Duration hrs	Max Current cms^{-1}	Min Current cms^{-1}
5-10	Ebb	5.8	8.4	11.6	0.6
11-17	Flood	6.5	4	15.7	1.3
18-23	Ebb	5.4	6.8	12.5	1.0
24-29	Flood	6	4.5	16.8	0.9
30-35	Ebb	5.3	8.1	13.6	0.9
36-43	Flood	6.8	4.2	14.6	0.6
Average	Ebb	5.5	7.8	12.6	0.8
Average	Flood	6.4	4.2	15.7	0.9

Observing the time lag between the tide and the current, the tide lags the current by 1.5hrs. For example, at 10-12hrs the current starts to fill while the sea level is falling, the sea level catches up with the current during its peak, and that the currents reach their lowest value (0.5cms-1) slightly later than slack water and is evidence of a progressive wave in the bay. Figure 5.3.2.5 compares, the mean sea level and the u-component for two days commencing from 1.09pm on 25/11/1999, it is obtained after decomposition the main current into its u and v components.

The results also show the tide lag the current by about 3 hrs. Diurnal inequality i.e. a lower magnitude of flooding current was followed by higher magnitude of flood current. Flood current occurring in the afternoon had a higher magnitude than the one occurring in the morning. The afternoon flood was enhanced by wind, which usually increased speed between 10 and 16hrs. Current during ebb shows less fluctuation than during flood. Towards the fourth day as the flood current increased in magnitude, the ebb current increased as well.
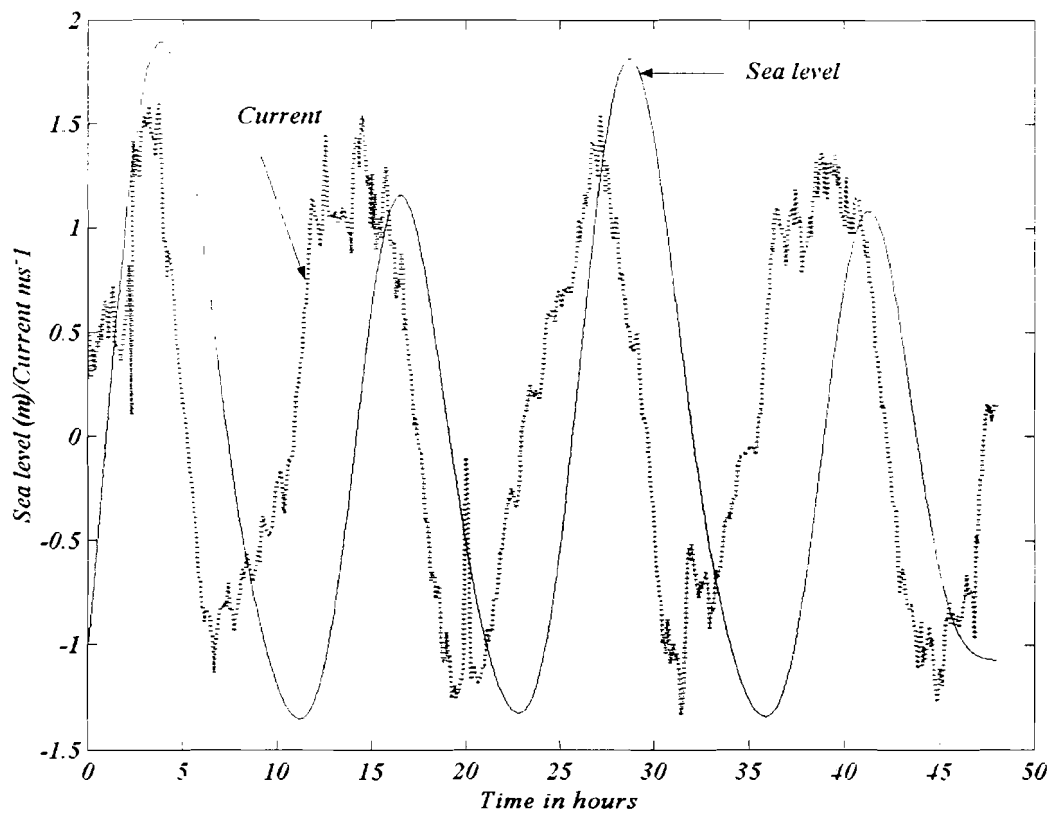
Figure 5.3.2.5 Comparison of sea level and along channel velocity, for two days starting from 1.09hrs on 25/11/1999, at the entrance to Gazi Bay.

Along and cross-channel velocity components

Expression 4.4.17 allows for the total current decomposition into a velocity component directed along the channel (longitudinal axis), where C is the speed measured and d the direction; D is the main direction (compass degrees 0-360°). u is the velocity component along D, and v is the velocity component perpendicular to the left of D.

208

$u = C.*\cos(a)$, and similarly for the cross-channel current is $v = C.*\sin(a)$, where $a = \pi/180(D-C)$, a function based on the decomposition computes the components when the desired direction is given.

The two main directions flood and ebb were in the range $0\text{-}20^{\circ}$ and $165\text{-}195^{\circ}$ respectively can be seen in Figure 5.3.2.3c. The consequence of the decomposition is that the velocities along the channel axis become asymmetrical with cross-channel velocity and somewhat reduced in amplitude. The results of the u-component and v-component are both shown in Figure 5.3.2.6, for the measurements from 25 November to 30 November 1999, where the inflow (flood) direction is considered positive and the outflow (ebb) direction negative.

Observing the current components, semidiurnal and diurnal variations are evident in the figure. Again, the general decrease in amplitude and magnitude from 25 November to 30 November 1999 indicates fortnightly spring and neap variations. The mean and maximum flood velocities are 6.2cms^{-1} and 16.9cms^{-1} respectively. The absolute maximum ebb velocity is $12.6\ \text{cms}^{-1}$, with a mean of 5.2cms^{-1}, whereas, the average flood and ebb durations are 6.64 hrs and 5.7 hrs respectively. Results giving duration in relation to tidal level is given in Section 5.3.3.3.
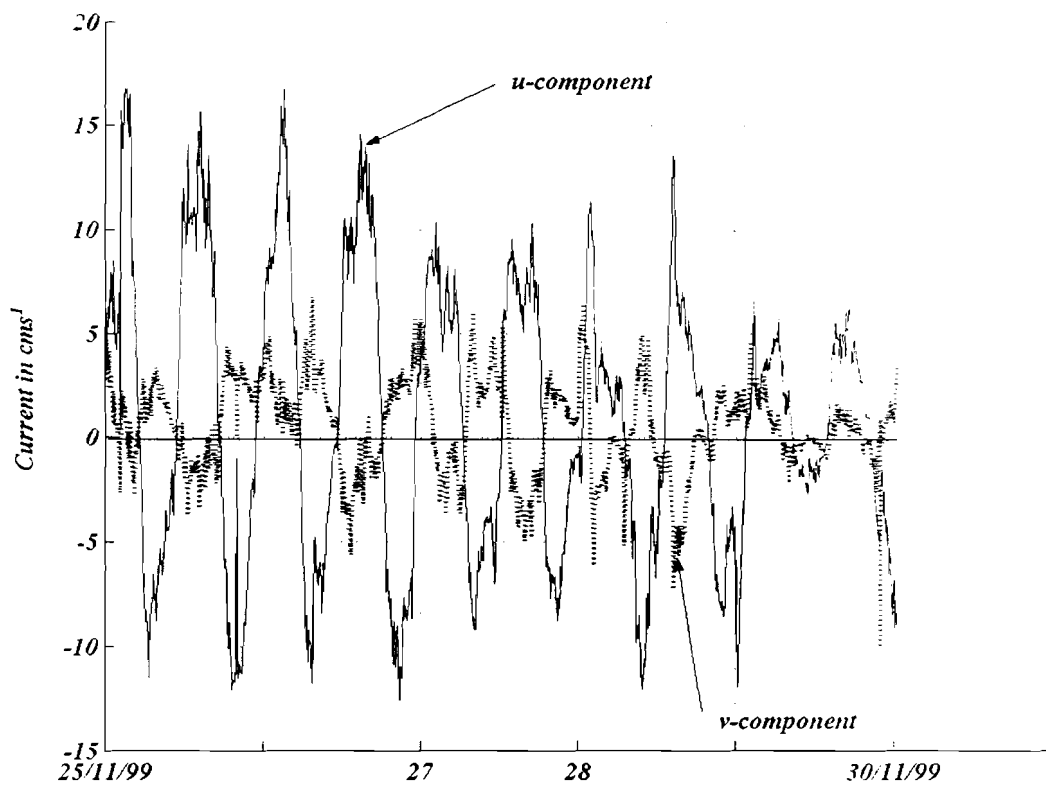
Figure 5.3.2.6 Decomposition into longitudinal (along channel) velocity (u-component 20° from north) and cross-axis velocity (v-component).

Thus, the flood and ebb currents illustrate clearly the time amplitude dominance of the longitudinal velocity similar to that of the total current shown early in Figure 5.3.2.4. The conclusion is that, the maximum and the mean flood velocity during the time of study were higher than the maximum ebb velocity and mean ebb velocity by 25.2 % and 16% respectively.

At this rate about 25% higher fluxes occur during flood than during ebb, implying that at some other position the net flow is opposite, or the water exits over the reef or through smaller channels in the reef. The difference of the mean flood and mean ebb is

210

1.6%, which is an indication that during the falling tide from spring to neap, the bay was gaining water.

Time after high water -hours at maximum flood/ebb velocities

The longitudinal velocity *vs* time after high tide was made by a polynomial fit of the mean curve through the plotted velocities (Figure.5.3.2.7). The curve indicates time asymmetry.
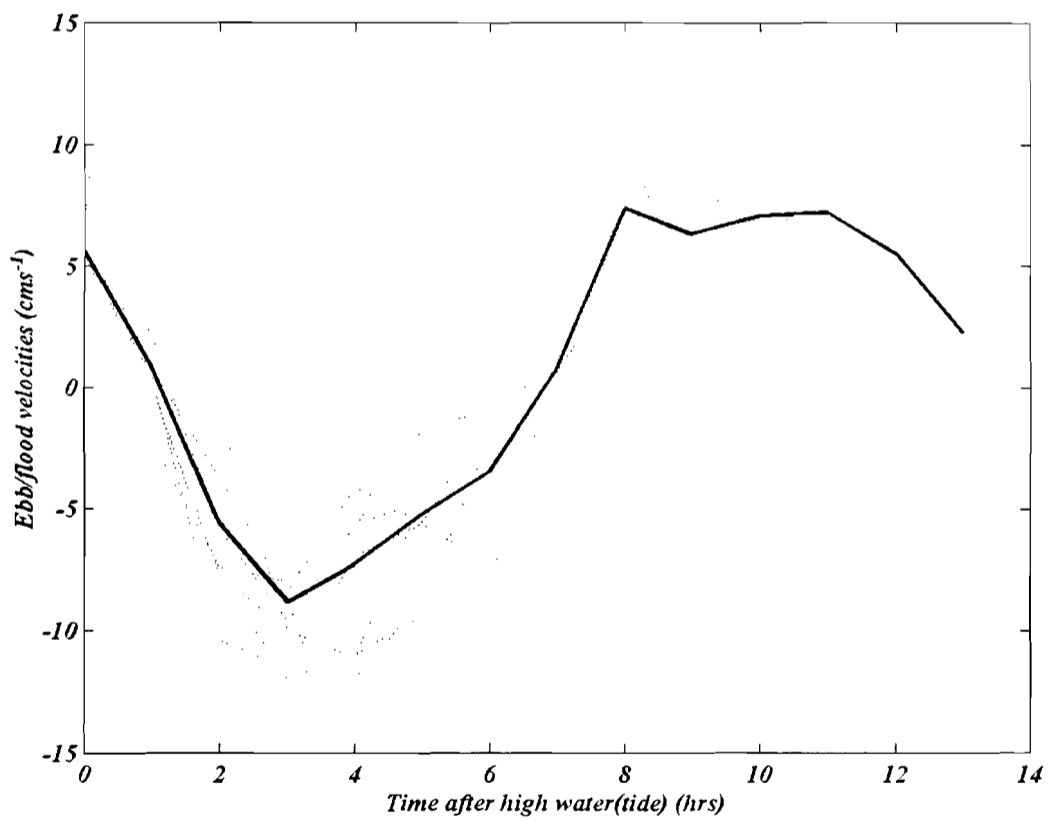
Figure 5.3.2.7 Longitudinal velocity vs time after high tide at Gazi bay entrance section. The solid line denotes the mean curve while the dotted lines denote measurements at 5 minutes interval for the period 25-30/11/1999.

211

Also seen from the figure is the time duration between ebb and flood velocity confirming, as earlier mentioned, that flood period is longer than the ebb period. Maximum flood velocities occurred about 1.2hrs before high tide, whereas maximum ebb velocity is 2hrs after high tide. The time of slack water is approximately 2 and 2.30 hrs after high and low water, respectively.

The velocities attained by the tidal flow in the bay depend partly on the characteristics of the tidal wave, for instance the tidal range and the tidal asymmetry, and partly on the morphology of the channel through which the current flows.

Taking the surface area upstream of the entrance channel to Gazi Bay as $1.8 \times 10^6 \mathrm{m}^2$. The cross-section area as $1.4 \times 10^3 \mathrm{m}^2$ (Table 5.3.2.3), and T=12.42hrs the period for semidiurnal tide (M_2) and the tidal ranges as given in Section 5.3.2.3, both average velocity and maximum velocity can be estimated according to Eqs. 4.4.20-21.

For the average tidal range of 3m and neap range of 1.4m (Section 5.3.2.3) the average tidal current is $\cong 17.3 \mathrm{cms}^{-1}$, during spring and neap respectively. The theoretical maximum current in the channel is $\cong 36 \mathrm{cms}^{-1}$. This shows that the observed current of $16.1 \mathrm{cms}^{-1}$ underestimates the maximum current almost by half. There are two reasons for this, the measurements were not done at full spring and the mooring position referred to earlier.

Currents induced particles excursion into the bay

The strong semidiurnal current in the bay allows for the estimate of tidal excursion, i.e. the resulting particle displacement as $\delta = UT/\pi$. Where the U is the current amplitude at a period T. Taking U to range from $17.3 \mathrm{cms}^{-1}$ and T =12.42hrs for M_2 currents, the resulting particle displacement rage is 2.46 km. From the entrance to the

to where Kinodo and Kidogweni Creeks start is almost equal to this tidal excursion, implying the bay is complete flushed within one tidal cycle.

On the other hand, the above current can also theoretical be estimated from Eq.4.4.23 if appropriate assumptions are made. If the distance from the mangrove edge is considered as the shoreline for Gazi Bay, to the average distance (D) from the shoreline to the end of shelf slope can be taken as 12 km, and the tidal range (H) varying from neap to spring as 1.4-4m (Section 5.3.2.3). The plume can be seen as overlaying a sub-surface layer of lesser mixing. Then application of Eq.4.4.23, gives an estimated range of 7.5-21.5cms^{-1} for neap-spring offshore-onshore current. Taking the mean tidal range of 3m, estimated onshore-offshore current is 16 cms^{-1}, which is in close agreement with the observed tidal current.

Residual currents

The horizontal and vertical salinity differences (Section 5.3.1.2) in the bay and the offshore water is caused by mixing of less dense saline (brakish) water that give rise to inclined isopycnals and isobaric surfaces along the axis of the bay and drive residual currents. Residual currents also result from tidal asymmetry as well as meteorological factors and even with low river discharge can drive residual gravity circulation an order of magnitude grater that peak river discharge (Schubel and Pritchard, 1972). These currents can be the main cause of water exchange.

The residual currents are those obtained after tidal analysis and correspond to the residual sea levels (Figure 5.3.2.8, panel c) or after averaging the tidal observed tidal current over 25hrs. Such currents reveal a lager fluctuation during spring period due to

213

increased turbulence. The fluctuations are probably due to other forcing mechanisms e.g. wind and seiches that were operational in the bay. It is important to note that the residual circulation is essentially the one associated with transport or flushing dissolved and suspended particulate materials, flotsam and bed load from the bay.

Efforts were made to determine residual currents using several PCMs. however, this proved problematic due the small depth in Gazi Bay and relatively warm water which the failure of the gelatin to coagulate on many occasions on account of high water temperatures. Few measurements were made during flood phase when cooler waters coming from the ocean helped the gelatin to coagulate fast enough. The few results obtained during flood period showed that the current near the surface, in the channel, had a maximum 26 cms^{-1} with an average of 20.5cms^{-1} near the surface. Thus, indicating that the current meter velocities were lower than those observed using the PCMs, however at the 5-7m depths the PCM velocities were close to those observed by the current meter during flooding phase (13-15cms^{-1}).

5.3.2.3   Tidal and spectral analysis

The method for tidal analysis was presented in Sections 4.4.4.1-2 together with the formula for tidal classification. As already mentioned, the aim of the analysis is to extract amplitudes, primary harmonic constituents, phases and their compound tides from sea level and current meter time series and find out the magnitudes of the key constituents, determine the degree of tidal asymmetry, and calculate phase differences. Analysis was carried out using 14 constituents. The constituents, with their names, symbols, and periods are Principal Lunar M_2, 12.42 hrs, Principal Solar S_2, 12.00 hrs,

215

Luni-Solar Semi-diurnal K_2 ,11.97hrs, Luni elliptic K_1 ,12.66hrs, Principle Lunar Diurnal, O_1, 25.82, Principle Solar Diurnal P_1, 24.07hrs, Lunar fortnightly M_f , 327.87hrs and five Shallow water tides $2SM_2$,11.61hrs , M_4,6.21hrs, S_4, 6.00hrs, M_6, 4.14hrs and $2MS_6$, 4.09hrs.

The results of the analysis are presented in Figure 5.3.2.8. The top panel (a) is the original record, panel (b) the computed record or the astronomical tide, panel (c) the residual record, the table to the right of the three panels gives the symbol, the amplitude, and the phase lag of each constituents. Similarly, Figure 5.3.2.9 gives results of tidal analysis of temperature records of the same tide gauge.

The M_2 has amplitude of 0.963m, S_2 and K_2 are next strong constituents both contribute 87.2% of M_2.
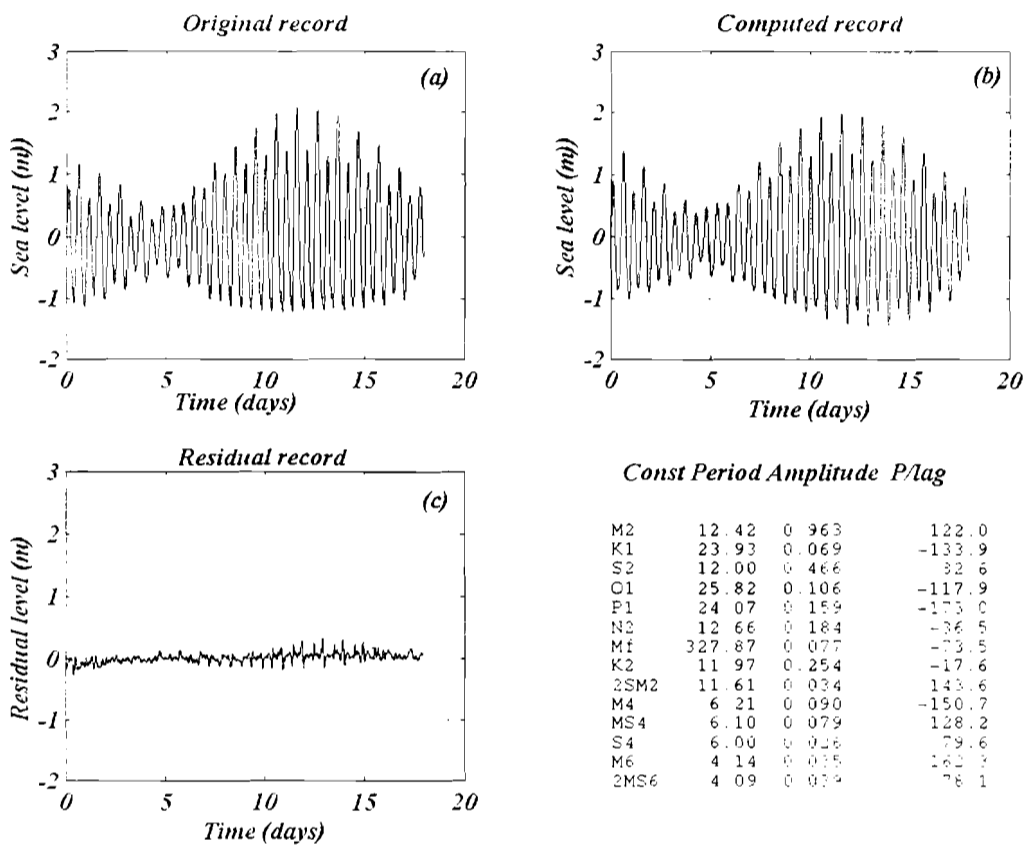
Figure 5.3.2.8 Harmonic analysis for Gazi Bay based on 18-day data record 12-30 November 1999 (a) observed (b) computed (astronomical tide) and (c) residual levels. The table in the fourth panel gives the period, amplitude and phase lag for the 14 components.

216
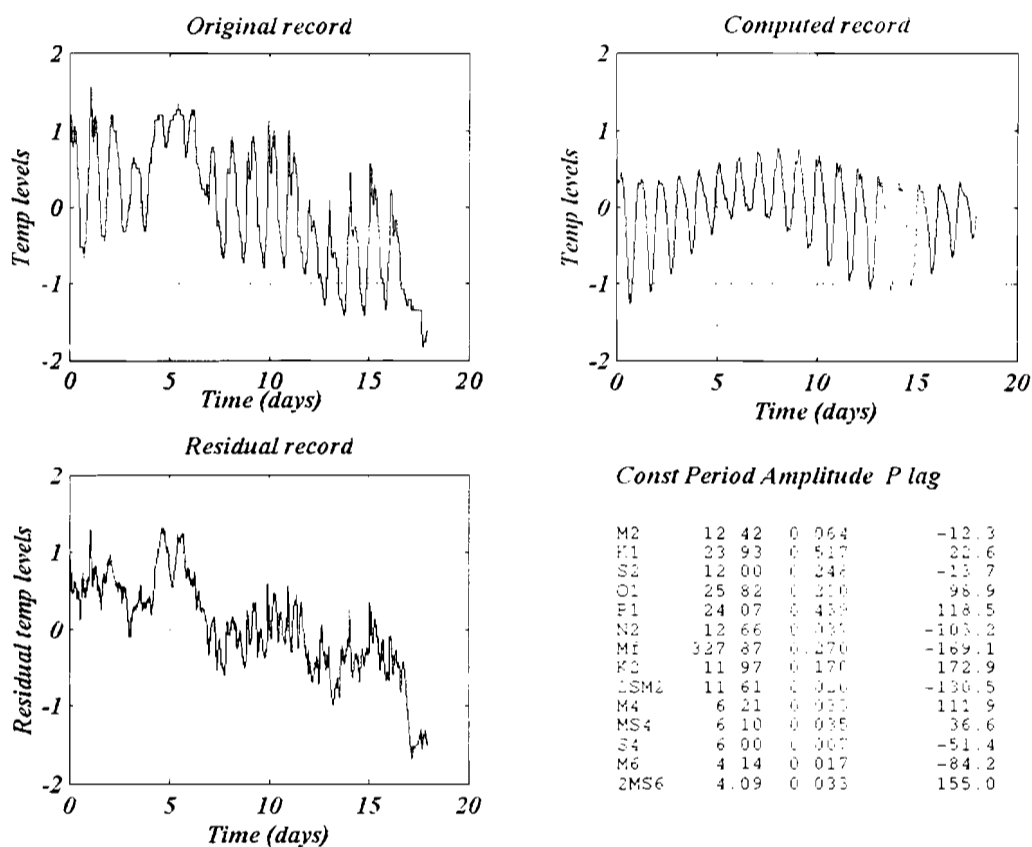
Figure 5.3.2.9 Harmonic analysis for Gazi Bay based on 18-day data record 12-30 November 1999 (a) observed (b) computed (astronomical tide) and (c) residual levels.

In Table 5.3.2.1 the four major astronomical components namely M_2, S_2 (semi-diurnal), K_1 (diurnal) and O_1 (diurnal) are shown. They are presented along with values of the same from the current meter time series. The formulas to compute derived parameters e.g. tidal ranges and form number (Eq.4.4.52) are also shown. Observing the results, Gazi Bay has a spring tidal range $2(M_2+S_2)$ of tidal range of about 4 m with a mean tidal range $2.2(M_2)$ of about 3m and a neap range $2(M_2-S_2)$ 1.4m. Owing to the

short records the results might slightly over estimate the true values by 20%. The dominant contribution is from the semidiurnal components (M_2 and S_2) as well as the Luni-solar diurnal (K_1) component. The amplitude of the S_2 is nearly half of that of M_2 indicating that during neap the S_2 and M_2 may not necessary cancel each other at neap tide. However, the ratio of the semidiurnal tide to that of diurnal tide is about 1.6 which means the semidiurnal tide must empty and fill the bay in nearly 1.6 times greater than diurnal tide. Hence, we expect the diurnal current velocities to be about half the semidiurnal ones.

Tidal phases differ between tidal elevation and tidal current at the entrance as seen in Table 5.3.2.1. Considering flood tide and current in Gazi Bay are northward the difference between tidal elevation and current of about 29 ° and -84 ° for M_2 and S_2 respectively indicate that the M_2 in Gazi Bay is a damped and progressive wave. For a purely progressive wave the phase difference is 0° or 90 ° (see Section 4. 4.4.1). For friction-damped waves the difference lies in the range 0 ° - 90 °. For standing wave the phase difference would be equal to 90 °, this suggests that S_2 tend to a standing travelling in a direction almost opposed to that of M_2.

The formula for the ratio of the major semidiurnal constituents and the major diurnal constituents gives a form of 1.36, which lies in the range 0.25-1.5. This leads to the conclusion that tides in Gazi Bay are predominantly semi-diurnal.

short records the results might slightly over estimate the true values by 20%. The dominant contribution is from the semidiurnal components (M_2 and S_2) as well as the Luni-solar diurnal (K_1) component. The amplitude of the S_2 is nearly half of that of M_2 indicating that during neap the S_2 and M_2 may not necessary cancel each other at neap tide. However, the ratio of the semidiurnal tide to that of diurnal tide is about 1.6 which means the semidiurnal tide must empty and fill the bay in nearly 1.6 times greater than diurnal tide. Hence, we expect the diurnal current velocities to be about half the semidiurnal ones.

Tidal phases differ between tidal elevation and tidal current at the entrance as seen in Table 5.3.2.1. Considering flood tide and current in Gazi Bay are northward the difference between tidal elevation and current of about 29 ° and -84 ° for M_2 and S_2 respectively indicate that the M_2 in Gazi Bay is a damped and progressive wave. For a purely progressive wave the phase difference is $0°$ or 90 ° (see Section 4. 4.4.1). For friction-damped waves the difference lies in the range 0 ° - 90 °. For standing wave the phase difference would be equal to 90 °, this suggests that S_2 tend to a standing travelling in a direction almost opposed to that of M_2.

The formula for the ratio of the major semidiurnal constituents and the major diurnal constituents gives a form of 1.36, which lies in the range 0.25-1.5. This leads to the conclusion that tides in Gazi Bay are predominantly semi-diurnal.

Table 5.3.2.1 Showing constituents from Gazi Bay, their amplitudes, phase lags, and some key parameter ranges for time series analysis of sea level, current and temperature for 18-days data (12-30/11/1999). R = Range.

Name of	Period	Sea level (MT2)		Current (RCM)		Temperature (MT2)	
Constituent	Hours	Amplitude η_{sl}	Phase θ_{sl}	Amplitude η_v	Phase θ_v	Amplitude η_T	Phase θ_T
M_2	12.42	0.963	115.4	1.293	144.6	1.050	347.5
K_1	23.93	0.069	47.9	0.342	276.5	0.805	54.9
S_2	12.00	0.680	177.4	2.118	92.7	0.126	41.0
O_1	25.82	0.172	58.4	0.584	218.4	0.340	118.8
Parameter	Formula	Parameter Value		Parameter Value		Parameter Value	
Mean R	$2.2M_2$	2.99		2.84		0.231	
Spring R	$2.0(M_2+S_2)$	4.09		6.82		0.462	
Neap R	$2.0(M_2-S_2)$	1.37		-1.65		-0.042	
Form Number	(K_1+O_1) $/(M_2+S_2)$	0.136		0.272		4.89	

Spectral analysis

Spectral analysis for the sea level and the current meter time series was carried out. The idea was to present the kinetic energy possessed by a parcel of water at any instant as the sum of energies of all the contributing to its motion as determine by the squires of their speed. Power density spectrum (PDS) (or energy density spectrum) was discusses briefly in Section 4.4.4.2. The PDS shows the magnitude of each cosine term in the summation series.

Figure 5.3.3.0 shows three panels of PDS based on 18 -day (a) sea level (b) temperature (c) 5-day current meter measurements in Gazi Bay (at MT2), from 12-30 November 1999. The portion that represents the kinetic energy fluctuating components, which account for the most of the energy of the flow, with only very small portion being contained in the mean motion, has been filtered out in the Programme used in the analysis leaving out mostly individual peaks. The individual peaks, appearing in each of the three panels of the energy density spectrums are the components of the flow that have specific periods (specific frequency). Boon (1981) pointed out that the concept time averaged tide can be used in isolating the lunar semidiurnal tide, M_2, and its associated shallow water tides, particularly the lunar quarter-diurnal tide, M_4. Observing the sea level spectrum, the peaks marked s_1 is between 6- 6.3hrs is probably a combination of shallow water waves M_4 and MS_4, whereas,s_2 and s_3 correspond to M_2 and S_3 respectively. M_4 causes the coarsest degree of distortion in the fundamental wave (Boon, 1981) and thus accounts for most of the flood and ebb duration observed in the mean direction in the forgoing Sections.

220
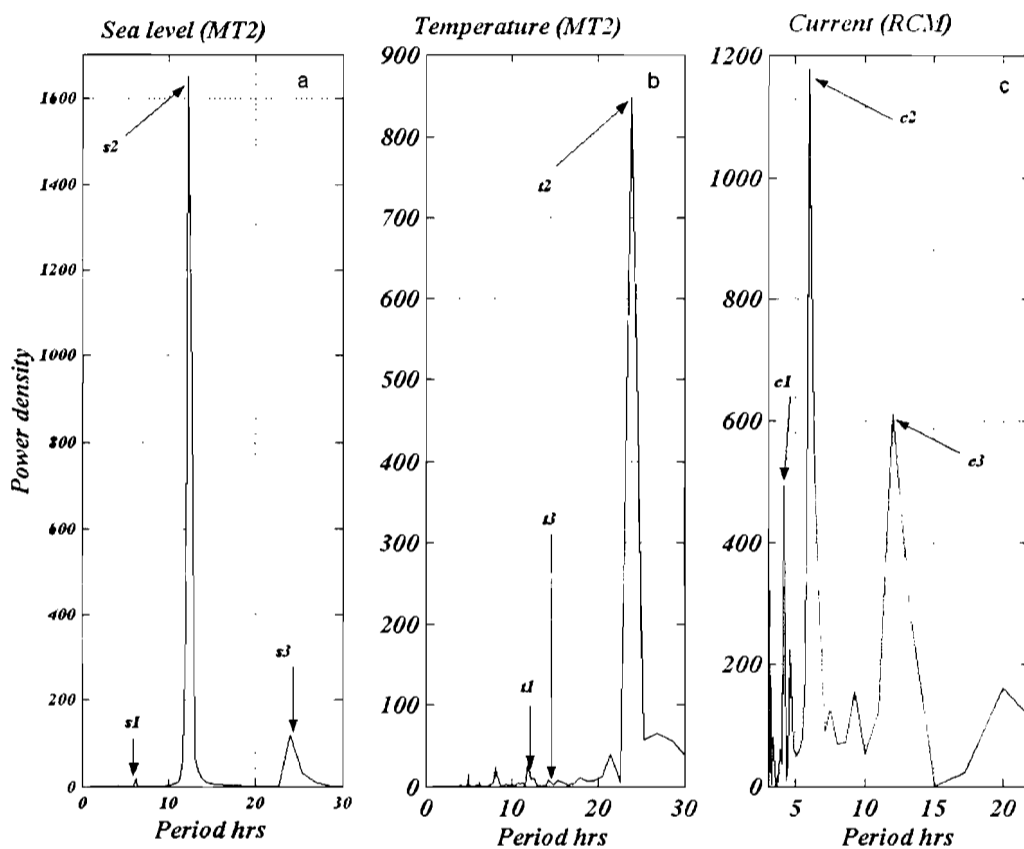
Figure 5.3.3.0 Power density (energy) spectrum based on 18 -day (a) sea level (b) temperature (c) 5-day current meter measurements in Gazi Bay (at MT2), between 12-30 November 1999.

The temperature energy spectrum shows peaks at period t_1 (11.95hrs), t_2 (23.91hrs), and t_3 (12.65hrs) corresponding to K_2, N_2 and K_1.

In the current energy spectrum the peaks marked c_1 and c_2, at periods of about 4hrs and 6hrs correspond to M_6 and S_4, while the peak marked c_3 is at 12.04 hours is most likely S_2.

221

5.3.3 Water exchange calculations

5.3.3.1 Morphology of the bay

In this section the results of water exchange are presented. Water exchange is a key factor when considering, for example, nutrient fluxes and water quality in general. Morphological characteristics of Gazi Bay were introduced in Section 4.3 while describing the study site. Here the parameters are tabulated with additional information such as tidal ranges and cross sectional areas (Table 5.3.2.3). As mentioned earlier we estimated the mean surface area of the catchment and that of the bay and its two small creeks from the total surface area (A) of the bay at high water level, from a topographic map (1:50,000).

Table 5.3.2.3 Morphological characteristics of Gazi Bay

GAZI BAY	
Catchment area (m^2)	2.5×10^8
Bay/creek surface area (As) (m^2)	1.8×10^6
Total surface area	2.68×10^8
Entrance section area (mean)	$\times 10^3$
Tidal range	2.8
Length (L)of Bay/Creek (m)	7×10^3
Mean depth (Hm) in the bay	2.5m
Mean depth /length of the entrance channel	10m/400m

The catchment area including the bay and creek are gave a total surface area of 2.68×10^8 m^2. The surface area of the bay ranges from 1.1×10^6m^2 during extremely low water and to approximately 1.8×10^6m^2 at maximum high water assuming that this extreme is above or below mean sea level at the entrance.

5.3.3.2 Water exchange generated by fresh water discharge

Fresh water outflow into Gazi Bay lowers the salinity, which produces a salinity (and density) difference (see Chapter 5.3.1.2). The density difference, particularly during the IMLR season, generates a baroclinic circulation. Since the salinity in the bay in this case is always lower than the salinity outside the bay the surface current is always directed out of the bay i.e. estuarine circulation. Baroclinic circulation is also driven by salinity fluctuations or changes (see later e.g. Tudor Creek, NEM season) out side the bay. When salinity increases outside the bay the water becomes denser. Water in the bay then flows out as a light surface current. Along the bottom of the bay saltier and denser water flows into the bay and thus increases the salinity. If the salinity outside the bay decreases the circulation reverses. If the salinity within the inner shallow basin increases e.g. during the dry season when evaporation from the mangroves and muddy inter-tidal areas withdraws fresh water from saline water at a rate of 0.6cmd^{-1}, a salinity maximum zone is created in the bay. Such a zone can effectively isolate the inner basin from the coastal water. Thus internal circulation is created in the dry season (Wolanski, 1986a). Salinity maximum was not evident in Gazi Bay. The circulation mechanism due to

baroclinic processes and remote forcing at the entrance is taken up in more detail in Tudor Creek.

When average values for river discharge and average salinity in the bay and outside the bay are considered the characteristic values for seasonal exchange can be obtained. During the IMLR and IMSR seasons difference in salinity exists between the bay and the oceanic water. For 1996, 1997, 1998 the typical salinity in the IMSR season were 32 in the bay and 35 in the ocean, and for the IMLR the value were and 30 and 35 respectively. The river discharge (R) for the IMLR was 5 m^3s^{-1}, for NEM season the range 0.4-0.2 m^3s^{-1} and SEM season the range of river discharge is 0.2-0.1 m^3s^{-1}. Using these values in equation 4.4.60 a typical estimate of exchange rate for the IMLR is 0.6 days, during IMSR season the estimated typical flushing rates are 2 days and greater than 3 days for NEM and SEM seasons. Compared to the flushing time of 6 days obtained by tidal prism method, it was suggested that the faster flushing rates are due to induced gravitational currents that give rise to the residual circulation whenever there is baroclinic forcing.

5.3.3.3 Water exchange generated by sea level

The modeling expression for hourly tidal discharge using tidal hypsometric flow model (Eq.4.4.13) in the theory and analysis Section 4.4.1 is used. The flood volume flux is expression as

$$Q_{flood} = A_m \frac{h}{Tf},$$

and for ebb volume flux

$$Q_{ebb} = A_m \frac{h}{Te},$$

Where T_f is the average mean flood duration, T_e the average ebb duration, h is the tidal range in the basin and A_m is the mean surface area of the basin upstream of the cross-section.

To obtain volume flux from the sea level data a hypsographic curve for the bay was first obtained. Four equally spaced cross-sections along the bay axis, one at the entrance, two in the middle and the fourth near the end of the bay. Four mean depths at each cross-section were then used together with the cross-section area to obtain hypsographic (depth-area) curve for the bay by interpolating between the cross-sections. A spline function was applied to generate the curve. A computer programmed using the above two computed the maximum, minimum and mean flood and ebb volume fluxes. Figure 5.3.2.2 gives spring and neap tides of 2.8m and 1.01m respectively. The average duration of the flood and ebb tide are 4.2hrs and 7.8hrs respectively. Thus, from the result we conclude that Gazi Bay is ebb dominant. The mean surface area of Gazi Bay is given in Table 5.3.2.3 is 1.8×10^6 m^3. The flood volume flux during obtained for the

(period closer to spring is as 1200 m^3 s^{-1} and for the period closer to neap is 233 m^3 s^{-1}. Thus, about 715 m^3 s^{-1} per tidal cycle during the period of study is exchanged.

Table 5.3.2.2 presents the spring, neap and mean tidal ranges as computed from tidal analysis, as 4.1m, 3m and 1.4m respectively. Taking the mean surface area of Gazi Bay as 1.8x10^{6}m^3 (Table 5.3.2.3) and assuming the tidal flood and ebb duration remain as given in Table 5.3.2.1, then the volume flux from tidal analysis can be estimated as, spring volume flux 1757 m^3 s^{-1}, neap volume flux 692 m^3 s^{-1} and mean volume flux as 1224 m^3 s^{-1}.

5.3.3.4 Water exchange generated by along-channel velocity

Calculations from the longitudinal velocity (along channel) obtained from the decomposition of the total current meter data was given in Section 5.3.2.2. In this section we use the velocity and the cross-section area to obtain instantaneous flood and ebb volume fluxes.

To estimate instantaneous volume flux from the u-velocity, the mean depth at the cross-section at VI (Figure 4.1.1.1) to was estimated at 4m and the width of the cross-section as 35000m (see Sketch Figure 5.3.3.2). From the sketch, the maximum cross-section area is about 8.5x10^3±1.78 m^2, the mean cross section area 3.6x10^{3}m^2, and the minimum area 1.6 x10^{3}m^2. The values obtained were, the instantaneous maximum flood volume flux as 2.35 x10^3 m^3 s^{-1} the maximum ebb volume flux as 1.76 x10^3 m^3 s^{-1} the mean flood flux 868 x10^3 m^3 s^{-1} and the mean ebb flux as 728 x10^3 m^3 s^{-1} Therefore the instantaneous (mean) net volume flux estimated from the current meter is about 140m^3. The volume flux and longitudinal current and sea level at the bay entrance are compared

in Figure 5.3.3.3. Currents in spring are stronger that in neap, consequently resulting in higher volume flux during spring than neap.
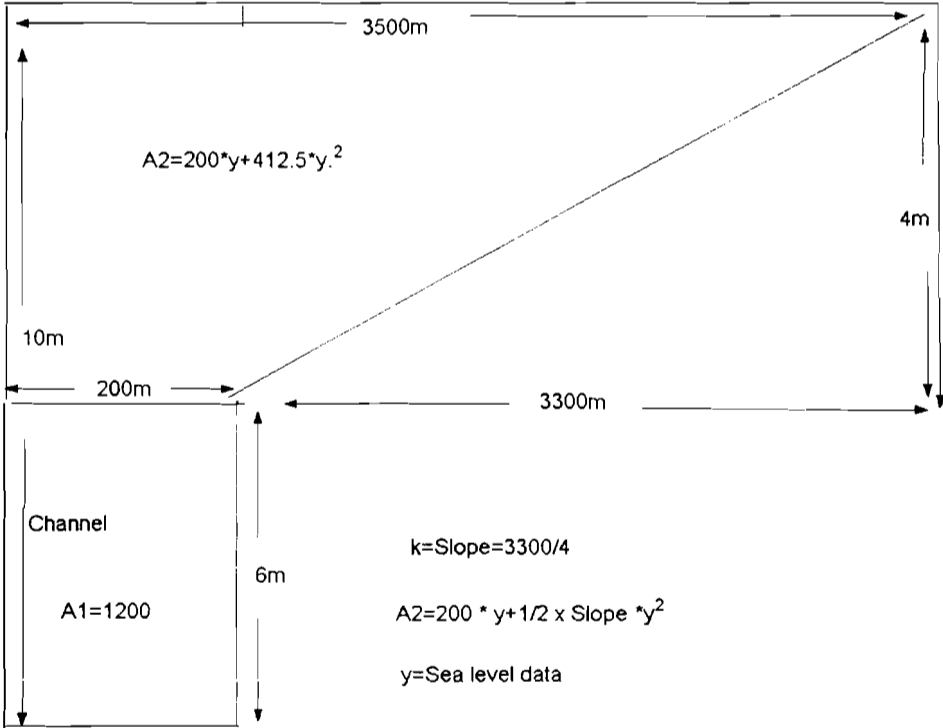
Figure 5.3.3.2 Sketch of Gazi Bay entrance cross-section area (A1+A2). A1 is the non-inter-tidal A2 is inter-tidal that is sea level varies with depth. Note the mean sea level must be set to zero above 6m.
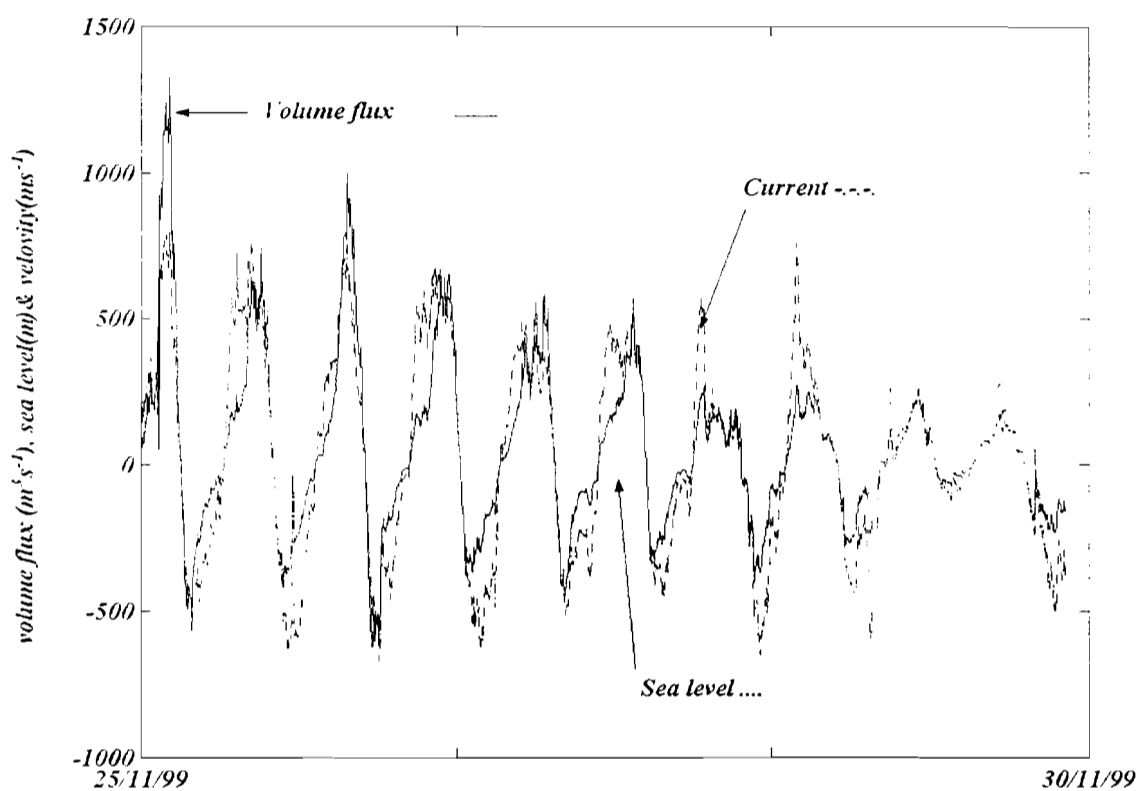
Figure 5.3.3.3 Comparison of volume flux, longitudinal current x50, and sea levelx100 for Gazi Bay entrance area.

Non-tidal flow was obtained by subtracting the ebb and flood of the tide from the total longitudinal flow and results expressed as cumulative net displacement. Displacement is defined as the product of the along-channel component speed and the time interval it represents. Net displacement is obtained by defining flow, for example, towards 20° in Gazi Bay as positive (flood).

The instantaneous volume flux has a maximum flood of 1326.3 ± 230.9 m^{3}s^{-1} , mean of

244.5 m^{3}s^{-1}and maximum ebb flood 623.29 ± 129.43 m^{3}s^{-1}mean of 168.03 m^{3}s^{-1}. Hence

we found a net inward flux of 76.2m^{3}s^{-1}.

Hence, in conclusion, the above approaches for water tidal water exchange give

values of similar magnitude. The computed velocities and fluxes maximum flux occurred

during spring, lowest during neap. In a tidal cycle slightly high volume flux occurred

during flood. The mean flood fluxes are higher than the mean ebb fluxes. The spring

fluxes are higher than the neap fluxes.

5.3.3.5 Water exchange generated by wind

Gazi Bay wider entrance, suggest enhanced water exchange due to wind. This can

be, for example via waves (infra-gravity) and a *lagoon current* flowing across the

entrance in the ambient water. Fishermen, in the location have reported such lagoon

current flowing along the lagoon off Charle Island and induced by waves. The horizontal

circulation arising from such a flow can be investigated analytically. This is sketched in

the Figure 4.4.1.2, and Eq.4.4. 19 is used, where angle φ is set to zero when the wind is

directed into the bay and 180° when the wind is directed out of the bay. This is done by

taking ρ_a =1.22kgm^{3}s^{-1} and ρ_b = 1025kgm^{3}s^{-1} the density of air and standard density of

sea water respectively. In addition it is assumed that the peaks in current fluctuations in

the observed current data were caused by wind stress and using a drag coefficient C_d

=0.0013 and a bottom coefficient of C_{db}= 0.002. For NEM and SEM seasons and the

value of wind obtained with the weather mast Section 5.1.2.2 (Figure 5.1.2.2) show that

the wind is of order 6ms^{-1}. The width (B) of the bay entrance is 3500m. When these

values are put in the equation, the result suggests overestimation of the flow. The reason for the over estimation is due to the fact that the equation does not take into account that the beach and the coral reefs stop the flow. Onshore wind pushes water into the bay the sea level rises, i.e. wind set up. The barotropic pressure gradient generates a barotropic out flow, and i.e. velocity is the same throughout the water column, which makes the water exchange generated by wind less effective. The flow is thus limited by the difference between the bay and ambient water and bottom friction. Waves also induce water exchange, they are referred to as Stokes' *waves*.

On seasonal scale wind may influence water exchange directly causing direct transport and indirectly by mixing as well as causing the thermocline to erode.

Mixing of coastal water by wind on seasonal time scale (3-6months) may affect the density of water by mixing salinity and temperature in the creeks and ocean water longitudinally and vertically, giving rise to slow gravitational currents that induce exchange. They are further considered in Section 5.3.5.3.

5.3.4 Other calculations

5.3.4.1 Bay tidal energy dissipation

Equation 4.4.40 allows for the determination of tidal energy in Gazi Bay. From Table 5.3.2.1, the tidal amplitude is found to be 0.963m, the tidal phase lag 115.4 ° and the current phase lag 144.6 ° this give a phase difference of 30°. g is 9.81ms-1, the standard density of water 1025kgm^{3}s^{-1} and the tidal current amplitude take as 0.13m. Using these values in the equation 4.4.40 gives tidal energy of flux of 97 Jm^{-2}s^{-1}.

5.3.4.2 1 -D model application

Gazi Bay was divided into 14 sections each about 1000m. The mean depth of each section was then determined and the cross-section area for each of the 14 sections calculated. Then One-D model for the bay was applied in order to calculate velocities and sea level and volume the flux across the entrance and compare the results with observation. The results from the model produced unsatisfactory results, unlike its application in Tudor Creek (see later). The reason for difficulties unsatisfactory results in has do with the fact that a large portion of the Gazi Bay is not covered by water during ebb and error associated with mean depth the estimate.

5.3.5 Advective and cumulative heat flux

Advective heat flux for Gazi Bay was estimated using the equations given in Section 4.4. The results are shown in Figures 5.3.5a and 5.3.5b for both advective and cumulative heat fluxes. Heat flux in Gazi Bay was estimated using the equations given in Section 4.4. However, the estimate required fist the use of the sea level and temperature time series (MT2) for the calculation of volume flux through the entrance cross-section area. This is done in Section 5.3.3. The sea level and temperature data produced more reliable results than the instantaneous current observations for reasons related to mooring arrangements (Section. 5.3.2.2). Gazi Bay instantaneous volume flux is given in Section 5.3.3.3 and illustrated by Figure 5.3.3.3 there. The results of heat flux through the Gazi Bay entrance are given in Figure 5.3.5.1a-b for both advective and cumulative heat fluxes. Detailed calculations for advective and diffusive heat flux are given in the Appendix B.

231
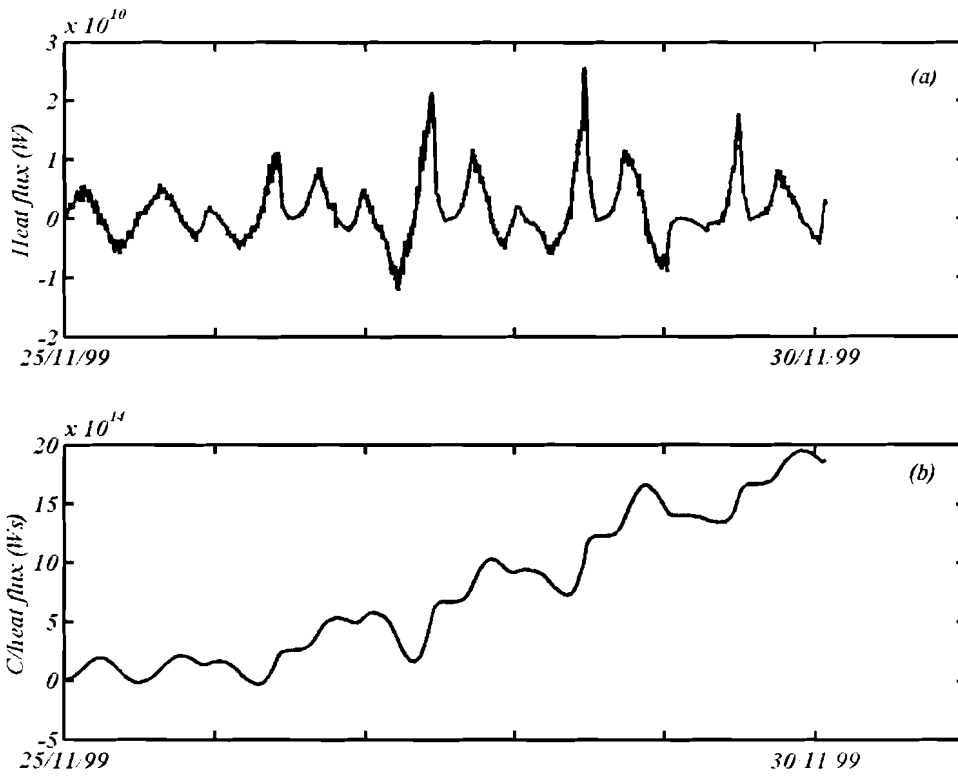
Figure 5.3.5.1a-b Instantaneous, Q_{ex} (positive inward) heat flux (panel (a)) across the entrance of Gazi Bay calculated from temperature time series data of November (IMSR season) 1999, panel (b) Cumulative (integrated) heat flux $Q_{ex}dt$, calculated from temperature time series data from the entrance to Gazi Bay during IMSR season 1999.

232

5.3.6 Flushing time

The water in Gazi Bay undergoes exchanges with the ocean. As mentioned earlier, these exchanges are driven by a combination of forces, including tides, wind and fresh water runoff. The rate of exchange can be expressed as in terms of flushing time, i.e. the time required to replace the water within the bay. Frequently the flushing time is referred to as the e-folding time, defined as the time required to decrease the volume of water in the bay to e^{-1} (about 37%) of its original volume, where e is the base of natural logarithms. If we now assume instantaneous and complete mixing of the tidal prism, each tidal cycle, after n tidal cycles the volume of this water still residing in the bay. We let (Vn) be the low tide volume of the bay. Then V divided by V plus the tidal prism (P) all raised to n multiplied by the volume of the water (Vo) originally in the bay (i.e. V= Vo) is equal to volume of water in the bay which is equal to $1.8 \times 10^6 m^3$ at a time t=0.

P is given by the average tidal range (3m) and the surface area and has a value of $5.4 \times 10^6 m^3$. Therefore the e-folding time is 12 tidal cycles (6 days). These is generally plausible because of the incomplete mixing within the appropriate portions of the bay, e.g. the water near the head of the bay or at the mouth of Kidogweni river may not reach the entrance to the bay during an ebb tide. In addition some of the water that does leave during the ebb may return on the flowing tide.

Estimate of flushing time was done using equation 4.4.62, which first allow the calculation of longitudinal eddy diffusion coefficient and then residence time. With evaporation rate of 0.5cm/day, salinity difference of 5, and reference ocean salinity of 35, and cross-section area $14.4 \times 10^3 m^2$ the eddy diffusion coefficient obtained leads to over

233

estimation of exchange time. These can be attributed to lack of large differences in salinity. Equation 4.4.62 is valid when there is a large salinity gradient.

When average values for river discharge and average salinity in the bay and outside the bay are considered then the characteristic values for seasonal exchange can be obtained. During the IMLR and IMSR seasons difference in salinity exists between the bay and the oceanic water. For 1996, 1997, 1998 the typical salinity in the IMSR season were 32 in the bay and 35 in the ocean, and for the IMLR the value were and 30 and 35 respectively. The river discharge (R) for the IMLR was 5 m^3s^{-1}, for NEM season the range 0.4-0.2 m^3s^{-1} and SEM season the range of river discharge is 0.2-0.1 m^3s^{-1}. Using these values in equation 4.4.60 a typical estimate of exchange rate for the IMLR is 0.6 days, during IMSR season the estimated typical flushing rates are 2 days and greater than 3 days for NEM and SEM seasons. Compared to the flushing time of 6 days obtained by tidal prism method, we suggested that the faster flushing rates are due to induced gravitational currents that give rise to the residual circulation whenever there is baroclinic forcing. In addition to tidal exchange, the single major factor affecting residence time in the bay is expected to be the windstorms, because of the relatively large entrance. Intense storms are capable of exchanging the bay's over a day or so.

5.4 TUDOR CREEK

5.4.1 HYDROGRAPHY

5.4.1.1 Creek temperature

We present results of the temperature time series measurements obtained from three tide gauges, at the entrance (oceanic), in the channel and in the upper reaches of the creek (basin area), to get a synoptic view of the temperature response to the tide. Another time series obtained from the salinity sensor is also presented for the same purpose and at the end of this subsection we examine the longitudinal structure of the water in the creek during the various monsoon seasons.

The three instruments worked for different duration. The two gauges, at the entrance and in the creek basin, the record is available for 36 days from November 1 to October 11 1998, while the one in the middle or in the channel recorded only for 25 days from November 1 to November 27 1998.

Spring, neap and daily temperature fluctuations

Statistics for the 36 days reveal maximum temperature of 30.08°C, minimum of 25.95°C with a mean of 28.65°C for the tide measurements in the creek basin. For the gauge at the entrance, the temperatures show a maximum of 27.90°C, minimum value of 26.20°C with a mean of 27.18°C. The 36-day temperature record shows a difference of 2.5°C between the creek basin and the entrance.

235

Figure 5.4.1.1a shows the temperature fluctuations for the 24 days mentioned from 2-26 November 1998, during which time the three instruments worked simultaneously. It is clear from this figure that temperature in the shallow creek basin are higher than in the channel and in the ocean, and that inside temperatures show high fluctuations.
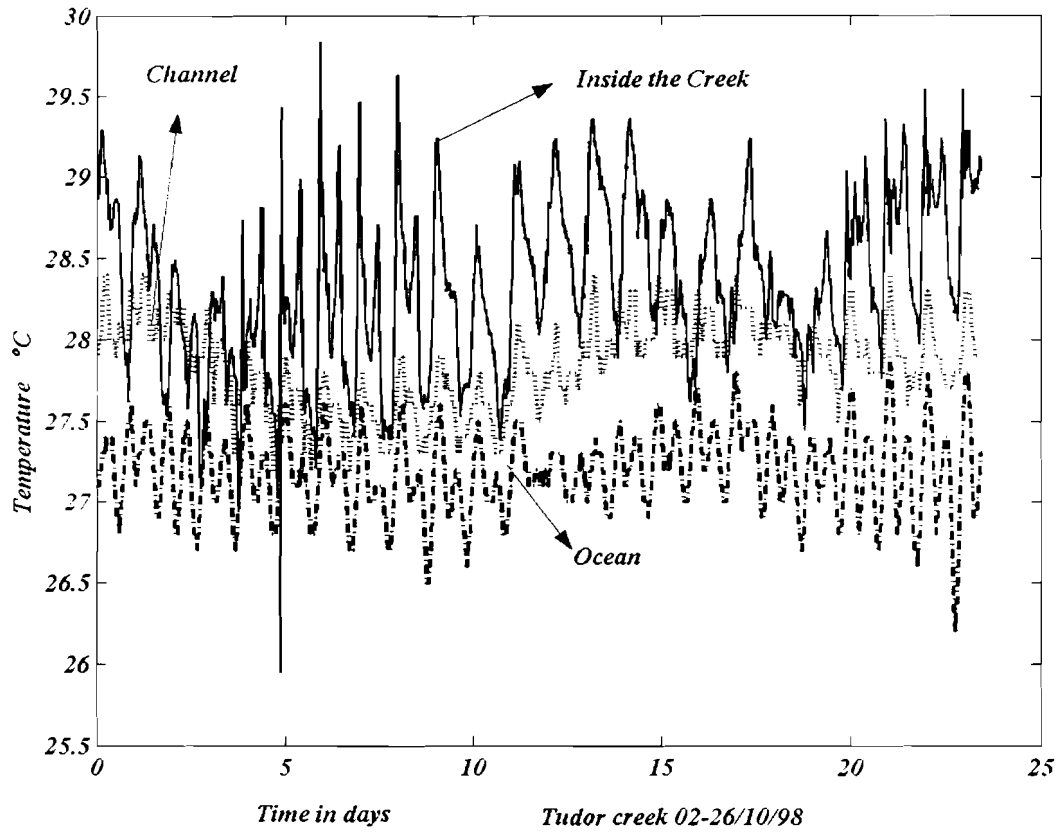
Figure 5.4.1.1a Comparison of temperature from three tide gauges in Tudor Creek at the entrance (Ocean), in the channel and inside the creek.

Like in Gazi Bay the spring period is characterised by fluctuations with the high amplitude, whereas the amplitudes are diminished during the neap periods. The highest

236

fluctuations, 75% for the total range of temperature for the three sets of records occur during spring in the shallow water within the creek basin. There the values fluctuate between a maximum of 29.84°C; and a minimum of 25.95 °C with a mean of 28.32°C and a range of 3.9°C. In the creek channel the fluctuations are diminished by 11%, with a range of 0.55°C, and values at 28.40°C, 27.20°C, and 27.85°C for the maximum, minimum and mean respectively. In the ocean station 14% of the fluctuations occur in a rage of 0.72°C, the temperature lie between a maximum of 27.90°C, minimum 26.20°C and a mean of 27.18°C. The temperature decreases longitudinally, from the creek basin to the entrance 1.95°C, which confirms that the temperature ocean water is cooler during this part of the season.

Comparison, of the three records reveals two interesting features. During spring the temperature in the creek basin appears to bodily surge downward diminishing the difference between the three curves and decrease by 1.5°C from previous values before swinging upward again. This cosine- like feature is not observed in the other two curves. Instead it can be seen that at the ocean side the temperature remains almost constant and in the creek basin curve there is a tendency for the mean temperature to increase with time suggesting that the basin is gaining heat. The down ward surging of temperature in the bay could be caused by rainfall, however because this does not happen in the two temperature signals, and also because of the increase towards neap, the phenomenon reveals more the effect of the tide in the shallow creek basin. We suggest that the downward surge of the curve or the decrease in temperature is caused by the large cooling effect as the less warm oceanic water is ejected into the creak basin during spring

tide. During neap, however, the bay warms up as less volume of water is available and less cold water ejected into the basin by tide.

Daily water temperature variation is compared with air temperature in Figure 5.4.1.1b, for one-day June 20 starting at 0.00hr. The figure shows that the creek water was warmer than the air-temperature by about 1°C. The mean temperature for water was 26.5°C while that for air temperature is about $25\ ^{\circ}$C.
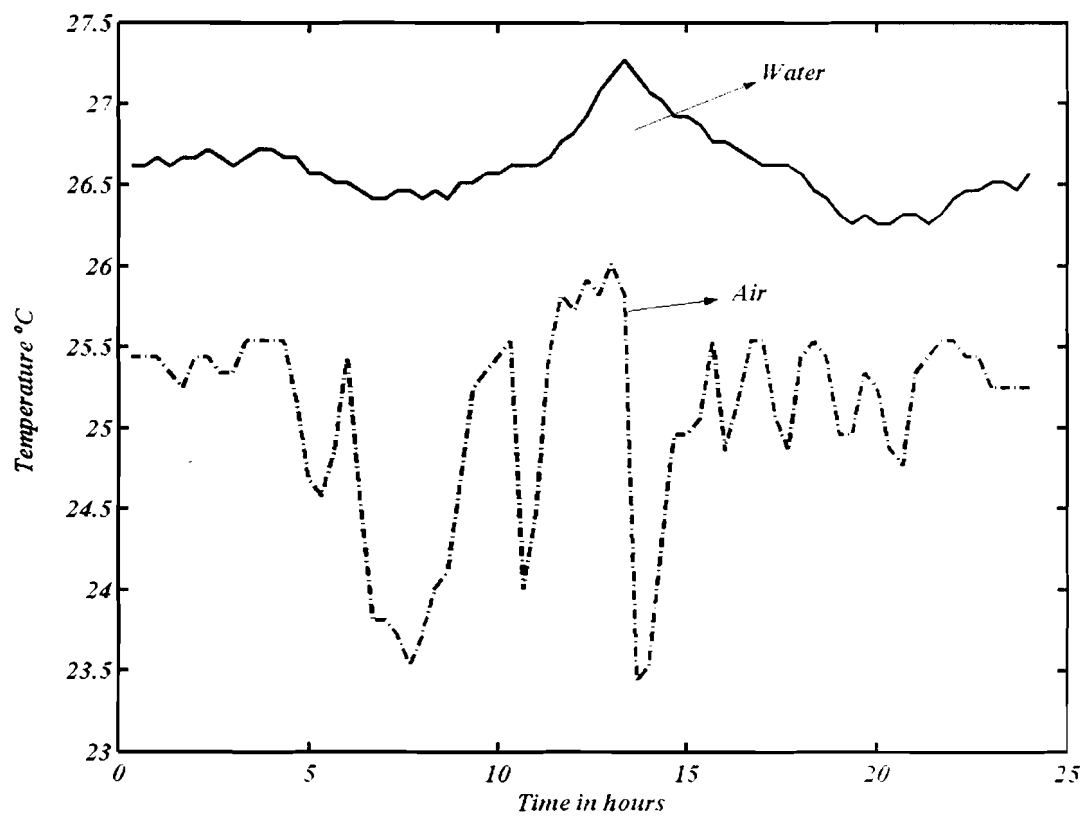
Figure 5.4.1.1b Daily fluctuation of water and air temperature in Tudor Creek entrance, June 20, 1996- starting 0.00hrs.

238

At about 13hrs the water attains its maximum temperature, while the air above the water attains its highest temperature also but with pronounced fluctuation. Solar heating causes the high temperatures in both, which is at maximum at the 13hr.

The daily temperature response is clearly illustrated in Figure 5.4.1.1c, which shows three temperature variations for three consecutive days, 3-6 November 1998. The dynamics of the temperature from the three panels can clearly be analysed. This can be done by considering the rising edge of the ocean curve as corresponding to the invasion of water from the ocean into the bay, and interpreted as warming up of the ocean water as it mixes and flows into the creek. The falling edge of the basin curve corresponds to cooling. Thus, starting for example with panel (a) maximum and minimum temperature appears opposed in the basin and ocean. As the less warm ocean water enters the creek, it warms and simultaneously cools the creek basin water, making the curves to approach each other, as can be seen by following the maximum-minimum (9-15hrs) toggling of the two curves in the three panels. The saw-tooth-feature in the basin curve panel (b) and (c) points to the reduced effect of mixing as more and more ocean water becomes trapped in the basin causing greater mixing and reduction of the creek basin temperature. The cooling produced by evaporation can be considered also as contributing to the saw tooth pattern.
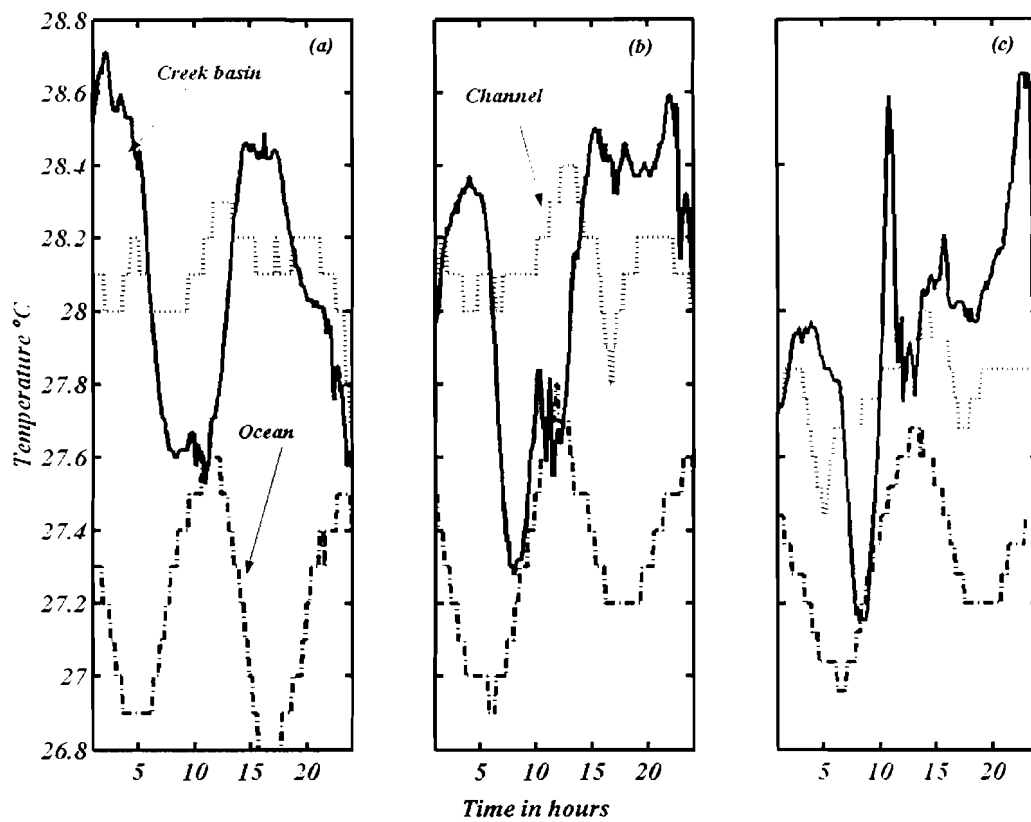
Figure 5.4.1.1c Illustrating the complex daily fluctuations in the temperature at the ocean station, the channel and the creek basin, for three consecutive days in three panels (a)-(c), 3-6 November 1998.

An example of the temperature observed at the weather mast stations from June 18 to July 27 1996 is also shown in Figure 5.4.1.1d. The figure indicates a decreasing trend in sea temperature. We observed that the mean temperature dropped from a

240

maximum of 26.5 °C in June to a minimum of 25 °C in mid-August, difference of 1.5 °C. Fortnightly inequality is clearly seen in the figure. The temperature gradients differ from one tidal phase to the next and are more pronounced in spring indicating of variable cooling rates in the creek waters.

The greatest variation in temperature occurs in each spring phase with maximum temperatures of 27 °C and minimum values of 26 °C in the months of June. In the spring neap cycle of the month of July the main temperatures dropped slightly to values less than 27 °C while the minimum temperature values dropped to 25.6 °C. The temperature decreased during the flood stage from a maximum of 27.3 °C to a minimum of 26.2 °C, indicating an average change of 1°C from flood slack water to ebb slack water. During neap however the temperature decreased from 26.5 °C to 25 °C thus showing a small range of temperature <1°C.

Seasonally influenced temperature structure in the creek

Monthly mean temperatures, from a series of vertical temperature measurements, for 1995, 1996, and 1997 are presented for the four-monsoon season.
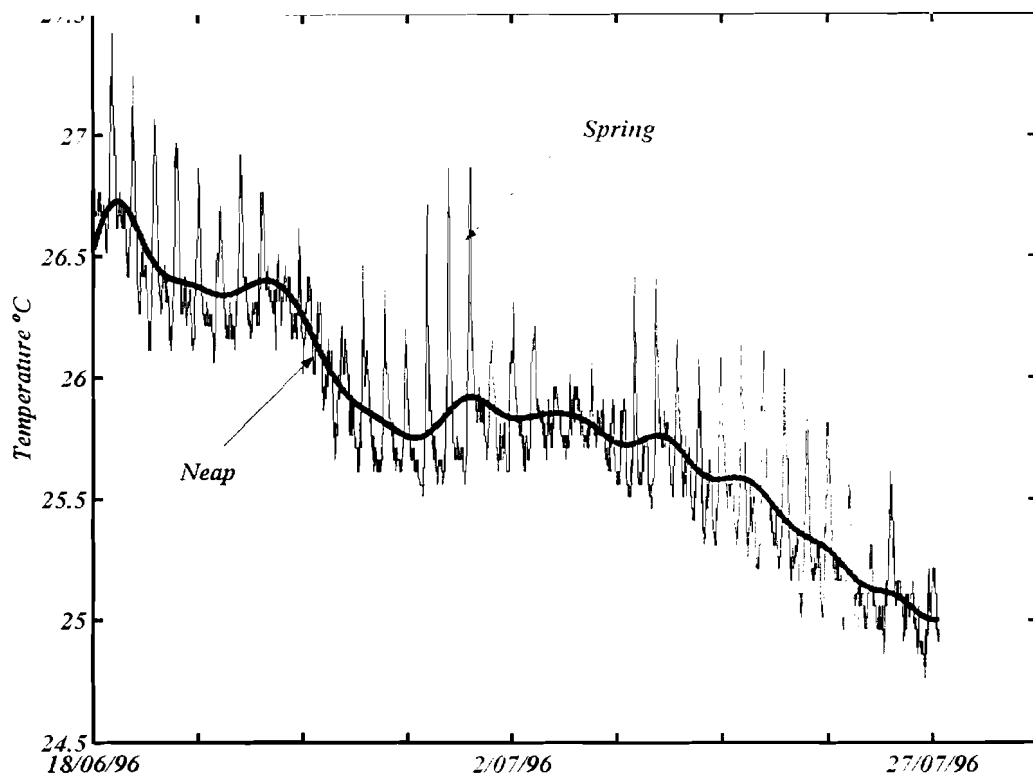
Figure 5.4.1.1d An example of variations in temperature in Tudor Creek from 18 June to July 27, 1996. Note neap corresponding low fluctuations.

We identify three regimes as mentioned before. The mangrove fringed inner part of the creek, which is referred to as shallow basin regime. The others are the channel regime, the entrance and the slope or offshore regimes respectively. We have presented the results in Figures 5.4.1.1e-h for the four monsoon seasons. The idea in this type of presentation is that the mean changes will reflect long-term gravitational circulation which in turn reflect the monsoon driven renewal of creek and the shelf water. Thus, although the parameter changes are small they suggest a 'net' structural response due to long-term water changes.

242

IMLR season

To illustrate the structural response of temperature during the IMLR season, a longitudinal vertical section, drawn from the inner basin of the creek to the entrance and including some part of the shelf water is shown in Figure 5.4.1.1e.
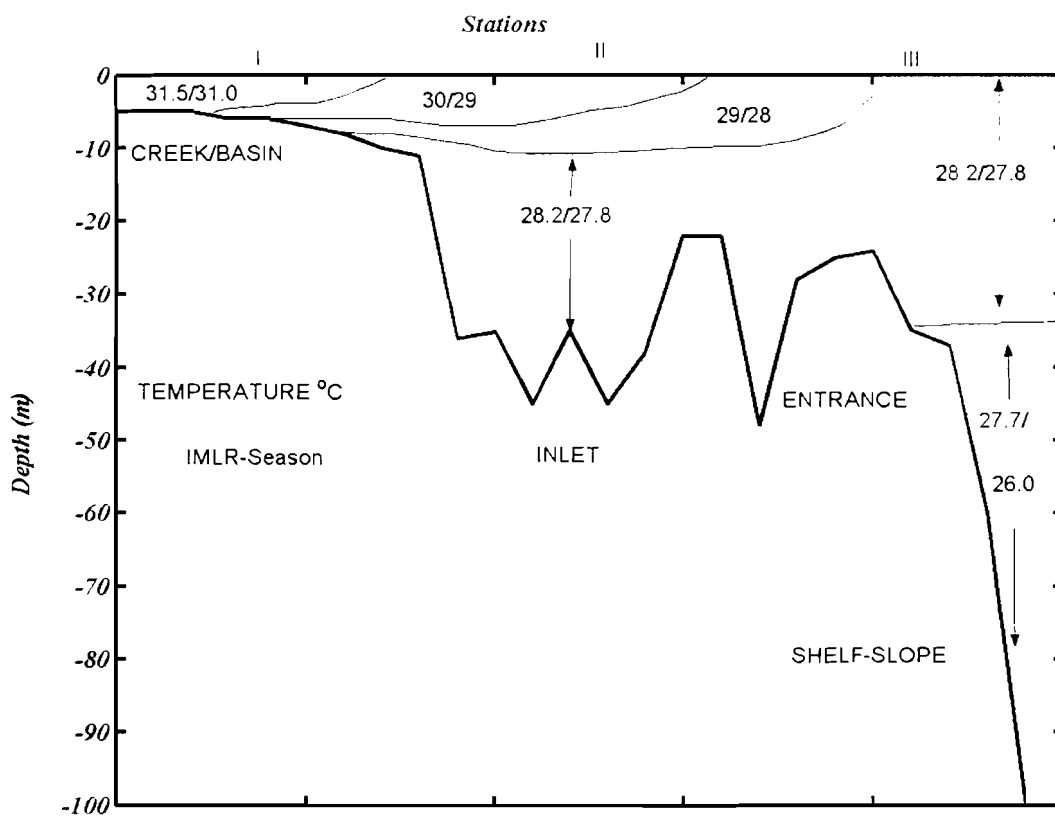
Figure 5.4.1.1e A vertical section showing longitudinal distribution of temperature in Tudor Creek during the IMLR season.

From these results a temperature gradient is evident from the inner basin to the entrance and the shelf slope area. The temperature range between the inner basin and the slope is 2 °C. The inner basin shows surface water temperature of 31.0°C, the inlet zone

29 °C and the shelf 28 °C. The average temperature for the creek is 29.7 °C. The temperature ranges are clearly observed. The surface to bottom ranges of temperature is 31.5-28.2 °C in the inner creek zone, 30-27.5 °C in the channel and 28.2-26°C at the shelf-slope zone.

SEM season

Figure 5.4.1.1f illustrates vertical temperature variations for the SEM season. The surface temperature decreases from an average value of 26.7°C at the shelf slope zone to 25.3 °C in the inner creek zone.
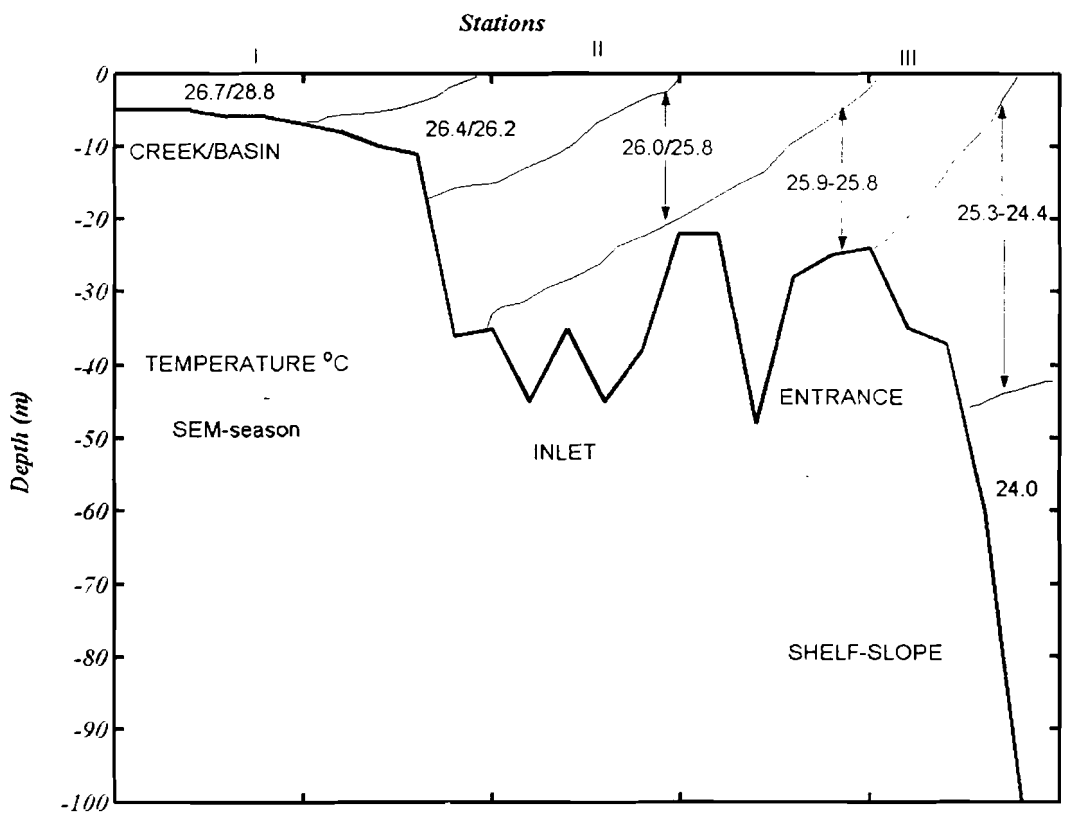
Figure 5.4.1.1f A vertical section showing longitudinal distribution of temperature in Tudor Creek during the SEM season (1996-98).

The surface to bottom range of temperature was 26.7-28.8 in the creek area, 26-25.8 °C in the channel and 25-24 °C in the water column above the shelf area. The mean surface temperature was 26 °C a decrease of about 3 °C from the previous season.

IMSR season

Vertical temperature structure for the IMSR season is shown in Figure 5.4.1.1g. A very slight temperature gradient is maintained between the shallow basin in the creek (29.0°C) and the entrance, inlet and surface water of the slope zone where the mean surface temperature is 28.6°C.
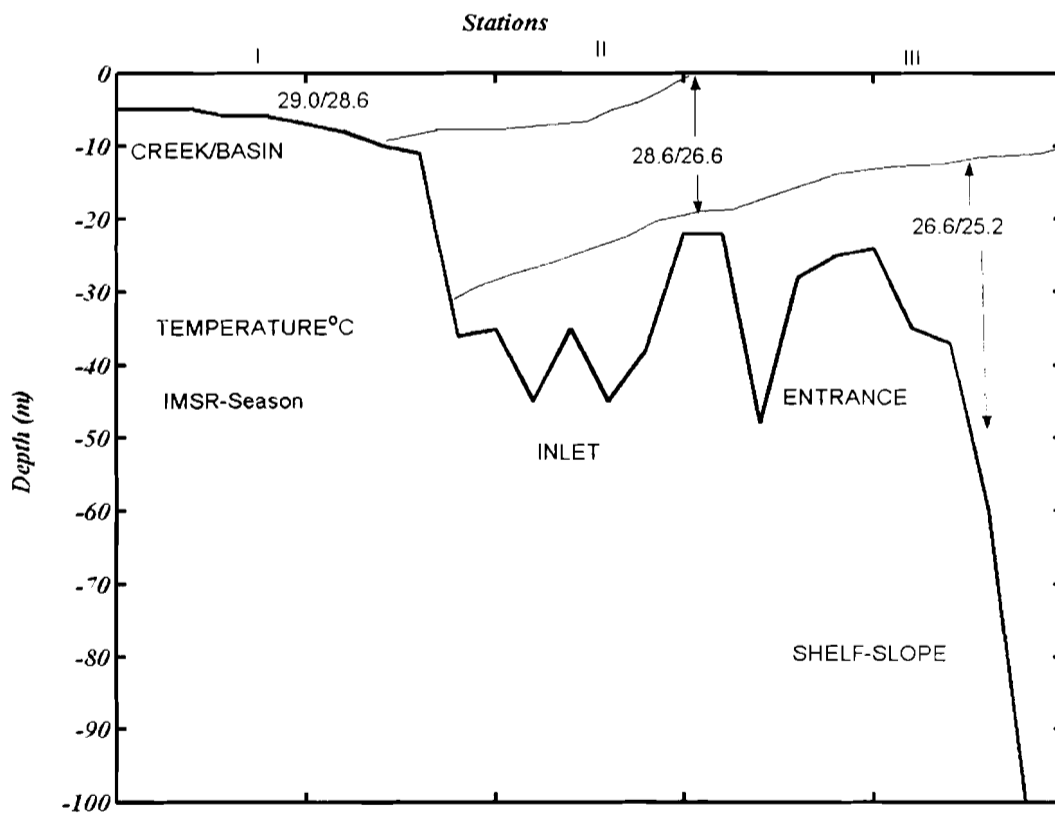
Figure 5.4.1.1g A vertical section showing longitudinal distribution of temperature in Tudor Creek during the IMSR season.

The mean vertical temperature range is 28.6-29.0 °C in the inner creek basin zone. In the inlet, entrance and slope zone an envelope of water of temperature range of 25.2-26.6 °C. This differs from the previous ones by having on average higher temperature.

NEM season

Temperature structure for the NEM season is shown in Figure 5.4.1.1h. This season shows the highest temperature with a mean value above 31°C.
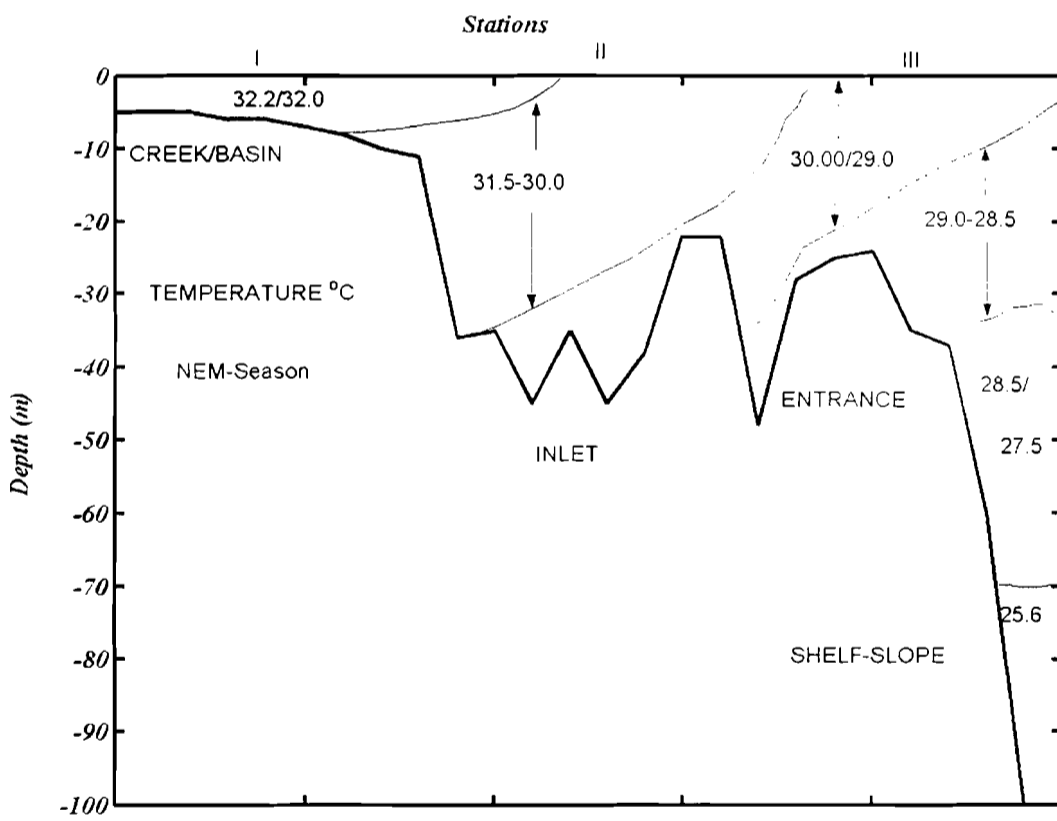
Figure 5.4.1.1h Vertical section showing longitudinal distribution of temperature in Tudor Creek during the NEM season.

The water on the shelf is slightly cooler with a vertical temperature ranging from 29-28°C, while the inlet and inner basin zone the values range from 30-31.5°C and 32.2-

32.0°C from surface to the bottom respectively. There is a longitudinal gradient of about 4.0°C between the inner creek area and the shelf-slope area

5.4.1.2 Creek salinity

Short-term salinity variations

Figure 5.4.1.2a illustrates salinity time series for data taken from 14 Jun to 8 August 1996. The figure shows salinity decreasing gradually after neap (25-27 June) from a maximum value of 34.91 to a minimum value of 24.53 in the first week of August. This is a difference of about 10.4 in salinity. The mean salinity for the entire period was 32.35 with a standard deviation of 2.12. The gradual decrease can be attributed to rainfall, which stood at about 500mm in the month of May and probably to the appearance of oceanic low salinity water that occur just (before) the start of the rain (Newell, 1959). The rainfall in the month of June is negligible being a mere 8mm in that month. In July however, the rainfall to about 60mm/month and although this may have contributed to the general trend in the decrease of salinity, its effect is more during ebb periods. For the 55 days shown, the rate of salinity decrease is 0.2/day. In addition however, there are considerable amounts of fluctuations particularly during spring period and at ebb tides, whereas the neap period is characterised by lower fluctuations than the spring period, which also is characterised by the presence of low salinity water during ebb. This suggests that spring tide flushes low salinity water from the creeks or its peripheral lagoons.

The tidal fluctuations of salinity are presented in Figure 5.4.1.2b, whereas those related to the rainfall effect in the month of July are presented in a Figure 5.4.1.2c.
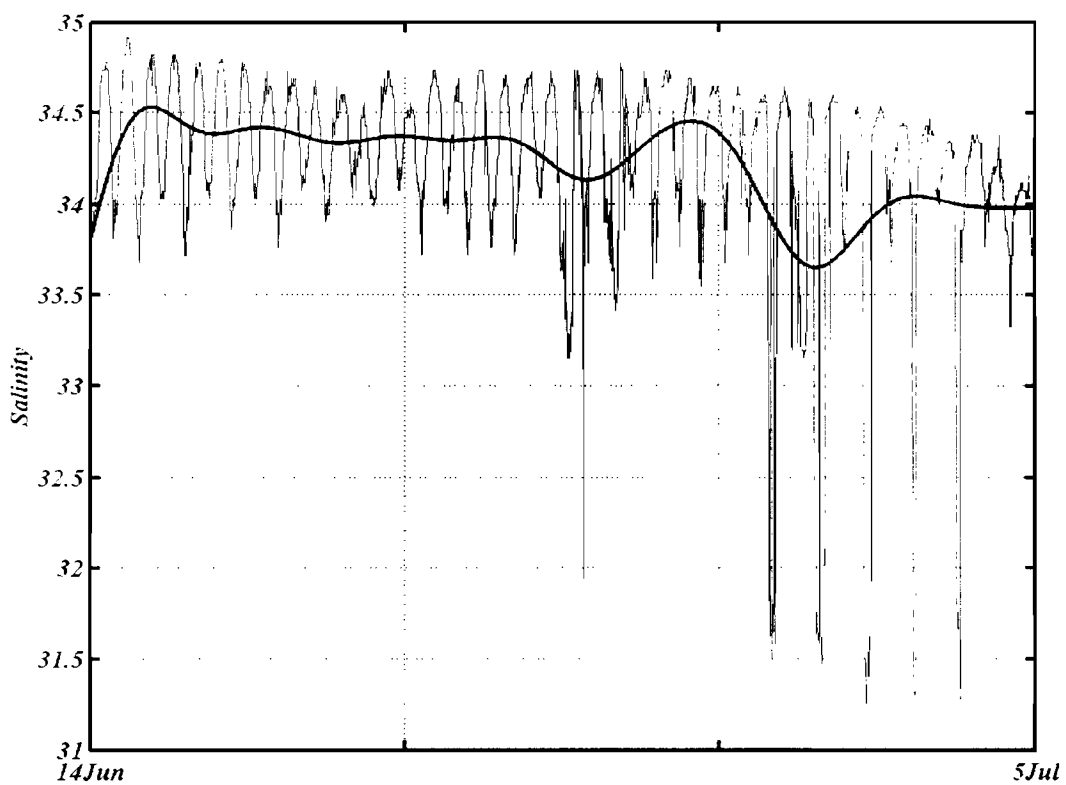
Figure 5.4.1.2a Salinity time series from Tudor Creek entrance area between from 14 June to 5 July 1996. Note the decreasing trend.

Figure 5.4.1.2b shows an example salinity fluctuation for 16-19 June 1996.

Throughout the two days shown, the salinity fluctuates between maximum and minimum

values during the flood tide and ebb tides. For example the flood of 16-17/6/1996 the

salinity increased from about 34.05 to maximum value of 34.82 during the slack water

flood.
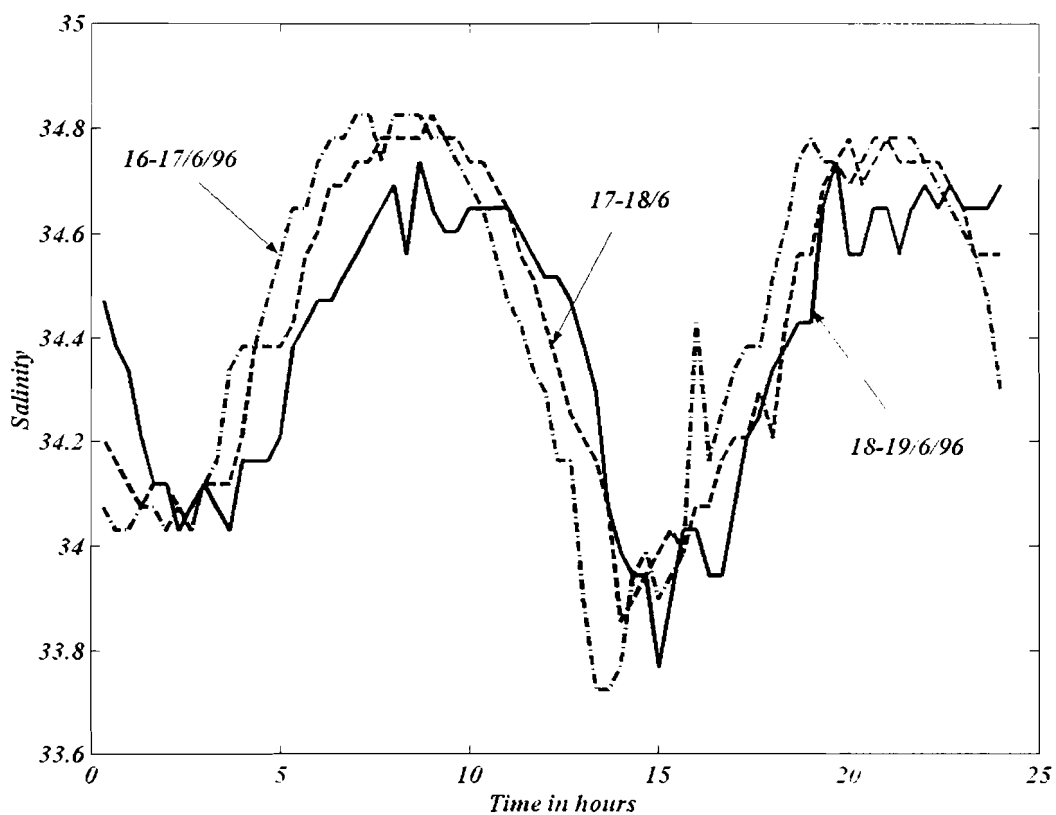
Figure 5.4.1.2b Daily salinity fluctuation (flood - ebb) in Tudor Creek, from 16-19

June 1996.

During ebb the salinity decreased to a minimum value of 33.72 at slack low water.

The high salinity is brought by the tide into the creek from the Ocean. The low salinity

seen during ebb water slack is brought from the inner parts of the creek. Looking at the

curves, everyday the salinity shifts to the right by 30min due to the tide, but also its rage decreases. The smallest range of the three data sets occurs in the third day. The salinity range for the three days is 1.025 and the mean is 34.41. However, for the daily fluctuations as shown on 16-17 June curve the salinity fluctuated with flood and ebb tide between a maximum value of 34.82 to a minimum value of 33.85 and a mean of 34.42.The mean value is different for each day. The differences are caused by diurnal inequality and mixing.

TUDOR CREEK-SALINITY (1996)
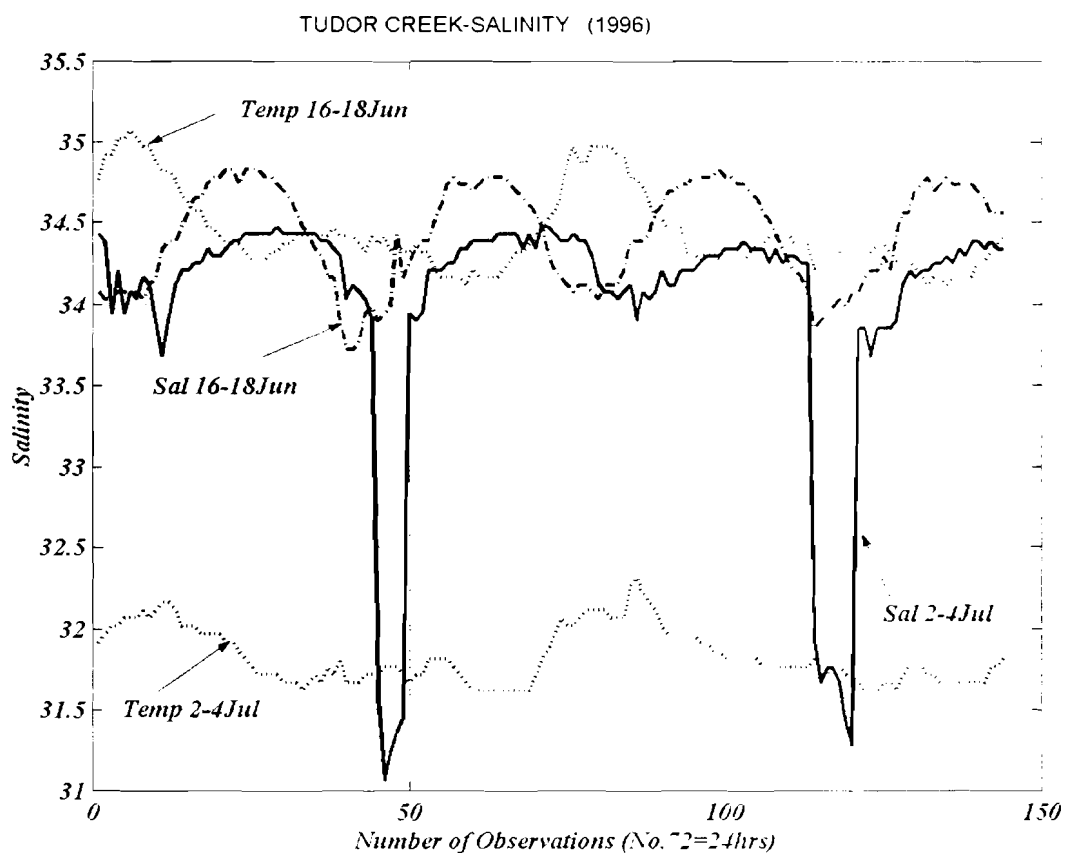
Figure 5.4.1.2c Composite presentation of salinity-salinity and salinity-temperature fluctuations between day 16-18June and 2-4July 1996.Note the appearance of low salinity parches (peaks) during ebb.

In the composite Figure 5.4.1.2c and Table 5.4.1.2 salinity and temperature fluctuations for two days 16-18 June and 2-4 July in 1996 from the same data series are shown. The temperature scale has been left out in the figure to enhance clarity and a constant added to the temperature valued so as to mirror the scale of salinity for easy display. The statistical values are, shown up in Table 5.4.1.2 for the same period.

Table 5.4.1.2 Statistics for salinity and temperature data for 12 tidal cycles in Tudor Creek entrance 1996.

Statistics	16 -18 June 1996		2 – 4 July 1996	
	Salinity	Temperature $^{\circ}$C	Salinity	Temperature $^{\circ}$C
Maximum	34.82	27.07	34.47	26.32
Minimum	33.72	26.11	31.06	25.61
Mean	34.43	26.42	34.00	25.83
Range	1.1	0.96	3.41	0.71
S/deviation	0.31	0.25	0.78	0.17

Again we observed, similar to Gazi Bay, maximum salinity occurred at the slack water after flood. Looking day-wise from 16-18 to 2-4 July values are in the range of 34.47-34.82 and temperature 27.07 -26.32°C and a mean of range of 34.43-34.00 and 26.42-25-83°C respectively. The day-wise decreasing trend in both salinity and temperature was mentioned earlier. However, what are clearly seen in the figure are the tidal rhythms in the salinity and low saline water events that appears in the 2-4 July curves. Tidal signal is also seen on the salinity curve. Observing the curve of 16-18 June we note clearly that maximum salinity occurs at slack water flood and minimum salinity

at slack water ebb. Salinity does not fall below 33.5 during ebb. The temperature is at its maximum between 14-15 hrs as a result of solar heating. The flooding oceanic water lowers the temperature by about 1°C and raises the salinity by about 1. Observing the curve of 2-4 July, and comparing it to that of June, interesting events appear to occur during ebb, which cause salinity to decrease further during ebb by a value of two to those at ebb in the June curve. The 'sword-like' salinity drops are most likely caused the passage of brackish water parches at the location of the sensor. These parches are not uniform in salinity and imbedded within them are very low salinity plume or 'bubbles' (Wolanski and van Senden, 1983). They are part of the inner creek low salinity water, which is advected seaward during ebb.

However, an even more interesting and surprising features are also high salinity 'bubbles imbedded within low sanity water. They probably originate from the peripheral cove, (near KMFRI) as a part of long-shore –rip current system. They masque the clockwise eddy during flood tide. The long-shore flow that is established strongly during certain parts of the flood tide stage carries with it re-suspended sediment from the beach cove and from further upstream, plus the high salinity water previously trapped in very shallow lagoon near the entrance. These are shown more clearly in the three panels of Figure 5.4.1.2d. Panel (a) high salinity trapped in low salinity water or plume during flood, while in panel (b) and (c) the trapping occur during ebb period. It should be noted that, the salinity sensor was at the location of headland (English Point) clockwise eddy (Kimaru, 1986), which acts as a trap of brackish plume and floating litter during certain stages of the tide. A salinity cross-section at this location indicated lower salinity on the side of the channel bank where the salinity sensor was deployed; thus indicating that

ebbing water hugs the left side of the channel facing downstream. Large temporal variations of salinity were found in the creeks during the IMLR and IMSR >. However, the spatial distribution of the brackish water parches was not measured. they occurred on the sides of the channel main channels influenced by the small side creeks or valleys that discharge runoff into the main Tudor inlet and the inner basin.
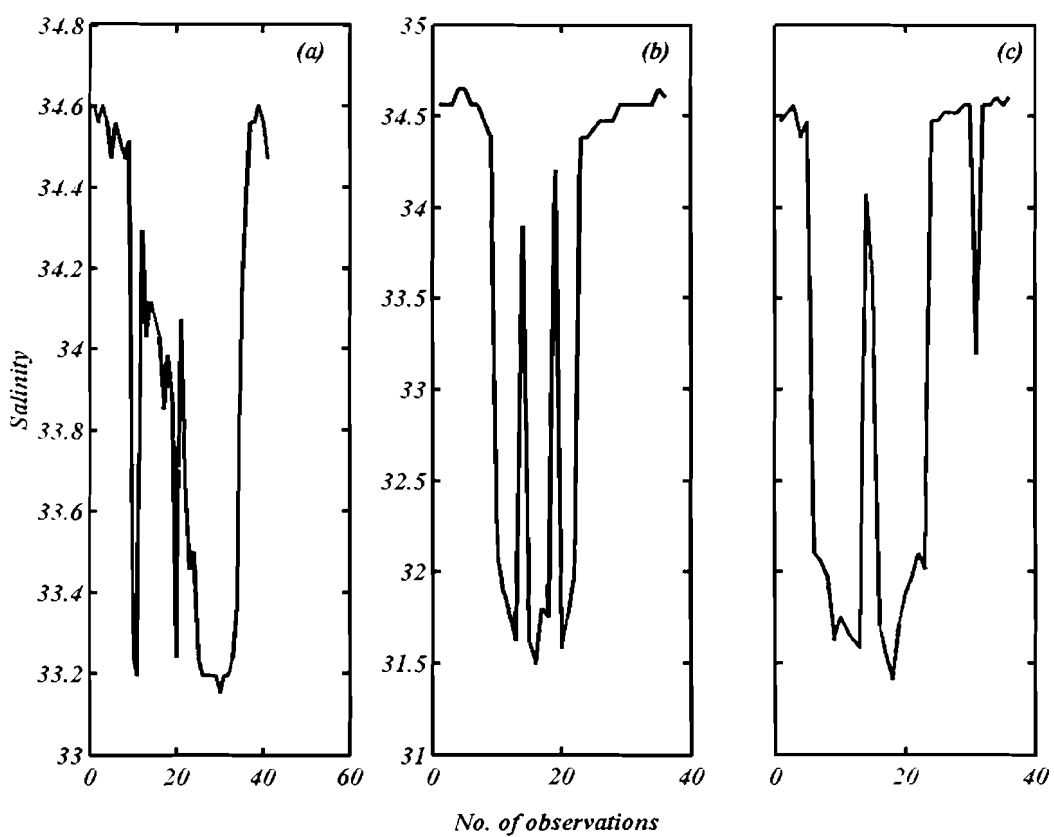
Figure 5.4.1.2d High salinity parches embedded in low salinity water during ebb period (b)-(c) and during flood period (a).

Seasonal salinity structure

IMLR season

The longitudinal section showing the response of the creek system to the 1996-98

rainfalls as a vertical structure of salinity is shown in Figure 5.4.1.2e.
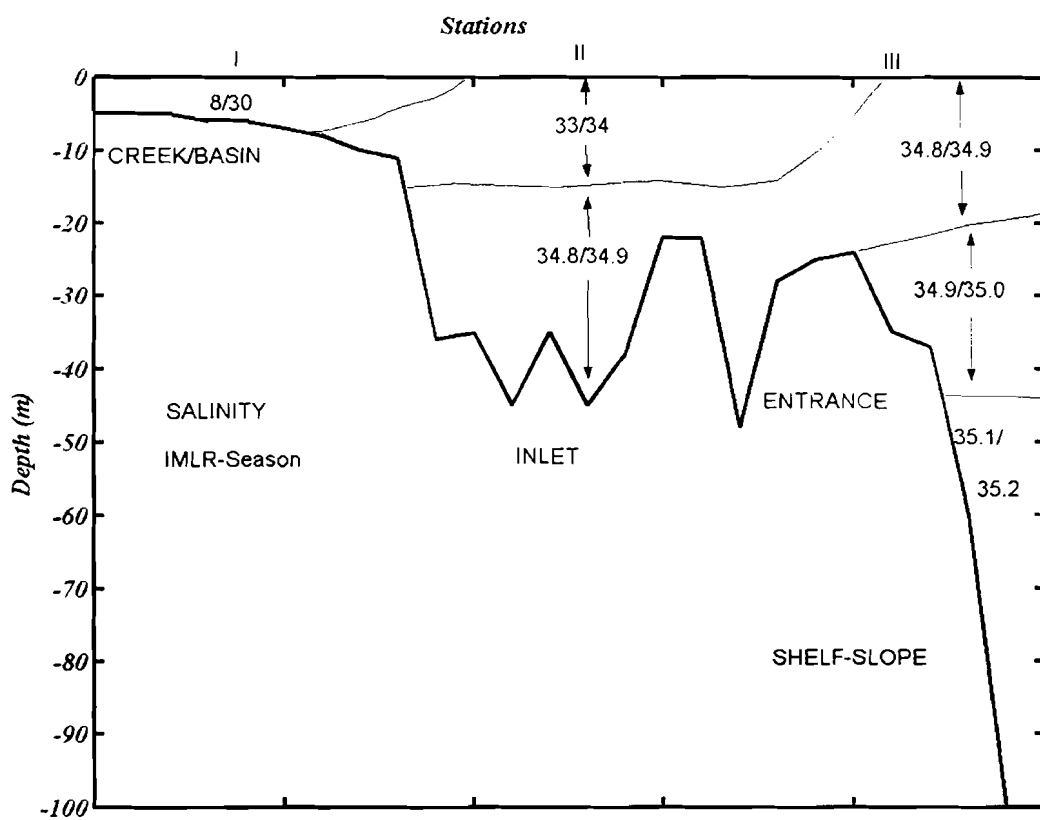
Figure 5.4.1.2e Vertical section showing longitudinal distribution of salinity in Tudor Creek during the IMLR season.

The surface to bottom salinity ranged from 8-30 in the inner creek zone, 33-34.9 in the inlet zone and 34.8-35.2 in the shelf slope zone. The total average salinity for the section was 29.3. The mean salinity for the inner creek zone was 19 and the slope water zone 35, which resulted in a salinity difference of 16 between the creek basin and the ocean.

SEM season

The dry period (July-October) experienced only 12% of the total annual rainfall in 1996, which lend to low discharge as shown earlier. Figure 5.4.1.2f shows vertical salinity structure for the four months of this season. The salinity response in the inner reaches of the creek was 35.8; an increase of about 80% from IMLR season, while a negative longitudinal gradient by a drop of about 4 was apparent from slightly decreasing salinity towards the ocean. At the ocean side salinity was higher in the surface waters (0-50m) as show by the range 35.26-35.31. Below the 50m the salinity range from 35.26-35.27. The surface to bottom range in the creek was negligibly small. The total mean salinity, calculated by averaging all the salinity observations for this season was 34.4, which was up from IMLR season by a value of 5.7. The small difference between the entrance and the inner shallow basin is an indication that the water content had withdrawn into the creeks and that low salinity water may be found only in the uppermost reaches within the narrow creeks. The water types (see Chapter 6) in the shallow mangrove basins are not very much influenced by the fresh water input. The relatively small rain and high evaporation mean that the salinity continues to increase. Thus setting a stage of high salinity just before the onset of both IMSR and NEM season.
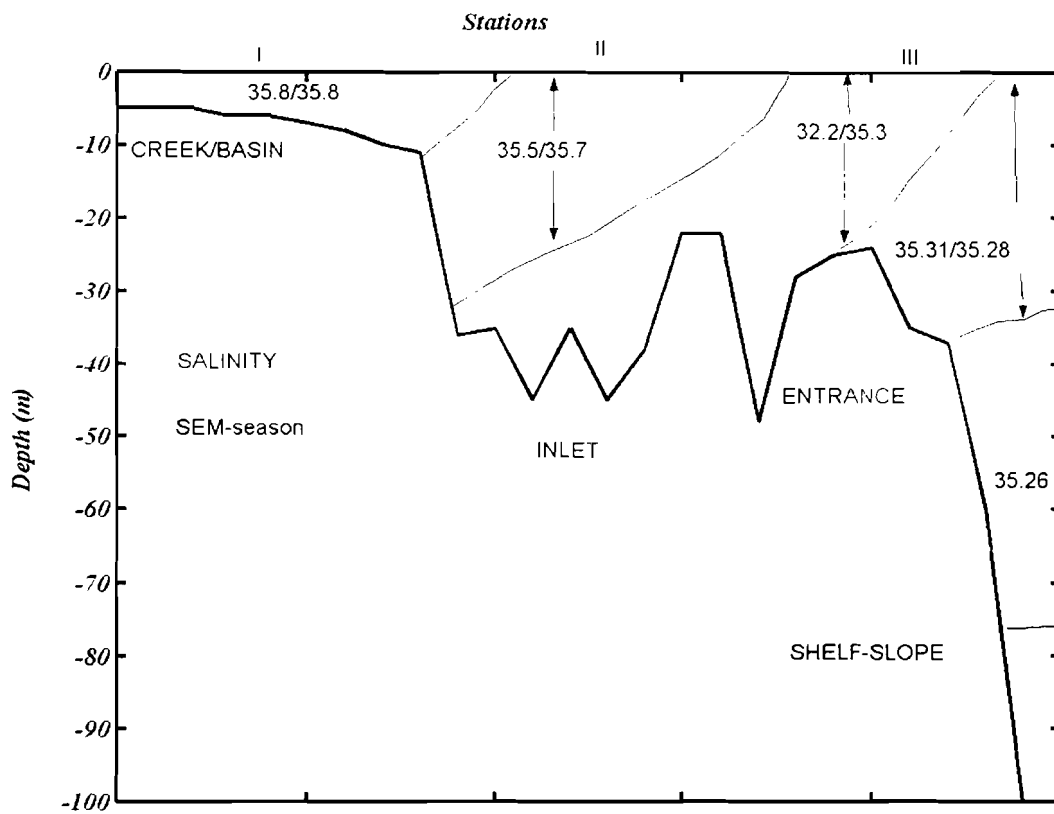
Figure 5.4.1.2f Vertical section showing longitudinal distribution of salinity in Tudor Creek during the SEM season.

IMSR season

As seen earlier the IMSR season has very variable rainfall, which may come as early as October or as late as in December. November represents the average conditions of this season and a longitudinal section is shown in Figure 5.4.1.2g. In the shallow inner part of the creek, the salinity is relatively high and homogeneous with values of 35.2-35.3 from inner part to the shelf slope and changing very slightly with depth. Thus the mean salinity is 35.2 for this season and is greater than the mean value for SEM season by 0.8. One reason for high salinity values is less rainfall. For example, in 1996, the rainfall was

36% of that year's annual value of 1050mm; other reasons are increased high evaporation

rates and the presence of oceanic water masses of relatively high salinity.
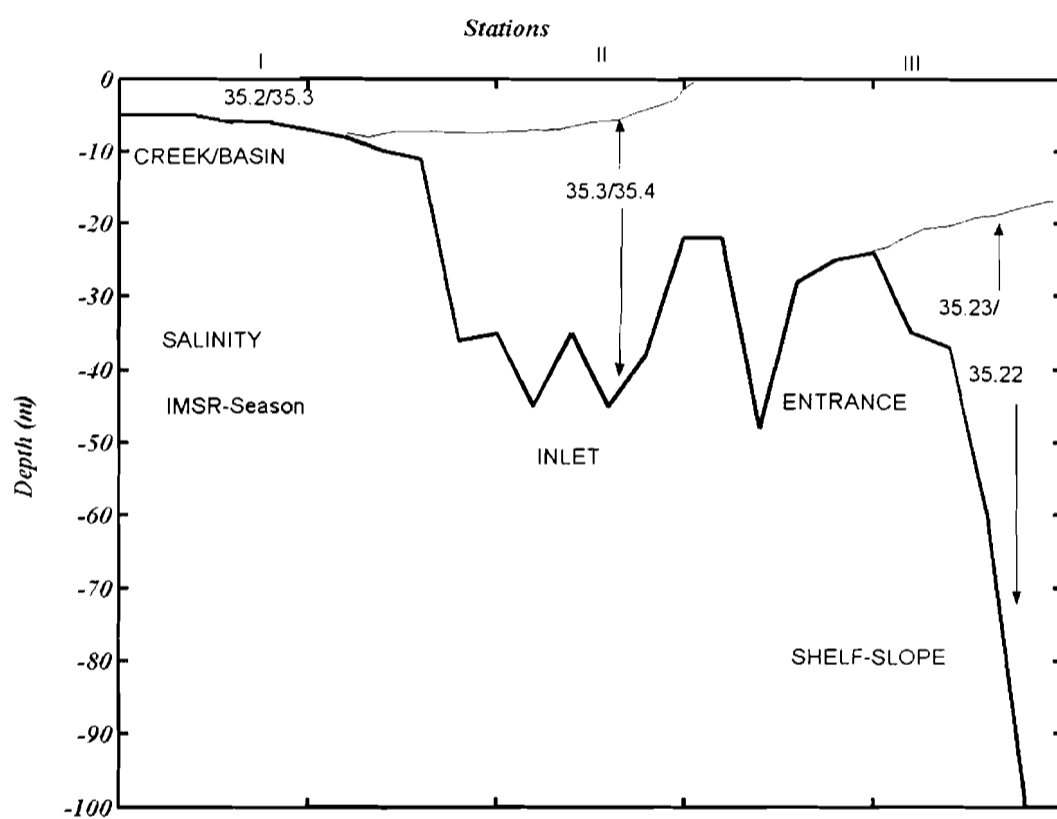
Figure 5.4.1.2g Vertical section showing longitudinal distribution of salinity in Tudor Creek during the IMSR season.

NEM season

Figure 5.4.1.2h shows vertical longitudinal section for the NEM season. The inner

creek zone up to mid reaches of the main channel had an average salinity exceeding 36,

which was the highest in the four seasons. The inner salinity (35.65) was higher than the surface slope water (35.0) almost 1.5. While the vertical change in salinity was less than 0.5. The salinity was 35.48 between 40-100m. These shelf values are slightly higher than those in the previous season. Thus indicating the entire creek system is gaining more salinity.
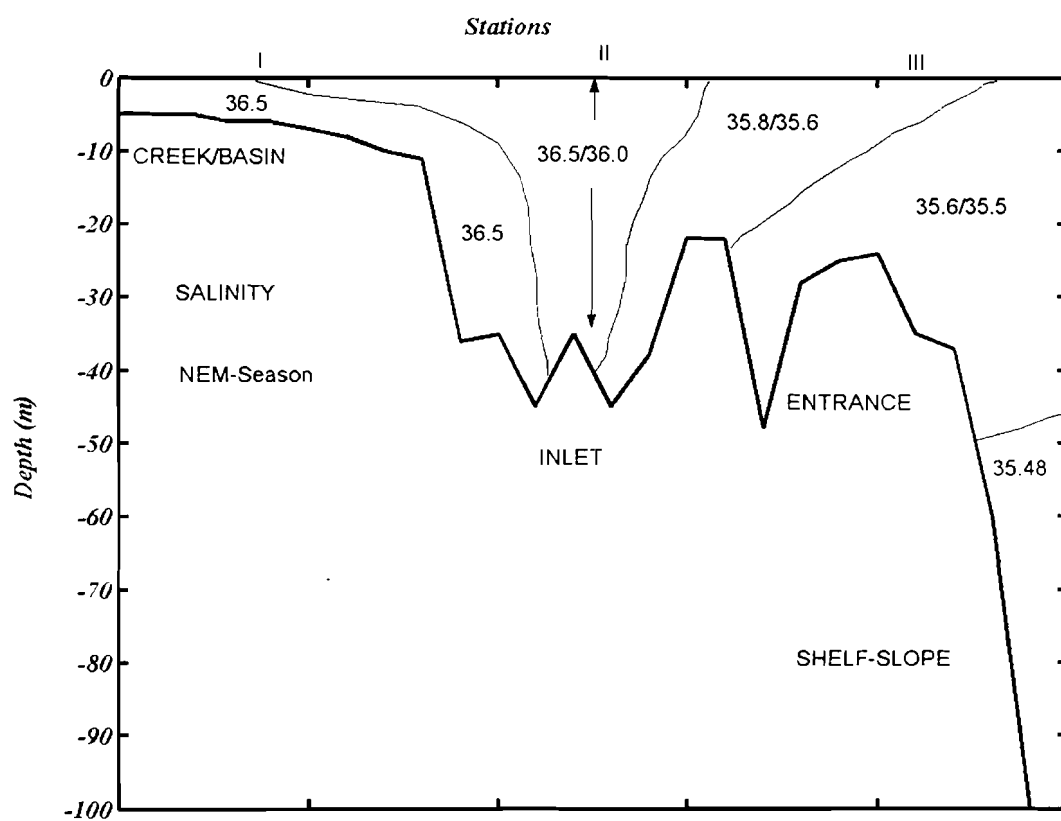
Figure 5.4.1.2h Vertical section showing longitudinal distribution of salinity in Tudor Creek during the NEM. Note highest salinity occurs in the inner basin.

The mean salinity of the entire creek system was 35.5. The difference in salinity between the creek and the ocean was less than 1. The mean salinity is not significantly

different from that of SEM season. Nonetheless the tendency for high salinity in the upper reaches of the creek is an indication that in NEM season the system tends to develop negative estuarine conditions, with an important implication to the creek circulation (See Chapter 7). The highest salinity was found close to the mangrove zones. Gradual increase in salt concentration in the creeks from the beginning of SEM season suggests a gradual inshore movement of water content from the Ocean into the creek systems. This movement generated an anti-clockwise circulation (see mechanisms, Section 7.4).

5.4.2 Currents, Sea level and Tidal analysis

5.4.2.1 Currents

Measured currents

Current measurements for Tudor Creek, for the period from 26 July to 2 August were shown in figure 4.3.3.3. The current magnitude together with direction is shown in Figure 5.4.2.1a in panel (a)-(b). The results reveal periodic tidal current with a maximum of 34.8 ± 7.2 cms^{-1} and the mean current is 10.9cm^{-1} for the duration of the six days.
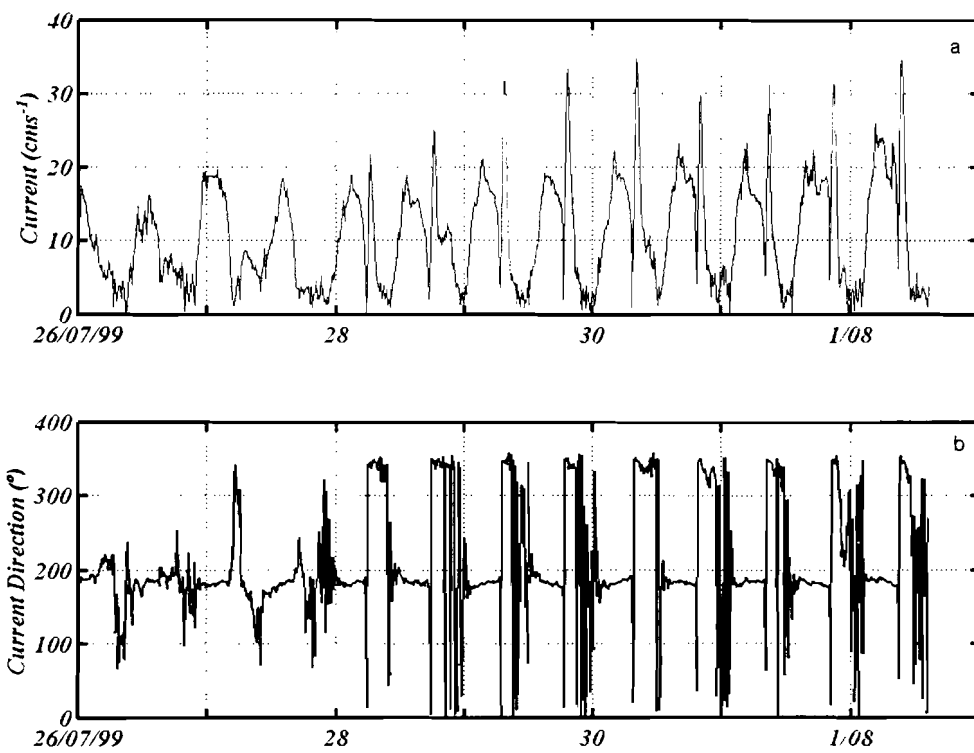
Figure 5.4.2.1a An example of current (panel a) direction (panel b) time series from

Tudor Creek entrance from 26 July to 2 August 1996.

260

Figure 5.4.2.1b is a scatter diagram showing the main ebb and flood directions for the same current meter. Results indicate that flood current into the creek occurs at 345 °, and the ebb current out of the creek occurs at 182 °.

b
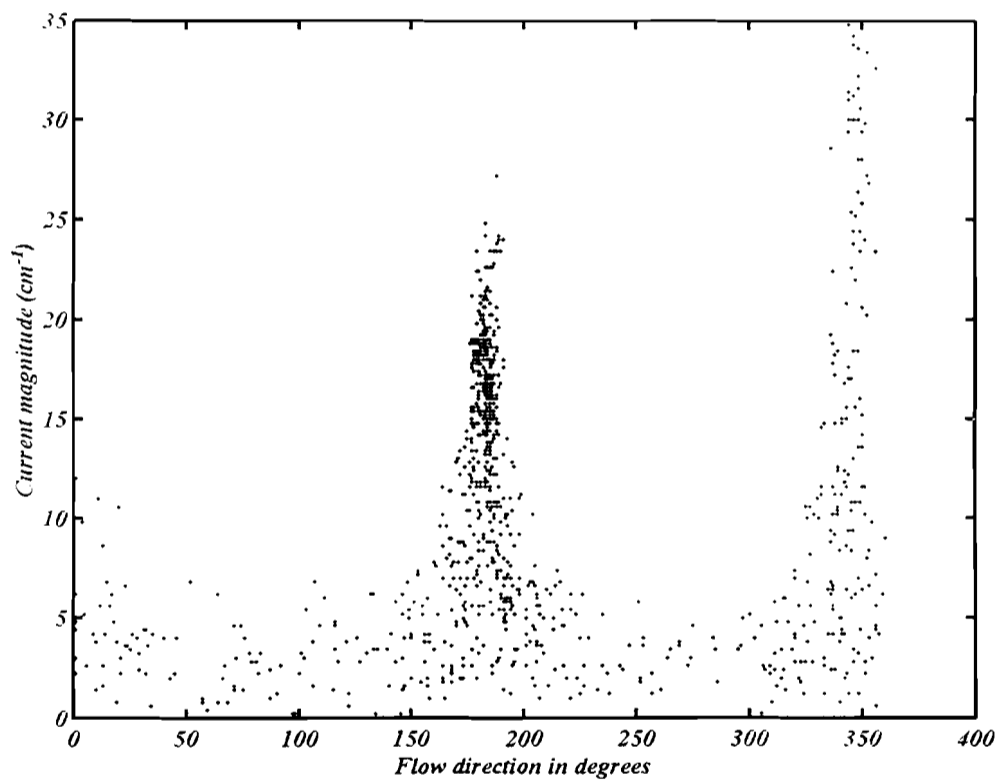
Figure 5.4.2.1¢ Scatter diagram showing the predominant flow direction in Tudor Creek from 26 July to 2 August 1996.

Thus current ebbs in a southerly direction and only 2 from 180 °, whereas flooding current enters the channel in a northerly direction 15 ° from 0 °. It can be from see from the scatter diagram that large currents (34 cms⁻¹) occur during flood than during ebb stage. It is instructive at this point, to consider results of current measurements taken

261

generally at the same location in 1993-4 (Nguli, 1994). Scatter diagram revealed that current ebbs in a southerly direction (171 $^{\circ}$) with maximum speed of about 28cms^{-1} while the flood current was northerly (338°) with a speed of 27cms^{-1}. The direction between flood and ebb was 167 $^{\circ}$, indicating that the ebb current deviated from 180 $^{\circ}$ by about 13 $^{\circ}$. There is slight difference in this results however, the slight deviations in the current direction and even speed is an indication that results may vary due to mooring locality.

Interesting features of current response pattern to topography is illustrated in Figure 5.4.2.1c which indicated current build up and related changes in fluctuations for 27-28/07/1996, and 29-31/07/1996. The current increased from neap to spring showing lower current speeds closer to neap and larger currents, and additional fluctuation as the current gradually increase towards spring. In this figure we can identify two discontinuities in the strength and nature of tidal current with increasing tidal height. For the day 27-28/07 the curve almost shows negligible busts of currents after high tide (e.g. at 10-15hrs, 25-30hrs). The reason for this could be because the tide is below mangrove banks. It is clear from the Figure 5.4.2.1c that burst of current appear to sent extra water into the creek, when the flood current occur close to 11am-2pm . These are over-bank tides, which occur when the tide water flows over the mangrove banks and rushes into the shallow peripheral lagoons.
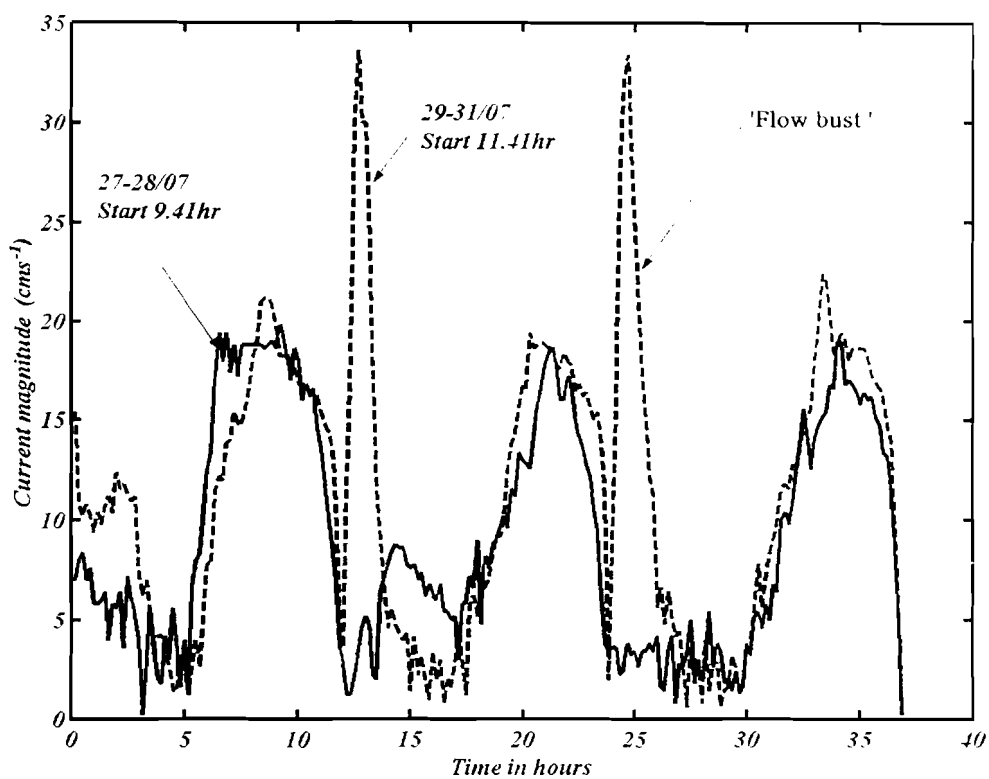
Figure 5.4.2.1c showing different current magnitudes between 27-31/07/ 2002 and an over-bank flow after high water is reached.

'Over-bank tides or flood pulses are characterised by the narrow current velocity spike up to 30cms^{-1} (marked as 'flow bust' in Figure 5.4.2.1c). A slight ebb pulses occur as oscillations and probably due to the shoaling of the depth as tidal level recedes.

Similarly tidal currents in the channel for the 1994 measurements were periodic and showed fluctuation in magnitude increasing from low values of 13-25cms^{-1} during

neap to 40-60cms^{-1} during spring. The mean current during neap was 19cms^{-1} while during spring the mean currents were about 50cms^{-1}.

Tidal asymmetry becomes important during spring period where the flow show tidal asymmetry with ebb current velocities exceeding flood current. The ebb current occurs with swift velocity for a shorter duration than the flood current that occur with lower velocity magnitude, but long flooding duration. Maximum velocities almost coincide with high and low water times.

Note there is significant difference between the ebb and flood velocities, with maximum ebb velocity of 80cms^{-1} and maximum flood velocity of 40cms^{-1}.

The average time between high water peaks and the highest flood tide velocity were 1.9 hours, whereas for low water highest ebb tide velocity was 3.34 hours. The average phase difference between the zero velocity time and the time when the water level are equal to mean sea level gave an average phase lag of 3.57 hours for both flood and ebb tide computation. The time between the lowest current velocities and high water was found to be 0.4hours, and 0.6 hours respectively, hence almost out of phase.

The results show that ebb flows occurred in the morning between 7-9 hours and in the afternoon between 19-22 hours, while maximum for the flood was at 2-3 hours and 16-17hrs.

Barotropic current

Barotropic current is computed as $U_n = \dfrac{1}{A_c}\left[A_s \left(\dfrac{\partial \eta}{\partial t} \right)\right]$, where A_c is the cross-section area of the inlet channel, A_s is the surface area of the creek and is the observed

neap to 40-60cms^{-1} during spring. The mean current during neap was 19cms^{-1} while during spring the mean currents were about 50cms^{-1}.

Tidal asymmetry becomes important during spring period where the flow show tidal asymmetry with ebb current velocities exceeding flood current. The ebb current occurs with swift velocity for a shorter duration than the flood current that occur with lower velocity magnitude, but long flooding duration. Maximum velocities almost coincide with high and low water times.

Note there is significant difference between the ebb and flood velocities, with maximum ebb velocity of 80cms^{-1} and maximum flood velocity of 40cms^{-1}.

The average time between high water peaks and the highest flood tide velocity were 1.9 hours, whereas for low water highest ebb tide velocity was 3.34 hours. The average phase difference between the zero velocity time and the time when the water level are equal to mean sea level gave an average phase lag of 3.57 hours for both flood and ebb tide computation. The time between the lowest current velocities and high water was found to be 0.4hours, and 0.6 hours respectively, hence almost out of phase.

The results show that ebb flows occurred in the morning between 7-9 hours and in the afternoon between 19-22 hours, while maximum for the flood was at 2-3 hours and 16-17hrs.

Barotropic current

Barotropic current is computed as $U_\eta = \dfrac{1}{A_c}\left[A_s\left(\frac{\partial \eta}{\partial t} \right) \right]$, where A_c is the cross-section area of the inlet channel, as is the surface area of the creek and is the observed

surface elevation in the creek. For Tudor Creek the surface area is $2.5*10^{-6}$ m^2, and the cross-section area is about 7000m^2.

Theoretical tidal current

The average onshore-offshore velocity may be expressed as:

$$U_m = \frac{2LH}{Td_{av}}$$

Where L is the distance from the shoreline to the shelf slope; H is the mean tidal range d_{av} is the mixing layer thickness. The area between the surface and the bottom, L, was calculated from the coastline to 4 km offshore (note almost the distance of excursion time for a particle in the creek. The square of the water depth divided this area at 4km to yield the required L/d_{av} relationship in the equation 4.4.22, this is done for 50m depth.

Non-tidal current circulation and secondary currents

The most of the creek is protected from direct wind from the open ocean. However, slight wind occurs at its wider and shallow basin and may drive a small residual circulation. Wave activities at the entrance are a frequent phenomenon. Wave set up at the reef entrance may be responsible for driving long shore drift along the eastern side of the entrance and probably most important for sand distribution along in the bends near the entrance. Suspended sediment entering the creek entrance during the flood phase could be due non-tidal circulation and waves.

5.4.2.2 Sea level

In Figure 4.3.3.4 sea level data was shown for Tudor Creek, for three tide gauges, deployed to measure water level simultaneously in the locations shown in Figures 4.1.1.2. An illustration of tidal fluctuation patterns is shown for 3 November 1998 (Figure 5.4.2.2a), similar pattern was observed for each during the entire duration (27 days) of measurements. The figure shows tidal curves for the tide gauge at the entrance area (MT1), in the channel (MT2) and at Jomvu Kuu (MT4). Time lag between the three curves is evident from the separation of the curves during the flood and ebb stages when the sea level is above 0.5m and below -1.5m respectively. As the creek starts to fill during flood tide the sea level rises at the entrance and then in the channel and finally in the shallow area as at Jomvu Kuu as evidenced by the progressive time lag between the three tidal curves. However, during the high water slack the sea level inside Jomvu is slightly higher than that indicated by the other two curves, and occurs slightly later. Thus tidal asymmetry and reflections are clearly observable. This is probably caused by water set-up in the shallow basin due to hydraulic effect. At the ebb stage the water level falls at the entrance followed by the level at the channel and finally at Jomvu Kuu. Between 0m and -1.5m the water level in the entire creek system is level with insignificant time lag between the three curves. Below -1.5m the sea level at Jomvu Kuu is distorted by shallow depth, this is the effect of M_4, as we saw earlier. At low slack water however the sea level at Jomvu Kuu is lower than in the channel and at the entrance, again indicating that during ebb water is pilled up in the channel-entrance area, which we can attribute to hydraulic jump.

266

The tidal range at the three locations varies. At the entrance the tidal range is

3.4m, in the channel 3.7m and at Jomvu Kuu, 3.9m. indicating that tidal range increases

along the creek and is highest in the shallow creek area. Higher tidal amplitude inside the

creek than at the entrance suggests that Tudor Creek amplifies the tidal wave entering at

the entrance. This is probably caused tidal reflection or oscillations in the shallow basin

areas; it also indicates that friction at the entrance and in the channel probably play

insignificant role in reducing the amplitude of the tidal wave as it propagates along the

channel. The tidal asymmetry near slack water may also suggest inner circulation due to

residual currents. We note this reflection due to shallow inner basin can perhaps be

advanced as one of the reasons for the difference in tidal dynamics between shallow

creeks in the tropical areas and other parts of the world e.g. where fjord like estuaries

occur (Stigebrndt, 1990).
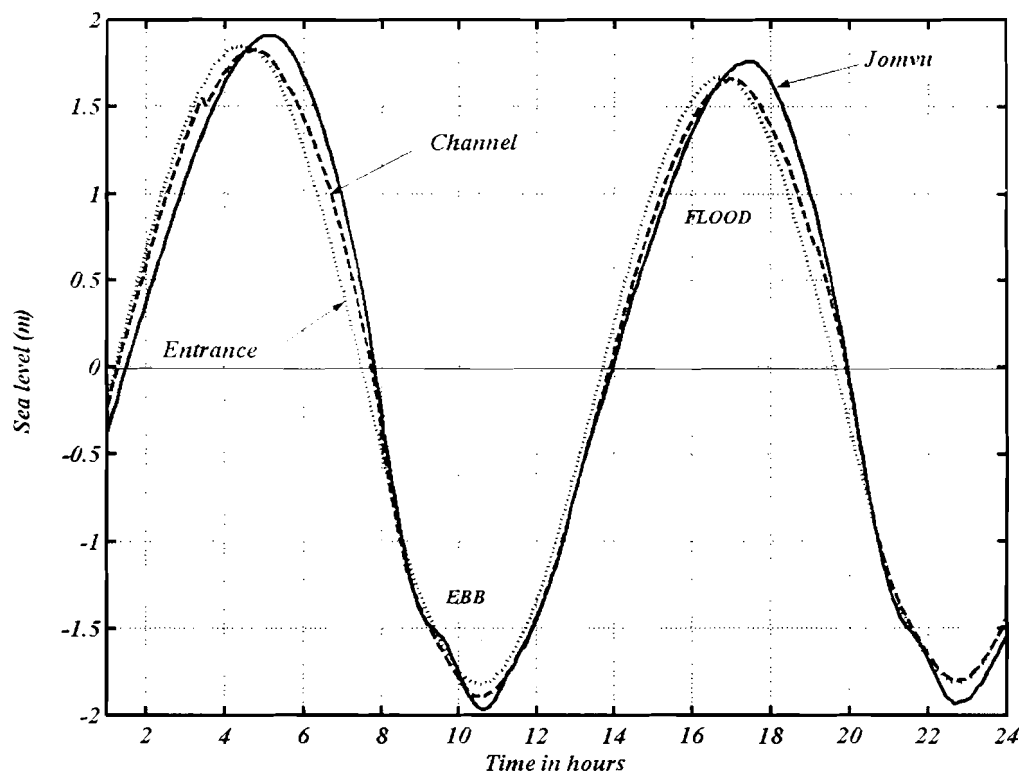
Figure 5.4.2.2a Comparison of the tidal curve at the entrance (MT1), Mid-channel (MT2) and in the shallow basin at Jomvu Kuu (MT4), for 3 November 1998. Note the time lag between curves and stretching of the tidal curve at Jomvu Kuu.

Figure 5.4.2.2b shows spring and neap tidal levels, on 7 and 13 November 1998 respectively, in panel a-c. Within the inner basin the spring, neap and mean ranges are 3.1m, 0.9m, and 2.2m respectively, while at the entrance the corresponding values are 2.8m, 0.9 m and 2m. Topographic effects are clearly seen in panel (c), for the depth below -1.5m. Harmonic analysis is carried out later in Section 5.4.2.4.

268
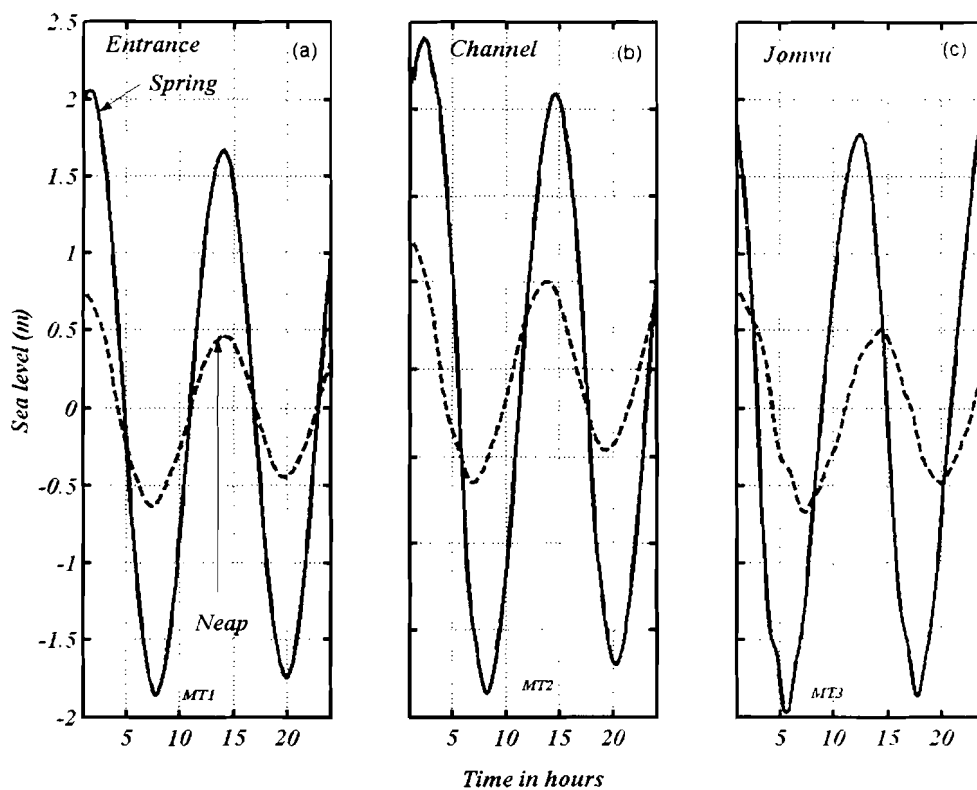
Figure 5.4.2.2b Illustrating spring (7/10/1998) and neap (13/10/1998) fluctuations at the entrance panel a Channel (MT2) and in the shallow basin at Jomvu Kuu. Note topographic effect (stretching) during both spring and neap.

5.4.2.3 Sea level from the GLOSS stations

Figure 5.4.2.3 panel (a-b) show sea level form GLOSS stations located in Mombasa and Lamu respectively, and which have been recording sea level data almost continuously. The sea level variations are shown together with the mean of annual monthly air pressure in Mombasa for 1995-1998 (panel b). GLOSS sea level stations in

the western Indian Ocean, is located near Tudor Creek (in the opposite entrance channel to Kilindini Harbor) this makes us consider results from this gauge along with those obtained from the Tudor Creek.
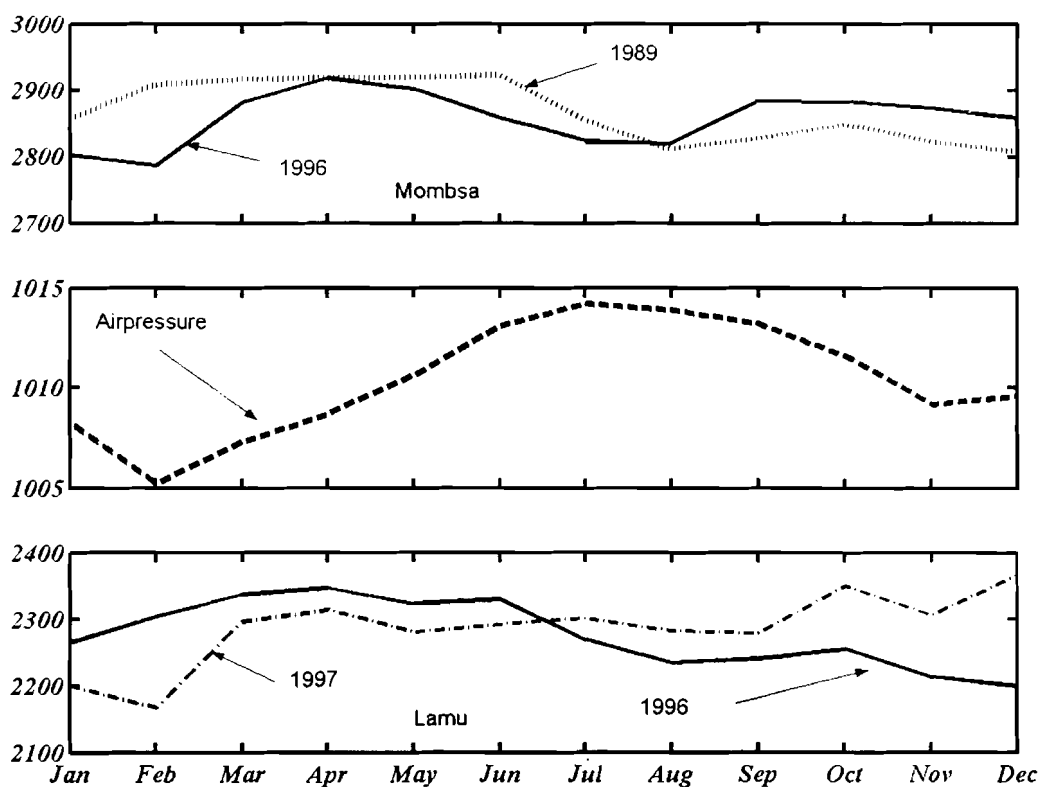
Figure 5.4.2.3 Panel (a) shows monthly sea level fluctuations (mm) from Mombasa for 1996 and 1997. Panel (b) shows also the mean of annual monthly air pressure in Mombasa for 1995-1998 and panel (c) shows similar fluctuations from Llama for 1996 and 1997.

It is clear from the figures that the sea level varies from one year to the next. In Mombasa the sea level is slightly higher by 550mm than in Lamu. Maximum values occur twice yearly with higher values during the April, and October. Minimum values

tend to occur in February and November low pressure corresponds to the onset of high sea level. It is evident that the sea level is higher during the NEM season than the SEM season due to barometric effect. The sea level curve of 1997 shows that sea level increased more than normal during SEM season probably due to buoyancy effect resulting in increased amount of fresh water after the extra-ordinary rains that year.

5.4.2.4 Harmonic and spectral analysis

Figure 5.4.2.4, illustrates the results of tidal analysis for sea level observations for 36 days from Tudor Creek, from 2 October to 7 November 1998. 14 principle harmonic constituents were used for harmonic and spectral analysis. In addition tidal analysis was carried out on temperature using similar number of constituents. The results of the analysis are given in a table (panel, d) of Figure 5.4.2.4 as tidal constituents, amplitude, period and phase lag, whereas panel (d) of Figure 5.4.2.5, gives similar analysis based on temperature analysis from the same tide gauge. These results show clearly that the M_2 constituent dominates, followed by S_2, other significant constituents are K_1, and N_2. Both S_2 and N_2 when added together contribute more than 90% of the M_2 amplitude, the other is K_1 and O_1 both of which contribute 25% and the shallow water tide 3.7%.
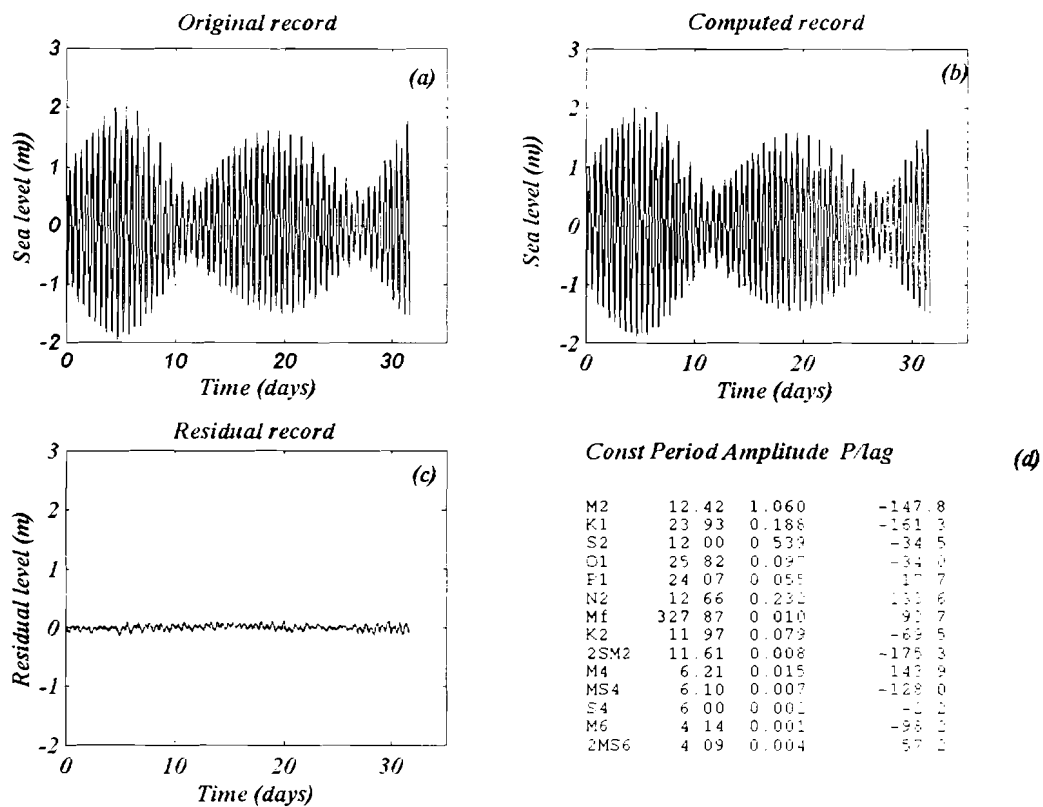
Original record

(a)

Sea level (m)

3
2
1
0
-1
-2

0   10   20   30

Time (days)

Computed record

(b)

Sea level (m)

3
2
1
0
-1
-2

0   10   20   30

Time (days)

Residual record

(c)

Residual level (m)

3
2
1
0
-1
-2

0   10   20   30

Time (days)

(d)

Const	Period	Amplitude	P/lag
M2	12.42	1.060	-147.8
K1	23.93	0.188	-161.3
S2	12.00	0.533	-34.5
O1	25.82	0.097	-34.0
P1	24.07	0.055	17.7
N2	12.66	0.232	131.6
Mf	327.87	0.010	91.7
K2	11.97	0.079	-69.5
2SM2	11.61	0.008	-175.3
M4	6.21	0.015	143.9
MS4	6.10	0.007	-128.0
S4	6.00	0.002	-2.2
M6	4.14	0.001	-98.2
2MS6	4.09	0.004	57.2

Figure 5.4.2.4 Illustrates the results of tidal analysis (a) original record (b) computed (or astronomical tides) (c) residual levels and (d) tabulated constituents, amplitudes and phase lags for sea level observations from Tudor Creek, 2 Oct-7 Nov 1998.

Analysis of temperatures indicates that M_2 and P_1 are important (Figure 5.4.2.5d), since P_1 contributes 63% of M_2. The original sea level is shown in panel (a) whereas panel (b) and panel (c) of the same figure shows the computed and residual records.
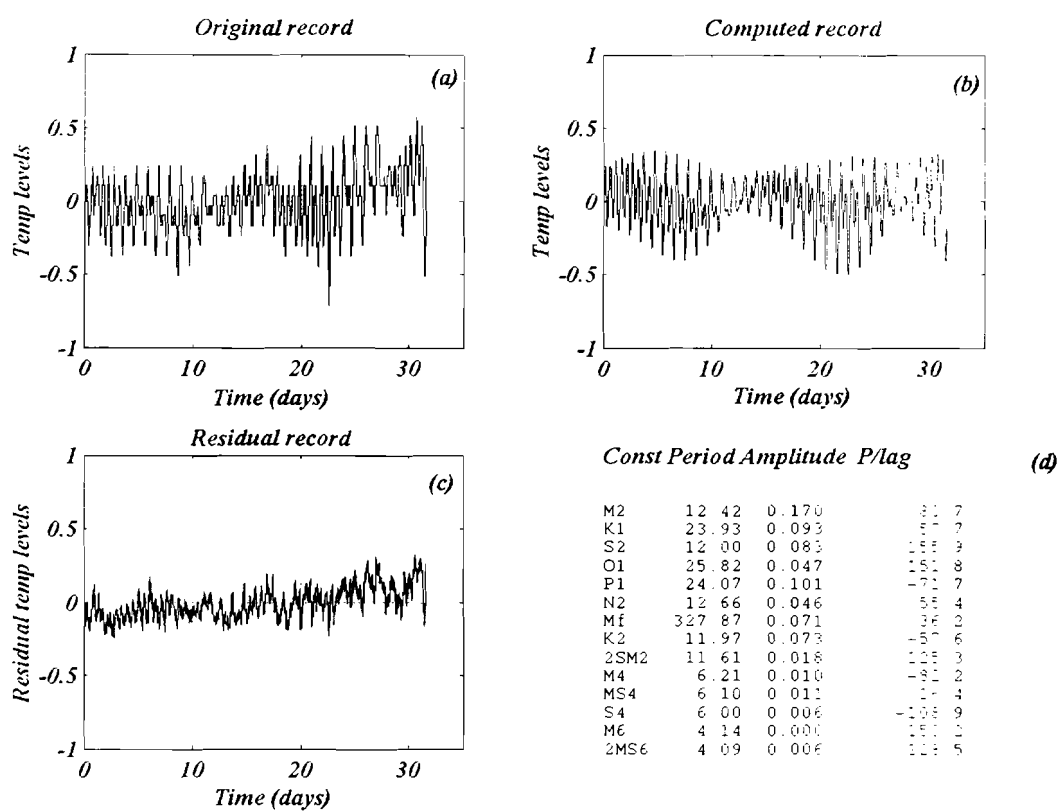
Figure 5.4.2.5 Illustrates the results of tidal analysis for temperature time series from Tudor Creek, from 2 October to 7 November 1998, where (a) original record (b), computed (or astronomical tides), (c) residual levels, and (d) tabulated constituents, amplitudes and phase lags.

Tidal analysis of the sea level inside that creek (Table 5.4.2.4a) showed no reduction of the amplitude of the M_2 indication that friction in the channel properly is playing insignificant role. S_2 also has similar amplitude; however, N_2 decreases by 16% of the M_2. K_2 amplitude appears to change by 50%.

Table 5.4.2.4a Amplitude and phase lag (relative to Greenwich) for seven principal constituents for the Tide gauge deployed in Tudor entrance channel and in the inner basin (KMC) compared to the Amplitudes and phase in Mombasa (Pugh, 1979).

C/Symbol	Period	Inner basin (KMC)		Tudor (Entrance)		Mombasa	
		Amplitude	Phase (deg.)	Amplitude	Phase (deg.)	Amplitude	Phase (deg.)
M_2	12.42	1.060	112.44	1.060	-147.8	1.055	0
S_2	12.00	0.541	-26.97	0.539	-34.5	0.521	-7.7
N_2	12.66	0.195	139.73	0.232	133.4	0.201	10.22
K_2	11.97	0.139	-77.16	0.079	-69.5	0.139	-7.72
K_1	23.93	0.224	-03.88	0.188	-161.3	0.191	20.02
O_1	25.84	0.089	-13.66	0.097	-34.0	0.113	21.02
P_1	24.07	0.150	111.25	0.055	-17.7	0.055	20.28

Table 5.4.2.4b Classification of the tides according to F-ratio.

Species	F-Value
Semi-diurnal	0<F<0.25
Mixed, Mainly Semi-diurnal	0.25<F<1.5
Mixed, Mainly diurnal	1.5<F<3.0
Diurnal	F>3.0

Table 5.4.2.4c Formulas for calculating various parameters such as the form number spring and neap tidal ranges, for stations inside and outside the creek and comparison with values obtained from Mombasa (Pugh, (1979).

Parameter	Formulae	Inner basin (KMC)	Entrance	Mombasa
Form number	$(K_1+O_1)/(M_2+S_2)$	0.195	0.178	0.193
Inequality phase relationship	$M_o^o(K_1^o+O_1^o)$	129.96	141.75	1
Phase Angle	$0.98(S_2-M_2)$	-136.62	-134.49	-7.546
Mean Range	$2.2M_2$	2.34m	2.33m	2.32m
Spring Range	$2(M_2+S_2)$	3.21m	3.198m	3.15m
Neap range	$2.0(M_2-S_2)$	1.05m	1.042m	1.07m
Tropical range	$2.0(K_1+O_1)$	0.63m	0.57m	0.61m
Diurnal Age	$0.91(K_1^o-O_1^o)$	8.89	-115.84	-37.34
Equatorial Range	$2.0(K_1-O_1)$	0.27m	0.182m	0.13

Note how the phase lag changes on using various constituent analyses in Tudor Creek 2 October 1998 November1998.

Using the above results the form number (F) is estimated as 0.21(see Table 5.4.2.4c, according to the classification F is found to lie at 0<F<0.25 which indicate that the semi-diurnal is dominant. Table 5.4.2.4c also shows various formulas for calculating the other tidal parameters.

Water exchange and Calculations

5.4.3 WATER EXCHANGE CALCULATIONS

5.4.3.1 Morphology of the creek

The catchment area and the free water surface area of 5.5×10^8 m^2 and 2.6×10^7 m^2 respectively (Table 5.4.3.1). The length of the creek is 10km and it has a mean depth of 10m. The cross-section at the entrance is 1770m^2. It will take less than one hour for tidal wave to propagate in the creek, due to its short length. The creek can be divided into three regimes according to the definition of estuaries: The shallow inner basin regime, the channel regime and the entrance regime. The shallow basin regime can be viewed as the composite mouth of the run off from several small valleys and the two main rivers that enter the Tudor Creeks; it has a mean depth of 3m above sea level. The channel regime is deeper and narrow and occasionally marked by small mangrove, channel bends and small headlands with a mean depth of 10m. The entrance shoals slightly into small sill at 10m, just 2km form the entrance the shelf slope rapidly to depths of 200m. The length of Tudor Creek, measured from the entrance (Stn VI) to the mouth of Kombeni River is 15km. However the mean length is 12km with the channel taking 4km. The mean surface area is 20km^2, with the channel constituting less than 10% of the total area. The average depth in the inner basin is 3m, above sea level, but maximum depth is 5m. Maximum depth in the channel is 50m and average depth in the channel is 12m. Taken together with the inner basin the creek has a mean depth of 10m. More than 70% of the total depth is in the channel. It should be noted that the inner basin has peripheral lagoons most of which are submerged during the spring high water but emerge during spring low water. The channel is sinusoidal, that is characterized by coves that create bends or headlands.

Table 5.4.3.1 Catchment and morphological characteristics of Tudor Creek.

TUDOR CREEK	
Catchment area (m^2)	5.5 x 10^8
Bay/creek surface area (m^2)	2.6 x 10^7
Total surface area	8.1x 10^8
Entrance section area	5 x 10^3
Tidal range	2.8
Length of Bay/Creek (m)	12x 10^3
Mean depth in the inner basin	4.8m
Maximum/mean depth /length of the entrance channel	50m/12m/4000m

5.4.3.2 Water exchange and circulation generated by fresh water

Application of Knudsen Equations

In order to estimate residence time using Eq.4.4.2.1, the results from meteorological observations i.e. precipitation (Qp), evaporation (Qe) and river discharge (Qr) are used, together with mean salinity in the creek and the ocean (entrance) for various monsoon periods. As pointed out earlier, the fresh water discharge into Tudor Creek is from River Kombeni. This seasonal river has two-peak discharge during IMLR

and IMSR seasonal. The discharge during IMLR is almost as twice the value of the IMSR season; SEM and NEM have small discharges. NEM is however drier than SEM.

The discharge was found to vary from year to year. In the so called 'El Nino years' the discharge increased considerably, for example, the year 1997-1998 the river discharged twice as much fresh water into the creeks. There was almost continuous rainfall that extended from the IMLR season through SEM into the IMSR season.

Table 5.4.3.2a Calculation of various parameters in Knudsen equation for Tudor Creek 1995.

		1995					Q_f
	Month	R/fall (mm)	Q_r x10^6m^3	Q_p x10^6m^3	Q_e x10^6m^3	Q_r+Q_p x10^6m^3	$(Q_r+Q_p)-Q_e$ x10^6m^3
NEM	Dec	32.9	3.2900	0.5922	3.4380	3.8822	0.4442
	Jan	2.5	0.25000	0.0450	3.7800	0.2950	-3.4850
	Feb	1.9	0.1900	0.0342	3.6540	0.2242	-3.4298
	Mar	47	4.7000	0.8460	3.9780	5.5460	1.5680
	122days	**84.300**	**8.4300**	**1.5174**	**14.850**	**9.9474**	**-4.9026**
IMLR	Apr	158.8	15.8800	2.8584	3.3120	18.7384	15.4264
	May	330.1	33.0100	5.9418	2.7900	38.9518	36.1618
	Jun	4.1	0.4100	0.0738	2.5920	0.4838	-2.1082
	91days	**493.00**	**49.300**	**8.8740**	**8.6940**	**58.1740**	**49.480**
SEM	Jul	69.4	6.9400	1.2492	2.4840	8.1892	5.7052
	Aug	180.1	18.0100	3.2418	2.8440	21.2518	18.4078
	Sept	44.6	4.4600	0.8028	3.2040	5.2628	2.0588
	Oct	154.1	15.4100	2.7738	3.4920	18.1838	14.6918
	123days	**448.200**	**44.820**	**8.0676**	**12.0240**	**52.8876**	**40.8636**
IMSR	Nov	98.0	9.8000	1.7640	3.3840	11.5640	8.1800
	30days	**98.0**	**9.8000**	**1.7640**	**3.3840**	**11.5640**	**8.1800**
	Total	1123.5	112.3500	20.2230	38.9520	132.5730	93.6210
	R/day	3.0781	0.3078	0.0554	0.1067	0.3632	0.2565

Table 5.4.3.2b Calculation of various parameters in Knudsen equation for Tudor Creek 1996.

	Month	R/fall (mm)	Q_r x10^{6}m^3	Q_p x10^{6}m^3	Q_e x10^{6}m^3	Q_r-Q_p x10^{6}m^3	Q_f (Q$_r$+Q$_p$)-Q$_e$ x10^{6}m^3
		1996					
NEM	Dec	0.5	0.0500	0.0090	3.4380	0.0590	0.0500
	Jan	10.1	1.0100	0.1818	3.7800	1.1918	-2.5882
	Feb	16.1	1.6100	0.2898	3.6540	1.8998	-1.7542
	Mar	136.6	13.660	2.4588	3.9780	16.1188	12.1408
	122days	**163.30**	**16.330**	**2.9394**	**14.850**	**19.2694**	**7.8484**
IMLR	Apr	106.4	10.6400	1.9152	3.3120	12.5552	9.2432
	May	499.9	49.9900	8.9982	2.7900	58.9882	56.1982
	Jun	7.5	0.7500	0.1350	2.5920	0.8850	-1.7070
	91days	**613.80**	**61.380**	**11.0484**	**8.6940**	**72.4284**	**63.7344**
SEM	Jul	57.1	5.7100	1.0278	2.4840	6.7378	4.2538
	Aug	24.8	2.4800	0.4464	2.8440	2.9264	0.0824
	Sept	11.6	1.1600	0.2088	3.2040	1.3688	-1.8352
	Oct	20.4	2.0400	0.3672	3.4920	2.4072	-1.0848
	123days	**113.90**	**11.390**	**1.0224**	**12.024**	**13.4402**	**1.4162**
IMSR	Nov	135.9	13.5900	2.4462	3.3840	16.0362	12.6522
	30days	**135.9**	**13.5900**	**2.4462**	**3.3840**	**16.0362**	**12.6522**
	Total	1026.9	102.690	18.4842	38.9520	121.1742	102.6900
	R/day	2.8134	0.2813	0.0506	0.1067	0.3319	0.2252

279

Table 5.4.3.2c Calculation of various parameters in Knudsen equation for Tudor Creek 1997.

		1997					Q_f
	Month	R/fall (mm)	Q_r $x10^6m^3$	Q_p $x10^6m^3$	Q_e $x10^6m^3$	Q_r+Q_p $x10^6m^3$	$(Q_r+Q_p)-Q_e$ $x10^6m^3$
NEM	Dec	284.7	28.4700	5.1246	3.4380	33.5946	30.1567
	Jan	2.0	0.2000	0.0360	3.7800	0.2360	-3.5440
	Feb	1.9	0.1900	0.0342	3.6540	0.2242	-3.4298
	Mar	3.10	0.3100	0.0558	3.9780	0.3658	-3.6122
	122days	**291.70**	**29.170**	**5.2506**	**14.850**	**34.4206**	**19.5707**
IMLR	Apr	268.3	26.8300	4.8294	3.3120	31.6594	28.3474
	May	279.1	27.9100	5.0238	2.7900	32.9338	30.1438
	Jun	80.1	8.0100	1.4418	2.5920	9.4518	6.8598
	91days	**627.50**	**62.750**	**11.2950**	**8.694**	**74.045**	**65.351**
SEM	Jul	43.1	4.3100	0.7758	2.4840	5.0858	2.6019
	Aug	54.1	5.4100	0.9738	2.8440	6.3838	3.5398
	Sept	18.5	81.8500	0.3330	3.2040	2.1830	78.9791
	Oct	825.7	82.5700	14.8626	3.4920	97.4326	93.9406
	123days	**941.40**	**174.14**	**16.945**	**12.0240**	**111.085**	**179.061**
IMSR	Nov	316.5	31.6500	5.6970	3.3840	37.3470	33.9630
	30days	**316.5**	**31.6500**	**5.6970**	**3.3840**	**37.3470**	**33.9630**
	Total	2177.1	217.710	39.1878	38.9520	256.897	217.945
	R/day	5.964	0.5965	0.1074	0.1067	0.7039	0.5972

Table 5.4.3.2d Calculation of for ΔS and $V \frac{\partial S}{\partial t}$ Tudor Creek 1995-1997

Period 1995	Q_f	$\bar{S}_{Creek}$	$\bar{S}_{Ocea}$	ΔS	$V \frac{\partial S}{\partial t}$
NEM	-4.9026				
IMLR	49.480				
SEM	40.8636				
IMSR	8.1800				
1996					
NEM	7.8484				
IMLR	63.7344	31.9250	34.8850	2.9600	
SEM	1.4162				
IMSR	12.6522				
1997					
NEM	19.4707				
IMLR	65.351	30.3700	34.7050	4.3350	
SEM	179.061	33.1950	34.9900	1.7950	
IMSR	33.9630				

Applying the Knudsen model.

$V = 18*10^6*2.5 m^3$

4-27 May 1996, Example: For spring to neap 4-27May. Salinity on 4 May=32.96, salinity on 27 May =30.89 the mean is 31.93. The number of days =24 or 86400 Seconds, Therefore

$dS1/dt = (32.96-31.93)/86400 = 1.1921e-005$

$Qe(24days) = (2.7900*10^6/30)*24 /(24*60*60) = 25.8333$

$Qp(24days) = (8.9982*10^6/30)*24 /(24*60*60) = 83.3167$

$Qr (24days) = (49.9900/30)*24 /(24*60*60) = 4.6287e-004$

$Qf = (Qr+Qp)-Qe = (83.3167+4.6287e-004)- 25.8333=57.4839$

$So-S1 = 34.8850-31.9250 =2.9600$

$(So-s1)Qo = [(18*10^6*2.5) *(1.1921e-005)]+ (32.90+30.89)/2=568.3400$

$Qo=568.3400/2.9600=192.0068 m^3s^{-1}$.

Residence Time $=V/Qo=18*10^6*2.5/192.0068$

$= 2.3437e+005 seconds/24*60*60?$

$=12.9days$

The residence time is the same order of magnitude as that obtained using expression 4.4.62 (Nguli, 1994).

5.4.3.3 Water exchange generated by the sea level

Calculations of the instantaneous tidal volume flux through creek entrance inlet were based on tide gauge measurements and the creek mean surface area using the equations given in Section 4.4. The average flood duration was found to be. 6.33hrs,

whereas the mean ebb duration is 6.08hrs, thus showing flood dominance. The surface area of Tudor Creek is $21 \times 10^6 m^2$, at HWS but reduces to about 20% of that value during LWS. Using the difference in volume of water in the creek between LWS and HWS; and LWN and HWN, the semi-tidal mean flood and ebb transport are worked out as in Table 5.4.3.1

Table 5.4.3.1 Volume at various maximum and minimum water levels and volume flux during flood and ebb in both springs and neap periods

	Spring	Neap
Volume at HWS	$9.478 \times 10^7 m^3$	$6.757 \times 10^7 m^3$
Volume at LWS	$4.111 \times 10^7 m^3$	$5.415 \times 10^7 m^3$
Q flood	$2354 m^3 s^{-1}$	$589 m^3 s^{-1}$
Q ebb	$2451 m^3 s^{-1}$	$613 m^3 s^{-1}$

As a result of precipitation and freshwater input referred to, the creeks undergo exchanges with the ocean. These exchanges are driven by salinity differences between the water in the creek basin and that in the ocean. It was observed that salinity difference existed between the creek basin and the ocean. The difference was large particularly following the IMLR season.

Calculation of the mean tidal volume fluxes through the entrances of Tudor Creek was based on the tide gauge measurements and the creeks and bay mean surface areas.

For the mean surface area at high water was calculated from topographic map scale1: 50,000.

Time after high water

Time after high water plot is shown in Figure 5.4.3.3 for Tudor Creek entrance area. From the figure it can be seen that the coldest water (dark blue) appears at high tide or a few hours later, when there is plenty of water in the creek. The warmest water (dark red) appears in the afternoon after low tide. The ebb coincides with colder water than flood indicating heat flux into the creek.

5.4.3.4 Water exchange due to flow across the entrance

A *lagoon current* in the Bamburi-Nyali lagoon has been found to move southward within the lagoon channel (Kirugara *et al.* 1996), and attributed to the wave set-up. The southward limit of the lagoon is the entrance to Tudor Creek. It is assumed that the southward flow in the lagoon channel extends flow across the entrance and may spread its motion into the creek (at least in its lower reaches) and enhance water movement in near the entrance.

284
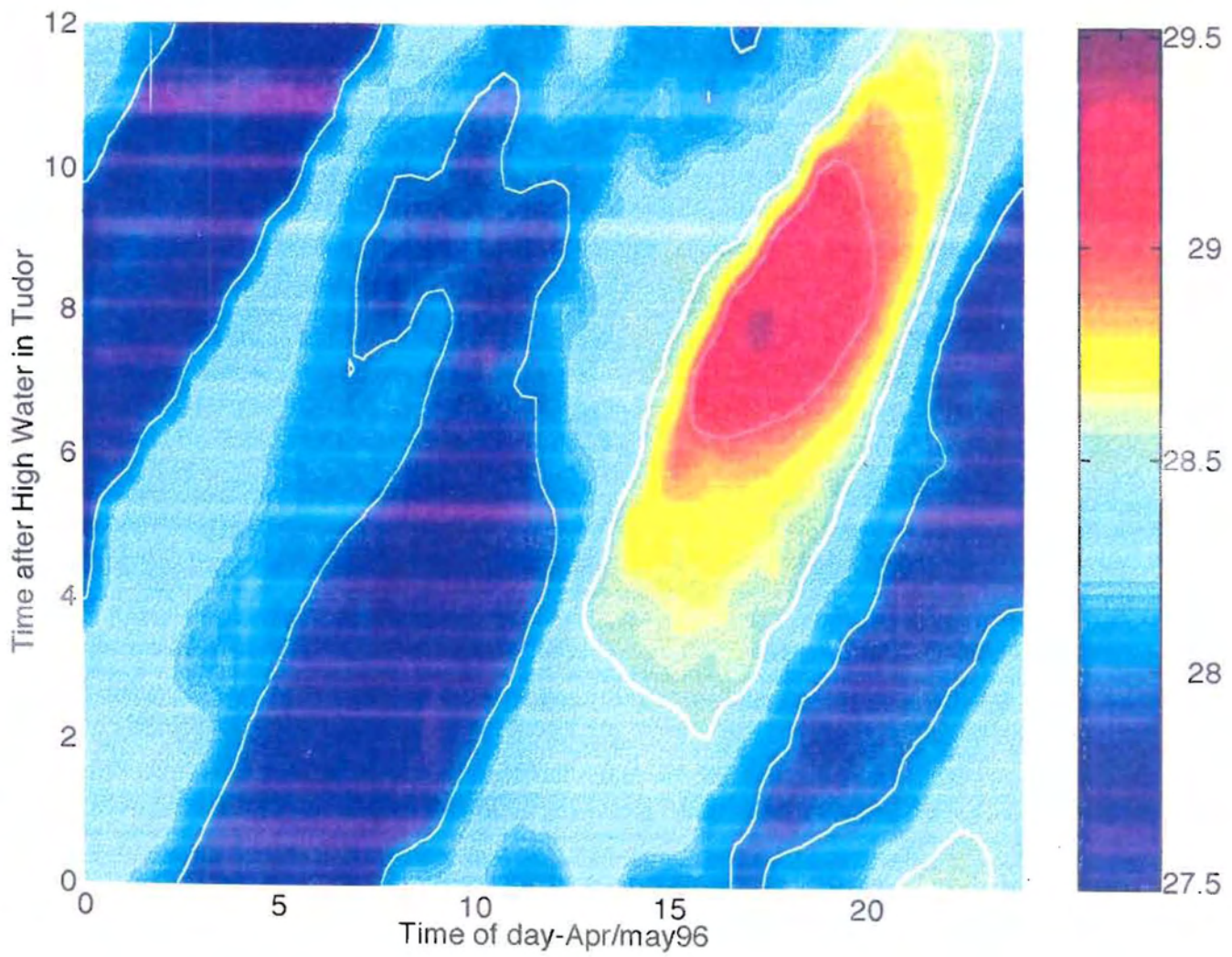
Figure 5.4.3.3 Temperature at the entrance to Tudor Creek for the month of April/May 1996 as a function of time after high tide and time of day.

285

5.4.3.5 Water exchange due to winds

Large-scale circulation could be thought of as causing water exchange between the creeks and the ocean by seasonal changes of the strength of the coastal current (EACC). The semi-annual sea level variability has virtually no effect on exchange, but it is related to the currents. Exchange may also be due to variable winds and related up welling, down welling events. Such events also affect the depth of the thermocline, which is often relatively shallow, whereas water of different character may reach into the creeks. In case of temperature and salinity variations specific volume change occurs and the column of water increases giving rise to what is referred to as steric height.

5.4.3.6 Flushing time

The calculation in Section 5.4.3.2 is an attempt to calculate flushing time using the Knudsen equation and that given by expression 4.4.60 is uncertain due to lack of precision in the amount of freshwater input into the creek. Since in the creek evaporation exceeds precipitation use of expression 4.4.63 and values for U_o=0.4ms-1,a=0.16, ε =8, A=bU_oH where b is a constant between 0.03-0.3 (Fischer et al., 1979), H the mean depth of 5m. The tidal averaged longitudinal eddy diffusivity (B) is of the order $300m^2s^{-1}$. Taking effective length of the creek as 8000m, the flushing time during spring is the order of 3 days, during neap tides, however when a small amount of water from the bay enters the creek, complete flushing of the swamp may take up to 6days. A parcel of water in the upper reaches of the creek however may take longer; probably the 13 days arrived at in Section 5.4.3.2.

5.4.4 Other calculations

5.4.4.1 Heat budget calculations and advective flux

Radiation balances from weather mast were shown earlier (Section 5.2). However, an alternative heat budget calculations and advective flux for Tudor creek are given in Appendix A and B. Advective and cumulative heat flux are shown in Figure 5.4.4.1a-b
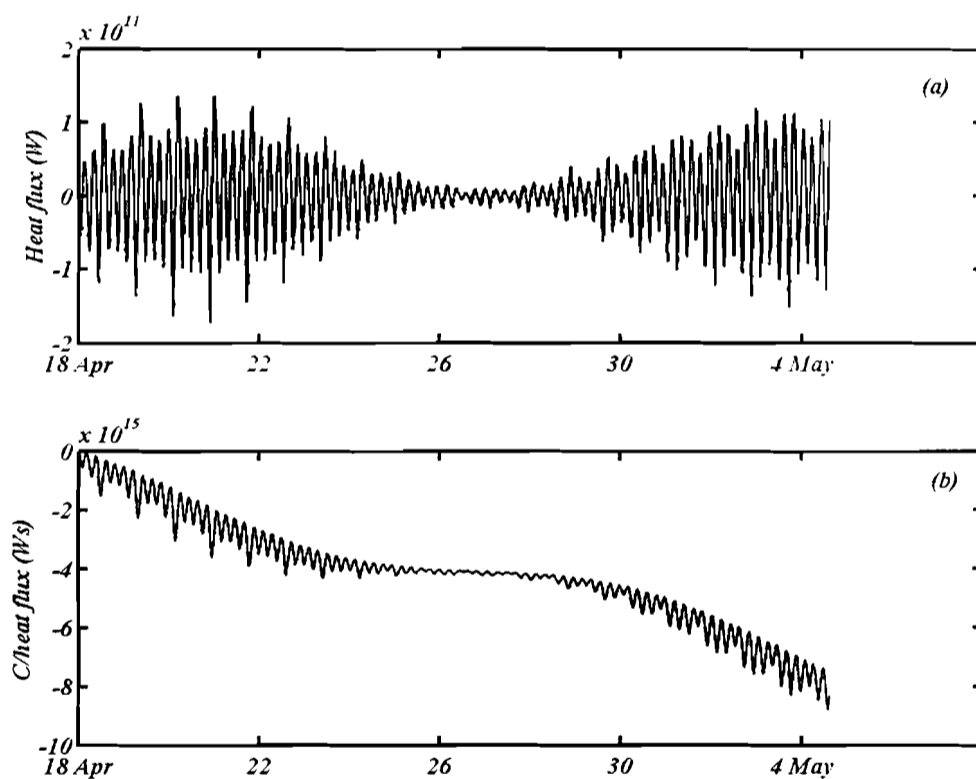
Figure 5.4.4.1a-b Instantaneous, Q_{ex} (positive inward) heat flux (panel (a)) across the entrance of Tudor Creek calculated from temperature time series data of 18 April -5May (IMLR season) 1996, panel (b) Cumulative (integrated) heat flux $Q_{ex}dt$, calculated from temperature time series data from the entrance to Tudor Creek.

Notice that in Figure 5.4.4.1panel (b) the cumulative heat flux is negative. This suggests a loss of heat from the creek. This is expected since temperature tends to decrease due to rainfall in the IMLR season as well as cold water advected by the EACC after the onset of SEM winds.

5.4.4.2 Creek energy dissipation

The two tide gauges that were successively deployed in Tudor Creek tended to show that sea level was amplified inside the creek rather than reduced. This unexpected finding meant that expression 4.4.65 and 4.4.72 could not be readily be used. A rough estimate using expression 4.4.40 given earlier for values of C_d=0.002, u_o^3 = 0.19ms^{-1} A=20*10^{6}m^2, ρ =1025kgms^{-1} resulted in energy dissipation of 1.59 x 10^0 Jm^{-2}s^{-1}. Caution should be taken for this result since the actual values for u_o^3 was not easy to obtain.

5.4.4.3 Bottom friction layer

The results for bottom layer determination were scanty, however, some calculation for Tudor entrance area are discussed in Appendix C.

5.4.4.4 Application of 1-D model

The aim of the one-dimension model is to compare the predicted and observed sea level and volume fluxes at various locations along the creek. We divided the creek into 19 sections; the distance between one section and another is 1000 meters. The width of the each section as well as the mean depth was noted. The depth multiplied by the width

selected the good set of sea level observations. The model was forced by sea level observations at the entrance. Taking a section for example, section 14 which is at Jomvu in the upper reaches of Tudor Creek, we observe that the predicted sea level compare well with the observed sea level (Figure 5.4.4.2a). Figure 5.4.4.2b is an example of sea level (panel a) and volume flux (panel b) volume flux obtained from the application of 1-D at section 14.
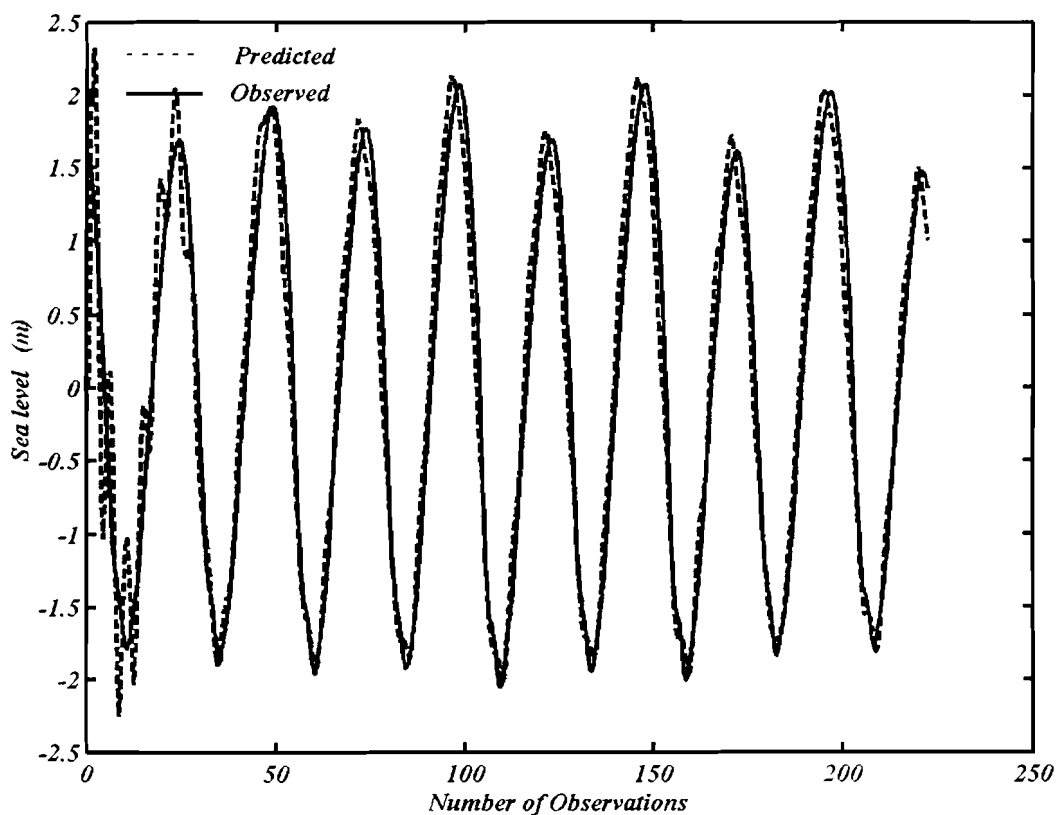
Figure 5.4.4.2a Comparison of the observed sea level at Jomvu Kuu with sea level predicted by 1-D model driven by actual sea level at the entrance.
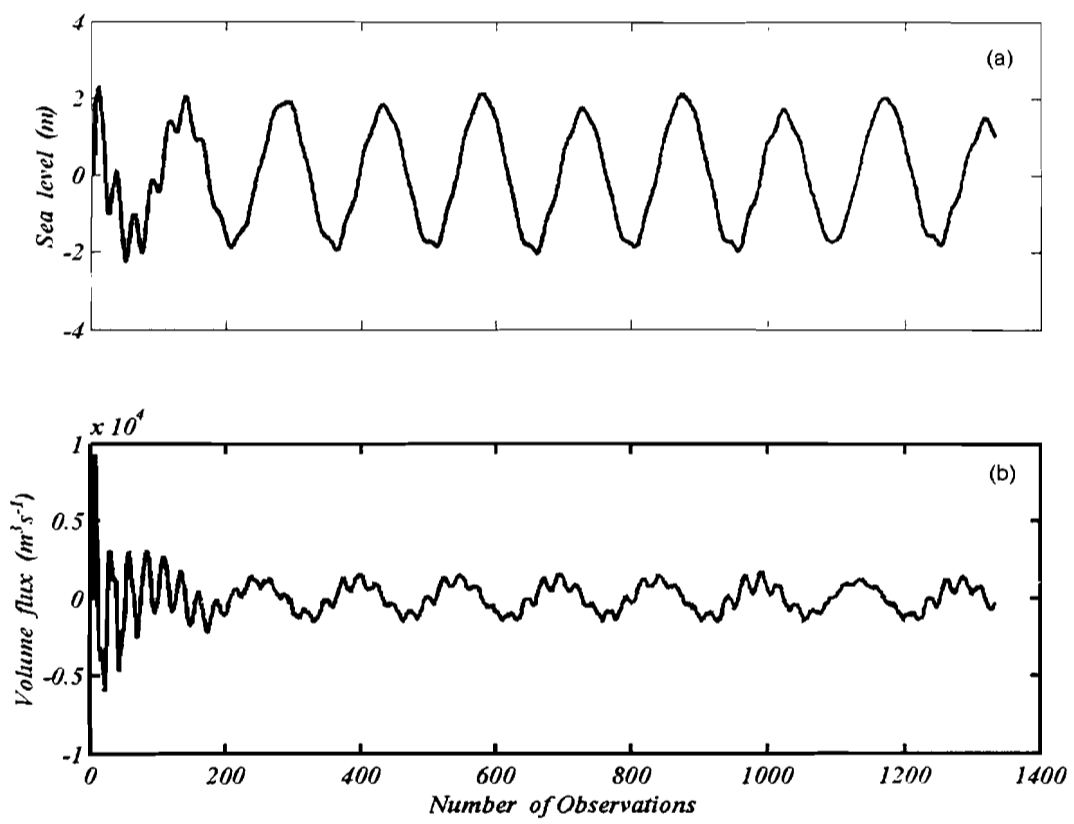
Figure 5.4.4.2b Example of sea level (panel a) and volume flux (panel b) volume flux obtained from the application of 1-D.

290

5.5 KILIFI CREEK

5.5.1 Hydrography

5.5.1.1 Temperature

Lengthwise temperature measurements were carried out in each monsoon period, in stations I to VI. Sampling was done during slack water for both flood and ebb period in similar manner to Gazi Bay and Tudor Creek. The data records were averaged to obtain mean for surface temperature, in each monsoon season for 1996, 1995 and 1997. The ranges of the mean values were also computed for the inner basin, mid-channel, and entrance. Oceanic values were obtained from ocean station in the near the study site. Values for the four seasons were close to those found in Tudor Creek and therefore it was decided to present values for Tudor Creek as a typical for water structural change in the two creeks

5.5.1.2 Salinity

Lengthwise salinity measurements were carried out in each monsoon period, in stations I to VI. Sampling was done during slack water for both flood and ebb period in similar manner to Gazi Bay and Tudor Creek. The data records were averaged to obtain mean for surface and bottom salinity, in each monsoon season for 1996, 1995 and 1997. The ranges of the mean values were also computed for the inner basin, mid-channel, and entrance. Oceanic values were obtained from ocean station in the near the study site. The values were almost similar to those obtained for Tudor Creek and were also treated as in Section 5.5.1.1

5.5.2 Currents, sea level, and tidal analysis

5.5.2.1 Currents

Figure 5.5.2.1a shows the magnitude of total tidal current (a) and its direction (b) in Kilifi Creek, taken in mid-channel location at 10m below the surface for six days starting from 11 July to 17 July 1977. Readily observable in panel (a) is the daily current fluctuations with magnitudes greater or less than 20 cms^{-1} whereas in panel (b) are the two main directions close to 100° and 300°. The fluctuations with values greater than 20 cms^{-1}, and in the direction greater than 250°, indicate flood tidal currents, whereas flows with fluctuation less than 20 cms^{-1} and direction less than 250° correspond to ebb tidal currents. For the ten days in this record, the daily maximum flood current increased from 28 cms^{-1} in 11/7/1997 to a maximum value of 38 cms^{-1} on 17 July 1997. During the ten days, the maximum tidal flood current was 38 cms^{-1}, with a mean of 21.3 cms^{-1}. The ebb tidal current fluctuated between a maximum of 27.3 cms^{-1} and a mean of 6.7 cms^{-1}.

Since the measurements were made around neap, the gradual increase in speed over the ten days is an indication that currents magnitudes become increasing higher as spring is approached, as a consequence of spring-neap or fortnightly inequality.

Within the same record diurnal inequality i.e. a lower magnitude of flooding current was followed by higher magnitude of flood current as readily observable. Flood currents occurring in the afternoon have higher magnitude than ones occurring in the morning do. The higher magnitude of the afternoon flood current is most likely caused by local wind. As the wind usually increased speed between 10 a.m. and 4 p.m. Similar fluctuations and gradual increase in ebb tidal current over the ten days is also observed. although this is not as conspicuous as in the case of flood tidal currents.

An interesting feature on the water exchange dynamics can be readily discerned from the appearance of the Figure 5.5.2.1a panel (a). Looking comparatively at the flood currents in one day one can readily say that the creek is flood dominant and that it appears to receive more water than it discharges during ebb. However, the regular pattern where high peak flood tidal current is followed consecutively by small ebb-relatively and smaller flood- ebb is an indication that the creek gradually retains part of the floodwater. This happens before the water is discharged during the subsequent ebb-flood-ebb phase (the three of which have lower amplitudes) and before the next higher flood. It is also an indication that the current meter, although in a position to record most of the flood current, was not suitably positioned the ebb tidal current creating what may be termed as 'deployment asymmetry'.
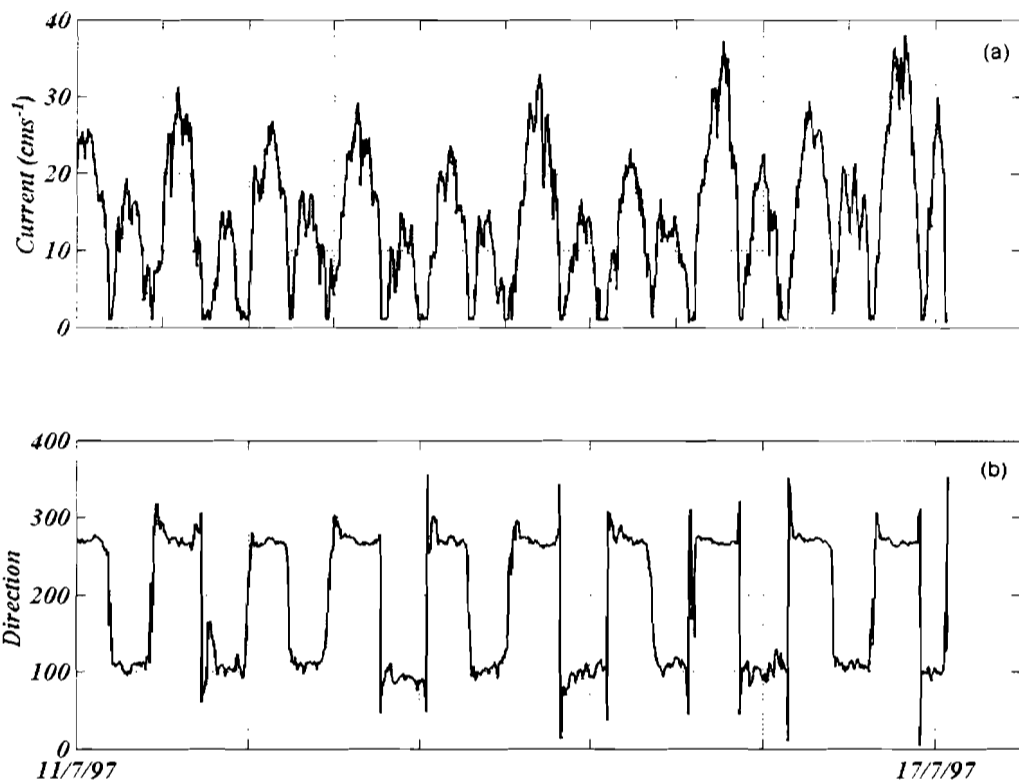
Figure 5.5.2.1a Measurements in Kilifi Creek, showing current (a) fluctuations (b) direction for 6 days measurements 11 -17 July 1977.

Figure 5.5.2.1b shows a scatter plot of current verses direction of the current meter records. Two main directions are clearly observed. The direction followed by ebb current range is 87- 112 $^\circ$ with a mean at 270 $^\circ$, whereas that of the followed by the flood current is 255-290 $^\circ$ with a mean of 270 $^\circ$.
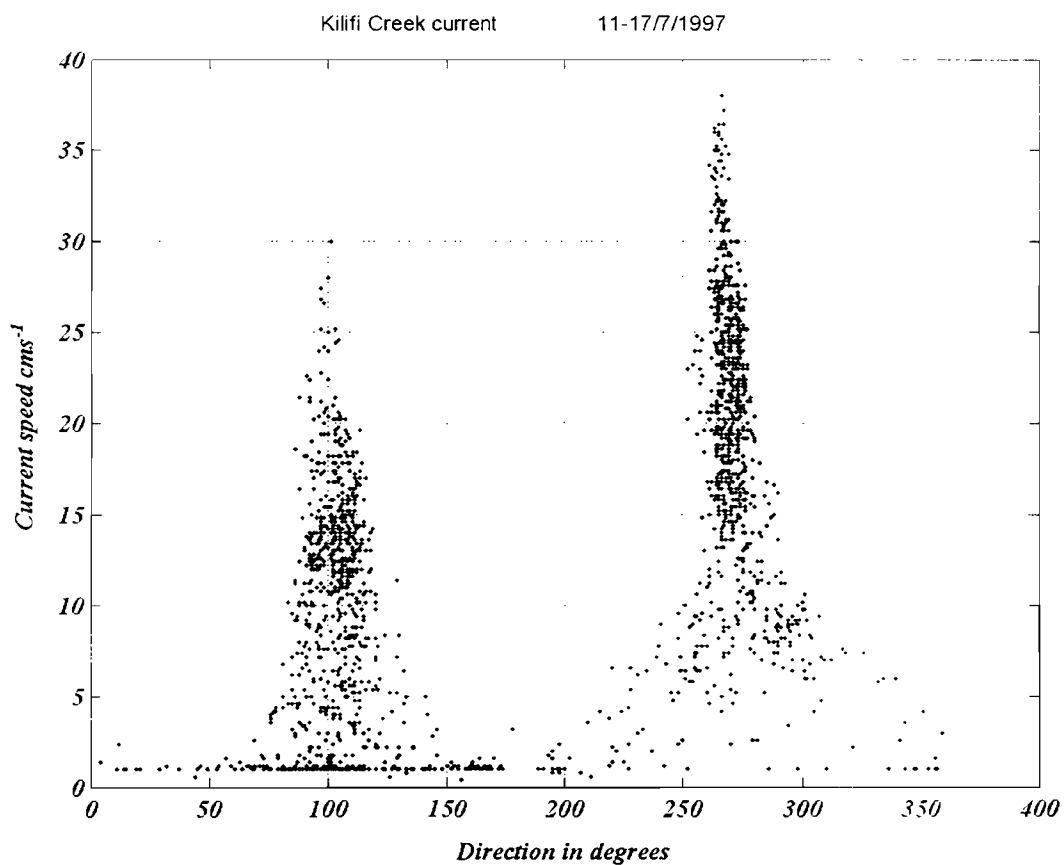
Figure 5.5.2.1b Direction of the current in Kilifi Creek

In order to establish the flood and the ebb direction observed with the current meter flood and ebb elevations are also used. The comparison is show in Figure 5.5.2.1c, which is an example of a composite plot for the three measurements for the period they worked simultaneously for 11-12/7/1997 starting at 23:55hrs.
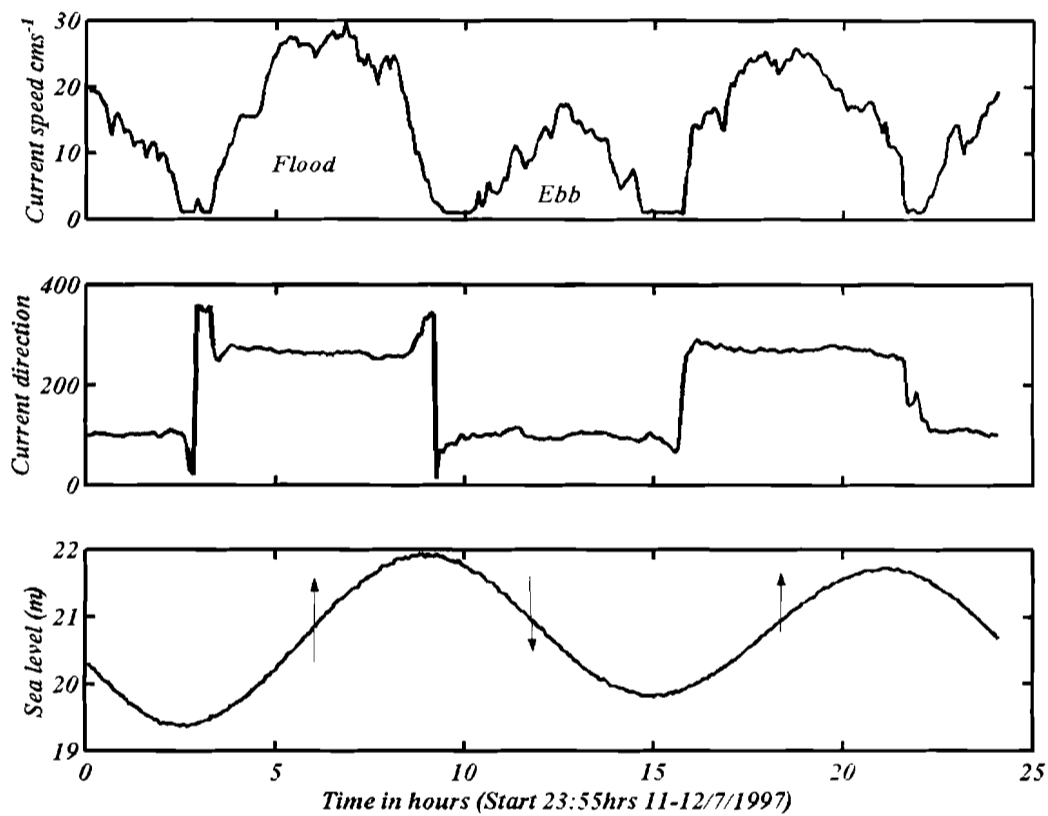
Figure 5.5.2.1c Time series showing simultaneous fluctuations of current, current direction and sea level (MT1) for a day, 11-12/7/1997, starting from 23.55hrs. The up-arrow indicates flood phase whereas the down-arrow shows ebb phases.

The flooding phase of the current coincides with the direction range $255\text{-}290°$, whereas the ebb coincides with the range $87\text{-}112°$, clearly collaborating previous observation. From this figure, it is apparent that the flood current has a higher magnitude

than the ebb current, the flood duration is longer, 28 minutes than the ebb duration, 14minutes. These suggest that the creek is flood dominant; however this is not wholly supported by the tidal measurements, thus indicating close similarity between the flood and ebb duration. Again, the reason for this is that the current meter was not deployed in suitable location to sufficiently resolve the flood and ebb flow.

In order to determine the current flowing in the along the channel, we resolved into along channel (*u*-velocity component) and across channel components (*v*-velocity component), by making use of the mean direction of the flood current.
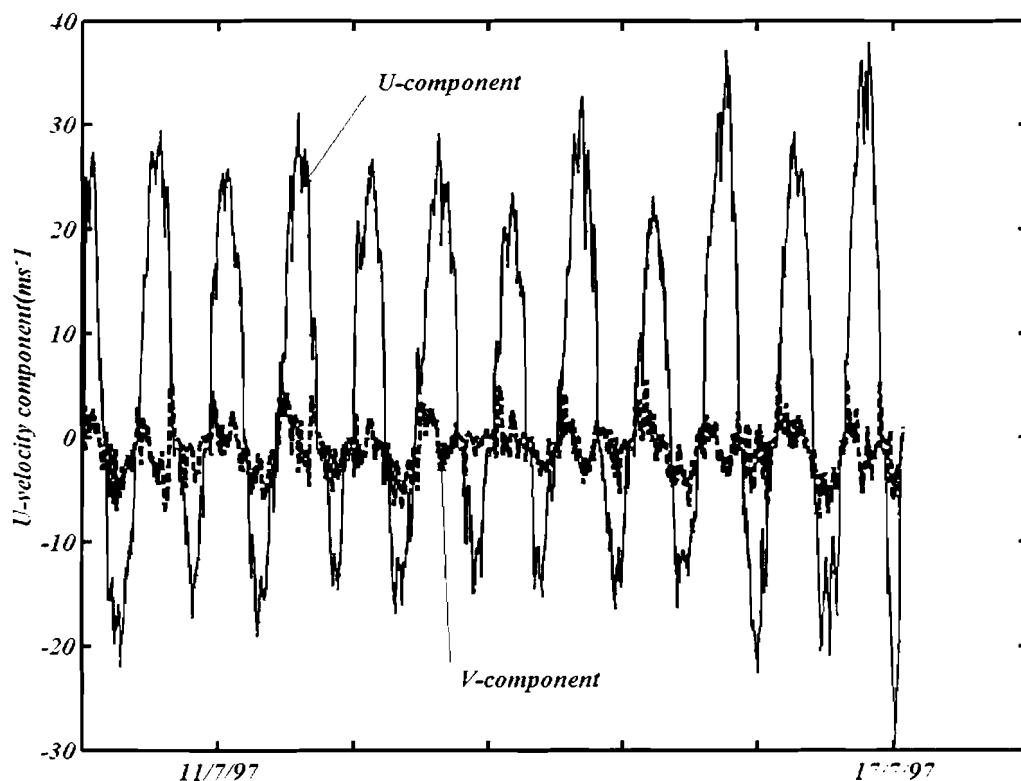
Figure 5.5.2.1d A plot showing *u*- and *v*- components from 11-17 July 1997

The resulting flow after computation of the U and V components show that the maximum flood is 37.9 cms^{-1}, the maximum ebb current is 29.4 cms^{-1}, whereas the mean flood current is 18 cms^{-1} and the mean ebb 9 cms^{-1}. The flood velocities are higher than the ebb velocities.

Barotropic current

In order to estimate the volume flux due to sea level variations we compute barotropic current which is computed as $U_\eta = \frac{1}{A_c}\left[A_s\left(\frac{\partial\eta}{\partial t}\right)\right]$, where A_c is the cross-section area of the inlet channel, A_s is the surface area of the creek and is the observed surface elevation in the creek. For Kilifi Creek $A_s=1.77*10^9$ m^2. $A_c=6.8*10^3$ m^2. Barotropic current is shown in Figure 5.5.2.1e.
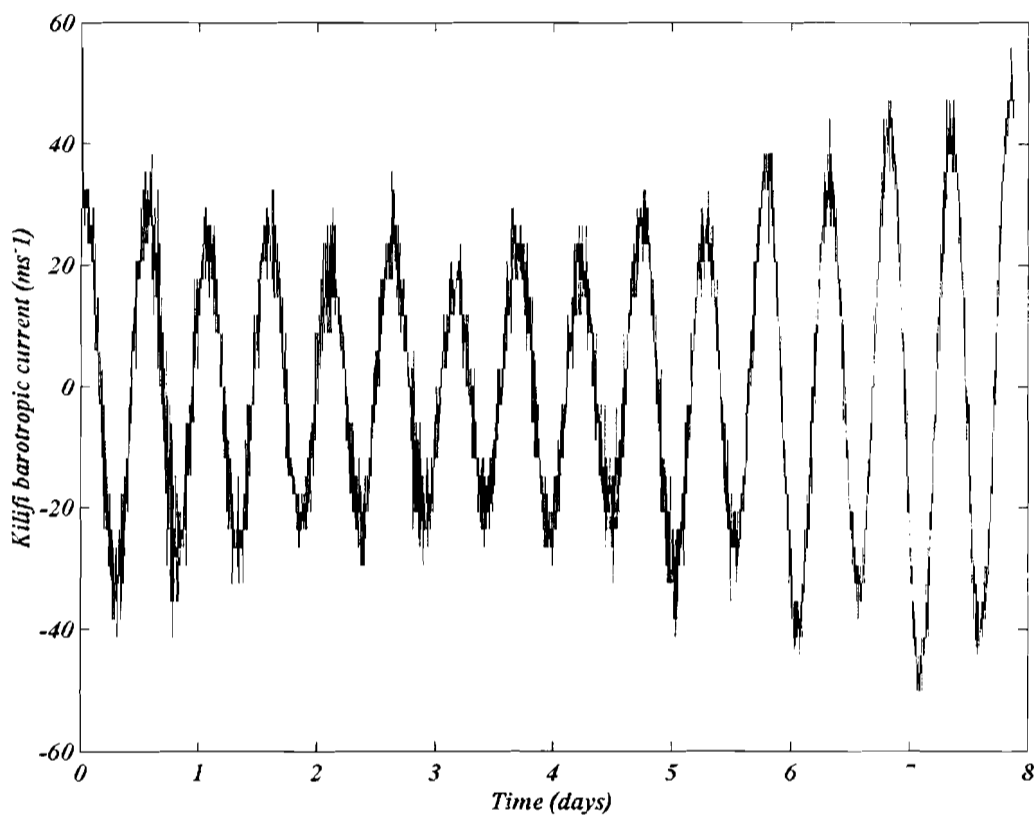
Figure 5.5.2.1e Barotropic current computed from the tide gauge at the entrance MT1 for the duration of 11-19 July 1997.

Theoretical estimation of current

To compute the theoretically the maximum spring and neap currents spring and neap tidal ranges are required. It was shown earlier that these are the average tidal range of 2.2m, maximum spring tidal range of 3.5m and neap of 1.7m. The theoretical current, however, give values, which are slightly greater than those of the current meter. There could are several reasons for this. First the current meter was probably not placed at the mid-position of the channel. The values obtain are closer to the values obtained from the PCM.

Non-tidal currents

Some observations were made on 12 July, using drifters for flood and ebb current, starting at the flood and ebb. Letter A-K in Figure 4.1.3.1 shows the locations from which some of the drifters were picked. Results from drift studies indicate that strong flood and ebb currents are found in the middle of the channel, but weaken on the side. The slowing down of drifter once they reached the inner entrance into the shallow bay indicate that slowing down as the current flows into the main basin away from the channel. The observation of some of the floaters taking a curved path to the right facing down stream indicated the tendency of the water to rotate. This was more evident, following collection of the some of the drifters to the right side of the channel during ebb. Some of the drifters stagnated in shallow water at D. It is interesting to note that drifters some of the drifters dropped at position A, B, C drifted shore ward. However, the ones dropped at position E, F, G, H, J, K and I drifted into the channel. This is an indication that in this part of the entrance the water is still ebbing, when flooding starts in the channel, thus indicating the water at the entrance may lag that in the creek. No drifter stagnated in the channel, for the obvious reason that the two-meter stretch is almost straight; with no bends like those found in Tudor channel area. Drifter K stagnated at point R because of being caught by mangroves on a small Island, while G and H moved to the center of the basin before being picked up J and I stagnated at point S1 and S2. Movement of the two innermost drifters towards the middle of the bay and their being collected at position S3 24 hours later indicated the anti-clockwise circulation during some part of flooding stage.

The trapping of mangrove litter and other debris re-suspended at the upper part of the

creek basin revealed non-tidal circulation prevailed in the inner basin.

5.5.2.2 Sea level

The three tide gauges in Kilifi Creek were deployed on the same day 11/7/1997 but

worked for different duration.
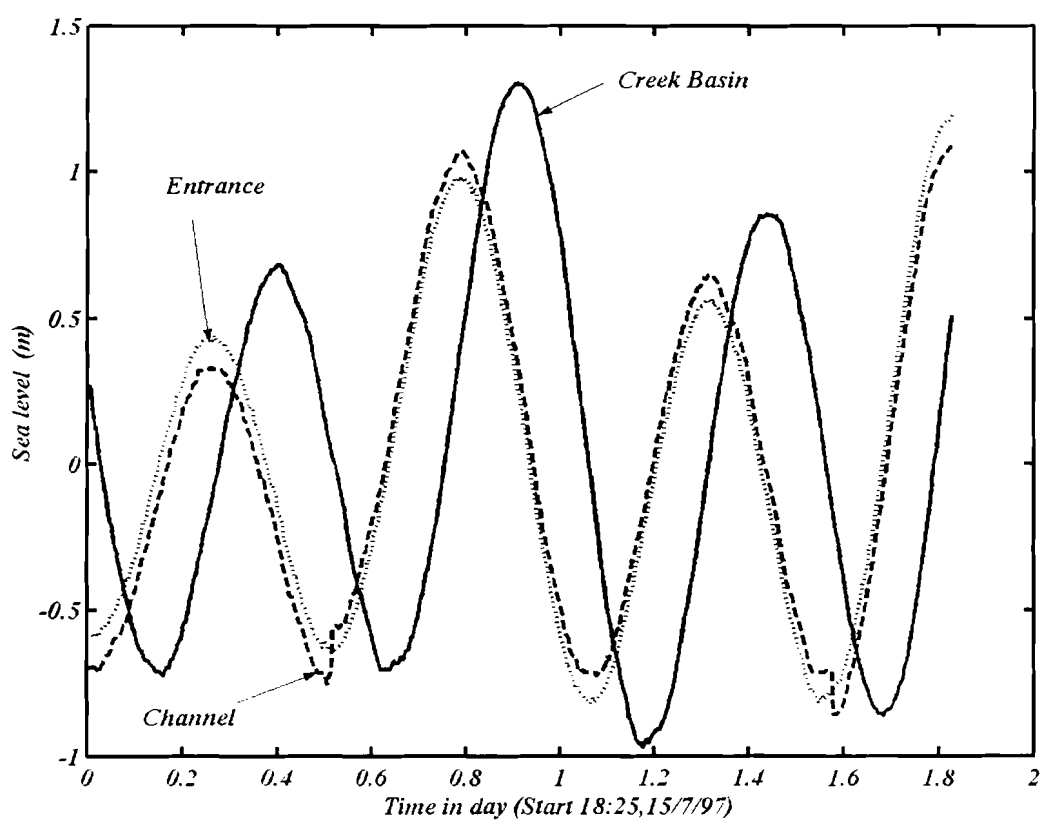
Figure 5.5.2.2a Sea level for the three tide gauges (MT1-entrance, MT2-channel, and

MT3-Creek basin) for two days simultaneous record 15-17/7/97.

301

The tide gauge located at the entrance (MT1) worked for ten days from 11-21/7/1997. The tide gauge in the channel at MT2 worked for 10 days .Out of the ten days, however, only two days from 15-17 July 1997 had reliable data. The inner tide gauge MT2 gave the longest record of more than 50 days. Figure 5.5.2.2a compares the part of the three gauges when they worked simultaneously for two days form 15-17/7/97.

The amplitude of the inner tide gauge (MT3) is higher than that of the other two gauges indicating that the tide was amplified in the basin rather than attenuated. The observation is similar to that made in Tudor Creek.
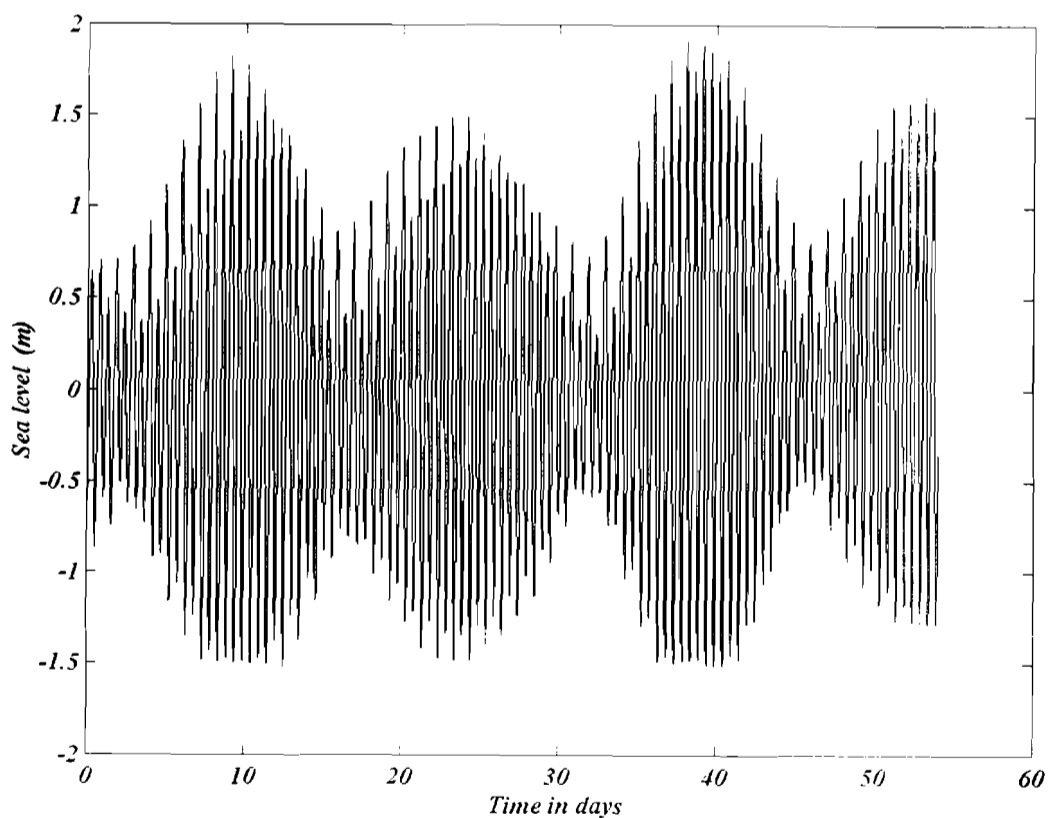
Figure 5.5.2.2b Showing the tide level for the inside Kilifi Creek from 11 July to 31 August 1977.

The lack of attenuation could be, again, due to tidal reflection in the bay, which results in standing wave inside the creek basin. The effects of friction in the lower part of the basin curve are not as evident as was in Tudor Creek. Sea level variations are shown in Figures 5.5.2.2b for the longest record.

Figure 5.5.2.2b shows clearly the tidal inequality in the spring periods, each tidal fluctuations or range is higher than that immediately preceding it. This inequality is not apparent in neap periods. The figure shows an average tidal range of 2.2m, maximum tidal range of 3.5m an average flood and ebb period of 6.23 and 6.21 hours respectively.
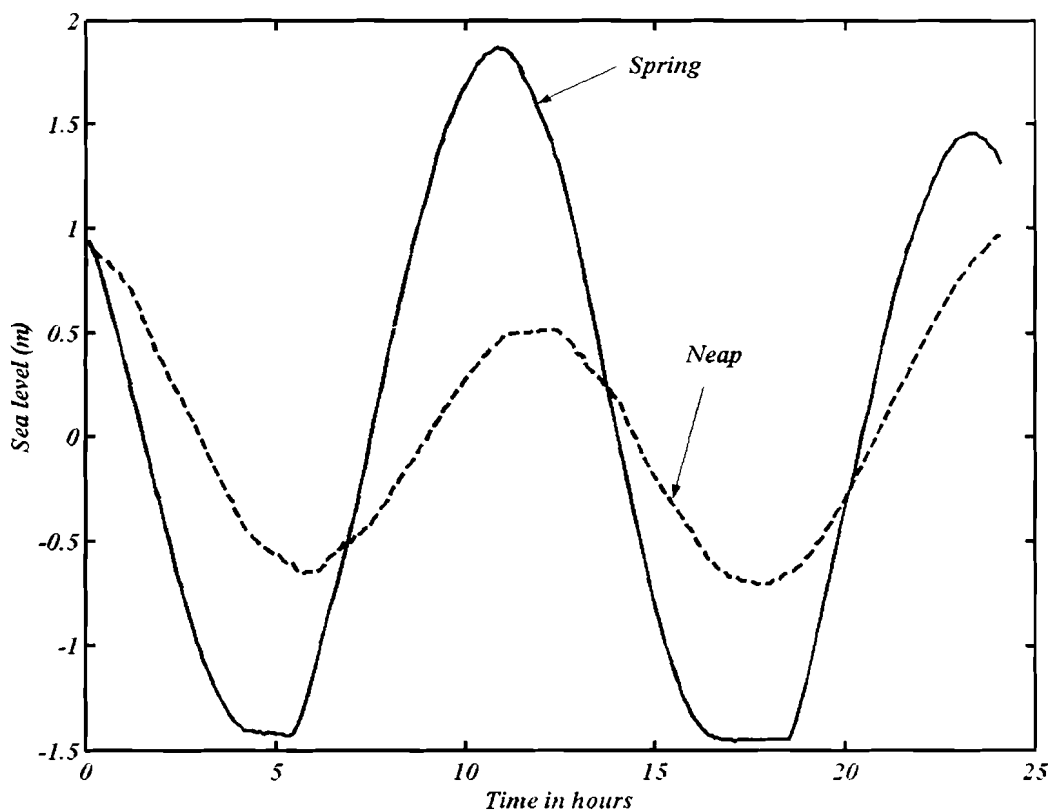
Figure 5.5.2.2c shows an example of sea level during spring and during neap ranges for 20/7/1997 and 27/7/1997 respectively.

Further examination of the curves, by comparing spring and neap tide for 20/7/1997 and 27/7/1997 reveals that the spring tidal range is higher range than neap tidal range (Figure 5.5.2.2c). Distortions caused by topographic effect can be seen more clearly near slack ebb water in the spring curve. In this particular example the neap range was 1.67m and the spring range 3.32m.

The flood and ebb duration during neap are equal (about 6.2hrs), however the ebb duration during spring is longer is slightly longer (6.5hrs) than flood duration (6.2hrs), indicating that in Kilifi Creek a small tidal asymmetry develops during spring tidal period. The analysis of the sea level data at the entrance (MT1) reveal that flood tide is 6.34hrs while ebb tide is 6.05 hrs indicating the at the entrance Kilifi Creek tends to be flood dominant.

Time after high water results

The average time between low water and the highest flood tide velocity was 3.6 hours, while that for highest ebb tide was 3 hrs after high water (Figure 5.5.2.2d). The average phase difference between the zero velocity time and the time when the water level are equal to mean sea level gave an average phase lag of 3.57 hours for both flood and ebb tide computation. The time between the lowest current velocities and high water was found to be 0.4hours, and 0.6 hours respectively, hence almost out of phase.

Figure 5.5.2.2d Time after high water calculated from using the tidal records from the entrance MT1 period 11 July 1997.

The results show that ebb flows occurred in the morning between 2-6 hours and in the afternoon between 12-14 hours, while maximum for the flood was at 4 hours and 9-11hours. The calculations gave average tidal current of 1.32 m, maximum tidal range 1.71m average flood period of 6.32 hrs and average ebb period of 6.24hrs. This indicated that the flood duration is longer than the ebb duration by 0.08 hrs. This again led to the tentative conclusion that the creek tends to be flood dominant.

Figure 5.5.2.2d Time after high water calculated from using the tidal records from the entrance MT1 period 11 July 1997.

The results show that ebb flows occurred in the morning between 2-6 hours and in the afternoon between 12-14 hours, while maximum for the flood was at 4 hours and 9-11hours. The calculations gave average tidal current of 1.32 m, maximum tidal range 1.71m average flood period of 6.32 hrs and average ebb period of 6.24hrs. This indicated that the flood duration is longer than the ebb duration by 0.08 hrs. This again led to the tentative conclusion that the creek tends to be flood dominant.

T. Tide and Spectral analyses (Found 19)

5.5.2.4 Tidal and spectral analysis

The tidal spectrum analysis was carried out for longest tidal data set of the tide gauge at MT3, which had a record of 52 days from 7 July to 28 August 1977. The results are shown in Figures 5.5.2.4a.

The constituents M_2 and S_2 are dominating (Table 5.5.2.4d) their values being very similar to those found in Tudor Creek. The very slightly decrease of the values in the could be to slightly more frictional response affecting the spring tide and probably induced by elongated secondary creeks in Kilifi. In additional to semidiurnal and diurnal constituent and other constituents such as, S_4, M_4, M_f and $2SM_2$ are also observed. The long period constituents have not been considered because to do so data for at least 2 years is needed. This long period constituents are small, and they depend largely upon regional meteorological conditions during the time when observations were made. The results of harmonic analysis of tide at in the creeks demonstrate the invariance of tidal constants, particularly for the major tidal constituents. Whereas M_f, S_4 and M_4 are strongly affected by variation of meteorological conditions and river discharge, the respective harmonic constants also vary.

The tidal energy is proportional to the amplitude squired of each constituent. At the entrance to Tudor creek, the sum M_2, S_2, K_2, N_2 and O_2 account for more than 91.7% of the tidal energy. P_1 is the largest minor constituent, which contributes 1.9%. The form number (F), which is the ratio of the sum of amplitudes of the diurnal tide species over the semidiurnal species Defant (1958), and can be used to characterise the tidal types as mentioned earlier is given as F= (0.13+0.25)/(1.57+0.68)=0.17. Hence the form number

for Kilifi Creek (inner basin) is 0.17, which is less than 0.25, and hence the tide at this

location can be characterised also as semidiurnal. They incline away from mixed

tide (F value between 0.25 and 3.0) by 35%. Figure 5.5.2.4b shows tidal analysis for

temperature time series. The dominance of the semi-diurnal tide is evident.

Const	Period	Amplitude	P/lag	(d)
M2	12.42	1 051	-129.3	
K1	23.93	0 164	-7.1	
S2	12.00	0 455	85.9	
O1	25.82	0 192	-149.5	
P1	24.07	046	36.6	
N2	12.66	214	76.2	
Mf	327.87	013	-30.0	
K2	11.97	0 118	-136.3	
2SM2	11.61	0 003	127.6	
M4	6.21	0 006	87.6	
MS4	6.10	0 009	-72.5	
S4	6.00	08	-178.9	
M6	4.14	006	100.3	
2MS6	4.09	6	-20.3	
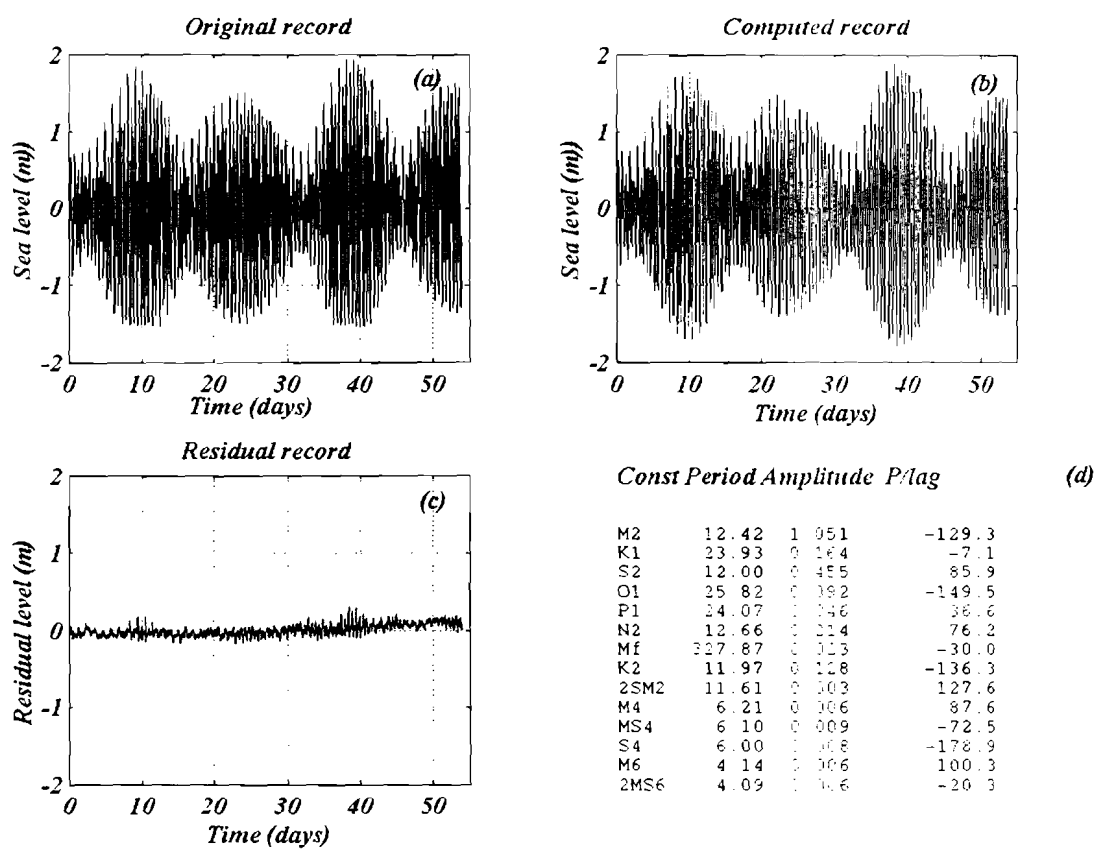
Figure 5.5.2.4a Illustrates the results of tidal analysis (a) original record (b)
Computed (or Astronomical tides) (c) residual levels (d) tabulated constituents,
amplitudes and phase lags for sea level observations from Kilifi Creek (11 July to 28
August 1977).

307

Original record

(a)

Temp levels
3
2
1
0
-1
-2

Time (days)
0   10   20   30   40   50

Computed record

(b)

Temp levels
3
2
1
0
-1
-2

Time (days)
0   10   20   30   40   50

Residual record

(c)

Residual temp levels
3
2
1
0
-1
-2

Time (days)
0   10   20   30   40   50

Const Period Amplitude P/lag   (d)

Const	Period	Amplitude	P/lag
M2	12 42	' 5	170.1
K1	23 93	6	125.5
S2	12 00	4	26.5
O1	25 82	7	115 8
P1	24 07	3	8 0
N2	12 66	4	36 4
M1	27 87	1	-42 2
K2	11 97	8	-178.0
2SM2	11 61	1	-83 4
M4	6 21	2	-178.4
MS4	6.10	4	120.5
S4	6 00	1	42 2
M6	4 14	2	-87.2
2MS6	4 09	6	166 6
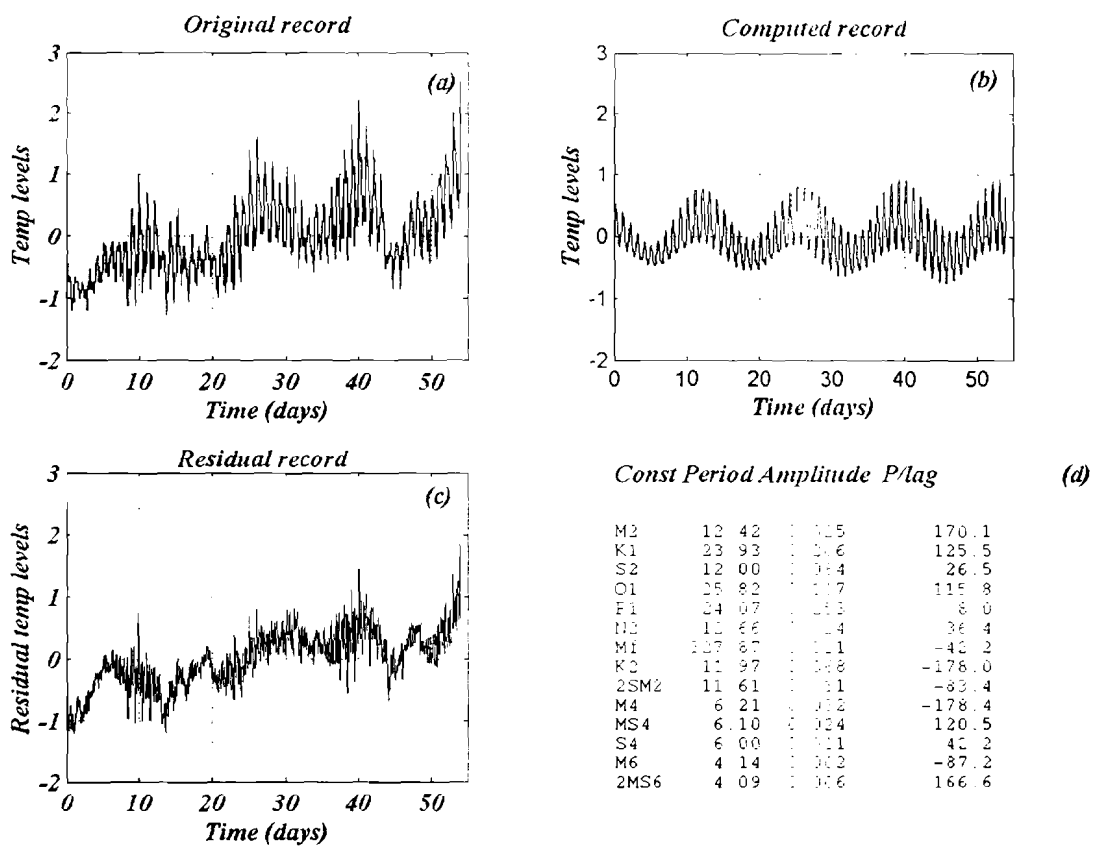
Figure 5.5.2.4b Illustrates the results of tidal analysis (a) original record (b) computed (or Astronomical tides) (c) residual levels (d) tabulated constituents, amplitudes and phase lags for temperature observations from Kilifi Creek (11 July to 28 August 1977). Note the tide gauge was inside the creek.

5.5.3 Water exchange calculations

5.5.3.1 Morphology of the creek

A summary of morphological characteristic is shown in Table.5.5.3.1.

The maximum length of Kilifi Creek is 17km, from the entrance to the extreme end of its longest creek. However, up to the end of the inner basin, the mean length is 14km. The main channel has a length of 2km and a mean width of 400m. The mean depth of the inner basin is 5m and that of the inlet channel is 12m, the maximum depth is 35m. The depth changes more or less gradually into the inner basin. The mean surface area of Kilifi is 2.1 x 10 ^{7} m^2 with the channel occupying 7% of the surface area. The upper part of the basin emerges during low water with large inter-tidal areas occurring in the inner part of 'Maya Creek', behind the mangroves. Except for the constriction at the entrance to the creek channel and change in depth both of which combine to give an anti-clockwise circulation during flood in the inner basin the entrance channel has no bends that cause lateral trapping like in Tudor Creek.

Compared to Tudor Creek, Kilifi Creek is rather shorter and more or less straight inlet, although a small promontory and a small island near the point where the channel begins to widen into the inner basin. The promontory can be thought of as enhancing turbulence in the basin during flood phase of the tide.

Table 5.5.3.1 Morphological characteristics of Kilifi Creek

KILIFI CREEK	
Catchment area (m^2)	1.75 x 10^9
Bay/creek surface area (m^2)	2.1 x 10^7
Total surface area	1.77 x 10^9
Entrance Cross-section area	6.8 x 10^3
Tidal range Neap Spring	2.8m
Length of Bay/Creek (m)	14 x 10^3
Mean depth in the inner basin	5m
Maximum/mean depth /length of the entrance channel	35m/12m/2000m

5.5.3.2 Fresh water discharge

There are two seasonal rivers discharging fresh water in Kilifi Creek.

Draining a catchment area of 1.75 x $10^9 m^2$ which is larger that that of Tudor Creek and that of Gazi Bay. Although the rainfall decreases as one moves northward the large surface area compensates this and consequently river discharge although still small is larger than that of the other two study sites.

5.5.3.3 Water exchange generated by sea level fluctuations

The barotropic current was computed in Section 5.5.2.2 .We now estimate the water exchange from through a cross-section in the channel using the barotropic current. Calculation of the mean tidal volume fluxes through the Kilifi Channel (entrances) is based on tide gauge measurements and the creeks mean surface areas.

The mean surface area of the creek was estimated from the total surface area (A) of the creek at high water level, calculated from a topographic map (1:50,000).

A_m is assumed to be equivalent to a surface area at low water of about 90%, of the high water area. That is A_m =95% for Kilifi Creek, and the mean surface area is 1.68x $10^9 m^2$.
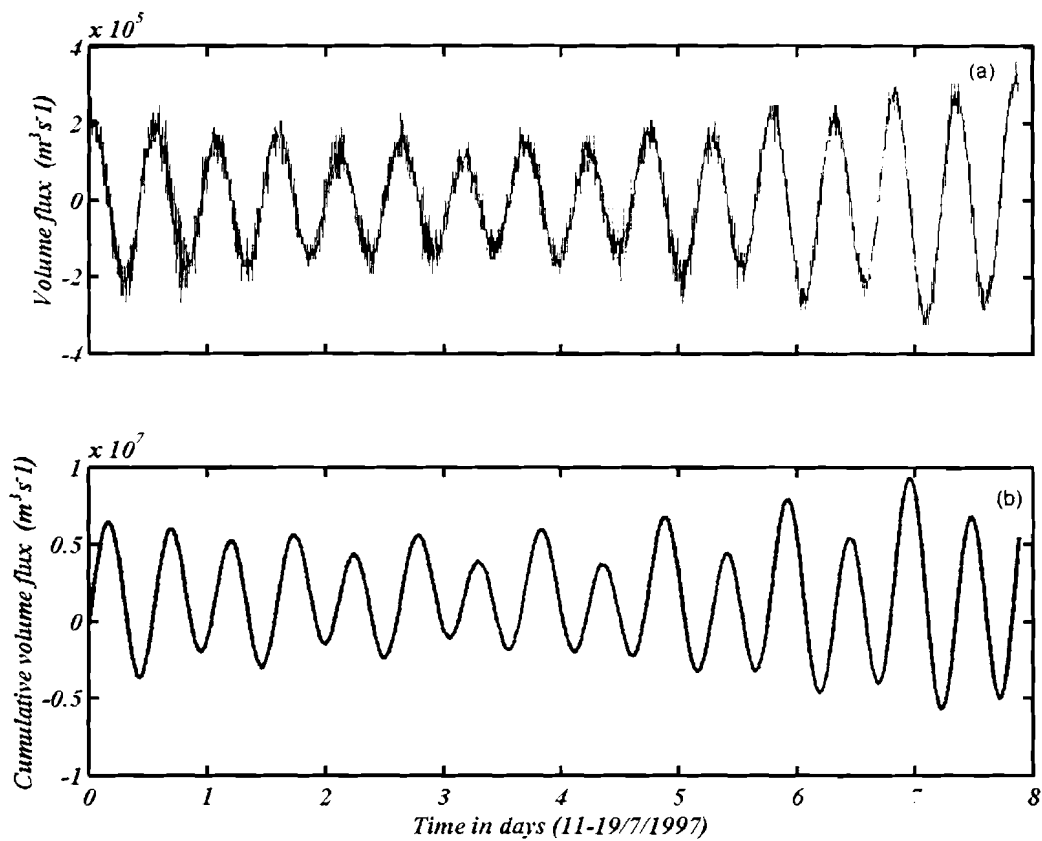
Figure 5.5.3.2 Example of (a) volume flux and, (b) cumulative volume flux across the entrance channel in Kilifi Creek, for the period 11-19 July 1977.

Figure 5.5.3.3 gives (a) volume flux and (b) cumulative volume flux across Kilifi Channel cross-section located near the MT1 and the current meter RCM, for the period of 8 days. The maximum flood volume flux is 3.2×10^5 m^3s^{-1}, while the ebb volume flux is 3.24×105 m^3s^{-1}. The mean volume flux is 2.4×10^5 m^3s^{-1} and the net volume flux is 38×10^3 m^3s^{-1} and a standard deviation of 1.4×10^5 m^3s^{-1}. The cumulative volume flux has a maximum of 9.3×10^6 m^3s^{-1} and a mean of 1.4×10^6 m^3s^{-1} and a standard deviation of $3.3x \times 10^5$ m^3s^{-1}.

312

5.5.3.4 Flushing time

Expression 4.4.63 is used with values for $U_o=0.36ms^{-1}$, $a=0.16$, $\varepsilon=8$, $A=bU_oH$ where b is as earlier shown and H is the mean depth of 5m. The tidal averaged longitudinal eddy diffusivity (B) is of the order 264 m^2s^{-1}. Taking effective length of the creek as 6000m, the flushing time during spring is the order of 2.4 days, which is closer to that of Tudor Creek. Also, during neap tides, however when a small amount of water from the bay enters the creek, complete flushing of the swamp may take more days. It should be noted, however, that Kilifi Creek inlet channel is less sinuous, than Tudor Creek and therefore water may be exchanged more readily in Kilifi Creek than in Tudor creek.

5.5.4 Other calculations

5.5.4.1 Creek energy dissipation

A rough of estimate of creek energy dissipation using expression 4.4.40 for values of $C_d=0.002$, $u_o^3=0.2ms^{-1}$ $A=21*10^6m^2$, $\rho=1025kgms^{-1}$ resulted in energy dissipation of the same order of magnitude to that calculated for Tudor Creek (2×10^6 $Jm^{-2}s^{-1}$). The result should be taken with great caution as the value for u_o^3 is possibly under estimated.

5.5.4.2 1-D Model application

Unlike in Tudor Creek insufficient sea level observations were not available for Kilifi Creek. The similarity of the two creeks is an indication that the One -D model applied in Tudor Creek could work in Kilifi Creek with proper tuning. Model development however was not part of the objectives of this study. Further work along this line is proposed however (see Recommendations).

313

5.6 SUMMARY AND CONCLUSIONS

Climatic and heat loss

Meteorological result reveals that from Mid-March to August as the atmosphere cools and creek water-cools as well. The reason for this change in temperature or loss of heat is due too increased wind, the arrival of cold air masses from southern Indian Ocean, arrival of clouds that cut off radiation and the invasion of the Gazi-Kilifi offshore water by cooler ocean water via the EACC. Thus the results point to the arrival of cold air mass from the southern Indian Ocean during SEM transported by the increasing wind speed during this time. Evaporation shows seasonality, with two high values and two low values. Highest evaporation occurs in February; in the NEM season time humidity is lowest. It decreases from March to reach lowest mean value in July when temperature is lowest. There after evaporation increases until October before decreasing slightly probably due to reduced heat and wind strength associated with switching of the SEM season in NEM season by the presence of cold front (associated with the position of the ITCZ).

Circulation, current, flood and ebb current asymmetry.

In the three systems studied the measured current were in the range 10-40 cms^{-1}, being lowest in Gazi Bay but higher in Tudor and Kilifi Creeks. Therefore currents did not reach the theoretical value of 100 cms^{-1}. Earlier, investigation had indicated that tidal velocities of close to 100 cms^{-1} were possible. However we found no such values and the reason could be due to positioning of the current meter and also the fact that all the

successful current measurements did not coincide with the peak monsoon winds. The current records revealed clear diurnal inequality i.e. a lower magnitude of flooding current was followed by higher magnitude of flood current. Flood current occurring in the afternoon had a higher magnitude than the one occurring in the morning. The afternoon flood was possibly due to enhancement by wind, which usually increased speed between 10-16hrs. Flood and ebb asymmetries are clearly indicated in the results and these are mostly caused by presence of mangroves, peripheral lagoons and other morphological features such as shoaling of depth. In the three systems studied the flood velocities were higher and their duration shorter time than currents and duration observed during ebb. However, the ebb tide duration was longer than the flood tide, in Gazi Bay hence leading to the conclusion that Gazi Bay displayed ebb dominance. Tudor and Kilifi Creek both displayed flood dominance. One would expect ebb dominance in the two creeks due to large mangroves and mud flats in the inner parts of the creeks, however the channeling effect of the tidal water entering the creeks probably shadow the effect of the mangroves and mudflats.

The average time between high water peaks and the highest flood tide velocity were 1.9 hours, while that for low water highest ebb tide velocity was 3.34 hours. The average phase difference between the zero velocity time and the time when the water level are equal to mean sea level gave an average phase lag of 3.57 hours for both flood and ebb tide computation. The time between the lowest current velocities and high water was found to be 0.4hours, and 0.6 hours respectively, hence almost out of phase.
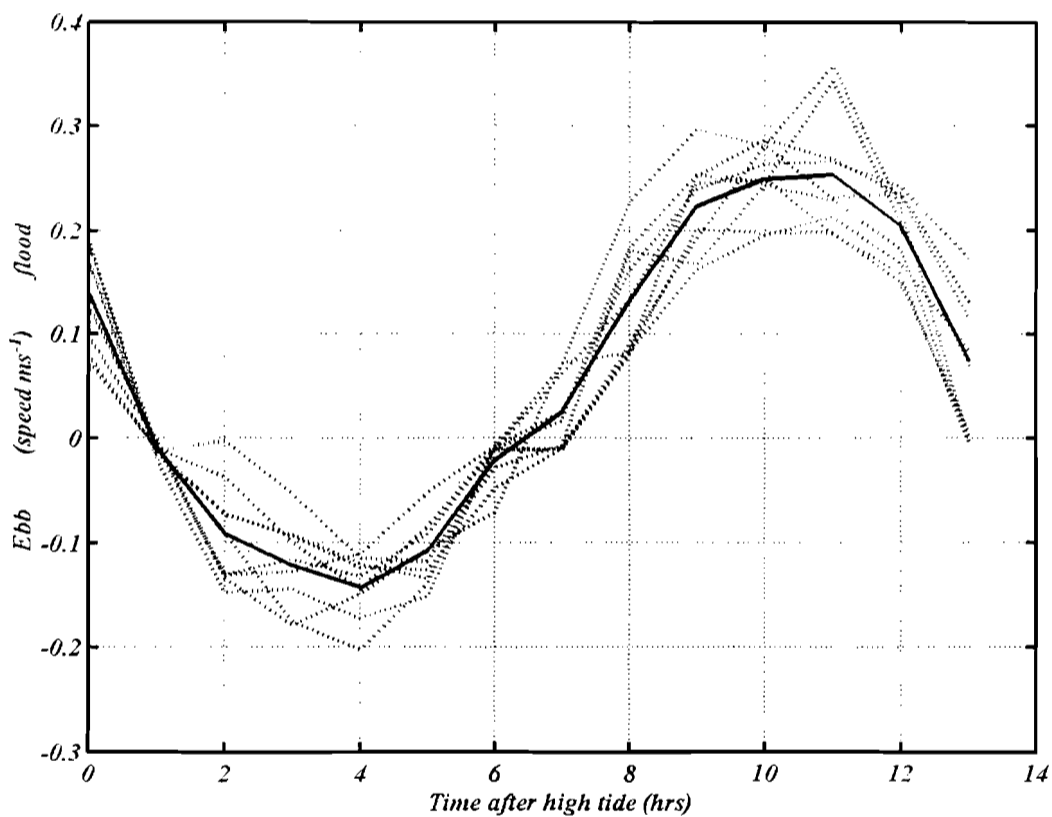
The results show that ebb flows occurred in the morning between 7-9 hours and in the afternoon between 19-22 hours, while maximum for the flood was at 2-3 hours and 16-17hours.

Comparison of the Kilifi Creek inlet channel and that of Tudor Creek reveal that the length of Kilifi inlet is half that of Tudor inlet moreover the inlet is less sinuous, with a more east-west orientation than that of Tudor Creek. From these observations it can be deduced that the two small creek systems and the inner basin in Kilifi Creek undergo exchanges with the adjacent offshore waters more readily than in Tudor Creek.

Salinity and temperature

Salinity and temperature, in Tudor Creek, ranged from 37.7 to 37.9% and 27.69 to 27.73°C respectively. Vertically, the low values of salinity and temperature occurred at the surface (3m) before decreasing between the depth of 6 and 8m. The decrease in salinity probably corresponds to the position of maximum current. The two parameters occurred below 10m, and tended to increase indicating the presence of the oceanic water or near entrance coastal water in the inlet closed to the seabed (below 17m). Temperature tended to increase while salinity decreased near the bottom. Salinity in the creeks decreased during ebb period, but increased during flood. This observation is clearly indicated by Figure 5.4.1.2b, which shows typical examples of how salinity changes with time. During ebb the salinity reach as low as 33.8 and maximum mean value of 34.8, during a typical flood stage at the entrance. Further, inside the creek salinity at ebb shows

a value of 22 and at flood slack water at 34.2, indicating that more fresh water has accumulated in the surface at this location than near the entrance.

Seasonality of salinity and temperature was evident. Highest values for both salinity and temperature occurred in February and early March at the time of the NEM season. The rain during the IMSR season had minimum effect of salinity and temperature. However the effect of rain in the IMLR season caused rapid drop in salinity and temperature. Salinity reached lowest value in May whereas the temperature reached minimum values in August. That is temperature-lagged salinity by 3 months.

CHAPTER SIX

OCEANOGRAPHY OF THE ADJOINING SHELF

6.1 COASTAL CURRENTS

The major coastal currents were referred to as the EACC, SC, SEC and ECC. We investigate the vertical structure velocity in the EACC off Gazi as a typical example. Coastal current observed between 5-100km, at depth 170-400m, off the Gazi Bay by means of free drift buoy (diameter=15cm) attached to a weight by one meter rope (Scheffers, 1981) are shown in Table 5.3.5. They are shown together with the wind speed for the month of February, July and October. That is NEM, SEM and IMSR (October) respectively. The results show the current at 170m have speed about of 130 cm s^{-1}, in the direction 190° -010° in NEM. During SEM, at a depth about 300m, the direction of the current change to 228° -048° with almost current of similar magnitude 120cms^{-1}, and in IMSR the current decrease slightly to 90 cm s^{-1} with a direction of 200°-020° at a depth of about 200m. In NEM the wind blow at a speed greater than 90 cms^{-1}. During the IMSR season the speed is less than 100cm s^{-1}. Thus, at a depth the depth between 170-400m the current flow remains essentially at 100 cm s^{-1} and in a south-north direction.

Oceanographic data off Gazi Bay available for May June November and December for the stations shown in Figure 4.1.5.1 was analyzed. These months represent the wet and the dry seasons, namely the IMLR, SEM, IMSR and the NEM seasons as mentioned earlier.

Table 6.1.1 Coastal current observed between 5-100km, at depth 170-400m, off the Gazi Bay by means of free drift buoy (diameter=15cm) attached to a weight by one meter rope (Scheffers, 1981).

Cruise	Date	Station Position		Avg. Depth	Dir	Cur(ms^{-1})	Wind Dir	Speed (ms^{-1})
8026		Lat	Long	(m)	X^o		X^o	
Feb 80	2	$04^o 37'$	$39^o 31'$	170	190-010	1.3	160	9.3
8022	25	$04^o 39'$	$39^o 47'$	310	330-150	0.6	170	6.7
July 80	25	$04^o 40'$	$39^o 40'$	305	200-020	1.0	190	6.7
	25	$04^o 41'$	$39^o 36'$	400	215-035	1.6	190	6.7
	25	$04^o 39'$	$39^o 31'$	355	200-020	1.5	180	4.3
8026	3	$04^o 39'$	$39^o 36'$	400	210-030	1.1	180	0.8
Oct 80	3	$04^o 39'$	$39^o 37'$	412	214-034	1.2	180	0.8
	3	$04^o 25'$	$39^o 43'$	472	180-360	0.4	180	0.8

The depth range of these stations varies from 0m to a maximum depth of 500m. At surface (0-5m) the temperature was 28.5°C, and at 10-50m it decreased from 27.95 to 26.18 °C. The shelf water was cooler than the bay water most of the seasons probably due to increasing solar radiation and heating by the bay bottom. In addition the cooler water

seems to be largely cooling by the Ocean at this time of the year (see TS diagram for station off Gazi Bay).

6.2 WATER STRUCTURE

6.2.1 Salinity and temperature

Several vertical data measurements on the Kenya shelf waters exist. Those taken off Mombasa shelf area to the north are from R.V.Tyro 1992/1993 and M.V. Kusi, 1979 (MONEX report, 1980). Those off Gazi Bay area are from Dr Fridjof Nansen 1985. The data considered here is taken selectively from Dr. Fidjof Nansen, and R.V.Tyro for the stations mainly for offshore water between Gazi Bay and Kilifi Creek.

Figures 6.2.1.1 and 6.2.1.2 illustrate typical vertical section contours of the temperature and salinity for May (IMLR) and November (IMSR) based on 7 offshore stations (source Dr Fridjof Nansen 1985) placed at 7 nautical miles apart on transect perpendicular to the coast. The two sets of figures differ by depth ranges so as to emphasize the vertical features in more details. Figure 6.2.1.1a-d emphasizes the shallow surface water (0-30m) temperature and salinity structure during the IMLR season (panels a, b) and IMSR seasons (panel c, d). In IMLR season low salinity coastal water is evident from station 1 to 4. A strong coastal front depicted by vertical isolines occurs between station 4 and 6. Water of lower salinity and temperature than the surface layer up-well form the bottom (panel a, b). In the IMSR season the front is weak, the surface layer is slightly cooler and salinity has increased by about 2 from the IMLR season values. The isotherms show that a diffuse ridge occur between stations 3 and 5 (panel c) whereas the vertical salinity isolines (panel d) indicate the front has move towards the shore.

A change in gradient is also evidenced in Figure 6.2.1.1a-d, by the large region between stations 1 and 4 where horizontal gradients are small, bounded by a narrow region, stations 4 and 6, where the horizontal gradients are large. Figure 6.2.1.2 a- b emphasizes the structure seen in Figure 6.2.1.1a-b but for depth up to 400m. The low salinity coastal water is evident in the surface layer as well as the front where the isotherms bend slightly upwards but sag blow the 200m (e.g.14°C isotherm). The intrusion of low salinity water is evident where the salinity contours attain a V-shaped feature.

Thus Figure 6.2.1.1a-d illustrate remarkably the effects of fresh water input characterized by a large parch of homogeneous low temperature (<28.2°C) and low salinity (<34.8) at station 1-4, whereas beyond station 6 water with high temperature (>28.5 $^{\circ}$C and high salinity (>35.28) is found. The two waters differ by temperature of about 0.6°C and salinity of 0.5.

Further examination of the prominent features in Figure 6.2.1.1-the coastal front between stations 4 -5, reveals a narrow high-gradient region of 20 nautical miles across. The isoclines, in the front, dive downward with a strong increasing contrast as can be seen in the temperature and salinity panel (Figure 6.2.1.2c-d). The front probably separate the coastal homogeneous water before station 1 to 3 (Figure 6.2.1.1a-d) from the surface oceanic water found in the EACC proper beyond station 6. These changes are intimately tied up with salinity and density and the contours of one variable appear similar to the contours of the other.
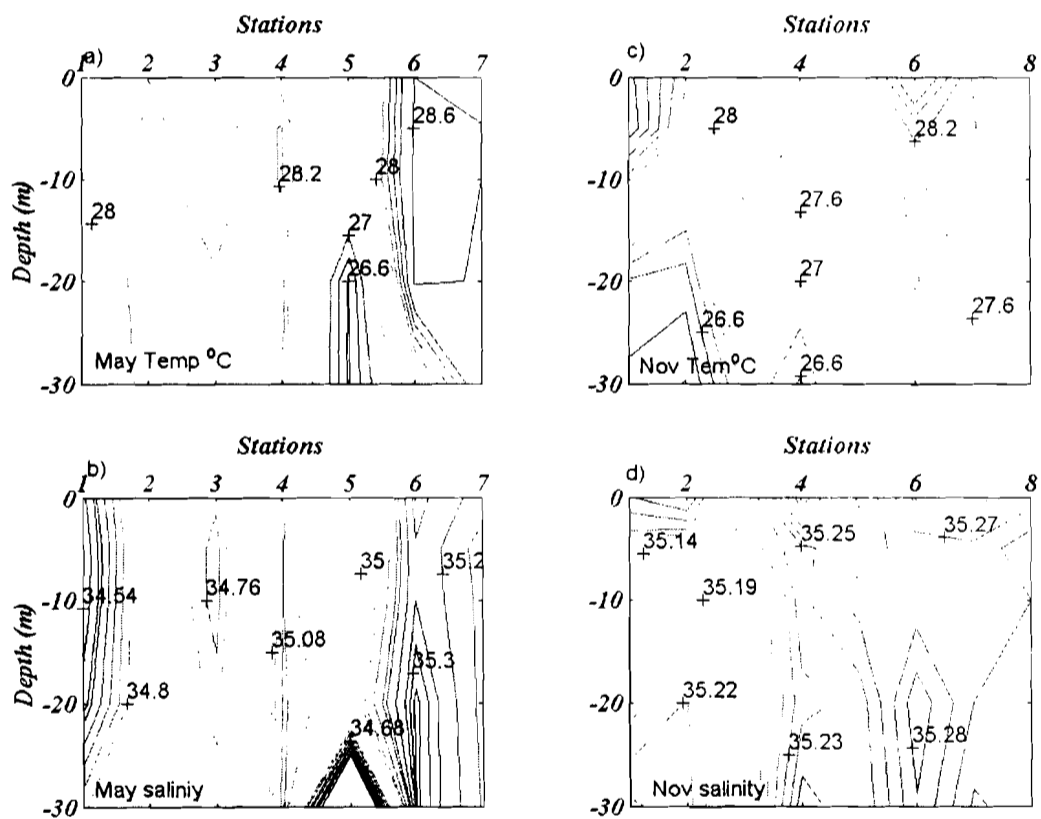
Figure 6.2.1.1 Vertical sections of surface (0-30m) (a) temperature and (b) salinity in May and (c) temperature (d) salinity in November off Gazi Bay. Note upwelling of cool water around Station 5.

Further observations reveal remarkable upwelling of low temperatures <27.5 °C and low salinity <34.7 in the middle of the front. For, example, following the isolines of salinity

in Figure 6.2.1.2b it can be seen that they slope up and in the lower parts they slope down. This observation suggests a tidal front, however, the rise of the isoline from one side of the front to the other create a horizontal gradient of density suggesting a flow into the paper (northward) in agreement with the northward direction of the EACC there. In the IMLR season the front appears intense well defined, probably locked in position by intense flow and topography and enhanced by fresh water flux. In IMSR season the front is still observable, but now, diffuse, spread out, and found closer to the surface and with eddy-like flow features in the in the upper layer (Figure 6.2.1.1c). It is also apparent that (Figure 6.2.1.2c-d) the less saline parch of water occurs at the coast in November and is evidence of smaller volume of freshwater input during IMSR season.

Further examination reveals that both the coastal waters oceanic water in November contains higher salinity and slightly lower temperature than in May. The results further suggest that the events that started at the onset of SEM season have by November reached the shallow waters, near the surface and gradually made their way to the creek entrance areas.

The cold-water intrusion or upwelling at the center of the front is seen in the right hand panel of Figure 6.2.1.1c-d where, a previously intense feature has been replaced by a more diffuse ridge below station 4 and which appear to be displaced closer to the shore. The isotherms are more stretched probably a consequence local wind effect and a general tendency for the water to spread offshore as well. Hence, there is a profound and striking difference as can be verified by comparing temperatures in the two upper panels of

Figure 6.2.1.2; the difference is probably a consequence of different circulation modes in the two seasons.
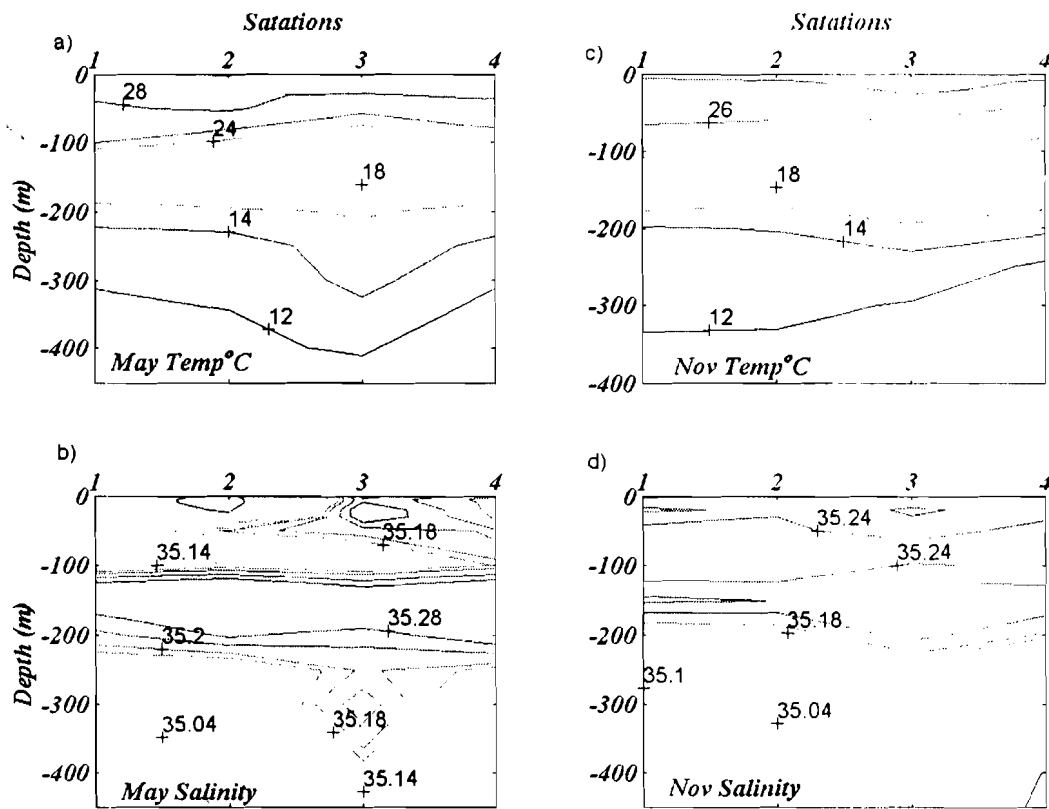
Figure 6.2.1.2 Vertical water structure off Gazi Bay showing contours of (a) temperature (panel a) salinity (panel b) for May (IMLR) and temperature (panel c) and salinity (panel d) for the November (IMSR) season.

The core structures, seen in May, disappear in November and water is more saline on the surface. The isotherms in the range 100-200m are inclining in the opposite

direction indicating a tendency for water to down well near the coast in May and vice versa in November.

6.2.2 Vertical temperature, salinity, density and oxygen variations

Vertical temperature, salinity, density and oxygen profiles are shown in Figures 6.2.2.1a-d. Surface mixed layer (50-150m) can be identified in these figures as a homogenous layer near the surface, with a tropical thermocline at about 20m. In addition the figure illustrates typical vertical variation in temperature, salinity and oxygen. The dotted profile is for a station close to the shore and the line a station further offshore. Temperature profile decreases with depth, more rapidly between 60-120m as indicated by the departure of the two profiles. The position of the permanent thermocline is about 75m. Temperature shows less decrease in waters below 400m. This is also observed in the salinity panel where it mirrors the temperature profile at deeper depth, but is the reverse above 200m, attaining salinity maximum of 35.35 and decreases to a surface value less than 34.85 for the ocean profile but slightly less value in the near shore profile.

Figure 6.2.2.1a typical vertical variation of panel (a) temperature, panel (b) salinity and panel (c) oxygen in ocean water off Gazi Bay during IMLR season (Source, R.V. Dr Fridjof Nansen 1982-1985) whereas Figures 6.2.2.1b-e show some examples of the salinity profiles in June for several stations along the coast, for salinity, temperature, oxygen and nutrients from R.V.Tyro 1996 June Cruise. Near the surface salinity ranges from 34.8-35.0. The lowest values of salinity, much like the temperature, occur in the landward stations due to river influence. The salinity increases in the

subsurface layer to a maximum value of 35.48 just below the thermocline. Between 300-550m the salinity has a mean value of 34.7. Another maximum of 35.3 occurs at 630m followed by a minimum at 1025m. At depths greater than 1500m the salinity value falls to 34.6. Slightly higher salinity occurs in the northern transects than in the southern ones for depths between 0-630m during the same cruise. The along shelf difference in salinity indicates that the EACC gradually gains salinity as it moves northward.

Maximum and minimum salinity occur between 50-75m for the near coast profile which indicate the possibility of more saline water inshore than offshore at the location of the thermocline. The decrease is probably a consequence of mass flux as mentioned earlier. Oxygen decreases first slowly in the surface layer value of $4.8m\mu l^{-1}$ but more sharply below the thermocline. A minimum of $3m\mu l^{-1}$ is reached just below the thermocline at about 150m but increases to a small maximum at 250m and thereafter becomes more gradual. This is probably a consequence of mixing of different water masses (see later) and other processes.
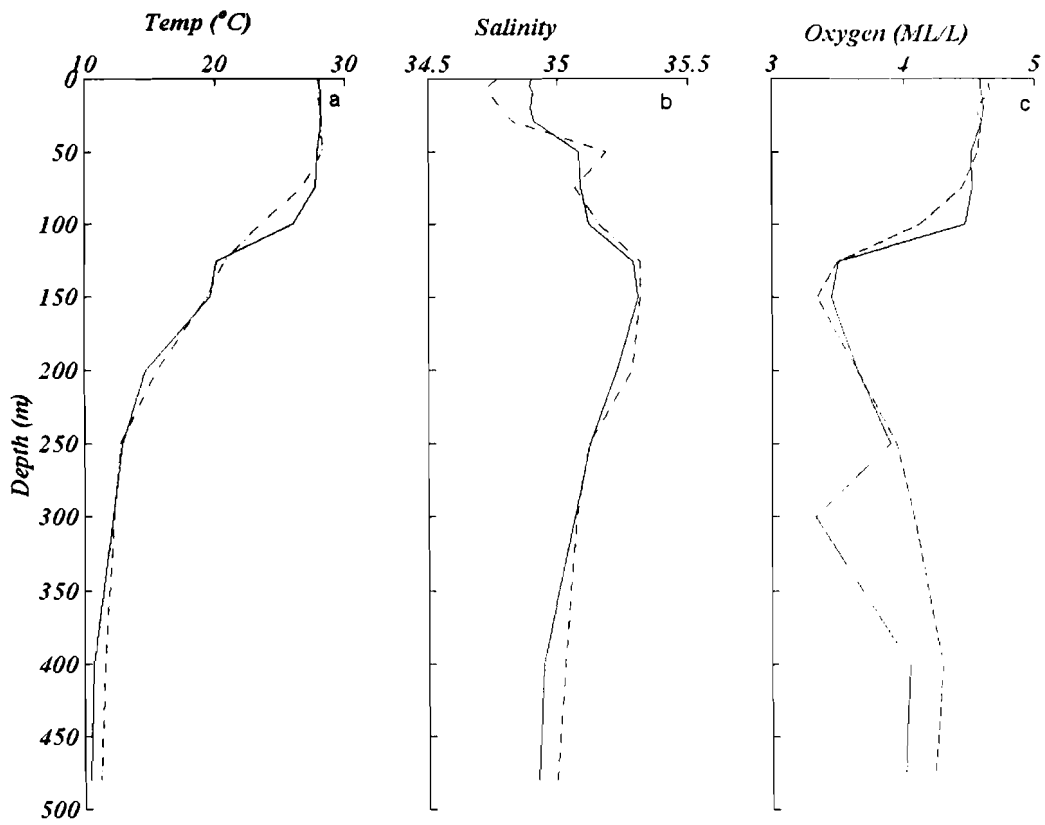
Figure 6.2.2.1a Typical vertical variation of (panel, a) temperature (panel, b) salinity and oxygen (panel, c) in ocean water off Gazi Bay during IMLR season (Source, R.V. Dr Fridjof Nansen 1982-1985).
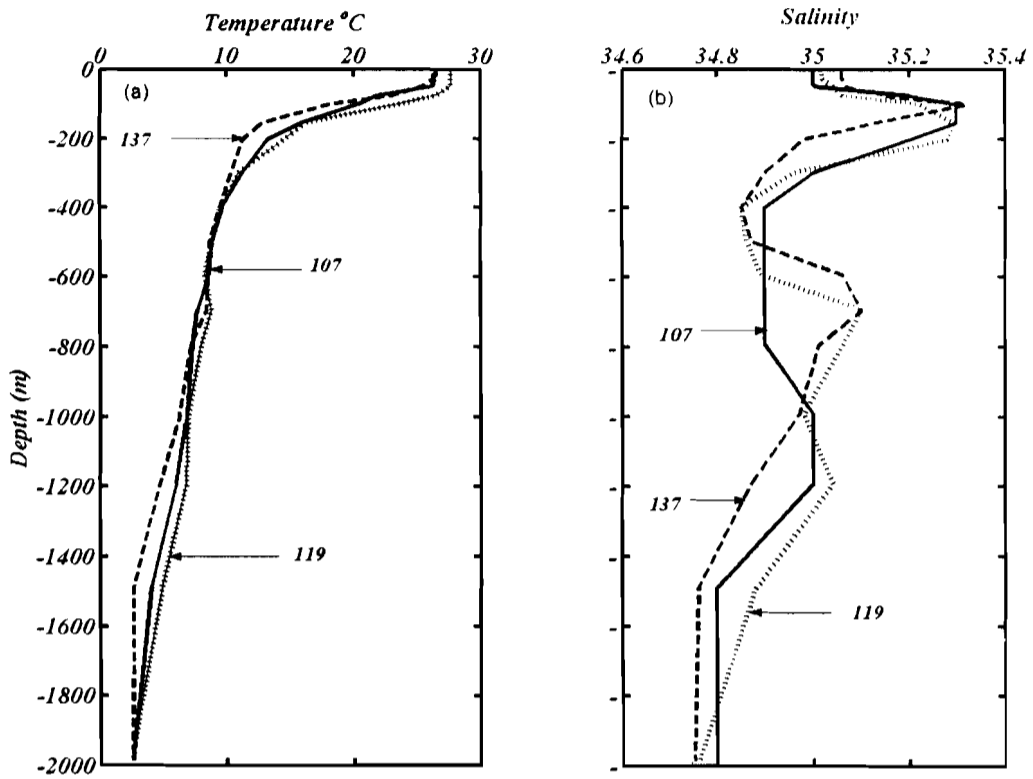
Figure 6.2.2.1b Vertical variation of temperature, (panel a) and salinity (panel, b) off Gazi-Kilifi shelf area in June and July (Source, R.V. Tyro 1992-93).
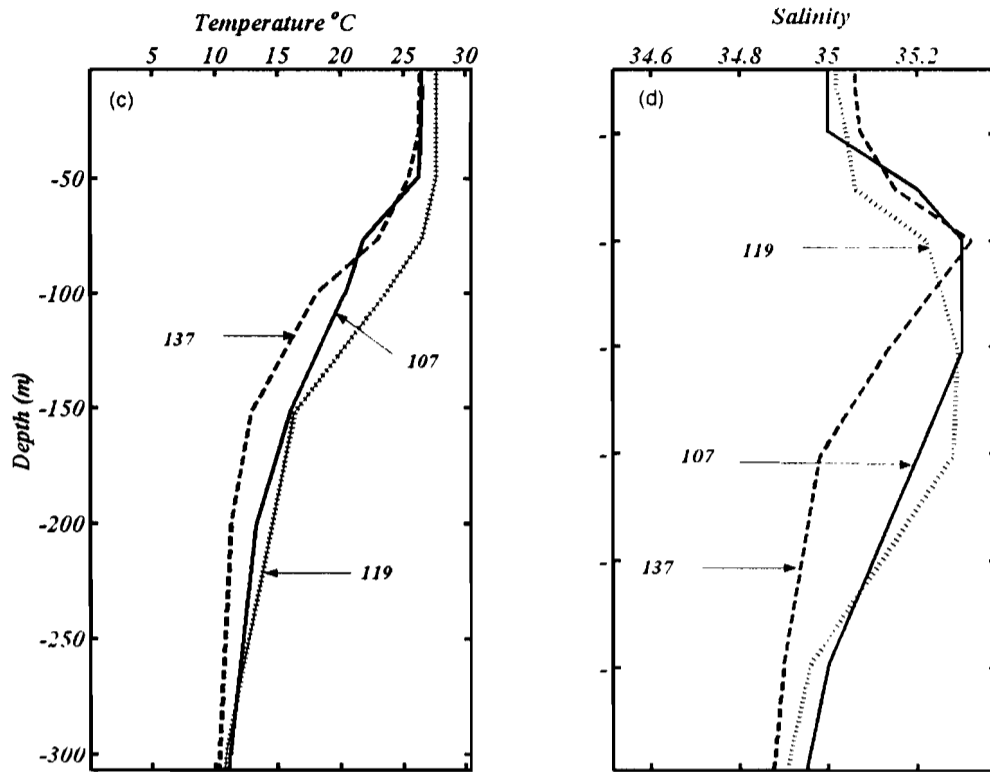
Figure 6.2.2.1c Vertical variation of temperature (c) salinity (d) off Gazi-Kilifi shelf area in June and July, (depth range 0-300m) (Source, R.V. Tyro 1992-93).
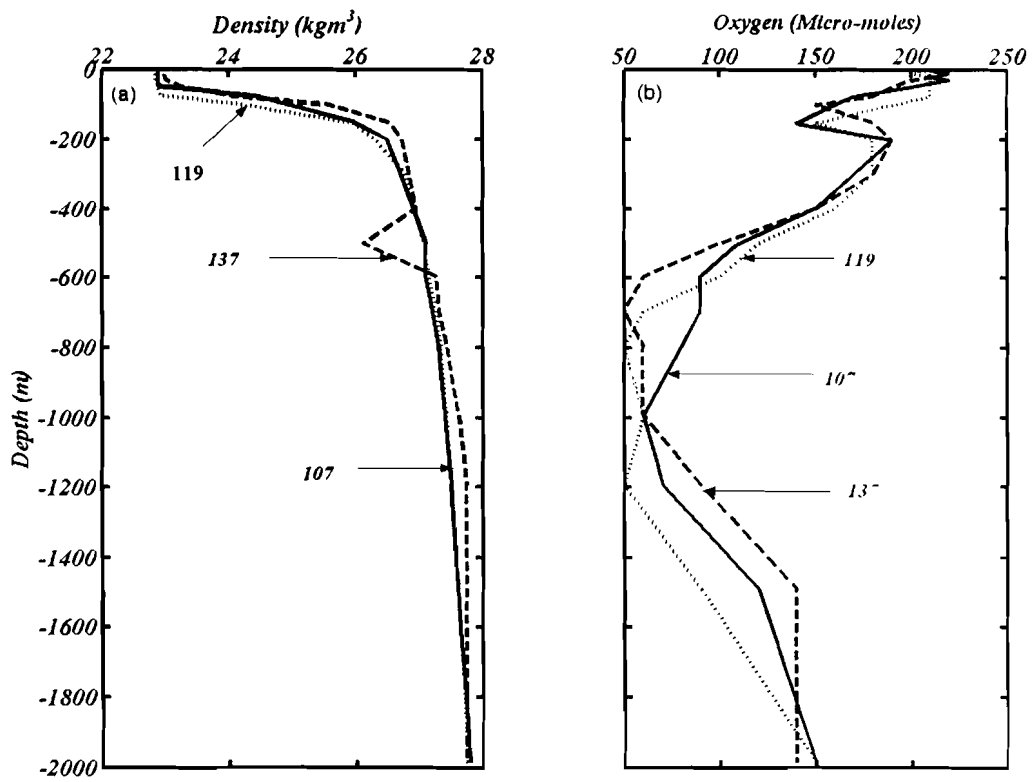
Figure 6.2.2.1d Vertical variation of density (panel, a) and Oxygen (panel b) off Gazi-Kilifi shelf area in June and July, (depth range 0-2000m) Stations101, 119, 137 (Source R.V. Tyro 1992-93. Stations 101,119 and 137).
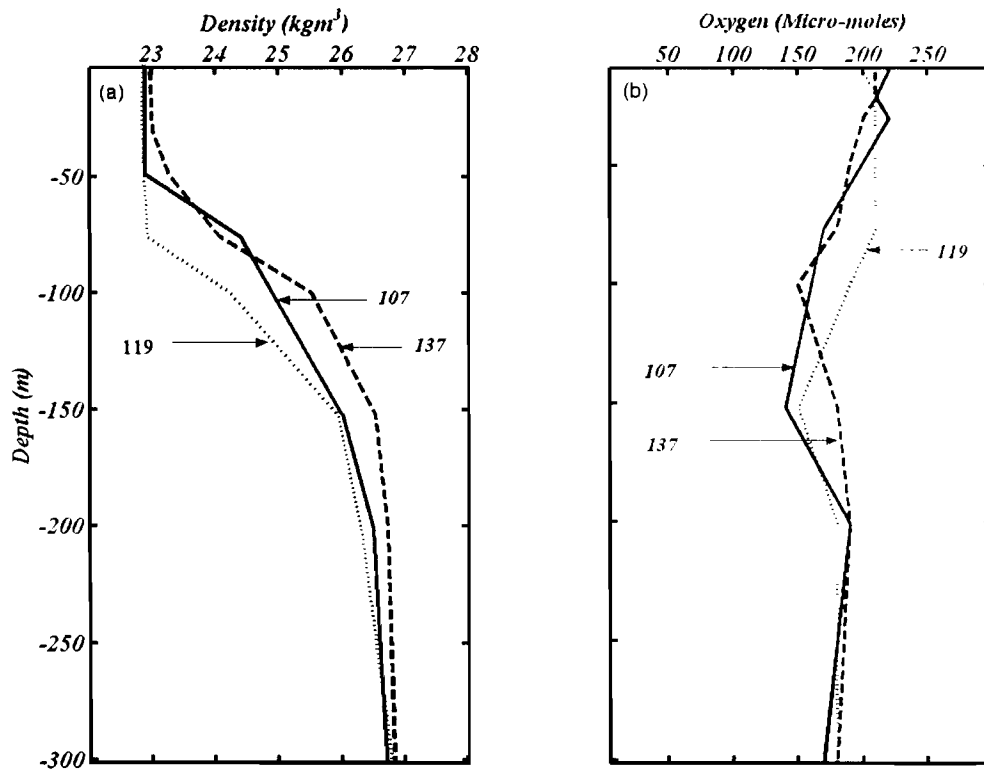
Figure 6.2.2.1e Vertical variation of density (panel a) Oxygen (panel d) off Gazi-Kilifi shelf area in June and July (Source, R.V. Tyro 1992-93. Stations 101, 119 and 137).

6.2.3 Surface salinity and temperature distribution

The surface salinity and temperature distribution off Kenya coast for the month of IMLR season (May), SEM season (August) and NEM season (December) are shown in Figure 6.2.3.1. The figure represents average values from 0-30m from MONEX data report 1980. Low salinity occurs in stations near the coast indicating that the water close to the shore has lower salinity due to river influence. Lowest salinity occurs in May as expected due to the long rains and fresh water discharge. The lowest values occur close to the mouth of Sabaki and Tana Rivers in Malindi-Ungwana Bay areas. December depict the highest surface salinity values whereas in August the salinity is intermediary. Temperature is lowest in August for reasons mentioned earlier. The salinity along the coast shows that compared to areas off Gazi Bay, the water off Kilifi Creek and to the north has lower salinity. Again this is due to the river input and also due to a northerly flow of river plume exiting from the Ungwana Bay. In August and December this situation seem to be reversed particularly in the furthest stations offshore, an indication of the arrival or occurrence of more saline water this time. This change could be partly due to intense mixing of various near surface and subsurface water masses during the SEM-season (Section 6.3.2).

332

40°E   41°E   :2°E

1°S   SOMALI   1°S

KENYA (inset)
AFRICA   40E   10°N   0°   10°S

MANDA

2°S   2°S

LAMU
(28·0)
[34·30]   (28·35)   (27·6)
KIPINI   [34·80]   [35·20] (27·35)
TANA RIVER   [35·21] (27·6)
[35·23]
(27·95)   (24·10)   (27·5)
[34·30]   [25·25]   [35·22] (28·2)
(28·3)   (24·45)   [35·32] (28·3)
KENYA   (27·70)   [34·7]   [35·34]   [35·31·]
[34·2]   (28·3)
SABAKI RIVER   (27·80)   (24·10)
[34·5]   [35·20] (24·3)
MALINDI   [35·27] (24·30)
[35·29]
(28·25)
(28·2)   [35·27] (28·25)
3°S   [34·3]   [35·28] (28·00)   3°S
KILIFI   (28·5)   [35·31]
[34·8]

MOMBASA

4°S   MAY   AUGUST   DECEMBER   4°S
(1983)   (1975)   (1982)

VANGA
(28·3)
[34·9]   (27·30)
[35·20]   (28·20)
(28·6)   [35·25]
[34·6]
TANZANIA
PEMBA ISLAND

Figure 6.2.3.1 Typical mean surface temperature and salinity off the Kenya coast

for the month of May, August and December (Source MONEX data Report 1979).

6.3 SEASONAL WATER TYPES AND OCEANIC WATER MASSES

6.3.1 Seasonal water types in the creeks and bay

In the previous section the off surface water was show to be different for different seasons. In the off shore area fresh water due from the creeks may combine with seepage to create yet new characteristics. At the shelf-edge, further characteristics may form due to upwelling of deeper water on and here a true separation of oceanic water from inshore may take place.

For the purpose of this thesis we classify as 'seasonal water type (SWT)' the water with its own characteristics created both within the creeks and lagoons and around the reefs, particularly where the mangroves and coral reefs are high and depended on the season. We use the term water mass to refer to more classical water types such as occur in oceanic conditions. We classify four seasonal water types on the basis of the seasonal structures in Figures 5.4.1.1e-h and 5.4.1.2e-h. The IMLR SWT has moderate temperature in the range 28-31°C and lowest salinity in the range 8-34.8. In SEM SWT has low temperature with a range of 24-27°C and moderate to high salinity in the range 32.2-35.8. The IMSR SWT has temperature of 26-29°C and salinity of 34.4-35.2 while the NEM SWT has high temperature 30.0-32.2 °C and very high salinity 36.5-35.4. One essential feature that occurs between the end of NEM season and the start of SEM season is the sudden decrease in salinity and temperature and probably more nutrients in the inner basin; the mangrove-creek environment is freshened! In the IMSR season, the end of SEM season and the start of NEM season the salinity and temperatures are high after being influenced by the events in SEM season, the relatively small rainfall has no significant effect on salinity. The four seasons are well known by the fishermen who refer

334

to the seasons in Kiswahili as Masika, Kusi, Vuli and Kazikazi for IMLR, SEM, IMSR and NEM seasons respectively. These seasons are associated with certain fishing traditions for the coastal people. Hence one can refer to 'Masika SWT', 'Kusi SWT', 'Vuli SWT' and 'Kazikazi SWT' to reflect the traditional ocean knowledge (TOK) yet untapped in the local fishermen. A case in point is 'the use of TOK for crustaceans and fish in certain creeks, lagoons, bays and offshore banks in one season rather than the other for maximum realisation of catches. The fishermen are able to identify areas where fish may be aggregated. They do this by identifying special flow features and location of slicks and small headlands and thus maximise catches-this point was a communication with one fisherman in what he called 'Misimu ya samaki' (Mr. Bakuli, Traditional fisherman in Kilifi Creek 1997 per comm.).

SWT can be envisaged as an elaborate interplay of the local fresh water input in the mangrove-creek and coral reef environment and the surface water of the East Africa Coastal Current. In the adjoining coastal water, the oceanic water masses are identified on the basis of the classification given mainly by Tomczac and Godfrey (1994).

6.3.2 The Adjoining coastal water

Surface water and thermocline layer

To bring out clearly the oceanic water masses (as opposed to SWT in the inshore) two figures are presented. The first (Figure 6.3.2.1a) uses data from Dr. Fridjof Nansen and depicts low salinity in the surface due to fresh water input in IMLR and IMSR seasons for the months of May and November (see also Figure 6.2.1e). We note however that the surface (e.g. 0 - 50m) is in direct contact with the atmosphere its temperature and

335

salinity are not sufficiently conservative to permit adequate definition of water mass, hence the reference to the water there as SWT. Figure 6.3.2.1a, however, reveals a top layer (0 - 20m) with warm fresher water than the underlying subsurface water with a maximum salinity of 35.45 at about 50m.
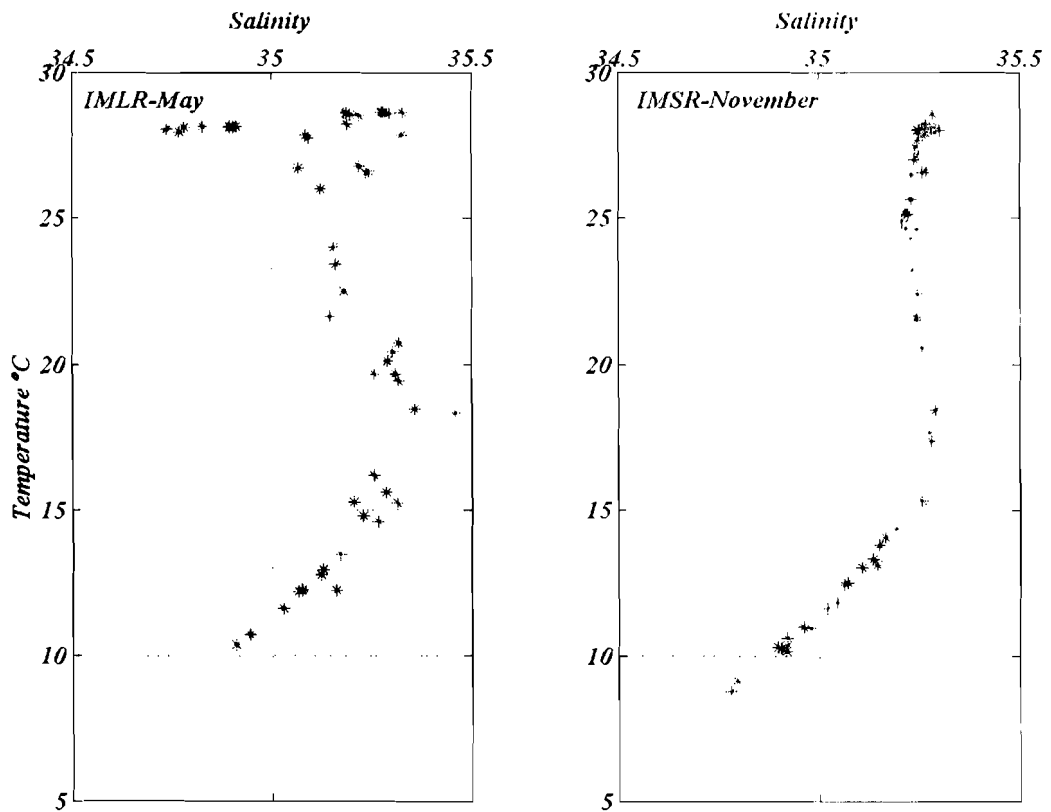
Figure 6.3.2.1a The T-S diagram illustrates the water masses found near the coast off Gazi Bay, in two panels (a) during May (IMLR) season and panel (b) November (IMSR seasons), (Source of raw data R.V. Dr. Fridgof Nansen 1982-85, KMFRI archives).

336

The second salinity maximum, at about 100 m, overrides a much cooler and fresher layer, which extends from 200m to 600m. Similarly the features are clearly emphasized in the second figure (Figure 6.3.2.1b) in which data from selected stations from R.V.Tyro 1992/1993 are used. The stations number is used are 107, 133,507, and 533.

The top layer of water is a mixture of the Bay of Bengal Water (BBW) from the Indian and Indochinese Subcontinent (Tomczac and Godfrey, 1994) and river discharge (Figures 6.3.2.1a-b; whereas we believe the subsurface maximum is caused by the high salinity end of Indian Central Water (ICW). Since the salinity maximum occurs within the thermocline layer (50-120m) we have referred to it as the BBW-ICW. Topography and seasonal reversals of the Somali Current influence the actual position of this maximum and structural complexity. The tongue of Arabia Sea water which William (1970) suggested as penetrating Kenya coast up to $3^{0}20'S$ and referred to as the "Somali water" is according to this classification, high salinity end of the ICW. However, the extent of the subsurface maximum as far South as Gazi is in agreement with Leetmaa and Truesdale (1972).

Intermediate and deep water

The T-S diagrams (Figure 6.3.2.1b) shows the complicated mingling of water masses at various levels. At the intermediate depth below the thermocline (200 – 2000 m) at least three water masses are capable of producing the complicated intermingling. The fresher layer below the maximum within the thermocline layer is due to the Australassian Mediterranean Water (AAMW) which is a tropical water mass derived from Pacific Ocean Central Water and formed during transit through the Australassian Mediterranean

337

sea (Tomczac and Godfrey, 1994). This is the water mass which Warren et al. (1966) and Invenkov and Gubin (1960) probably referred to as the upper branch of subtropical surface water of salinity 34.7 - 35.5 and temperature 7 - 15^{0}C. The salinity maximum that occurs in the layer 600 – 800 m and coinciding with the oxygen minimum is very likely caused by the Red Sea water which originates from north Indian Ocean and moves southward sinking to deeper water on account of its high density. The water below 1000 m, where oxygen concentration increases slightly, can be associated with the Antarctic Intermediate Water (AIW) with salinity less than 34.65 and temperature 3.5 - 7^{0}C. This water mass has its origin at the sea surface in the vicinity of the subtropical convergence near 40^{0}S (Warren et al., 1966).
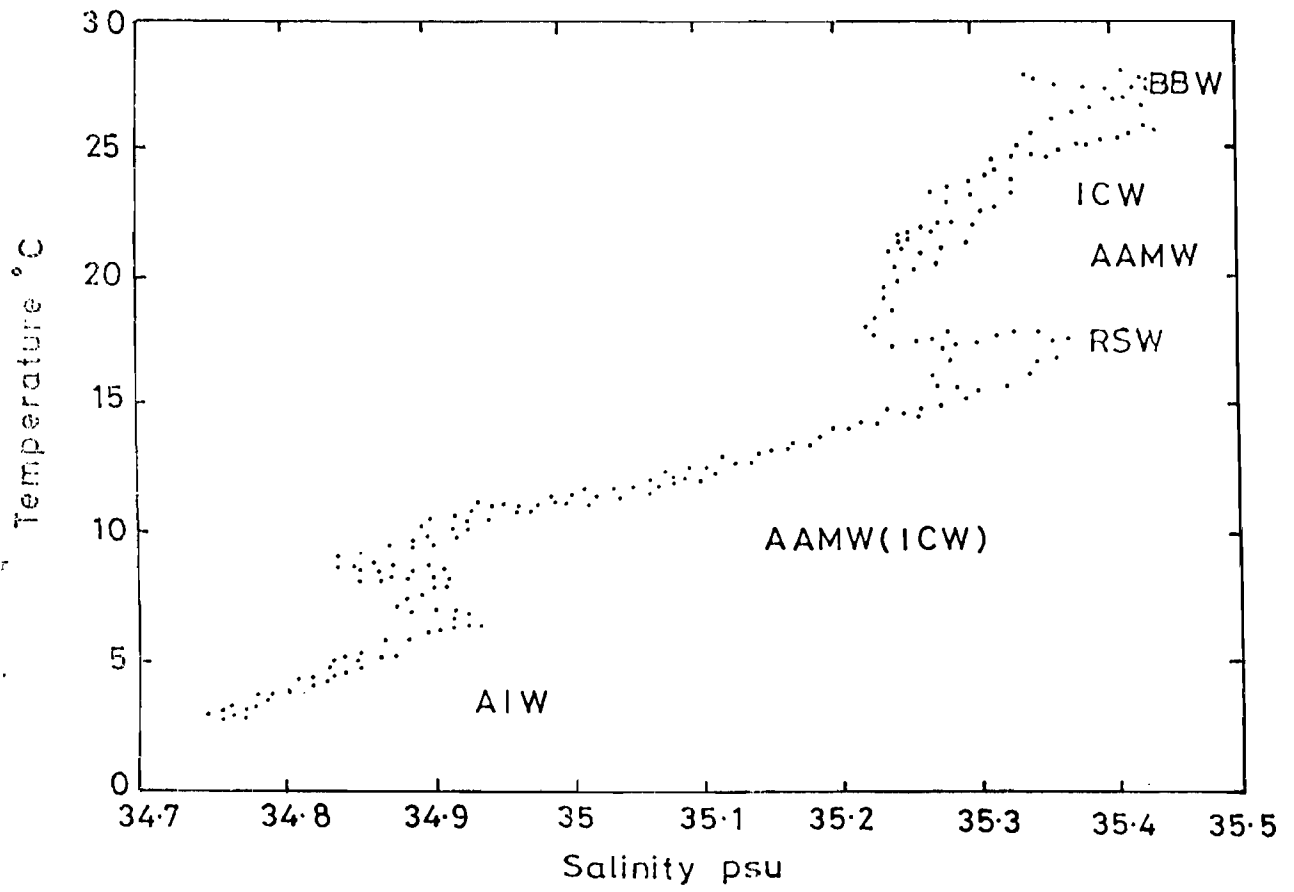
Figure 6.3.2.1b An example of T-S diagram illustrates the water masses found off Kenya coast (Source, R.V. Tyro 1992/93, Cruise).

6.4 NUTRIENT CONCENTRATION AND DISTRIBUTION

6.4.1 Vertical variation of nutrient off Gazi-Kilifi shelf

Nutrients and primary production were found to be relative low in the surface water during the two cruises, although they were slightly higher in December particularly in the northern transects. There was a general increase in nutrient with depth and away from the shallow stations suggesting that the nutrients were largely of oceanic origin. Above the thermocline silicate, phosphate and nitrate were less than 3 $m\mu l^{-1}$, 0.6 $m\mu l^{-1}$ and 2 $m\mu l^{-1}$ respectively. Nitrite was very low in June but appeared more in December with apparent maximum at about 70 - 100 m and a minimum at 20m. Further, silicate and nitrate, nitrite and phosphate variation with depth are shown in Figure 6.4.1.1 for June 1992, whereas Figure 6.4.1.2 show silicate and nitrate concentrations for three stations in the month of June/July. Phosphate and nitrite are also shown in Figure 6.4.1.3. In general nutrients were found to be low in the upper surface layer but increased within the thermocline layer.

In the intermediate water silicate, phosphate and nitrate showed highest concentration of 114$m\mu l^{-1}$, 2.54$m\mu l^{-1}$ and 36 $m\mu l^{-1}$ respectively with very low nitrite concentration. Oxygen concentration was higher in the upper layers of the surface layer with values between 240 – 200$m\mu l^{-1}$. The concentration fell to half this value between 150 - 300 $m\mu l^{-1}$ but dropped to minimum of about 60$m\mu l^{-1}$ in the intermediate waters. The position of this minimum occurred at about 400 – 800 m. The concentration increased slightly in deeper waters below 1500 m.

The position of this minimum occurred at about 400 – 800 m. The concentration increased slightly in deeper waters below 1500 m.

The higher nutrients and primary productivity especially in the deep water off Kilifi-Gazi shelf can be explained by the presence of another ecosystem different from that of that of Kilifi-Gazi shelf dominated by the EACC. This other ecosystem is that off north of Malindi Bay and characterised by the influence of the fresh water and arrival of higher salinity water from the north and complicated currents.

6.4.2 Inshore-offshore nutrient change

Table 6.4.2a indicates how offshore nutrients, oxygen, temperature and salinity change with depth off Gazi Bay. An example of how inshore nutrients (Stations I-VI) compare with those offshore for each season is illustrated in Table 6.4.2b.The highest nutrient concentrations occur in the IMLR season in the inshore areas, while the ocean shows very low concentrations during this time. The high concentration is associated with nutrient input from land as a result of large fresh water input in the inshore area. Nutrient concentrations are lowest in SEM season. In the IMSR season nutrients are lower than in IMLR season, an indication of less rain. In the Ocean the nutrients are higher in NEM season than in SEM season probably due to circulation mechanism that favors nutrient enhancement (see Chapter 7).

Table 6.4.2c also summarizes measurements by Kazungu 1998 in Tudor Creek, which were largely taken during the wet season. Norconsult also collected nutrients during various months and are also reflected for comparison. The results were obtained by averaging four samples and near bottom valued from samples collected in from station I-IV, VI and the ocean stations. The results serve to emphasize the availability of high nutrients in the inshore water during the IMLR season.

341

SO4 and NO3 (In Micro-Moles)

NO2 and PO4 (In Micro-Moles)
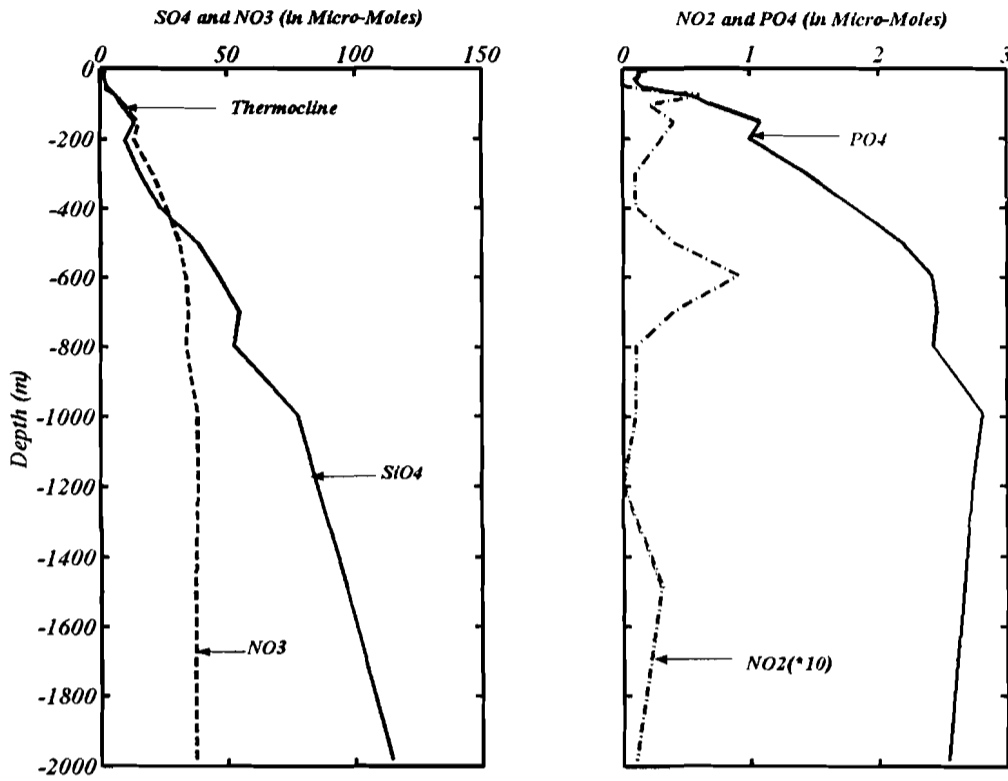
Figure 6.4.1.1 Vertical variation with depth of nutrients, Silicate and Nitrate

(panel, a), Phosphate and Nitrite off Gazi-Kilifi Shelf for June 1992.

342
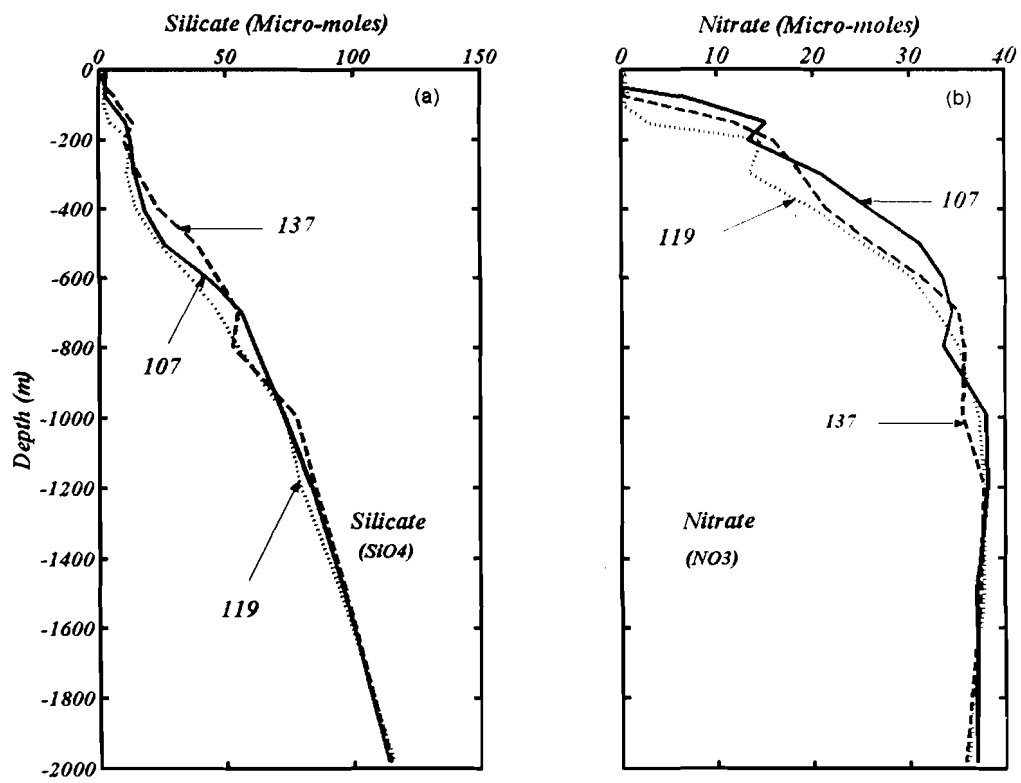
Figure 6.4.1.2 Vertical variation of nutrients: panel (a) Silicate and panel (b) Nitrate off Gazi-Kilifi shelf area for June and July 1992/3.
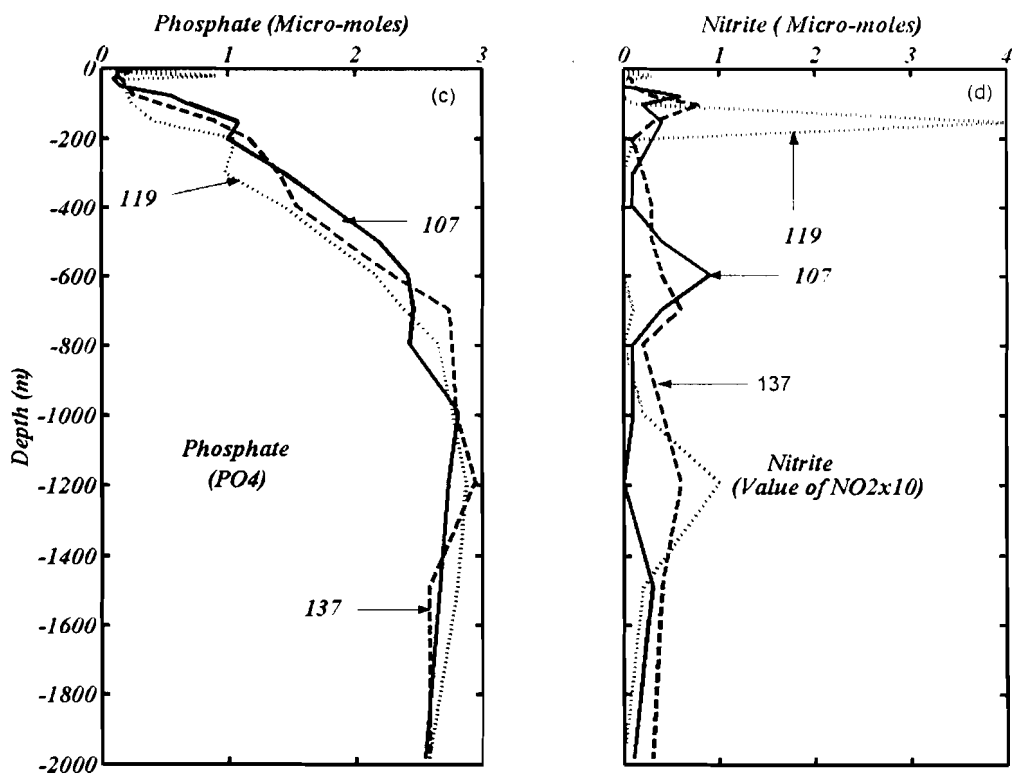
Figure 6.4.1.3 Vertical variation of nutrients: (a) Phosphate and Nitrite off Gazi -

Kilifi shelf area for June and July 1992.

2 ‹‹

Table 6.4.1a Nutrients concentrations with depth off Gazi Bay showing ammonia, oxygen, temperature and salinity

Depth(m)	Nutrients					Oxygen	Temp	Sal
	SiO_4^-	PO_4^-	NO_3^-	NO_2^-	NH_4	O_2		
0-8	0.6	0.21	0.10	0.00	0.08	220	28.10	35.35
10	0.9	0.22	0.11	0.00	0.08	230	27.94	35.34
25	0.8	0.25	0.05	0.00	0.09	220	27.85	35.34
50	0.7	0.27	0.09	0.00	0.09	220	26.18	35.34
75	6.9	0.76	8.40	0.67	0.08	160	22.06	35.24
100	11.0	1.09	14.34	0.02	0.09	140	18.31	35.22
150	13.2	1.26	16.75	0.00	0.11	160	13.78	35.10
200	12.1	1.27	16.87	0.04	0.14	190	12.06	35.05
500	35.3	2.12	29.58	0.11	0.09	120	8.88	34.86
700	56.9	2.63	34.81	0.02	0.06	80	7.99	34.89
1000	81.1	2.85	38.11	0.04	0.08	70	6.47	34.92
1500	103.0	2.83	38.19	0.01	0.08	100	4.37	34.85
2000	116.9	2.66	36.09	0.08	0.08	150	2.68	34.76

Table 6.4.2b Average values of Nitrate, Phosphate, Silicate for Gazi Bay stations I-VI and offshore during different monsoon seasons.

Date	Season	Stn I-IV			Stn VI			Ocean		
1996		NO_3^-	PO_4^-	SiO_4^-	NO_3^-	PO_4^-	Si	NO_3^-	PO_4^-	SiO_4^-
May	IMLR	16.6	1.12	124.50	2.00	0.42	36.00	0.2	0.09	3.7
Aug	SEM	0.14	0.38	18.00	0.32	0.53	3.50	0.06	0.14	2.51
Nov	IMSR	6.32	0.13	12.41	0.11	0.25	2.5	0.01	0.22	1.2
March	NEM	5.43	1.15	3.5	0.22	0.55	3.52	0.54	0.37	0.63
Annual mean		7.12	0.69	39.6	0.66	0.44	11.38	0.20	0.20	2.01

Table 6.4.2c Typical average values of Nitrate, Phosphate, Silicate for Stations I-VI in April, May and June (Source, Kazungu, 1998).

Season	Stn I-IV			Stn VI		
	NO_3^-	PO_4^-	SiO_4^-	NO_3^-	PO_4^-	Si
April	0.15-3.10	0.30-1.41	3.50-70.00	3.40-9.25	0.51-1.51	0.47-0.63
IMLR	2.80-52.0	0.36-0.64	45-64	9.30-28.50	0.68-2.04	116.00-185.36
June	0.15-0.72	0.22-1.02	4-13.80	0.15-0.60	0.42-0.62	0.13-0.27

6.5 SUMMARY AND CONCLUSIONS

Salinity structure indicated that both surface and bottom salinity varied from one monsoon season to another, although not by large magnitude. It was established that in the shallow reaches of the basin creek area low salinity water occurs in the upper reaches of the creeks due to river discharge, runoff and seepage. These areas have also large tidal range and as a result are well mixed. Temperature gradients exist from the shallow inner water to the ocean. The mean temperature difference between the creek and the ocean varied with tide and season. The maximum temperature occurs in NEM season (February-March) and to lowest in SEM (August). But increases less rapidly from mid-SEM to high values in NEM. For instance, in the creek the temperature increased from 22.75° C at the entrance to $24.86\ ^\circ$C inside the creek in November. The temperature was intermediary in the IMLR and IMSR seasons. The cooling is associated with cooler winds in SEM season that also drive cooler oceanic water into the study area from the southern part of the Indian Ocean via the EACC. A striking difference between, between IMLR and IMSR indicated that near surface sea temperatures could be due to the coupling between wind and the coastal flow and presence of remote water masses. The salinity also showed similar changes. It decreased from high values in NEM season to lower values during the onset of IMLR season and in earlier part of SEM season. For larger part of SEM season a longitudinal salinity gradient existed, but was more pronounced during IMLR season. This occurred just before the onset of the rains in March April where the difference between the ocean and the inner part of the creeks was observed to range between 5-16, depending on the amount of rainfall, creek and tidal

347

conditions. The structure differences were the basis for classification of the inshore water types: 'Masika SWT', 'Kusi SWT', 'Vuli SWT' and 'Kazikazi SWT'.

A complex shelf edge front, clearly identified during the wet period, suggested a feature that is formed by friction effect when the EACC comes into contact with shoaling shelf bottom. This was suggested as isolating the inshore water from the offshore .The front was also though as due to the wake caused by the Pemba Island which lie on the path of the EACC, and that it may coincide with the internal radius of deformation. The water off the shelf edge consisted of various water masses from different parts of the Indian Ocean.

Nutrients are generally low in the ocean surface layer although they were higher in the NEM than SEM season. Nutrient in the inshore water is higher than offshore. Nutrient increased with depth reaching maximum values within the thermocline region or just below it before changing almost uniformly with depth in deep water (depths>1000m). Oxygen has three maximums in the surface layer just below the thermocline and in the waters near 1600m. Two minimum values occur. One of the minimums occurs within the thermocline, and the other occurs below 600 and 1200m. The differences are cause by different water masses.

It was hypothesised that the EACC does not directly inject its water into the creeks, but rather the dynamics triggered at the beginning of the transition of the monsoon create conditions (events) which gradually propagate into the coastal area. The low salinity water appearing along the coast just before the onset of the IMLR season (Newell, 1959). They are partly due to the arrival of the front or its upwelling centre at the lower ends of the creeks; however, the warm temperatures are due to the

overwhelming solar radiation effect during NEM. The high salinity water in the coastal area at this end of NEM season may suppress intense localised upwelling along the shelf edge. See Kelvin wave upwelling events taken up in the discussion Chapter.

CHAPTER SEVEN

DISCUSSION ON CLIMATE, HYDROGRAPHY, TIDES AND MECHANISMS OF TIDAL EXCHANGE

7.1 CLIMATIC CHARACTERISTICS OF THE STUDY AREA

The meteorological observations for the 1995-1998 periods show that Gazi Bay, Tudor and Kilifi Creeks, like the rest of the Kenya, experience monsoon climate, with seasonally varying pressure, wind, humidity, cloud cover, rainfall, radiation, air temperature and evaporation. The observations confirm findings by previous workers, for example by Newell (1957, 1959), McClanahan (1999) and Okemwa (1989), whom, refer to seasonality in the context of two monsoon seasons. In this investigation we have considered climatic characteristics in the context of four seasons. The underpinning reason is the emphasis of fresh water forcing and the seasonal ventilation effected by non-local gravitationally driven water exchange. The four seasons are the Northeast monsoon (NEM) represented by the wind blowing from Northeast in the months between December and March. The SEM season is predominated by the southeasterly winds from June through October (Note, when reference is made of two seasons, the SEM period can be thought of as starting from mid-march to the end of October). The IMLR and the IMSR season are the onset of SEM season and NEM season respectively and represent the times when the monsoon wind bring rain in the study area, and in Eastern Africa as a whole. The rains occur in the months of April-May and in November respectively.

350

Observation indicated that for 1995-1998 stronger wind occurred in the SEM season than in NEM season. The IMLR season marked the passage of the Inter-tropical Convergence Zone (ITCZ) that ushered in the SEM season with cooler temperatures (25-26°C), and lasted up to October. The IMSR season occurred in November and from December to March the NEM was established by Northeast wind, which brought the usual dry warm (>30°C) temperatures in January and February. Cerdelöf et al. (1995) also report similar observations on Chwaka Bay in Tanzania. The variation of the atmospheric pressure is a key factor controlled indirectly not only by the distribution of air pressure at sea level, but also particularly by the movement of the ITCZ and through the associated wind systems (Wright, 1988). The climatic conditions observed in this study are supported by previous work. For example by Akoola, (1984) who rightly argue that the meteorological conditions along the coast depend on changes in low level pressure systems to the north and to the south, particularly near the Southern Hemisphere subtropical ridge and, the resultant wind changes. In the month of July, for example, the ITCZ is crossing over East Africa; by this time we have high pressure in the southern Indian Ocean and a low pressure over Arabia (Tomczak and Godfrey, 1994). This establishes a pressure gradient of 20mb and causes maximum wind (about $10ms^{-1}$) to blow over the study area. In January, say the peak of NEM, the ITCZ is established over Red Sea, and a low pressure (1010mb) occurs over southern Indian Ocean in the neighborhood of the Mozambique Channel and the Mascarene Islands. At the same time a high pressure (1020mb) occurs over Arabia, thus giving a lesser gradient of 10mb and hence less strong winds. The relationship between the movement of the ITCZ and the extent of the semi-permanent anticyclones in the Middle East and the southwest Indian

351

Ocean have been discussed by Sansom (1955) who has pointed out that the Southeast monsoon, was to a large extent controlled by the Mascarene high. Lumb (1966) has also discusses a weak pressure ridge that forms and extends to the northeast from the Malagasy region. He has also discussed the orographically induced ridge to the east of Malagasy Republic, which leads to a better defined trough between the East African Coast and Seychelles Island. The trough is probably the cause of a 'northeast-belt of clouds' casually observed off the coast of Kenya, almost every morning but particularly in the SEM season. The casual observation of cloud was useful for confirming the general passage of the ITCZ in the region, since the arrival of the front is marked by appearance of rain clouds followed by rain and change of winds.

More over, Ramsay (1971) investigated pressure gradient and the surface winds between the Kenya Coast and the region to the south and found a significant gradient and noted that pressure rise near 15°S lead to increases in the surface wind speed at Mombasa within 12 hours. Findlater (1994) showed that low easterly wind during IMLR and IMSR seasons develop into easterly jet.

In addition to the atmospheric pressure discussed above, the seasonal variability in air temperature, humidity and evaporation is also caused by the monsoon. As mentioned earlier, in 1992-1998 the SEM brought cool air from the south, increased cloud cover and reduced sun radiation, causing the air to cool and temperature to drop to as low as 24°C in July. This corresponded to an increase in humidity. With the reduction of clouds towards the end of SEM season the air temperature gradually increased, and was still high in November during IMSR season when the winds blow more or less eastward. The flow turned northeastward in NEM bringing with it dry and hot air from

the north causing the air temperature to reach maximum in February- March, which corresponded with the time of highest evaporation and low humidity. Decrease in temperature results in increase of relative humidity, since the capacity of the air to hold cooling lower water vapor and rise in air temperature results in decrease in relative humidity.

On daily scale humidity changes are due to daily evaporation from coastal and creek waters hence the observed humidity fluctuations during the night and early in the morning are 92-94% but drops to 60-70% in the afternoon. Diurnal variability of atmospheric pressure indicated that like humidity the pressure is higher in the morning than in the afternoon. The pressure difference is cause of land - sea breeze, which also reveals diurnal variability. The local winds strongly influence the Northeast monsoon but this influence appeared to be insignificant in the SEM season. The local winds are generally strong during the day and night and reach daily maximum velocity of about $9.5ms^{-1}$, with a yearly average of $6ms^{-1}$. More often the direction of local wind follows that of the main monsoon wind. Daily cycles of air temperatures were found to be almost smooth curves throughout the day, with only one high and one low point. The low points occur early in the morning between 5-6 a.m. While the temperature begins rising in the morning at about 8 a.m. and increases to a maximum between 2-3p.m. The fluctuations are probably caused by differential insolation on the ground. Since the ground radiates heat energy in relation to the fourth power of its absolute temperature, the temperature curves trend upward throughout the morning hours. The rise continues through out the afternoon and later in the evening. This is probably due to heating of the lower air largely by long wave ground radiation, which continues at a time the insolation albeit weak. The

353

annual curves for mean monthly temperature are somewhat similar to those of daily temperature. The highest temperatures occur in February-March (>30°C) when the sun is almost overhead and slowly moving to the north. This is the time of maximum insolation (time of equinox) and also the time when there is a considerable amount of clouds in the sky, which probably contribute significantly in heating the air by long wave radiation. The air temperature, although expected to be lowest in June and December which are the summer and winter solstice when the sun is furthest to the north and south respectively, show minimum air temperatures in August only. This can partly be explained by the loss of heat through enhanced evaporation by peak monsoon winds and clear skies in July and by the cooling caused by the Southeast monsoon winds. There appears to be no lag between insolation and annual temperature.

Variability in climatic parameters is also primarily caused by radiation. Air temperature both in annual and diurnal time scales can best be described on the basis of the solar radiation incident in this area. The radiation was highest in between November and March and lowest between May and July. The yearly average was about 200 W m^{-2}, with monthly variation between 175 and 239W m^{-2}. The values from weather mast agree well with the long-term values, and falls within the range of 40 Wm^{-2} to over 350 Wm^{-2}. The values generally increase from south of Gazi to north of Kilifi indicating, along the coast, differences in solar input for the each creek system. It appears the boundary shift occur slightly north of Kilifi and shift furthest north /south during the month of July-August/January-February respectively. These correspond with the peak summer seasons for the northern and the southern hemispheres respectively and the position of the ITCZ.

354

Although time series variability in solar radiation were observed with the weather mast there was a slight difference when compared with radiation values obtained from other coastal stations e.g. MIAMS, and is probably evidence for spatial radiation patterns. Spatial pattern has been studied in Kenya before (Obasi and Rao, 1976a; Okoola, 1982; Ogallo and Rumamu, 1998) whose studies focused on the spatial and temporal characteristics of the extreme solar energy over 40 Kenyan locations using the daily maximum and minimum total radiation energy values. Their maximum value ranged from about 300 to over $400Wm^{-2}$. The minimum values were however below $50Wm^{-2}$ at some of this location indicating large diurnal and seasonal ranges between the maximum and minimum power values. The largest power values were concentrated within December to March corresponding to the month of maximum evaporation. This is the time when most part of the coastal region has low cloud cover.

The magnitudes of the power values were relatively low during IMLR and IMLR seasons as a result of dominant cumululiforms clouds. which caused depletion of the available solar radiation in the atmosphere and reduction of loss of heat from the creeks by the long wave radiation. Under typical overcast conditions, the heat loss of the earth is reduced to about 15% of the loss with clear skies. The months of July and August are also dominated with Stratford clouds and low-level temperature inversion (Ogallo and Ramuna, 1998) and hence are accompanied by low solar values. Observation of the predominant direction from which the rain arrives at the coast has shown that the short rains appear to approach from the mainland. Thus suggesting that they are probably caused by the influx of the unstable moist air mass from the Atlantic and moist Congo/Zaire basin, which are locally known as the Congo Zaire air mass.

7.2 DISCUSSION ON SEASONALITY IN HYDROGRAPHIC PARAMETERS AND WATER EXCHANGE

Fresh water in put, decrease in salinity and estuarine circulation

Due to the semi-arid nature of catchment of Gazi Bay, Tudor Creek and Kilifi Creek, the rivers entering these shallow ecosystems are merely seasonal and hence fresh water input into the creeks is dominated by runoff and that high runoff implies a high total fresh water input or discharge. The fresh water input as well as excess evaporation has profound impact on the creek and the adjoining coastal waters. During the IMLR and IMSR seasons, the water level in the creeks increases rapidly the effect increases seaward transport and flushing of brackish or the seasonal water types. As a result the turbidity, in the main creek channels and the adjacent coastal water increase because of sediment-laden runoff. Density-driven or gravitational circulation then takes place within the creek coastal boundary layer or coastal fronts. Such boundary is viewed as commonly occurring near-shore water mass and mixing zone that exhibits characteristics of estuarine environment, rather than continental shelf waters (Kjerve, 1984). As the fresh water discharge rate increase so does the total load of sediment washed into the creeks and the size of the creek plume debauched to create a much extensive coastal boundary plume. The fresh water discharge and flooding in the upper creek areas causes large shifts in salinity particularly in the upper reaches of the creeks (e.g. Figure 5.4.1.1e). As the runoff from the catchment areas peaks up within the shallow mangrove fringed basins the resident water is rapidly advected out of the systems and salinity drops in the creeks, to low values, such as was observed in IMLR season (Figure 5.4.1.1e). Hence, variations of

356

discharge affect the salinity supply in the creeks, causing longitudinal temperature and salinity differences. Baroclinic forcing is due to salinity differences. The fresh water added to the inner creek basins are mixed by the tide with the ambient water into homogeneously mixed water types characteristic of each season as mentioned earlier.

Decrease in fresh water input and evaporation effect on circulation

As decrease in precipitation occurs (Figure 5.1.3.6) after IMLR and IMSR seasons respectively and the diminution of fresh water discharge (Figures 5.1.3.1 also occurs (Figures 5.1.3.8), the salinity in the creek returns at an exponential rate to previous levels. This was indicated by increase in salinity towards the end of SEM season. Tidal mixing causes the change. It should be noted that also when this mass flux become negligible during NEM season, the salinity increases further beyond the oceanic value of 35 to values ranging from 35.2-36 (Figure 5.4.1.2h). The excess salinity values are most likely caused by evapo-transpiration, which has two effects. First, the water left behind becomes saltier, because only the water and not much of its included salt is added to the air; the remaining water becomes cooler due to the loss of heat during the evaporation process. Secondly, the heat that is lost from the creeks is added to the atmosphere, thereby warming the air adjacent to the water. Thus much of the heat transferred from the systems to the atmosphere is transferred through evaporation. The increase in salinity (salt content) and the decrease in temperature make the remaining water denser (heavier per unit volume). This means that the cold salt water, which is heavier, occupies less space than it would if it were warm fresh water. Because water has been lost directly to the air and because the remaining water occupies less space due to increased density, the

surface of the water in the systems is actually lowered by evaporation (this is part of the negative circulation). This means that as evaporation increases to maximum values in NEM season a reversed density gradient develops from the ocean to the shallow inner basins in the creeks, the result is negative estuarine condition that produces a reverse baroclinic forcing in the creek. Evaporation almost exceeds precipitation almost through the year. During much of the SEM and even at the times of IMSR the salinity rebounds to original high values. In NEM season minimum evaporation occurs, and coincides with periods of maximum salinity before the mass influx brings the salinity down to minimum values in April-May-June. Thus the monthly change in the mean sea level is essentially influenced by the differences between each season averages of net inflow and evaporation.

Elsewhere, there is evidence to support this. For example, Sikora and Kjerve (1985) reports of a restricted lagoon, much like the creeks considered here, in Lousiana, where the lagoon become totally fresh within two days of the opening a spillway during May-July 1973 flood on Mississippi River. After the flood receded and the spillway structure was closed, it took three months for the salinity to return to its pre-flood level of 5.

It is interesting to note that the rebound in salinity occurs from November to March a time when the increase in mean sea level from one month to another is appreciable, which can be seen as mirroring the spring tide. Also the minimum net inflow takes place in April-July when the mean sea level is decreasing at the creek entrances. It appears evaporation and precipitation drives negative and positive estuarine circulation. Elsewhere evidence exist, for example, Bogdanova (1974) on his

investigation of water exchange in the Red Sea through the Strait of Bab-el Mandab, on the basis of observations made by Morcos (1959), found that evaporation drives negative estuarine circulation. A schematic showing the type of circulation that is envisaged for this 'trans-monsoon' inflow-outflow mechanism is depicted. Fresh water with denser saline oceanic water in the creek channel results in inclined isopycnals and isobaric surfaces. The surfaces, along the axis of the creek that slope down towards the ocean in the surface layer and drive a residual seaward current.

Moreover in addition to localised evaporation in the creek, relatively warm water with high salinity observed in early month of NEM season, is advected southward by the Somali Current (Swallow et al., 1992) is probably responsible for the increase of salinity shown in Figure 5.4.1.2h. For example, in lower Tudor salinity and temperature follow similar patterns, during the investigation salinity and temperature were about 30 and 28°C respectively. In mid-Tudor the estuary the salinity were shown to be 28. Thus along channel temperature remained more and less uniform but salinity varied from 27 to 30.5 indicating salinity gradient of 3.5 (example, Figures 5.4.1.2f and 5.4.1.1f). The gradient is however not as strong as would be expected during rain period and suggested small rainfall and river influence in the shallow and wide reaches of the inlet at the time of study. A front, was observed within the creek between the shallow basin brackish water and the channel near Ras Juda, and separates more saline water in the channel from the less saline water in the shallow inner basin. The water in this area showed a strongly turbulent zone with water tending to rotate clockwise during flood and vise versa during ebb near Ras Juda and the disturbances extending a considerable distance down stream. The front may indicate internal hydraulic control, with sub-critical conditions within the

shallow estuarine basin changing to supercritical in the plume. Kazungu (1996) had observed similar front occurred in the same neighbourhood. The channel is very dynamic part of the creek systems and can be considered as a frontal zone dividing the shallow mangrove-fringed inner basin from the ocean. One can then imagine the front being push back and forth like a piston in some part of the creek and above the shelf slope.

7.3 CIRCULATION, CURRENTS AND TIDAL HEIGHT CHARACTERISTICS, AND WATER EXCHANGE

Baroclinically driven circulation governing net water exchange

The currents patterns inside the shallow mangrove fringed basins, in the channels and beyond are altered by strong baroclinic forcing with the river discharge and runoff. Fresh water is appreciably lighter than the salt water and makes its way through the creeks it as a surface layer it absorbs and entrains some of the saltier water from below as it progresses. Therefore the saltiness of the surface layer increases longitudinally (down-creek) as observed (Figure 5.4.1.2e), while that of the lower layer decreases up-creek. In this manner there is no loss of salt within the creek as salt entrained and carried seaward by the top layer is replaced by an increased inflow of salt in the bottom layer, thus creating estuarine circulation. In the creeks investigated a two districts layer situation was not evident, there being a small difference between the surface water and the bottom water and on account of large tidal prism and small river discharge. However, true estuarine circulation, albeit ephemeral and during periods of large runoff and river input with would probably occur in the uppermost parts of the secondary creeks that constitute

the mouth of the seasonal rivers such as Kombeni and Mkurumuji. Often the "jet" of river that enters the mangrove-fringed secondary creeks and the shallow inner basins remains partly intact, and moves down the small channel as a thin ribbon of brackish surface flow.

The estuarine circulation and the circulation generated by wind set-up in some parts of the inner basin or by wind blowing directly along the creek channel constitute gravitational, non-tidal or residual circulation related to residual sea levels. Some evidence for this occurs in Gazi Bay (Figure 5.3.2.9) where the residual oscillations are larger than those of Tudor Creek (Figure 5.4.2.1a, panel c) which is more protected from wind influence from the open sea. The large shallow water and peripheral lagoons observed in the creeks might also give rise to residual or secondary circulation that is responsible for net exchange of water between the creeks and the ocean. Casual observations revealed that secondary circulation were evident in embayments and near promontories. For example a known case is one in Tudor Creek near KMFRI characterized by a clockwise eddy during ebb (Kimaru, 1986).

Tidal currents, direction and asymmetry

Tidal current and direction presented, for example in Figure 5.3.2.3a for measurement taken close to the height of spring and ending close neap period, show tidal currents are greater during spring than during neap and also showed semidiurnal as well as diurnal and fortnightly spring neap variations. The greater tidal currents means larger volumes of water are exchanged across any given cross-section during spring than during neap on account of larger tidal prism. The currents as well as the surface currents were

361

found to change magnitude with time and tidal heights and behaved differently in each study site. Currents are fastest during spring than during normal tide and neap tide. This of course is expected given the differences in the tidal prism in each creek. Maximum current velocities are experienced at mid-high water and mid-low water. Extremely low current velocities characterise slack waters. Surface current were greater in the main channels, but decrease inside the inner creeks basins on account of channel effect in the inlet, and reduced velocity by friction through shoaling depths and widening in each inner basin. Currents were found to be slowest in Gazi Bay where no channelling effect is present. There is a tendency for the water to rotate clockwise, during flooding stage, in the shallow inner basins.

In Tudor Creek with its peculiar headlands and more coves than the other two systems, side eddies were formed in the coves of each side of the headlands and showed opposite sense of rotation. One unique characteristic of circulation in Tudor Creek, is the presence of, clockwise eddies generated at the entrance of Tudor Creek and carrying with them plume suspended from the creek bottom during peak flood stage. Currents in each creek showed variations, which were probably, related to the tidal prism differences and probably influence of wind or seiches.

In the mangrove tidal creeks, no strong ebb-flood current asymmetry was observed as the magnitude of ebb and flood currents are almost of the same level. Measurements conducted during the pre-NEM showed the flood currents to be dominant in terms of magnitude and duration as compared to ebb currents.

Such currents have been found elsewhere to enhance the export of nutrients from the inner mangrove areas to the open waters (Wolanski et al., 1980; Pylee et al. 1990; Van de Kreek, 1976).

Diurnal inequality

Diurnal inequality, that is the difference in height between the higher high water level and the lower low water is not equal and, is more pronounced at spring period when the fluctuations are largest. Topographic influence was not evident in the tide gauges records moored in relatively deeper water near the entrance or mind channel in Tudor and Kilifi Creek. However for mooring in the shallow depths for example, in Gazi Bay, and the shallow water parts of Tudor Creek (Jomvu Kuu), the lower part of the spring period the inequality was removed and the curve distorted due to friction. During neap the inequality is less observable particularly in the lower parts of the curve, hence, indicating that the effect felt during spring low water is less felt during neap. However, inequality is removed at the top during two to three cycles in neap; probably as a result of thermal influence as suggested elsewhere in this study. The tidal amplitudes during neap are reduced by almost 30% of their spring values. There is also the diurnal inequality between lower low water and higher low water and a daily inequality in the time intervals between pairs of high tides.

The tides cause a twice-daily exchange of water between the inner creek basins and the ocean. Basically, the changes occurred because the volume of water from the inner creek basins and the entrance areas was carried into the middle of the creeks and mixed. The simultaneous response of temperature during low (ebb) and high (flood) water for example in Gazi Bay, clearly illustrates this point. At low tide the oceanic water, the mid-

363

reaches and the water from the inner bay areas all appear to have temperature close to each other and relatively lower compared to that in the upper reaches of the bay. During high water however the cooler oceanic temperature is found at the entrance and the highest temperature in the upper reaches. This also indicates that during flood the different water types occur in different parts of the bay. Water types can also occur in relation to seasonal characteristics and this has already been pointed out in Section 6 where it was suggested as a basis for various seasonal water types. During ebb the mixed water has lower temperatures and displays more stable water mass reflected by the closeness of the temperature curves.

7.4 THERMOCLINE RESPONSES AND ITS EFFECT ON WATER EXCHANGE

The circulation off Kenya coast was referred to in the introduction. Various key coastal currents were mention that shift speed and direction with seasons. On the discussion referring to seasonal mechanisms that influence the water exchange we focus more on the EACC and the Somali Current. Figure 7.4.1 is 3-Dimension schematic diagram bringing together the SEM season (Panel (a)) and NEM season (panel b) response of current direction, thermocline, and depth range of the BBW-ICW (Section 6.3.2). Additional responses, which are listed in panel (b), and indicated in panel (a), are reversed in SEM season. We now look at the mechanisms underpinning the deepening of the mixed layer and the strengthening of the thermocline in the offshore waters and consequently shoaling of the thermocline.

A combination of factors mainly related to flow is at play. In SEM season and particularly in July-August Southeast winds are in their maximum strength and correspondingly the EACC reaches its maximum speed of more than $2ms^{-1}$ (Newell, 1957, 1959, Swallow et al., 1992) along the coast and mainly directed northwards in Gazi-Kilifi shelf area. Viewed in south-north direction, the Southeast winds would produce down-welling favourable conditions on the Kenya shelf as indicated in Panel (a) in Figure 7.4.1, where the BBW-ICW thermocline is schematised as down welling to 150m. In the Northern Hemisphere the Somali upwelling occurs during this season. The effect of the strong monsoon winds during this period mixing is enhanced and an almost homogeneous surface layer and deepening of the thermocline to about 80-120m occurs (Morgan, 1959). We found the themocline to be at 75m during for SEM season. In the creeks, during SEM season, the variations of surface temperature, salinity, rainfall, wind and waves of the Kenya coast reflect the observed changes.

The upwelling favourable conditions for NEM season are also schematised in the three-dimensional Figure 7.4.1. In this schematic the BBW-ICW thermocline is shown to occur a depth of 50m.
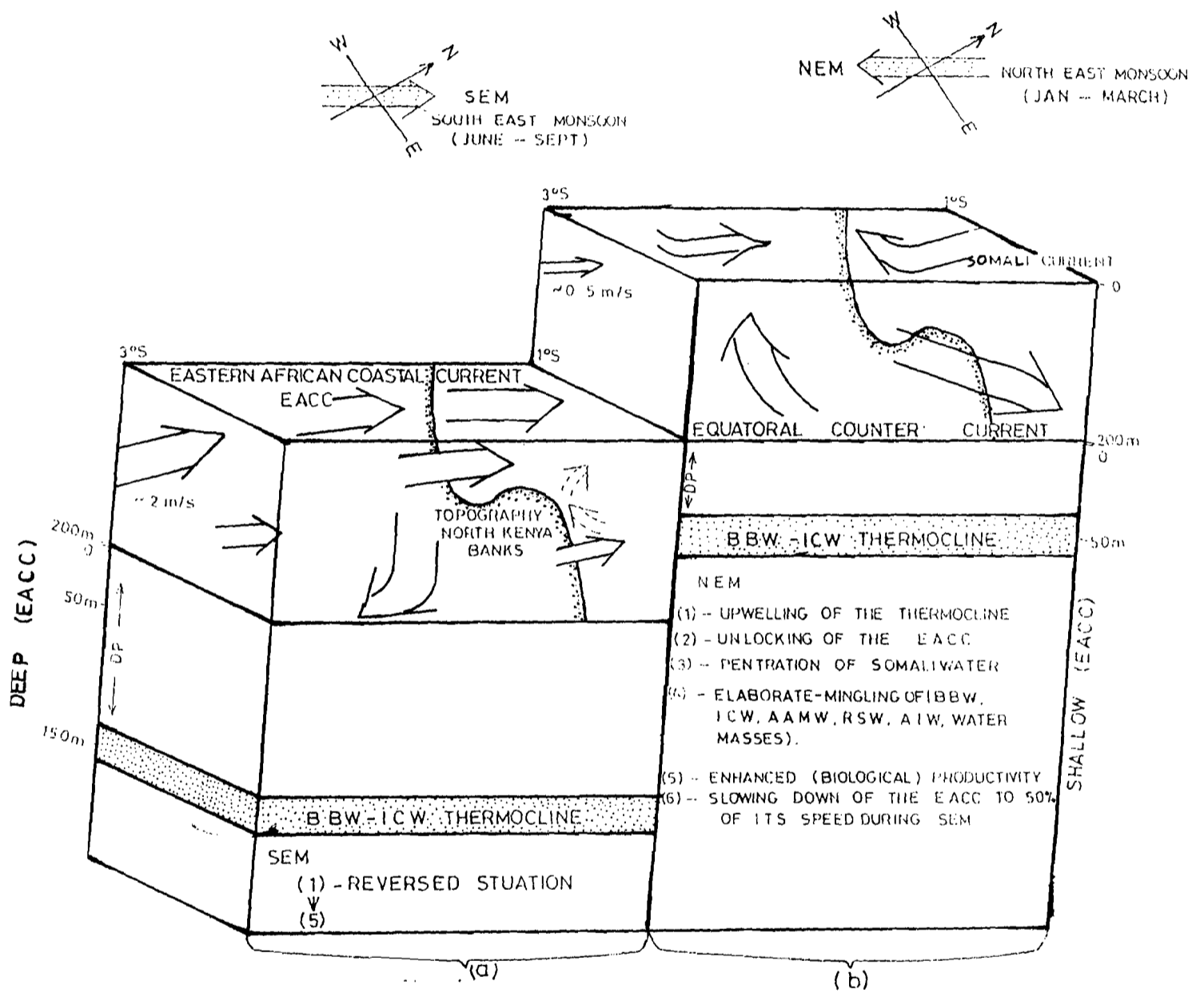
Figure 7.4.1 3-D schematic diagram showing the SEM seasonal (panel a), and the NEM season (panel b), response of current direction, thermocline, depth range of BBW-ICW and other effects.

We can further speculate on the effect of the offshore currents dynamics on the creek-ocean water exchange. Johnson et al., (1982), argued that vorticity change at the North Kenya Banks (NKB) was responsible for switching the EACC. It can be suggested that during SEM season the EACC merely serve to increase the distance between two juxtaposed ecosystems (EACC and SC) which can be visualised as having two different surfaces of constant potential temperature. As the surfaces move apart due to increasing wind the EACC overshoots the NKB and greater rate of spin or vorticity ensures. As the potential vorticity increases, hence the thermocline deepens and the surface layer become homogenous (see shelf slope of Figure 5.4.1.1e and 5.4.1.2e) while the sea level falls, as water is drawn form the EAB. Increased coastal flow across the entrance to the creeks implies rapid exchange as the estuarine plume exiting from the creeks is quickly advected from the entrance and replaced by different water. During this period a tongue of low salinity from the previous IMLR season, can be observed along the coast near the Pemba channel as see in the Indian Ocean Atlas (Wyrtki, 1972). It is likely that such water gravitational circulation in the creeks and promotes rapid exchange during IMLR season as well as in the earlier period of SEM season.

During NEM season, the potential vorticity is such that the EACC gains in potential energy, and the flow of the EACC is reduced almost by half. The sea level rises as the water backs up in the south due to wind reversal and anti-clockwise circulation, e.g. when NEC is established in the Arabian seas. Note the current is northward of northward off Gazi Kilifi offshore area. To the north of Kilifi Creek in the region of Malindi-Ungwana Bay area the current is to the south (Jonson et al., 1982). During this period however an equatorial jet ensures that water is drawn away from the coast by the

ECC (Findlater, 1972). Such a flow and the easterly winds ensure upwelling favorable conditions, which may be visualized as schematized in panel (b) Figure 7.4.1 on the Kenya shelf. Shoaling of the thermocline occurs after November, as mentioned by Kabanova (1968), and may be as high as 50m at the peak of the NEM season as schematized in panel (b) of Figure 7.4.1. Further evidence is seen in Figure 7.4.2 where the isolines (above 50m depth), for different oceanographic parameters in various cross-sections, up-well (Source Dr. R.V. Fridjof Nansen Data 1982-1985). Thus during the IMLR and NEM season the water surface has warmer and lighter water floating on the top of a much deeper layer. During this period the main thermocline taken as the base of the surface mixed layer and appeared at 43m its position being estimated as the location where the temperature is one degree below that on the sea surface. Morgan, (1977) gave the position as 50m. The slight difference could be due to non-specification of the explicit month the measurements were made, as the position could be different depending on the wind regimes at the time.

The implication of a shallow thermocline close to the creek entrance is evident. Since the ebb current speed may reach close to $1ms^{-1}$, it is likely, to lift the thermocline water from a depth 50m and entrain it in the lower part of the plume and later drive the seawater into the inlet during flood. The mechanism has been referred to as tidal pumping (Wolanski, 1980) and has been shown, for ebb currents of $1ms^{-1}$, water can be drown from a depth of 100m. We note also that the upwelling is probably initiated in October by an eastward equatorial jet caused by westerly winds (Findlater, 1972; Wyrtki, 1973; Duing and Schott, 1977; O'Brien and Hurburt, 1974), which appears during the inter-monsoon months.
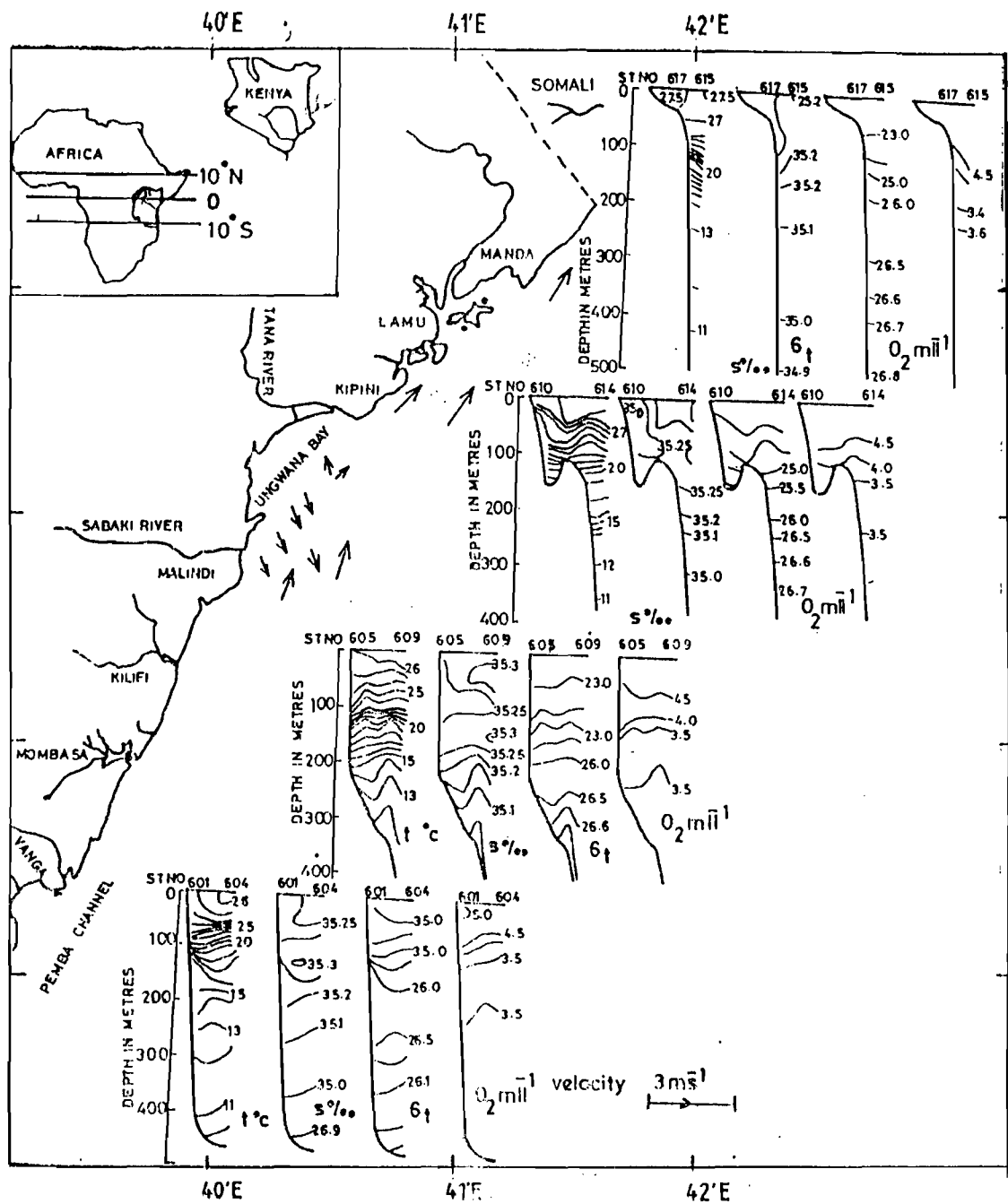
Figure 7.4.2 Composite diagram showing cross-section (I-IV) for temperature,

salinity, density, oxygen and currents for December off Kenya Coast (Source, R.V.

Tyro). Note, upwelling isolines in the surface layer.

To add more on the evidence to support upwelling favourable conditions we point out that Stomel et al., (1992), has shown that there is a tendency for offshore water to leave the coast, between Pemba and Malindi. In addition from heat budget, Hastenrath and Lamp, (1980) have argued that the area north of 10°S along the East African Coast and Arabia play a substantial role in the heat budget and vertical motion of the northern Hemispheric Indian Ocean for the year as a whole.

Another reason is that the three study areas are close to the upwelling equatorial region. It has been estimated the total heat loss from May to August is $\sim 2.8 \pm 2.0 \times 10^{21}$J whereas the net heat gains from September to April is $\sim 4.6 \times 10^{21}$ J (Hastenrath and Lamb, 1980).

7.5 MECHANISMS OF WATER EXCHANGE IMPLICATION TO ENHANCED BIOLOGICAL PRODUCTIVITY

Biological scientists from the region have insisted that the physical oceanographers explain to them the physical mechanism leading to the occurrence of high biological productivity on the shelf both in terms of plankton and fish landing, particularly in the immediate slope waters near the creek entrances, during NEM. Recent observation (Ruwa, per comm.) indicates that the waters in the creeks are more productive in the SEM season whereas waters at the entrance and coral reef areas are more productive in NEM season (see Pugh, 1984). Pugh attributed the unusually enriched water to decay matter related to periods of exposure in the inter-tidal zone. Biological

enhancement in the reef area can be related to periods of submergence and exposure of the inter-tidal areas.

It can also be related to localized upwelling in reef channels such as noted by Wolanski et al. (1980), on study of tidal flow through Ribbon Reefs in the northern Great Barrier Reef of Australia. However, these two explanations in part explain enrichment process. There other explanation most likely is caused by intricate interplay between the terrestrial and oceanic influences on in the coastal ecosystems, and particularly as it relates to water exchange processes and circulation mechanisms.

The response of the shallow inner mangrove basins to seasonal dynamics related to the monsoon can be understood better by comparing the response to tidal rhythm. The high sea level in the NEM season and low sea level in the SEM season can be viewed as similar to flood and ebb tides. Thus the meeting of the EACC and SC resembles like 'backs up' of the acts like flood tide, albeit on annual time scale. So the water on the shelf and in the creeks 'floods' during the NEM season whereas it 'ebbs' during the SEM seasons. We can infer from this argument that, as a general rule, the shallow mangrove fringed basins dynamics and creek morphology are controlled by lowering of the sea level during SEM season. Thus we associate the creek scouring and erosion processes in the creeks with the SEM season, since ebb tides are associated with this processes phenomena (Ranwell, 1972). Similarly accretion processes can be seen as occurring in the NEM season. There are inshore and offshore circulation patterns or mechanisms associated with this seasonal 'floods' and 'ebbs'. The mechanisms can be linked with biological enrichment. Figure 7.5.1a are presented for the purpose of suggesting mechanisms responsible for biological enhancement and fish landings. During the NEM

season, excess weather conditions lead to the occurrence of highest salinity and temperature in the creeks and in the offshore (see Figures 5.4.1.1e and 5.4.1.2e). The hypersaline condition occurs in the creeks shallow basins due to excess evapo-transpiration. This condition is enhanced by diminished of fresh water input during NEM season. The result is the production of dense water, which locally induces a net clockwise circulation in the shallow water basin, as shown in Figure 7.5.1a cell A. At the ocean side warm water of high salinity and temperature albeit of slightly lower values than those observed within the creek are transported into this region from the northwestern Indian Ocean. During this time the sea level is high and the thermocline is close to the surface (See Schematic 7.5.1a). Because of temperature, and reduction of density between the base of the thermocline and the surface water, increase in vertical transport is expected (cell B of Figure 7.5.1.a) hence the nutrients move (diffuse) from lower water to the surface. Evidence for the circulation B, the upwelling NEM upwelling favorable condition is shown in Figure 7.4.2 by upwelling isolines in the surface layer (0-50m).

During SEM season the fresh water condition are much weaker (Figure 5.4.1.2g). Plausibly, the gravitational circulation pattern that is set up within the creeks and ocean water at the slope is that of dry condition and is depicted in Schematic Figure 7.5.1c. Figure 7.5.1d is a COMEC-model schematic for the SEM season down-welling favorable conditions.
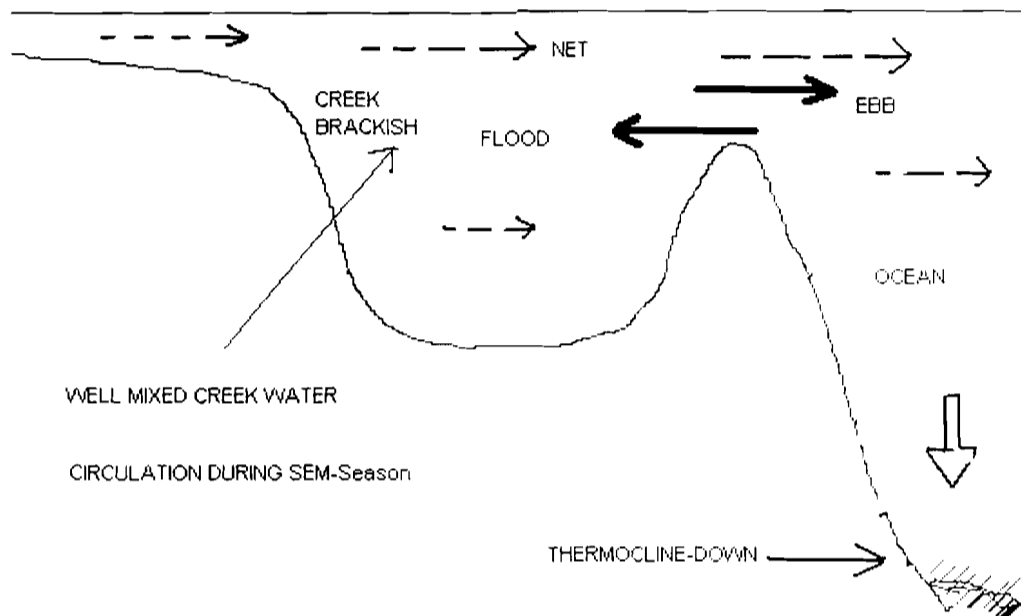
Figure 7.5.1c Schematic model showing internal creek circulation during SEM season when positive estuarine conditions prevails and thermocline down-wells.

The SEM season hydrographic conditions in the creeks are such that a net clockwise (gravitational) circulation induced by fresh water condition during the IMLR season persists. The brackish water conditions gradually recede into the creeks with the diminishing fresh water and the gradually encroaching southern ocean oceanic conditions

376

MIXING ZONE

A

CREEK INTERNAL NET
CIRCULATION

NEM-Season

FORCED SHELF
CIRCULATION

OCEAN

B
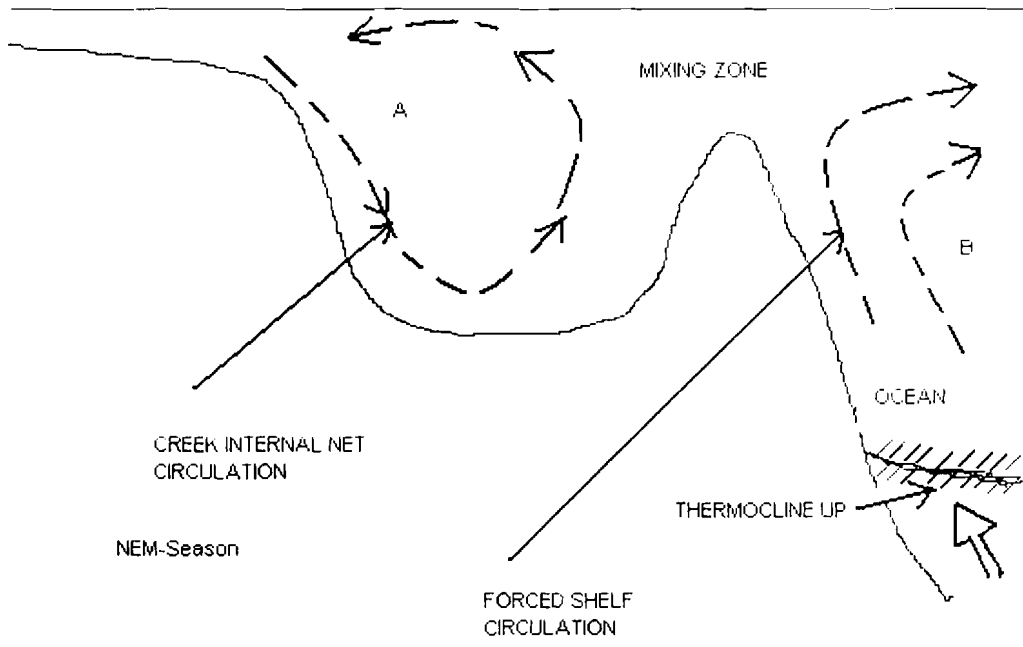
THERMOCLINE UP

Figure 7.5.1a Schematic model showing internal creek circulation during NEM season when negative estuarine (dry-season) conditions prevail, and thermocline response on the shelf.

The upwelling tendency coupled with Ekman transport produces an upwelling favorable circulation scenario at the shelf slope as mentioned earlier, thus causing nutrients to be available at the slope. Gradual increase in salinity inside the creeks imply that the net movement of water is from the ocean into the creeks, a process that is probably speeded by the Equatorial Jet stream (Findlater, 1973) associated the Ekman process. In addition higher values of sea level in NEM, implies increased flow and hence more stirring of the bottom sediment on the leeward side of the reef. A large volume of seaweed on beaches, during NEM season, indicates increased speed of currents on the shelf edge and in the lagoons (Fishery Dept. comm.). Increased currents may mean greater out-welling estuarine and coral plume in inlets that cut across the fringing coral reef, thus again favoring higher biological productivity scenario.

The foregoing are just simple explanations of an otherwise intricate response of the shallow ecosystems (eco-response) to the inter-monsoon and monsoon cycles. Figure 7.5.1b depicts a cross-shelf eco-process schematic for transect across the coast illustrating the processes of the upwelling favorable scenario, created as the result of ocean-ward drift, albeit of the sub-surface layer, following the convergence of the SC and the EACC. Notice that the cross-section cuts across a number of coastal ecosystems e.g. the shelf-slope, the coral reef, the seagrass and the mangrove-creek environment, which constitute the most important critical habitats (Ruwa, 1996) in these equatorial internal waters. This can be referred to as 'Creek-Ocean-Monsoon Eco-process model ' in short 'COMEC-model' which is a conceptual presentation of multi-process conditions that lead to hydro-meteorological variability that in turn lead to enrichment of coastal waters and fisheries of the EAB. The implication is that shelf-break upwelling occurs, intense tidal mixing

374

and pumping at leeward of the fringing coral reefs, elevation of the thermocline is due to the enhancement of the vertical motion north of 10°S as pointed out by Hastenrath and Lamp (1980). The events can also be linked to monsoon driven Kelvin waves (Gill, 1982) along the East Africa Coast. The outcome of this process is that the biological activities and fish landings for both commercial and artisanal fishery (Nzioka, 1979) are enhanced.
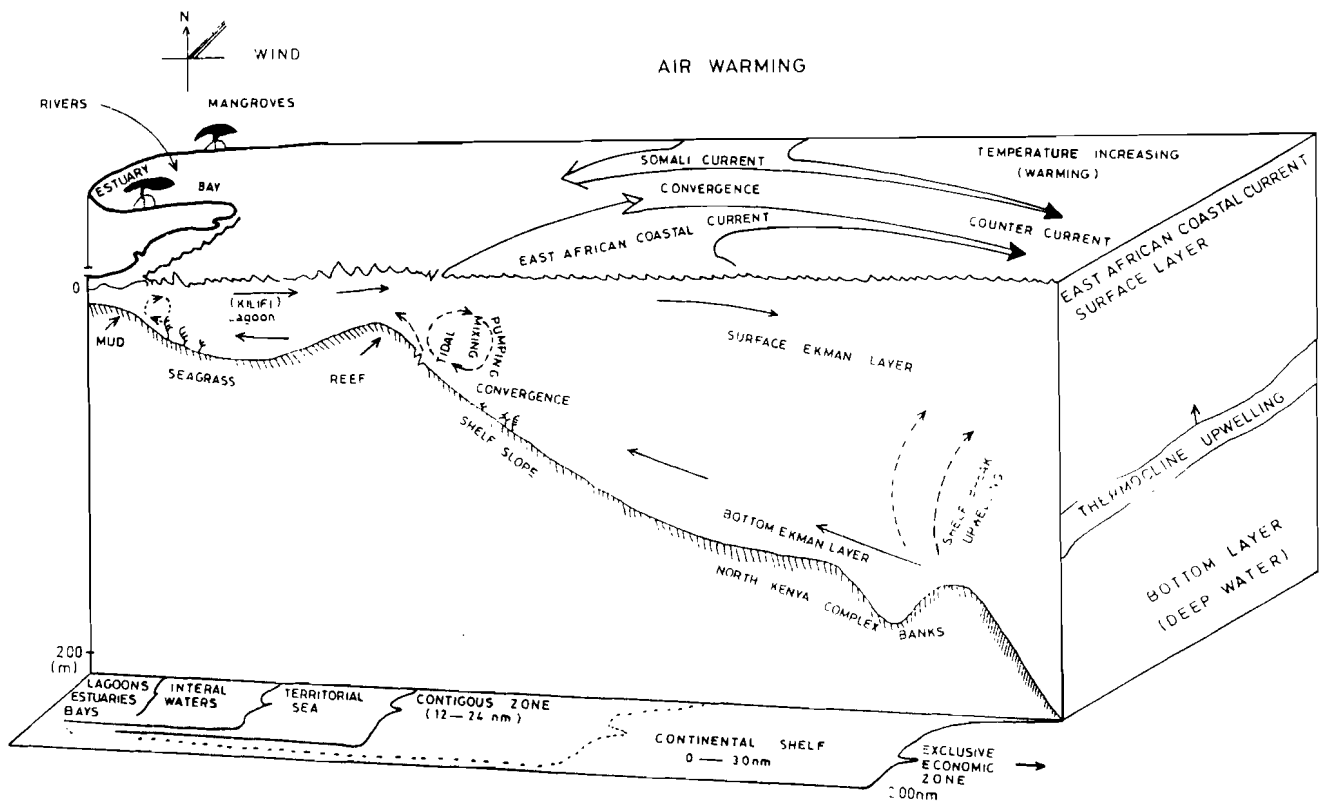
Figure 7.5.1b Eco-process schematic of a typical creek- to-ocean cross-section during the thermocline 'upwelling favorable conditions' (NEM season) in Kenya coast.

into the creeks. The down welling of the thermocline is reminiscent of anti-clockwise

circulation near the entrance, the situation is similar to dry condition described e.g. by

Wolanski (1993). Thus an upwelling tendency occurs within the upper reaches of the

creek and down-welling condition at the entrance-slope area. The evidence for this is the

low sea level that occurs during the SEM season (Figure 5.4.2.3).
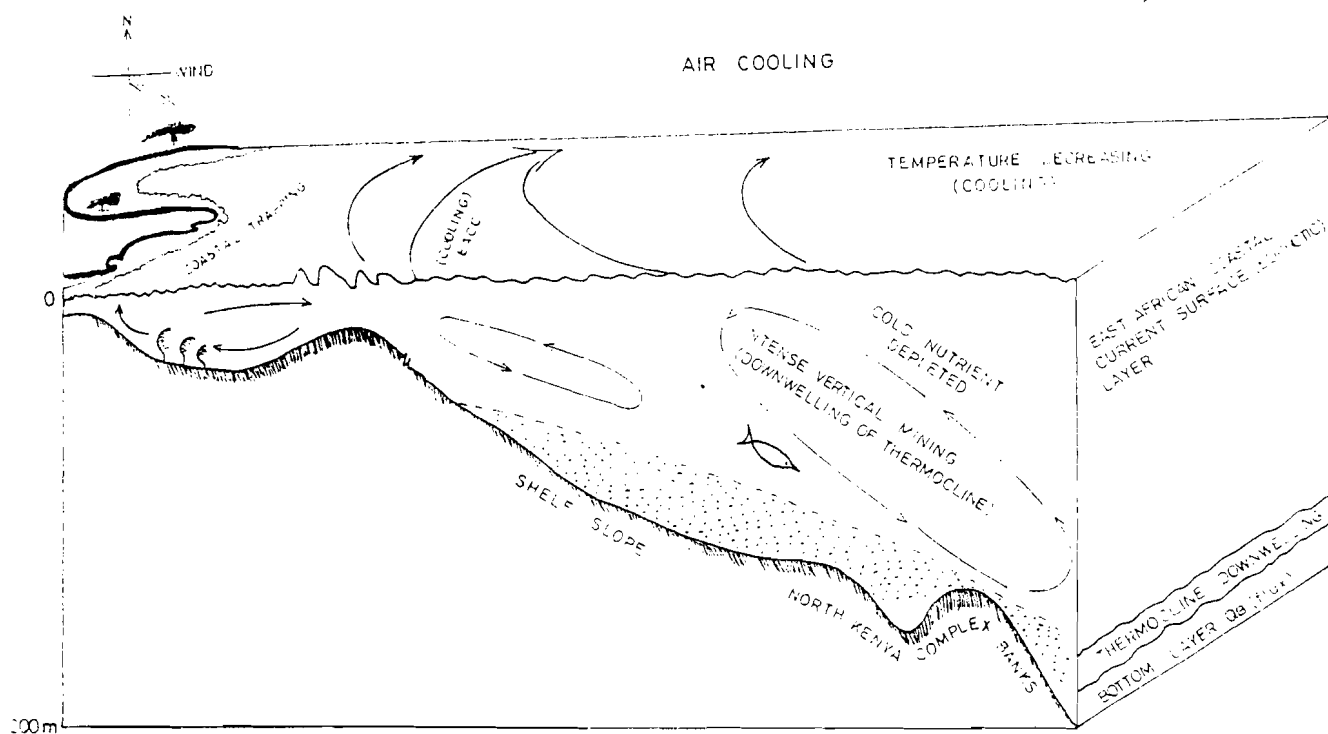
Figure 7.5.1d Eco-process schematic of a typical creek- to-ocean cross-section during the thermocline 'downwelling favorable conditions' (SEM season) in Kenya coast.

These patterns of circulation scenario favors enhanced productivity in the inner creek area and limited productivity at the entrance and slope water area. In addition it can be speculated, that 'the terrestrial influence' characterized by enhanced fresh water influx during IMLR season, result in high nutrient concentration in the creeks, which probably remain trapped in the upper reaches of the creeks due to a receding frontal feature. During IMLR and SEM season the presence of rainfall, lower temperatures, stronger coastal current means that salinity difference between the surface layer and the base of the mixed layer is increased leading to suppressed vertical transport. Hence, low concentrations of nutrients appear in the surface of water at this time, hence the scenario is the reverse of the one occurring offshore during NEM season. The annual progression of the hydro-meteorological parameters is shown in the integrated Figure 7.5.1e, which is a complex plot. The Purse seine and artisanal fish landing are also shown in the lower panel. High fish landings along the coast occur between October and February IMSR and NEM seasons when the thermocline is shallow. It is suggested that the presence of large marine games near the creek is a result of water circulation dynamics. Particularly the upwelling favorable conditions established during the NEM season bring them close to the creek entrances (Fishery Dept. personal comm.). Their southward movement further south into EAB later in the season, may be due to enhanced upwelling tendencies related to arrival of less saline water via SEC in the earlier parts o IMLR season and calmer waters in the EAB south of Pemba.
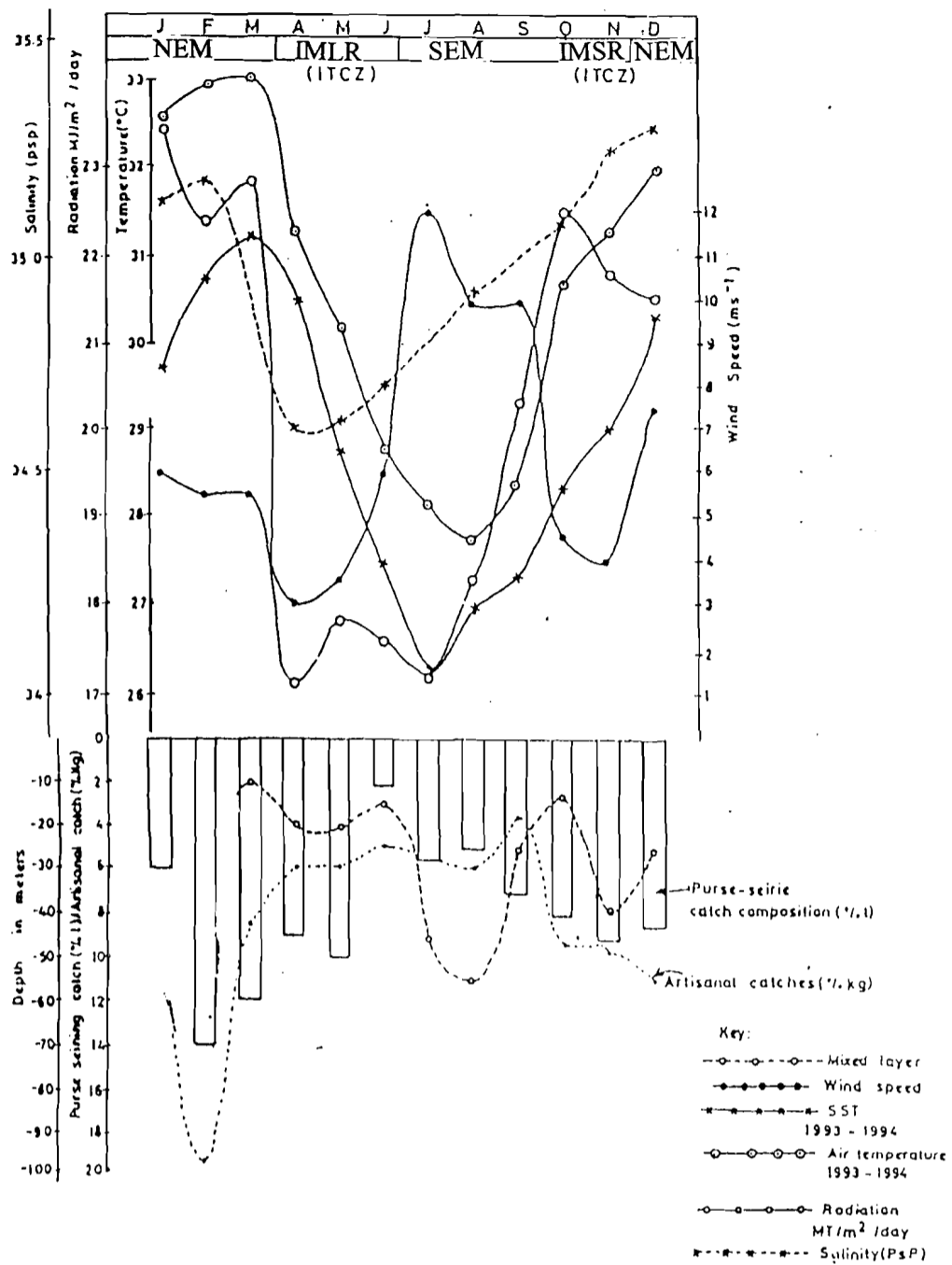
Figure 7.5.1.e A complex showing time progression of meteorological and oceanographic parameters (source Nguli 1999, withdrawn paper, Institute of Marine science Conference 1999 , submitted abstact).

CHAPTER EIGHT

SUMMARY, CONCLUSIONS AND RECOMMENDATIONS

8.1 SUMMARY AND CONCLUSIONS

Water exchange, circulation and heat budget in a shallow bay and two relatively deep creeks in the Kenya coast were investigated. To understand better the forcing factors governing water exchange and circulation were quantified and discuss in the context of inter-monsoon long rain season (IMLR), Southeast monsoon (SEM), the inter-monsoon short season (IMSR) and the Northeast monsoon (NEM). The climate of the study areas is shown to be monsoon related. Rains occur in May and November with maximum in May, winds change direction and blow almost in east-west direction in April and October- November but at the peak of each SEM-season and NEM season they are strong and blow from Southeast and Northeast respectively. Highest wind speeds are in July-August and lowest in April and November, whereas air temperatures are highest in February-March and lowest in August.

The temperatures and salinity show seasonal fluctuations. Flood tides brought cool temperature and waters of higher salinity from the ocean and lowered the creek temperature by 1-3 °C and salinity by 1PSU. During ebb tide water of lower salinity was found near the entrance and vice versa during flood tide. Water temperatures were also higher during neap than spring periods. High salinity bubbles were also found during ebb tides at the entrance and indicated entrained pockets of high salinity water from inner parts of the creeks. Seasonality was also observed on monsoon scale.

379

Heat flux estimate for Tudor Creek, showed that the net value for advective heat flux was $6Wm^{-2}$ into the creek and diffusive heat flux of $17Wm^{-2}$ out of the creek. Therefore a net heat flux of $11Wm^{-2}$ when a net volume flux of $62m^3s^{-1}$ and typical temperature difference of 1.5^0C between the creek and the ocean were used.

NEM season reflected highest salinity and sea temperatures than the other three seasons. The high salinity was caused by excess evaporation in the creeks as well as the presence of oceanic water masses of high salinity probably from the SC. Lowest salinity occurred in IMLR season as a result of rainfall and invasion of water of lower salinity brought by the EACC. The surface mixed layer and the thermocline shoaled (upwelled) during NEM-season but deepened during SEM season. Observations showed lower and higher salinity in the inner basin of the creeks than the ocean during IMLR (wet) season and NEM (dry) season respectively. Salinity differences produce density difference and generate baroclinic circulation with surface current always directed out of the bay i.e. estuarine circulation. Salinity within the inner shallow basin increases during the dry season as a result of evaporation from the mangroves and muddy inter-tidal areas at a rate of $0.6cmd^{-1}$ of water. Then a salinity maximum zone is created, and an internal circulation set up, that may effectively isolate the inner basin from the coastal water.

Semi-diurnal tide (M_2) with strong diurnal inequality dominated the tidal circulation in the three study sites. Thus the dominant flow was barotropic. Flood currents were stronger than the ebb currents with a maximum of the order of $40cms^{-1}$ in Tudor and Kilifi Creeks entrance area but less by half the value in Gazi Bay. The stronger currents were attributed to narrower channel effect in the two creeks whereas the weaker currents in Gazi Bay were due to the wide entrance. In the three-study sites spring tidal

currents were higher than neap currents and diurnal and fortnight inequality was also observed in the currents corresponding to the tidal inequality. Tidal excursion was estimated at 2.5km. Tidal asymmetry was evident in all the study sites and was attributed to the presence of shallow mangrove areas and mud flats with the creek inner basins. Gazi Bay was found to be ebb dominant with ebb tide duration exceeding flood duration, where as Tudor and Kilifi creeks showed flood dominance. The tidal currents are asymmetrical in Tudor and Kilifi Creeks with swift flood currents of shorter duration than the ebb currents of small magnitude and longer duration. Tidal asymmetry tended to disappear during neap periods in Gazi Bay. Tidal ranges were found to be variable, for instance, in Gazi Bay, the spring, neap and mean tidal ranges were 4.1m, 3.1m and 1.4m respectively and spring volume flux of 1757 $m^3 s^{-1}$, neap volume flux of 692 $m^3 s^{-1}$ and mean volume flux of 1224 $m^3 s^{-1}$. Sea level in Tudor Creek was found to be higher than in the ocean, a difference that was attributed to tidal oscillations within the shallow inner basin of the creek, in the same creek 'over-bank tides' or flood pulses were characterized by narrow current velocity spike of up to $30cms^{-1}$. Slight ebb pulses occurred probably due to shoaling of depth as the tidal level recedes.

On seasonal scale, sea level was higher during NEM season than during SEM season, this phenomenon was attributed, in part, to the 'back up' of the coastal water when the SC meets the EACC and non-local forcing possibly related to monsoon Kelvin wave events in the region. The creeks were found to flush in less than 3 days although the uppermost reaches of the creeks might take longer periods to flush. On longer time scales, however, the creeks are well ventilated in IMLR and SEM but less so in NEM season on account of opposed gravitational circulation which can be described in two

fold mechanisms: the dowelling favorable conditions and upwelling favorable conditions during SEM and NEM seasons respectively. The mechanisms are given the acronym: Creek-Ocean Monsoon Eco-process models (COMEC models) and schematized as long-term internal and offshore gravitation circulation. In SEM season the circulation is such that water exchange is more enhance and internal circulation enhances 'localizes upwelling' inside the creeks thus enhancing biological productivity there, but offshore water 'down wells' as evidenced by deepening of the thermocline. In NEM season internal gravitation enhance trapping in the creeks and the set up circulation pattern that favor upwelling at the entrance and in the offshore thus enhancing biological activities. The shoaling of the thermocline during NEM season is the evidence advanced for this circulation scenario.

8.2 RECOMMENDATION AND FUTURE WORK

Management of the shallow water ecosystem as well as the time depended currents off Kenya coast and the rest of the East Africa Bight should be based on a sound understanding of the key aspects of water circulation, water exchange and variability of the physical and biological components. Water circulation and exchange control the advection and dispersion of eggs and larvae from fish, crustaceans and corals when they are in pelagic dispersal phases. Water circulation also controls the shuttling of fish in and out of the creeks and lagoons on tidal scales and inter-monsoon scales and the southern movement of the migratory fisheries into and out of the East Africa Bight. There is urgent need to collate the bight-wide existing oceanographic data in order to explore further the seasonal processes that enhance the upwelling and down welling favorable conditions and produce a more detailed link between the fisheries and the physical processes. It appears that there are specific periods in the year that the crustacean larvae find their way into the creek systems and leave the creeks for recruitment further offshore or within the deeper parts of the creek systems. The time needs to be determined and the related water conditions established for better management of the crustaceans. More over water circulation and exchange controls the transport of pollutants such as nutrients from sewage. The circulation also controls agricultural runoff, pesticides, and mud from dredging of harbors and also erosion and accretion of on the shoreline e.g. in Malindi-Ungwana Bay and Dar es Salaam and in turn affect marine life. Circulation and re-suspension of silt in shallow entrance or shelf area could be responsible for fish kills often reported along the coast (Wawiye, 1996 per comm.) is due to silt re-suspension of

383

sediments in some parts of the shelf edge due to strong bursts of tidal currents and residual circulation.

To improve our understanding and answer pressing management questions more field data need to be gathered which should be done together with raising the awareness of fishermen on the benefit of research so as to limit loss or interference of any deployed research equipment. Future research should concentrate on mechanism governing mixing processes and causing plankton patchiness in the creeks and in back reef lagoons. Detailed work needs to be done in numerical modeling of the creek systems in order to simulate circulation and assist in the description of the hydrodynamics of the creek.

Proper bathymetric surveys campaign should also be carried out in creeks, lagoons and bays of interest and information archived to ensure better geomorphologic information, that can facilitate more detailed research in these ecosystems, for example in accessing suitable positions for deploying equipment e.g. current meter.

REFERENCE

1   Abuodha, J.O.Z. (1989). Morphodynamics and sedimentology of the malindi-Fundisa coastal area associated with the heavy mineral deposition. Unpbl. M.Sc. thesi, Univ. Nairobi, 258p.

2   Abuodha, P.A.W. (1992). Geomorphology and sedimentology of the Mombasa-Diani area: Implications for the coastal zone management. Unpubl. M.Sc. Thesis,Univ. Nairobi, 155P.

3   Andersson, L. and Rydberg, L. (1993). Exchange of water and nutrients between the Skagerrak and the Kattegat, Estuarine, Coastal and Shelf Science.3.6 (2), 159-181.

4   Andersson, L. and Rydberg, L. (1988). Trends in nutrient and oxygen conditions within the Kattegat:effects of local nutrient supply. Estuarine, Coastal and Shelf sciences, 2.6, 259-579.

5   Angstrom, A. (1924). Solar and terrestrial radiation. Quart. J.R. Met. Soc. 50: 121-125.

6   Anderson, D. L.T. and Rowlands, P.B. (1976). The Somali Current response to the Southwest Monsoon: the relative importance of local and remote forcing. J. Mar. Res., 34, 395-417.

7   Anonymous, (1981). The general water movement off the Kenya Coast. Project KEN/74/023 work report no.1,2 and 3respectively the survey activities in 1979, 1980 and 1981. Unpubl. Manuscript, Kenya Marine and Fisheries Res. Inst.

385

8   Ase, L.E.(1978). Preliminary report on studies of shore displacement at the southern coast of Kenya. Geografisker Annaler, 60A, 3-4, 209-221.

9   Ase, L.E. (1981). Studies of the shores and shore displacement on the southern coast of Kenya-especially in Kilifi District. Geografisker Annaler, 63A, 3-4, 303-310.

10   Anderson, L. and Rahm, L. (1986). Heat balance of a shallow cove,estuarine , coastal and shelf sciences, 23,705-724.

11   Anwar, H.O, (1983).Turbulence measurements in stratified and well-mixed estuaries flows. East Coast. Est. Shelf. Sci. 17 243-260.

12   Bell, B. E.(1972). Marine fisheries, in east africa: Its people and resources, edited by W.T.W. Morgan, 2nd ed., pp. 243-253, Oxford University Press, New York..

14   Bigendako, P.R. (1984). An investigation into the behaviour of tidal elevation at the Kundichi beach by the harmonic analysis Method. M.Sc. Thesis, University of Dar es Salaam.

15   Bird, E.C.F. (1969). Coasts: An introduction to systematic geomorphology. The MIT Press, Cambridge, 246p.

16   Bogdanova, A.K. (1974). Indirect estimation of the seasonal variation of the water exchange through Bab-el-Mandab. L'oceanographie physique de la mere rouge, Publication du CNEXO, Serie: Actes de colloque, 2, 253-265.

17   Boon, J.D. 1975. Tidal discharge asymmetry in a salt marsh drainage system. Limnol. and Oceanogr.,20:71-80.

18 Boon J.D. III. and Kiley, K.P. (1978). Harmonic analysis and tidal prediction by the method of least squire. Spec. report No. 189. Virginia Institute of Marine Science, Gloucester Pt. VA. 49pp.

19 Boon (1981),J.D.III and Byrne, R.J.1981. On basin hypsometry and morpholodynamic response of coastal inlets systems. Marine Geology.40:27-48.

20 Boto, K.G. and Bunt, J.S. (1981). Tidal export of particulate organic matter from a northern Australian mangrove system. Estuarine, Coastal and Shelf Sciences. 1.3, 247-255.

21 Bowers D.G. and Lennon G.W. (1990). Estuarine, coastal and shel sciences 30, 17-34.

22 Bowden, K.F. (1983). Physical oceanography of coastal waters. Chister:Ellis horwood, Chichester,302pp.

23 Brakel, W.H. (1984). Seasonal dynamics of suspended sediment plume ins from the Tana and Sabaki Rivers, kenya: Analysis of Landsat Imagery. Remote Sensing of Environ., 16, 165-173.

24 Bruce, J.C. and Volkmann, G.H. (1969). Some mesurements of current off the Somali coast during the north east Monsoon. J.Geophy. Res., 74(8), 1958-1967.

25 Bryceson, I. (1982). Seasonality of oceanographic conditions and phytoplankton in Dar es Salaam waters.University Science Journal (Dar es Salaam). 8, 66-76.

26 Carpenter, L., and D.G. Capone. New York: Academic Press, pp. 1-35.

27 Cartwrite, D., Munk, W.H. and Zetler, B.(1969). Pelagic tidal measurements. EOS,50, 472-477.

28   Carlsson, M. (1997). Sea level and salinity variations in the Baltic Sea-An Oceanographic study using historical data. PhD Thesis, 1997 Department of oceanography, Göteborg

29   Caswell, P.V.(1956). Geology of the Kilifi-Mazeras area. Geol. Surv. Kenya Rep., 34, 54p.

30   Caswell, P.V.(1953). Geology of the Mombasa-Kwale area. Geol.Surv.Kenya Rep.,24,69p.

31   Crame, J.A. (1980). Succession and diversity in the pleistocene coral reefs of the Kenya coast. Palaentology 23(1):1-37.

32   Crame, J.A. (1981), Ecological stratification in the pleistocene coral reefs of the Kenya Coast. Paleontology, 24(3): 609-646.

33   Cederlöf Ulf, (1993). Post Graduate Lecture Notes in Fluid Mechanics (with some application of matlab techniques for time series analysis), Department of Oceanography University of Gothenburg.

34   Cederlöf Ulf, Rydberg, L., Mgendi, M. and Mwaipopo, O. (1995). Tidal exchange in a warm tropical lagoon. Chwaka Bay, Zanzibar. Ambio 24, 458-464.

35   Cederlöf, U., Rodhe, J., Rydberg, L.,Sehlstedt P. (1996). Performance study of the Haamer gelatin pendulum current meter. To appear in The Netherlands Journal of Sea Research.

36   Chandrakath, G., Ranganna, G., and James, E.J. (1987). Mixing and circulation processes- Parenje estuary(Karnataka) Proc.Natn.Sem. Estuarine management, 1987, Trivandrum: 67 - 69.

37   Cheng, T.R., Casulli, V. and Gartner, W.J. (1993). Tidal, residue, Intertidal Mudfat (TRIM) model and its application to San Fransisco Bay,California. Estuarine and Coastal and Shelf Science. 3.6, 235-280.

38   Citeau, J. Piton, B. and Magnier, Y. (1973). Sur la circulation geostorphique dans l'oest de l'ocan indien sud-equatorial, Doc.ORS-TOM 31,32pp., Inst, fr. De Rech. Sci. Pour le Develop. En coop., Brest, France.

39   Courtier, A. 1933. Maree-Serv. Hydrr. De la Marine. Paris.

40   Cox, M.D. (1976). Equatorial trapped waves and the generation of the Somali Current. Deep-Sea Res.,23(12), 1139-1152.

41   Curl, H. (1959). The Hydrography of the inshore northeastern gulf of Mexico. Pub. Inst. Mar. Sci. Univ. Tex.6:193-205.

42   Denes, T.A. and Caffrey, J. M. (1988). Changes in seasonal water transport in a Louisiana Estuary, Four league bay, Louisiana. Estuaries Vol.II No.3: 184 - 191.

43   Duing, W. and Schott, F. (1977). Measurements in the source region of the Somali Current.J. Phys. Oceanogr. 8:278-289

44   Duing, W. and Schott, F. (1978) Measurement in the source region of the Somali current during the monsoon reversal J. Phys. Oceanogr. 8: 278-289.

45   Duing, W. and Szekielda, K.H.(1971). Monsoon response in the Western Indian Ocean. J. Geophys. RES., 76(18), 4181-4187.

46   Dyer, K.R. (1986). Estuarine and Coastal Sediment Dynamics. Wiley,Chichester, 342.

47   Eiser, W. C. and Kjerve, B. (1986). Marsh topographic characteristics of South Carolina salt marsh basin. Estuarine, Coastal and Shelf Science 23:595-605.

48   Fairbridge, R.W. (1980). The estuary: its definition and geodynamic cycle. In: E. Olausson and I. Cato (Editors), Chemistry and Biogeochemistry of Estuaries. Wiley, New York, pp.1-35.

49   Filloux, J.H., Snyder, R.L. (1979). A study of tides set up and bottom friction in a shallow semi-enclosed basin. Part I: Field Experiment and Harmonic analysis. Journal of Physical oceanography 9, 158-169.

50   Fieux, M. and Stommel, H. (1977). Onset of the Southwest Monsoon over the Arabian Sea from Marine Report of the Surface winds: Structure and variability. Monthly Weather Review, 105(2) 231-236.

51   Fisher, H.B. (1972). Mass transport mechanism in partially stratified estuaries. J.Fluid Mech. 53, 672-687.

52   Findlater, J. (1971). Mean monthly airflow at levels over the Western Indian Ocean. Geophys. Mem.,115,53.

53   Findlater, J. (1977). Observational aspect of the low level cross-equatorial jet stream of Western Indian Ocean. Pure Appl. Geophy. 115:2151-1261.

54   Garvin, R.W. (1995). A simple model of estuarine subtidal fluctuation forced by local and remote wind stress. J. Geophysical Res.,96(C6),11945-11948.

55   Garvin, R. W. (1985). A simple model of estuarine subtidal fluctuation forced by local and remote wind stress. J. Geophys. Res. 90,11945-11945.

56   Garvin, R.W. (1991). Subtidal frequency estuary-shelf interaction: Observations near Deaware Bay. J. Geophys. Res., 96(C4), 7049-7064.

57   Glibert, P.M. (1988). Primary productivity and pelagic nitrogen cycling. In: Nitrogen cycling in coastal marine environment. T.H. and Jan Sornsen Eds. John Wiley and Sons Pulication.

58   Graneli, E., Graneli, W., and Rydberg, L. (1986). Nutrient limitation at the ecosystem and the phytoplankton community level in the laholm Bay, south-east Kattegat. Ophelia 26:181-194.

59   Han, G. and Niedrauer T. (1981). Hydraphic observations and mixing processes in the New York Bight, 1975-77. Limu.Oceanogr. 26:1126-41.

60   Hansen, D. V. and Rattray, M. Jr. (1966). New dimensions in estuary classification. Linnolo. Oceanog. 11, 319-326.

61   Hansen, D.V. and Rattray, M. (1965). Gravitational circulation in straights and estuaries. J. Mar. Res.,23:104 –122.

62   Heath, R.A. (1977). Heat balance in a small coastal inlet Pauatahanui Inlet, North Island, New Zealand. Estuarine, Coastal and Shelf Science. 5, 783-792.

63   Hemminga, M.A., Slim,F. J., Kazungu, J., Ganssen, G.M., Necuwehuize, J. and Kruyt, N.M. (1994).   Carbon outwelling from a mangrove forest with adjacent seagrass beds and coral reefs (Gazi bay Kenya). Marine Ecology Progress Series. 106, 291-301.(Goreau T.J., and Hayes, R.M. (1994), Coral bleaching and Ocean 'hot spots'. Ambio 23,176-80).

64   Harvey, J. (1977). Some aspects of hydrography of waters of the coast of Tanzania. Dar. Univ.Sci., Vol.3 (1&2).

65   Hill, A.E. (1994). Fortinitely tides in a lagoon with variable choking. Estuarine, Coastal Shelf Science. 38, 423-434.

66   Hove, A.R.T.(1980a). Some aspects of current sedimentation, depositional environments and submarine geomorpology of the Kenya's sumerged continental margins. Univ. Nairobi, IDS/OP 28, 127-144.

67   Hunt, J.N. (1964). Tidal oscillations in estuaries. Geophysical journal of Royal Astronomical society 8, 440-455.

69   Hutinngford,G.W.B. (1980). The Periplus of the Erythraean Sea, 225pp.,Hakluyt Society, London.

70   Inman, D.L. and Nordstom,C.E.(1971). On the tectonic and morphologic classification of coasts. Journ. Geol., 79(1),1-21.

71   Invankov, V.N. and Gubin, F.A. (1960). Water masses and hydrochemistry of the Western and Southern parts of the Indian Ocean. Eng. transl: Trans. Mar. Hydrophys. Inst., Acad. Sci. U.S.S.R. 22, 27-99. A.G.U.

72   Inversen, S.A. (1984).Kenya marine resources in waters deeper than 10m investigated by R/V "Dr. Fridt of Nansen". In: of the Norad-Kenya Seminar to review the Marine Fish stock and Fisheries in Kenya. Institute of Marine Research, Bergen, Norway.

74   Inversen, S.A. and Myklevol, S. (1984). Kenya Marlin fish resources in waters deeper than 10m investigated by R.v Dr."Fridjof Nansen" in.(Iversen S. A.and Myklevoll S.(eds.) the proceedings of Norad fish stocks and fisheries in Kenya. 210pp.

75   Ivanoff, A. (1977). Ocean absorption of solar energy, pp. 47-71. In: E.B. Kraus (Ed.). Modelling and prediction of the Upper Layer of the Ocean. Perganon Press, New York.

76   Jackson, R.G. (1976). Sedimentological and fluid-dynamic implication of turbulent bursting process in a geophysical flows. J. Fluid.Mech. 77, 531-560.

77   James I. D. 1980, Estuarine coastal and Marne Science 10,597-607.

78   Jiahao, Y. (1987). Analysis of circulation and salt flux in the changjiang (Yangtze) estuar China Ocean Engineering Vol.7 No.4. 77 - 88.

79   Johnson D.R., Nguli, M.M. and. Kimani, E.J. (1982). Response to annually reversing monsoon winds at the Southern boundary of the Somali current. Deep Sea Res. 29:1217-1227.

80   Joseph, J. and Kwup, P.G. (1987). Tidal response and circulation of the Cochis estuary. Pr Natn. Sem. Estuarine management Trivandrum: 88 - 92.

81   Kabanova, Yu.G, (1968). Primary production in the northern part of the Indian Ocean. Oceanology, 8(2): 214-275.

82   Kazungu, J. M. (1989). Seasonal fluctuation of nitrate-nitrogen concentration in Tudor estuary, Mombasa Kenya.Journal of science and technology series A: Vol.10.

83   Kazungu, J.M. (1986).Kenya Belgium report. Kenya Marine and Fisheries Research Institute 1986-1987.

84   Kazungu, J.M., Dehairs, F.and Goeyens, L. (1988). Nutrient distribution patterns in Tudor estuary (Mombasa Kenya) during rainy season. Kenya Journal of Science and Technology. Series B. Vol. 10.

85   Ketchum, B.H. (195). The exchange of fresh and salt water in tidal estuaries. Journal of Marine research 10, 18-38.

            .

86   Kimaro, A. (1986). The composition and abundance of near-surface zooplankton, MSc. Thesis, University of Nairobi.

87   Kitheka, J. (1996).   Water circulation dynamics in tropical mangrove-fringed bay in Kenya.To appear in Limnology and Oceanography.

88   Kjerfve, B.J. and Magill, K.E. (1989). Geophysical and hydrodynamics characteriestics of shallow coastal lagoons. Marine Geology. 88, 187-199.

89   Kjerfve, B.J. Greer, J.E. and Crout, R.L. (1978). Low frequency response of estuarine sea level to nonlocal forcing. In Estuarine Interactions (Wiley, M., Ed.).Academic press, New York. pp. 497-513.

90   Kjerfve, B., Stevenson, L.H. and Proehl, J.A. (1981). Estimation of material fluxes in an estuarine cross - section: A critical analysis of spatial density and errors. In Limnol. Oceanogr. 26 (2) : 325 -335.

91   Kromkamp, J., Ham, E. and Peene, J. (1992). Primary Production along the Kenyan coast during the rain period at the end of the Southeast monsoon. R.V.Tyro shipboard report.

92   Kruyt, N..M. and Van de Berg, J.H. (1993). Hydrography of Gazi.In dynamics and assessment of the Kenya mangrove ecosystem No. TS2-0240-C (GDF) 221-237 Woitchnik A.F. (editor).

93   Kundu, P.J.(1997). Fluid Mechanics, Academic press,223-226.

94   Kuo-Chuin, Wong and Joy, E., Moses H. (1998). The tidally and subtidal variations in the transverse salinity and current distribution across a coastal plain estuary. Journal of marine Research, 56, 489-517.

95 Lankford, R.R.(1976). Coastal lagoons of Mexico: their origin and classification. In: M.L. Wiley (Editor), Estuarine processes. Academic Press, New York, Vol.2, pp.182-215.

96 Leetmaa, A. (1973). The response of the Somali current at 2°S to the southwest monsoon of 1971, Deep-sea Res; 20 (4), 397-400.

97 Leetmaa, A. and Truesdale, V. (1972). Changes in the Somali current in 1970 off the east Africa coast with the onset of the southeast monsoon. J.Geophys. Res., 77(18), 3281-3283.

98 Leetmaa, A. (1973). The response of the Somali Current to the Southwest monsoon of 1971, Deep Sea Res. 20, 297-304.

99 Leetmaa, A. (1972). The response of the Somali Current to the South West monsoon of 1970. Deep Sea Res. 19, 319-325.

100 Linden and Niki, (1999). Coral reef degradation in the Indian Ocean status reports and prosects, 1999. Editors: Olof Linden and Niki Sporrong, Page 99

101 Lutjeharms, J.R.E. (1972). A Guide to research Done Concerning Ocean Currents and water masses in the South West indian Ocean, 577 pp., University of cape Town, soth Africa.

102 Lwiza, K. M. M. & Bigendako P.R. (1988). Kunduchi Tides. Tanz. J.Sci.Vol. 14, 65-76.

103 Mahoney, P.J.B. (1980). African Pilot vol III-south and east coast of Africa from Cape Algulhas to Ras Binnar, Including the Island of Zanzibar and Pemba. Third edition. Hydrographer of the Navy, 25-44.

104   Magnier, Y. and Piton, B. (1974). Les particularites de la couche 0-600m dans l'ouest de l'ocean Indien sud-equatorial, Cah. ORSTOM, Ser. Oceanogr., 12(3), 143-158.

105   Magnier, Y. and Piton, B. (1973). Les masses d'eau de l'ocean indien, a l'ouest et au nord de Madagascar au debut de l'ete austral, Cah. ORSTOM, Ser. Oceanogr., 11(1), 97-113.

106   Mandelli, E.F. (1981). On the hydrography of some coastal lagoons of the pacific coast of mexico. In: Coastal lagoon Research: Present and Future. UNESCO, Paris, pp.81-95).

107   Marleen de Troch, Jan Mees and Wakwabi, E. (1998). Diets of abundant fishes from beach seine catches in seagrass beds of the tropical bay (Gazi Bay, Kenya). Belg. J. Zool.-Vol. 128 (1998) pp 135-154.

108   Mede, R.H. (1969). Land ward transport of bottom sediments in estuaries of Atlantic Coastal Plain. J. Sediment petrol., 39:22-234. Van Dorn. W.G., 1953. Wind stress on an artificial pond. J. Mar. Res., 12:249-276.

109   Medeiros,C. and Kjerfve, B. (1993). Hydrology of a tropical estuary system: Itamaraca, Bazil.Estuarine Coastal and Shelf Science. 36,495-515.

110   Morcos, S. A. (1959). Uber die Veränderugen der Schichtung und Zirkulation im Suez-Kanal. Doctor-Dissertation. University of Kiel,202 pp.

111   McCathy, J.J., Kaplan, W.A. and Nevins J.L. (1984). Chesapeake Bay nutrient and plankton dynamics and source and sinks of nitrite. Limnol.Oceanogr.29, 84-98.(Prichard and trite, 1956, in Journal of Fisheries Research Board of Canada,vol.14 (4) 605-616.

112   Mclanahan, T.R. (1988). Seasonality in the Eastern Africa's coastal water.Marine Ecology Progress Series. 44, 191-199.

113   Mclanahan,T.R. and Sharif, S.H. (1990). Courses and consequences of sea urchin abundance and diversity in Kenya coral reef lagoon. Occanologia. 83, 362-370.

114   MONEX (1980),   Data Report Monsoon Experiment(MONEX). Kenya.The Office of Naval Research. Contract. No. W00014-75-C-0173.

115   Morgans, J.F.C. (1979). The sea we fish in E. Africa Agric. J.25:91-96.

116   Morgans, J.F.C. (1959). The north Kenya Banks. Nature 184, 259-2260.

117   Mukolwe, E. (1973). Regreeion analysis of the mean monthly sunshine and radiation in East Africa, Dept. of Meteorology, University of Nairobi.

118   Munk, W.H. and Carwright ,D.E. (1966). Tidal spectroscopy and predictions. Philosophical transactions of the Royal Society of London. 259,533-581

119   Munk,W.H. and Cartwright, D.E. (1966). Tidal spectroscopy and prediction. Phylosophical transactions of the Royal Society of London,259 533-581.

120   Munk, W.H. and Hasselman, K. (1964). Super-resolution tides. Studies in Oceanography, Univ. of Washington Press. Pp. 339-344.

121   Munk , W. H. and Hasselman, K. (1964). Superior-resolution of tides. Studies in Oceanograpaphy univ. Press. Pp. 339-344.

122   Munyao, T.M.(1992). Sedimentology of the shirazi-Funzi lagoon. M. Phil thesis, Moi Univ.

123   Newell, B.S. (1959). The hydrography of the East African coastal waters. Part II.Fish Publ. London No. 12:18pp.

397

124   Newell, B. S. (1957). A preliminary Survey of the hydrography of British East African Coastal waters. Fish Publ. London No. 9:20pp.

125   Nichols, M. M. and Biggs, R.B. (1985). Estuaries. In: R.A. Davis Jr. (Editor). Coastal Environments. Springer, New York, pp. 77-187.

126   Nichols, M. M. and Biggs, R.B. (1985). Estuaries. In: R.A. Davis Jr. (Editor). Coastal Environments. Springer, New York, pp. 77-187.

127   Nguli, M.M. (1994). Water exchange and channel friction related to tidal flow in Tudor creek,Kenya coast,Western Indian Ocean.   MSc. Thesis Gothenburg University. 32 pp.

128   Nguli, M. M. Ochumba, P.O. and Othina, A.N.(1991). The diurnal variability of some hydrographic properties in Tudor creek Kenya.Workshop on Tropical Coastal Lagoon Ecosystems, Inhaca Island, Mozambique.

129   Norconsult, A.S. (1975). .Mombasa water pollution and waste disposal study: Report to the Ministry of Local government, Vol. VI. 104 pp.

130   Obasi, G.O.P. and Rao, N. N. (1976a): A detailed study of solar radiation and potential in Kenya.UNESCO/WMO Solar energy Symposium Poc. WMO.477:114-124.

131   O'Brien, J.J. and Hurburt, J.E. (1974). Equatorial jet in the Indian Ocean. Theory. Science, 184:1075-1077.

132   Odido, M.O. (1994). Tidal dynamics of Tudor creek. Mombasa Kenya, MSc.Thesis, Gothenburg University. 30 pp. R.V. Kusi (1979), in Monex Data Report,(1980) KMFRI data achives.

133 Okemwa, E. (1990). A study of pelagic copepods (COPEPODA:CRUSTACEA) in a tropical marine creek,Tudor Mombasa Kenya,with special reference to their community structure,biomass and productivity. Ph.D. Thesis, VUB.

134 Okemwa, E. and Revis, N. (1988). Planktonic copepods from coastal and inshore waters of Tudor creek, Mombasa.Kenya Journal of Science and Technology series B: 7 pp.27-34.

135 Okoola R. (1982). Solar power potential in Kenya. Kenya J.T.Sc. Tech (A) 4:53-64. WMO 1981: Meteorological aspect of the utilization of solar radiation as an energy source WMO.No.577.

136 Onjay, F. F.(1984). Some aspects of the geomorphic evolution of the Kenya coast with special reference to the kambe limestone rocks of the Kilifi are. In: natural and Man-Induced Environmental Charges in the tropical africa: case studies in Camerroon and Kenya. A preliminary report of the Tropical Africa geomorphology and late-Quaternary paleoenvironment Research project 1982/83, sapporo, Japan, 117-127.

137 Onyango, H. B.A.(1989). Numerical Modeling of Gazi creek (South Coast,Kenya) I:Hydrodynamic model II: Descriptive Ecological Model, MSc.Thesis, VUB.

138 Pejrup, M.,Batholdy, J. and Jensen, A.(1993). Supply and exchange of water and nutrients in the Grådb tidal area, Denmark. Estuarine, Coastal and Shelf Science. 36, 221-234.

139 Phylee, A., Varma, P.U. and Revichandvan, C. (1990). Some aspects of circulation and mixing in lower reaches of Periyar estuary West Coast of India. Indian journal of marine sciences,

Vol.19: 32-35.

140 Pritchard, D.W. (1956). The dynamic structure of coastal plain estuary. J. Mar res. 15, 33-42.

141 Pritchard, D.W. (1954). A study of salt balance in a coastal plain estuary. J. Mar res. 13, 133-144.

142 Pugh, D.T. (1979). Sea level at Aldabra Atoll, Mombasa and Mahc. Western Equatorial Indian Ocean, related to tides, meteorology and circulation.Deep Sea Research. 26, 237-258.

143 Pugh, D.T. and Rayner, R.F. (1981). The tidal regimes of three Indian atolls and some ecological implications. Estuarine Coastal and Shelf Science. 13, 389-409.

144 Quardfasel, D.R. and Schott, F. (1982). Water mass distribution at the intermediate layers off the Somali coast during the onset of the South West monsoon, Journal Physical oceanography. 12, 1358-1352.

155 Revis, N. and Okemwa, E.(1988). Additional records of species of copeponds and their distribution in the coast and inshore waters of Kenya. Kenya Journal of Science series B.8:123-127.

156 Redfield, A.C. (1950). The analysis of tidal phenomenoa in narrow embayments. Papers in Physical Oceanography Meteorology 11 (4),1-36.

157 Ridd, P.W., Sandstrom, M.W. and Wolanski, E. (1988). Outwelling from tropical tidal salt flats. Estuarine, coastal and Shelf Sciences. 26, 243-253.

158 Robertson, A. L. and Duke, N.C. (1987). Mangrove as nursary sites: Comparisons of abundance and species composition of fish and crustaceans in

mangroves and other near shore habitats in tropical Australia. Marine Biology. 96, 193-205.

159   Rydberg, L. (1986). Observations on nutrient fluxes through the coastal zone.Rapp.Negambo Lagoon, Sri Lanka.To appear in Estuaries 19 (3).

160   Schroeder W.W., Scott, P. D. and Wiseman,W.JR. 1990. Salinity stratification in a River-Dominated Estuary. Estuaries Vol.13 No.2. p.145-154.

161   Schubel, J.R. and Pritchard, D.W. (1972). The estuarine ennvironment. J.Geo. Edu.,20: 60-68.

162   Ranwell 1972 Ecology of salt marshes and sand dunes.Chapman and Hall, London.xiv,258pp.

163   Ruwa, 1996 Intertidal wetlands, in McClanaham T.R. and Young T.R. eds., New York, Oxford Univesity press,101-130.

164   Ryther, J.H. (1956). Photosynthesis in the ocean as a function of light intensity. Limnol. Oceanograp.1:61-70.

165   R.V.Tyro (1992-93). Ship Cruise Data report, KMFRI data archives.

166   Seeling, W.N. and Sorensen, RM.1978. Numerical model investigation of selected tidal inlet-bay system characteristics. Am. Soc.civ.Eng., Proc. 16th Coastal Eng. Conf.,Hamburg, West German,pp.1302-1319.

167   Seeling, W.N., Harris, D.L. and Herchenroder, B.E. 1977. A spatially integrated numerical model of inlet hydraulics.Coastal Eng.Res.Cent., Fort Belvoir, Va., GITI Rep.,14.99pp.

168   Simmons, H.B. (1955). Some effects of upland discharge on estuarine hydraulic. Proc. Am. Soc. Civ. Eng. 81, No. 792.

169 Sharp, J.H. (1983). The distribution of inorganic nitrogen and dissolved particulate inorganic nitrogen in the sea. Nitrogen in Marine Environment (edited by E.J.

170 Skyum, P. and Lund-Hansen, L.C. (1982). Barotropic and Baroclinic forcing of a semi – enclosed bay. Geogr. ann 74A(4): 363-373.

171 Schott C.F. (1993). Canonical parameters for estuarine classification. Est. Coast.Shelf. Sci. 36, 529-540.

172 Schureman, P. (1971). Manual of Harmonic Analysis and Prediction of Tides.U.S.Dept. of Commerce Coast and Geodetic Survey; Special Publ.No.98, Revised 1940, Published 1971.

173 Smith, N.P. (1979).Tidal dynamics and low frequency exchanges in the Aranses pass, Texas. Estuarine. 2, 218-227.

175 Smith, D. (1986). In Subtidal Exchanges between Corpus Christi Bay and Texas inner shelf Waters, in Lecture notes on Coastal and Estuarine Studies, Physics of Shallow Estuaries and Bays, J. van de Kreeke Edt. P 143-152

176 Smith, S.L. and Codisporti, L.A.(1990). Southwest monsoon of 1979.Chemical and biological respons of Somali coast waters. Science 209:597-599.

177 Soderkvist, J.(1997). Water exchange in a shallow bay, Gothenburg University , ISSN 14000-3821. 24p.

178 Stigebrandt, A. (1980). Barotropic and baroclinic response of semi-enclosed basin to barotropic forcing from the sea.In the sea.Fjord Oceanography. eds Freeland et al., Plenus Publishing, New York.

179   Stigebrandt, A. (1983). A model for the exchange of water and salt between the Baltic and the Skagerrak.Journal of Physical Oceanography, 13, 412-427.

180   Strahler, A.N.1952.Hypsometric(area-altitude)analysis of erosional topography. Bull. Geol.Soc. Am., 63:1117-1142.

181   Strickland, J.D.H.and Parsons, T.R. (1972). A practical handbook of Seawater analysis. Bulletin 167 Fisheries Research Board Canada. 311 pp.

182   Sultan S.A.R. and Ahmad F. (1994).Heat budget of the coastal waters of Kuwait: a preliminary study. Estuarine, Coastal and Shelf Science. 38, 319-325.

183   Swallow, J.C. and Bruce, J.C. (1966). Current measurement off the Somali coast during the southwest monsoon of 1964. Deep Sea Res. 13.,.861-888.

184   Swenson, E.M. and Chuang, W.S. (1983).Tidal and sub tidal water volume exchange in an estuarine system. Estuarine, Coastal and shelf science Vol.16: 229 - 240.

185   Swallow,J. C., Schott, F. and Fieux, M. (1992). Structure and Transport of the East African Coastal Current.J.Geophy.Res., 93:(12), 22, 245-22,570.

186   Tchernia, P., Lacombe, H. and Guilbout, P. (1958)..Sur quelqhes nouvelles observations hydrologiques relative a'la re'gion equatoriale de l'occ'an Indien. Bull. Inf. Com. Cont. Oce'anogr. Etude Cotes 10: 115-143.

187   Thompson, A.O.(1956). Geology of the malindi are. Geol. Surv. Kenya, Rep.36,63p.

188   Thomson, R.E. (1981). The Oceanography of the British Columbia Coast. Can. Spec. Publ. Fish. Aquat. Sci.56: 291p.

189   Tomczac, M. and J.S.Godfrey, (1994). Regional Oceanography,An Introduction pp 221-236 Perganon Press.

190   Turyahikayo, G.R. (1987). Wave characteritics off the East African coast. Kenya Journ. Sci., A8, 1-2, 33-58.

191   Uncles R. J, Bale A. J Hollard R.J.M. , Morries, A.W. and Elliot, R.C.A. (1983). Salinities of surface water in a partially mixed estuaries and its dispersion at low run-off. Oceanol. Acta 6,289-296.

192   Uncles R.J., Ong, J.E. and Gong, W.K. (1990). Observations and Analysis of Stratification-Destratification Event in a Tropical Estuary. Estuarine, Coastal and Shelf Science 31, 651-665.

193   Warren, B., Stomnel, H. and Swallow, J.C. (1966). Water masses and patterns of flow in the Somali basin during the Southwest Monsoon of 1964. Deep-Sea Res., 13: 825-860.

194   Wattayakorn, G., Wolanski, E. and Kjerve, B. (1990). Mixing, trapping and outwelling in Klong Ngao mangrove swamp,Thailand. Estuarine, Coastal and Shelf Science. 31, 667-688.

195   Wang, X.H. and Craig, P.D. (1993). An analytical model of Tidal circulation in a narrow estuary.Journal of Marine Research, 51, 447-465.

196   Wei Shi, Marrisson, J. M., Bohm, E. and Vijayakumar, M. (1999). Deep Sea Research II 46 (1999) 1551-1575.

197   Weisberg R.H. (1976): The non-tidal flow in the providence river of Narrangasett bay: A stocchastic approach to estuarine circulation. Journal of Physical Oceanography.

198   Wolanski, E. (1990). Hydrodynamics of tropical coastal marine systems pollution in tropical aquatic systems.

199   Wolanski, E. (1989). Measurements and modelling of the water circulation in mangrove swamps. COMARAF seric documentaire No.3.

200   Wolanski, E. (1986). Tidal mixing and trapping in mangrove swamp. Estuarine, Coastal and Shelf Sciences. 23, 759-771.

201   William, F.(1970). The sport fishery for sail fish at Malindi, Kenya 1958-1968, with some biological notes. Bulletin of Marine Science 20 : 831-852.

202   Wolanski, E., Jones, M. and Bunt, J.S. (1980). Hydrodynamics of a tidal creek - mangrove swamp system. Austr.J Mar.Freshwater Res.Vol 31:431-450.

203   Wolanski, E., Mazda, Y., King, B. and Gay, S. (1990). Dynamics flashing and trapping in Hichbrook channel, Estuarine, Coastal and Shelf Science. 31, 550-580.

204   Wolanski, E. and Senden, D.V. (1983). Mixing of Burdekin river flood waters in the Great Barrier Reef. In the Austr. Journal of Marine and Freshwater Research. Vol.34: 49 - 63.

205   Wolanski, E. and Thomson, R.E. (1984). Wind-driven circulation on the northern great Barrier reef continental shelf in summer. Estuarine coastal and shelf science, Vol.18.

206   Wyrtki, K. (1973). An Equatorial Jet in the Indian Ocean. Science. 181: 262-264.

207   Wyrtki, K. (1971). Oceanographic Atlas of the International Indian Ocean Expedition, 531 pp., National science Foundation, Washington, D.C.

208   Zingde, M.D., Sharma, P. and Sabris, M. M. (1985). Physico - chemical investigations in Awanga river estuary (Gujarat). Madagascar - Bulletin of the National Institute Oceanography, Vol.18 (2). 307 - 321.

Appendix A

Heat Exchange

Radiation balance

Flood usually implies that colder oceanic water is brought into the Tudor creek system while the ebb removes mixed creek water containing excess heat. Since the water exchange and the temperatures of the different waters have been measured (both within the hydrographic survey program and through tide gauge measurements), it is principally possible to calculate heat flux through the channel. We shall also establish a heat budget for the area.

The average heat flux through the Tudor channel per unit surface area is given by

$$Q_T = (Q_{sr} - Q_{lrbr} - Q_{ehl}) - Q_{rsr} - Q_{hcf}$$

where,

Q_{sr} is the solar radiation input,

Q_{rsr} is the reflected solar radiation,

Q_{lrbr} is the net longwave back radiation,

Q_{ehl} is the heat loss by evaporation ,

Q_{hcf} is the heat loss by conduction, biological processes etc.

Q_{sr} is given by $\beta S \cos(\sigma t)\cos(\lambda+\delta)$, $Q_{sr} > 0$ or otherwise zero (see Pugh and Rayner 1981, Sultan and Ahmad, 1993, Reeds ,1977, Reeds,1983, Gill, 1982) ,where β is the atmospheric extinction coefficient, which is approximately 0.7 for vertical transimission (Defant, 1961), S is the solar constant which is equal to $1390 Wm^{-2}$, σ is the solar angular speed, λ is the solar declinatin, δ is the station latitude. Since the creek is near the equator we set λ and δ equal to zero. Q_{rsr} is 10% of Qsr and may be negleted. $Q_{sr} = 180\ Wm^{-2}$.

Using Brunts formula

$$Q_{lrbr} = 0.985 \psi Tw^4 (0.39 - 0.05 e_a^{1/2})$$

where ψ is the Stefanal-Bolzman Constant. Tw is the water temperature, e_a is the vapour pressure of air in mb. Taking e_a, of 25 mb and Tw, of 25^{0}C, $Q_{lrbr} = 62Wm^2$.

$Q_{ehl} = (11.2 + 4.1W)(e_s - e_a)$ (see Pugh and Rayner ,1981),

where W is the wind speed in m s^{-1}, e_a is the air vapour pressure, and e_s is the saturated vapour air pressure at the sea temperature. Taking e_s at 33 mb (75% saturated at 25^{0}C and wind at zero, $Q_{ehl} = 90$ W m^{-2}.

$Q_{hcf} = 0.47(11.2 + 4.1W)(Ts-Ta)$ W m^{-2} ,

where Ts is the water temperature, and Ta is the air the air temperature.

Ts-Ta is 1.25 ^{0}C. $Q_{hcf} = 15$ W m^{-2}. The net heat balance becomes $Q_T = Q_{sr} - Q_{lrbr} - Q_{ehl} - Q_{hcf} = 180-62-90-15 = 13$W m^{-2}.

Q_T can be interpreted the heat flux (adv + diff) through the channel which thus can be calculated from the observations.

Appendix B

Advective and diffusive flux

The ebbing water must on average be warmer, by an amount δT, than the flood water. That is the net heat output by the water exchange equals the net heat gain from radiation. The net heat flux can be estimated from the sum of the advective and the diffusive flux ($Q_T = Q_{T_{adv}} + Q_{T_{dif}}$) as follows:

$$Q_{T_{adv}} A_c = \rho c_p Q_e T_o, / A_c \quad \text{and} \quad A_c Q_{T_{dif}} = \rho c_p Q_{max} \delta T / A_c$$

$Q_{T_{adv}}$ is the advective heat flux, $Q_{T_{dif}}$ is the diffusive heat flux, Q_{max} (aproximately Q_1 is the net volume flux, δT is the temperature difference from the creek and the ocean during North peak dry season. Q_e is the evaporative volume flux, A_c is the surface area of the creek

T_o is the temperature in the ocean side, ρ is the density of the sea water, c_p is the specific heat of the sea water ,

$c_p = 4000 \ J(kg^oC)^{-1}$; $\rho = 1000 \ kgm^{-3}$, $Q_e = 1.6 \ m^3 s^{-1}$, $T_o = 27.8^oC$, $A_c = 22 \times 10^6 \ m^3$.

$Q_{max} = 62 m^3 s^{-1}$, and $\delta T = 1.5^oC$

Therefore the value for advective heat flux $Q_{T_{adv}} = 6 Wm^{-2}$ (inwards) and diffusive heat flux $QT_{dif} = 17 \ W \ m^{-2}$ (outwards) the net heat flux is $11 W \ m^{-2}$.

The results from the calculation of heat flux must be treated with great caution. It is based on measurements of temperature during day time, while during the night the difference in temperature is probably smaller (fig.10). The estimate of Q_{max} is also made on too few data and a not very precise estimate of Q_e . However, it indicates the correct order of magnitude of the heat flux or the budget equation qiven above.

Alternatively the heat flux can be calculated from the current meter data simply by using the formula :

$$Q_T = \int_\tau \rho c_p A_{xs} U(t) T(t) c$$

where U is velocity and T is temperature, and τ is the period of observation, which has to be of the order of the residence time.

Appendix C

The Bottom Layer at the Exchange Section

Estimations of friction velocity,drag coefficient and the depth of the boundary layer.

The pendelums measurements nearest to the bottom in the mid channel position (figs. 4.1.2a-b.) were placed 1, 2 , 3 and 4 (corresponding to pendelum # 20,19,18 and 17 in meters from the channel-bed . These current measurements, made twice a month during three months at flood and ebb and at spring and neap periods, provide motivation for a simple study of the bottom friction layer. Fig.12. show some of the profiles of the measurments from the pendelums measurements From the profiles U(z) we try to determine the friction the bottom stress, the roughness depth and the quadratic drag coefficient and the depth of the logarithmic layer.

The expression for the friction layer is as follows:

$$U(z) = (U^*/k) \ln(z/z_0),$$

where U(z) is the horizontal velocity profile in the boundary layer. U^* is the friction velocity and k is a universal constant known as von Karman's constant (0. 42). In our above interpretation

z is the vertical distance from the sea bed.

z_0 is the roughness length, which is a function the bottom stucture.

The friction velocity,U^* can be defined by the expression

$$U^* = \sqrt{\frac{\tau}{\rho}}$$

from which

$$\tau = \rho U^{*2}$$

where τ is the bottom shear stress and ρ is density of water.

The quadratic drag coefficient (C_d) is given by the expression,

$$\tau = \rho c_d U_o^2$$

where U_o is the velocity outside the boundary layer,

thus

$$c_d = \frac{\tau}{\rho U_o^2}$$

The above parameters were determined from a matlab program that estimates the friction velocity and roughness length by least square fit of the current data to the logarithmic profile (fig.12). This was done by rearranging equation 4. 4.1a as follows:

$$U(z) = \frac{U^*}{k} \ln z - \frac{U^*}{k} \ln z_o$$
,

and performing linear regression to the straight line equation ;

$$y = mx + C$$,

where

the slope $= \dfrac{U^{*}}{k}$,

the intercept $C = -\dfrac{U^{*}}{k}\ln z_{o}$,

and

$z_{o} = e^{kc/U^{*}}$.

U_{o} is the mean velocity in the layer above the friction layer and was estimated and used in the program for each set of measurments. Table 8 shows the values for the parameters.

The exponential depth scale of the bottom friction layer

Wang and Craig (1993), point out that the depth scale of the constant eddy viscosity layer (the bottom friction layer) can be calculated, if the frequency (ω) of the dominant tidal component and the eddy viscocity (μ) are known, from the expression

$$D = \sqrt{(\dfrac{2\mu}{\omega})}$$

where D is the exponential depth scale of the constant eddy viscousity layer, μ , the friction

coefficient . It should be noted that the eddy viscosity layer is above the constant shear stress layer (the logarithmic layer) of which length can be estimated as from 0-4m above the sea-bed.

Common representation of the interior eddy viscosity (Wang and Craig,1993) is

$\mu=cU^*H$, where H is the depth of the water and U^* the friction velocity. c is a constant

ranging from 0.01 to 0.1. From the logarithimic profiles (fig.12) , almost constant velocity

occur in the range from near the surface to about 11m below the surface. The curves

suggest that the depth of the constant eddy viscosity layer lies between 4m

and 9m above the sea- bed. Thus conveniently chosing the value for c as 0.01 allows

us to determine the value for D. When the values for U^* of 0.04m s^{-1} from previous

calculation (assuming this is the value at the base of the eddy viscous layer) and H taken

as 20 m coincinding with the general depth of the channel at the mooring site. The value

for μ is found to be 0.0082 m^2s^{-1}. Wang and craig foud a value of 0.0028 $m^2s^{-1}$for

similar system. When ω is taken as $2\pi/T$, where T is 12.42 hrs, the value for the depth of

the eddy viscocity layer is 10.8 m, this is compares well with the values of 9m obtained

by Wang and craig for similar system. This shows that the currents in the channel do

reach constant values towards the surface. The observations also confirm that the

position of RCMs 10 m was suitably selected and further that the three lowest pendelums

were within the boundary layer.

It should also be noted that the depth of the constant eddy viscous layer can be taken

as the height where the mean flow velocity in the upper layer drops to about 90% of it's

value. In some cases the boundary layer never grows to its maximum steady state value

because it's build up (growth) time is close to the tidal cycle i.e. the current switches

direction before the boundary layer is fully developed. .